ParisTech
INSTITUT DES SCIENCES ET TECHNOLOGIES
PARIS INSTITUTE OF TECHNOLOGY

MINES ParisTech

École doctorale n° 432 : Sciences des Métiers de l'Ingénieur

Doctorat ParisTech

T H È S E

pour obtenir le grade de docteur délivré par

l'École nationale supérieure des mines de Paris

Spécialité « Génie des Procédés »

présentée et soutenue publiquement par

Caleb NARASIGADU

le 06 septembre 2011

Conception d'une Micro-Cellule pour Mesures d'Équilibres de Phases : Mesures et Modélisation

Design of a Static Micro-Cell for Phase Equilibrium Measurements : Measurements and Modelling

Directeurs de thèse : **Dominique RICHON et Deresh RAMJUGERNATH**
Co-encadrements de la thèse : **Christophe COQUELET et Paramespri NAIDOO**

Jury

M. Jean-Nöel JAUBERT, Professeur, Institut National Polytechnique de Lorraine	**Rapporteur**
M. Serge LAUGIER, Maitre de Conférence, E.N.S.C.B.P.	**Rapporteur**
M. Johan David RAAL, Professeur Emerite, University of KwaZulu-Natal	**Examinateur**
M. Pascal MOUGIN, Ingénieur de Recherche, Institut français du pétrole	**Examinateur**
M. Deresh RAMJUGERNATH, Professeur, University of KwaZulu-Natal	**Examinateur**
M. Dominique RICHON, Directeur de Recherche, MINES ParisTech	**Examinateur**
M. Christophe COQUELET, Maitre Assistant, MINES ParisTech	**Examinateur**

T H È S E

MINES ParisTech
Centre Énergétique et Procédés – Laboratoire CEP/TEP
35, rue Saint Honoré, 77305 Fontainebleau cedex, France

DESIGN OF A STATIC MICRO-CELL FOR PHASE EQUILIBRIUM MEASUREMENTS: MEASUREMENTS AND MODELLING

by

CALEB NARASIGADU

[MSc. (Eng)]
University of KwaZulu Natal

Submitted in fulfillment of the academic requirements for
the degree of Doctor of Philosophy in Engineering at the School
of Chemical Engineering, University of KwaZulu Natal and
L'Ecole Nationale Supérieure des Mines de Paris
as agreed in the convention for international joint doctorate supervision
entered into by these two institutions

Durban
2011

ABSTRACT

Vapour-Liquid Equilibrium (VLE), Liquid-Liquid Equilibrium (LLE) and Vapour-Liquid-Liquid Equilibrium (VLLE) are of special interest in chemical engineering as these types of data form the basis for the design and optimization of separation processes such as distillation and extraction, which involve phase contacting. Of recent, chemical companies/industries have required thermodynamic data (especially phase equilibrium data) for chemicals that are expensive or costly to synthesize. Phase equilibrium data for such chemicals are scarce in the open literature since most apparatus used for phase equilibrium measurements require large volumes (on average 120 cm^3) of chemicals. Therefore, new techniques and equipment have to be developed to measure phase equilibrium for small volumes across reasonable temperature and pressure ranges.

This study covers the design of a new apparatus that enables reliable vapour pressure and equilibria measurements for multiple liquid and vapour phases of small volumes (a maximum of 18 cm^3). These phase equilibria measurements include: VLE, LLE and VLLE. The operating temperature of the apparatus ranges from 253 to 473 K and the operating pressure ranges from absolute vacuum to 1600 kPa. The sampling of the phases are accomplished using a single Rapid-OnLine-Sampler-Injector (ROLSI^{TM}) that is capable of withdrawing as little as 1µl of sample from each phase. This ensures that the equilibrium condition is not disturbed during the sampling and analysis process. As an added advantage, a short equilibrium time is generally associated with a small volume apparatus. This enables rapid measurement of multiple phase equilibria. A novel technique is used to achieve sampling for each phase. The technique made use of a metallic rod (similar in dimension to the capillary of the ROLSI^{TM}) in an arrangement to compensate for volume changes during sampling.

As part of this study, vapour pressure and phase equilibrium data were measured to test the operation of the newly developed apparatus that include the following systems:

- VLE for 2-methoxy-2-methylpropane + ethyl acetate at 373.17 K
- LLE for methanol + heptane at 350 kPa
- LLE for hexane + acetonitrile at 350 kPa
- VLLE for hexane + acetonitrile at 348.20 K

New experimental vapour pressure and VLE data were also measured for systems of interest to petrochemical companies. These measurements include:

- VLE for methanol + butan-2-one at 383.25, 398.14 and 413.20 K

- VLE for ethanol + butan-2-one at 383.26, 398.23 and 413.21 K
- VLE for ethanol + 2-methoxy-2-methylbutane at 398.25 and 413.19 K
- VLE for ethanol + 2-methylpent-2-ene at 383.20 K

These measurements were undertaken to understand the thermodynamic interactions of light alcohols and carbonyls as part of a number of distillation systems in synthetic fuel refining processes which are currently not well described. Two of these above mentioned systems include expensive chemicals: 2-methoxy-2-methylbutane and 2-methylpent-2-ene.

The experimental vapour pressure data obtained were regressed using the extended Antoine and Wagner equations. The experimental VLE data measured were regressed with thermodynamic models using the direct and combined methods. For the direct method the Soave-Redlich-Kwong and Peng-Robinson equations of state were used with the temperature dependent function (α) of Mathias and Copeman (1983). For the combined method, the virial equation of state with the second virial coefficient correlation of Tsonopoulos (1974) was used together with one of the following liquid-phase activity coefficient models: TK-Wilson, NRTL and modified UNIQUAC. Thermodynamic consistency testing was also performed for all the VLE experimental data measured where almost all the systems measured showed good thermodynamic consistency for the point test of Van Ness et al. (1973) and direct test of Van Ness (1995).

PREFACE

The work presented in this thesis was performed at the University of KwaZulu-Natal and L'Ecole Nationale Supérieure des Mines de Paris from January 2008 to March 2011 as stipulated in the convention for international joint doctorate supervision entered into by these two institutions. The work was supervised by Professor D. Ramjugernath and Doctor P. Naidoo at the University of KwaZulu-Natal and Prof. D. Richon and Doctor C. Coquelet at L'Ecole Nationale Supérieure des Mines de Paris.

This thesis is submitted as the full requirement for the degree PhD in chemical engineering.

I, Caleb Narasigadu declare that:

i) The research in this dissertation, except where otherwise stated, is my original work.

ii) This thesis has not been submitted for any degree or examination at any other university.

iii) This thesis does not contain other persons' data, pictures, graphs or other information, unless specifically acknowledged as being sourced from other persons.

iv) This thesis does not contain other persons' writing, unless specifically acknowledged as being sourced from other researchers. Where other written sources have been quoted then:

   a) Their words have been re-written but the general information attributed to them has been referenced;

   b) Where their exact words have been used, their writing has been placed inside quotation marks and referenced.

v) This thesis does not contain text, graphics or tables copied and pasted from the internet, unless specifically acknowledged and the source being detailed in the thesis and in the References section.

_____

C. Narasigadu

As supervisor of this candidate, I approve this dissertation for submission:

_____	_____
Professor D. Ramjugernath	Doctor P. Naidoo
_____	_____
Professor D. Richon	Doctor C. Coquelet

ACKNOWLEDGEMENTS

I would like to take this opportunity to acknowledge and thank the following who have made a tremendous contribution to this work:

- Firstly, my Lord and Saviour, Jesus Christ, Who has made my tertiary education a reality. Lord, I am eternally grateful to You.

- My supervisors, Professor D. Ramjugernath, Doctor P. Naidoo, Doctor C. Coquelet and Professor D. Richon for their expert knowledge, guidance and support.

- SASOL Ltd. for their financial assistance.

- The technical staff at the School of Chemical Engineering University of KwaZulu Natal, in particular Kelly Robertson for his invaluable contribution to this work in terms of construction work.

- Alan Raymond Foster and Warren Errol Sheahan for their assistance with the schematic drawings.

- My mum, Linda, my sister, Lisa, and my uncle and aunt, Jiva and Sylvia, for their many years of wholehearted support, prayer, encouragement, love and motivation.

- My extended family, fellow postgraduate colleagues, friends and especially the congregation of Christian Revival Centre Tongaat church for their invaluable advice, prayer, support and friendship.

DEDICATION

To

my Lord and Saviour, Jesus Christ

But without faith it is impossible to please and be satisfactory to Him.
For whoever would come near to God must [necessarily] believe
that God exists and that He is the rewarder of those who
earnestly and diligently seek Him [out].

HEBREWS 11:6
(AMPLIFIED BIBLE)

TABLE OF CONTENTS

LIST OF FIGURES

Chapter 2

Chapter 3

Chapter 4

Chapter 5

Chapter 6

Chapter 7

Appendix C

Appendix D

Appendix E

Appendix F

LIST OF PHOTOGRAPHS

Chapter 4

LIST OF TABLES

Chapter 3

Chapter 6

Chapter 7

Appendix B

Appendix C

NOMENCLATURE

English Letters

$A^{'}$	Parameter in the extended Antoine vapour pressure equation
$A^{''}$	Parameter in the Wagner vapour pressure equation
A_{∞}^{E}	Excess Helmholtz free energy at infinite pressure [J.mol^{-1}]
A_m	Mixture parameter in a cubic equation of state
A_i^*	Peak area for species *i* obtained from the gas chromatograph
AVD	Average absolute deviation of a property
a	Intermolecular attraction force parameter in a cubic equation of state
a_{ij}	TK-Wilson model energy interaction parameter of Tsuboka and Katayama (1975) [J.mol^{-1}]
a_m	Mixture intermolecular attraction force parameter in a cubic equation of state
a_t	Polar contribution parameter in correlation of Tsonopoulos (1974)
$B^{'}$	Parameter in the extended Antoine vapour pressure equation
$B^{''}$	Parameter in the Wagner vapour pressure equation
B_{ij}	Interaction second Virial coefficient [cm^3.mol^{-1}]
B_m	Mixture parameter in a cubic equation of state
$B_{mixture}$	Second Virial coefficient of a mixture, defined by Equation (3-27) [cm^3.mol^{-1}]
B_{virial}	Second Virial coefficient, density expansion [cm^3.mol^{-1}]
b	Molecular size parameter in a cubic equation of state
b_m	Mixture intermolecular attraction force parameter in a cubic equation of state
b_t	Polar contribution parameter in correlation of Tsonopoulos (1974)
$C^{'}$	Parameter in the extended Antoine vapour pressure equation
$C^{''}$	Parameter in the Wagner vapour pressure equation
c	Parameter in the mixing rule of Wong and Sandler (1992)
D	Summation term in the mixing rule of Wong and Sandler (1992)
$D^{'}$	Parameter in the extended Antoine vapour pressure equation
$D^{''}$	Parameter in the Wagner vapour pressure equation

E'	Parameter in the extended Antoine vapour pressure equation
F	Objective function in an iteration scheme
F_i	Response factor of species *i* from gas chromatograph
f_i	Fugacity, pure species *i* [kPa]
$\hat{f}_i$	Fugacity, species *i* in solution [kPa]
$f^{(0)}$	Term in correlation of Tsonopoulos (1974), defined by Equation (3-31)
$f^{(1)}$	Term in correlation of Tsonopoulos (1974), defined by Equation (3-32)
$f^{(2)}$	Term in correlation of Tsonopoulos (1974), defined by Equation (3-34)
G	Molar Gibbs energy [J.mol^{-1}]
G_{ij}	Parameter in the NRTL model of Renon and Prausnitz (1968)
$\overline{G}_i$	Partial Gibbs energy, species *i*
ΔG	Gibbs energy change of mixing [J.mol^{-1}]
g_{ij}	NRTL model energy interaction parameter of Renon and Prausnitz (1968) [J.mol^{-1}]
H	Molar enthalpy [J.mol^{-1}]
$\overline{H}_i$	Partial enthalpy, species *i* in solution
K_i	Vapour-liquid equilibrium ratio for species *i*
k_{ij}	Binary interaction parameter
l_i	Parameter in the UNIQUAC model of Abrams and Prausnitz (1975)
N	Number of chemical species
n	Number of moles
n_i	Number of moles, species *i*
n_T	Total number of moles in a system
P	Absolute pressure [kPa]
P_i^{sat}	Saturation vapour pressure, species *i* [kPa]
Q	Quadratic summation term in the mixing rule of Wong and Sandler (1992)
q_i	Area parameter for UNIQUAC model of Abrams and Prausnitz (1975)
q_i'	Area parameter for modified UNIQUAC model of Anderson and Prausnitz (1978)
R	Universal gas constant [J.mol^{-1}.K^{-1}]
RMSD	Root mean squared deviation

r_i	Volume parameter for UNIQUAC model of Abrams and Prausnitz (1975)
S	Molar entropy [J.mol^{-1}.K^{-1}]
T	Absolute temperature [K]
u_{ij}	Energy interaction parameter of UNIQUAC model of Abrams and Prausnitz (1975) [J.mol^{-1}]
V	Molar volume [cm^3.mol^{-1}]
$\overline{V_i}$	Partial molar volume, species *i* in solution
x'	Term used in the Wagner vapour pressure equation, defined by Equation (7-4)
x_i	Mole fraction, species *i*, liquid phase
y_i	Mole fraction, species *i*, vapour phase
Z	Compressibility factor
z	Overall mole fraction

Greek Letters

α	Scaling factor function in a cubic equation of state
α_{ij}	Non-randomness parameter in the NRTL model of Renon and Prausnitz (1968)
β	Parameter in the TK-Wilson model of Tsuboka and Katayama (1975)
β_v	Parameter in the TK-Wilson model of Tsuboka and Katayama (1975)
Φ_i	Ratio of fugacity coefficients, defined by Equation (3-24)
Φ_i^*	Volume fraction in the UNIQUAC model of Abrams and Prausnitz (1975)
ϕ_i	Fugacity coefficient, pure species *i*
$\hat{\phi}_i$	Fugacity coefficient, species *i* in solution
Γ_i	Integration constant
γ_i	Activity coefficient, species *i* in solution
δ	Denotes a residual for a property
δ_{ij}	Parameter that relates second Virial coefficients, defined by Equation (3-29)
$\varepsilon, \varepsilon_A, \varepsilon_B$	Tolerances used for objective functions
$\varepsilon^*, \varepsilon_P^*, \varepsilon_T^*$	Constant terms in the direct test of Van Ness (1995)
κ	Characteristic constant in a cubic equation of state

$\kappa_1, \kappa_2, \kappa_3$	Parameters in the scaling factor function of Mathias and Copeman (1983)
Λ_{ij}	Parameter in the TK-Wilson model of Tsuboka and Katayama (1975)
λ_{ij}	Parameter in the TK-Wilson model of Tsuboka and Katayama (1975)
μ_i	Chemical potential, species *i*
θ_i	Area fraction in the UNIQUAC model of Abrams and Prausnitz (1975)
θ_i'	Area fraction in the modified UNIQUAC model of Anderson and Prausnitz (1978)
τ_{ij}	Parameter in the NRTL model of Renon and Prausnitz (1968)
ω	Acentric factor

Subscript

c	Denotes a critical property
cal	Denotes a calculated value from a model
exp	Denotes an experimental value
i	Denotes species *i*
j	Denotes species *j*
new	Denotes the current value of a property in an iteration scheme
old	Denotes the previous value of a property in an iteration scheme
r	Denotes a reduced property
1	Denotes species *1*
2	Denotes species *2*

Superscript

E	Denotes an excess property
id	Denotes value for an ideal solution
ig	Denotes value for an ideal gas
l	Denotes liquid phase
sat	Denotes a saturated value
v	Denotes vapour phase
α	Denotes a phase
β	Denotes a phase

π	Number of phases
∞	Denotes a value at infinite dilution

Notes

Δ	Difference operator

Les industries chimiques ont un besoin constant de données d'équilibre de phase (diagrammes de phases) précises (particulièrement pour les nouveaux produits chimiques dont la synthèse est coûteuse pour) afin concevoir avec succès des procédés de séparation efficaces et économes facile à mettre en œuvre. Pour déterminer ces diagrammes de phases, il est nécessaire de disposer d'un appareillage fiable associé à une méthodologie expérimentale bien adaptée. Bien qu'il soit facile de trouver dans la littérature de nombreux types d'appareillages destinés à la mesure d'équilibres de phase, seulement peu d'entre eux ont été conçus pour travailler sur de petits volumes de produits chimiques (inférieurs à 20 cm^3). Cette étude concerne donc une prise de recul face à l'existant, une réflexion critique et enfin la conception et le développement d'un nouvel équipement expérimental de mesure de tension de vapeur et des équilibres multiphasiques sur de petits volumes de l'ordre de 18 cm^3. La température de fonctionnement de cet équipement expérimental s'étend de 253 à 473 K et la pression de fonctionnement s'étend du vide à 1 600 kPa. En complément de cette étude, de nouvelles données expérimentales d'équilibre de phase ont été obtenues, sur des systèmes binaires comprenant un alcool léger et un composé carbonylé, pour le compte d'une compagnie pétrochimique Sud-Africaine.

1

CHAPTER ONE

INTRODUCTION

Phase equilibrium is of special interest in chemical engineering as this type of data forms the basis for the design of separation processes such as distillation and extraction, which involve phase contacting. In the light of chemical companies/industries manufacturing new chemicals, there is an important need for thermodynamic data, especially phase equilibrium measurements. These new chemicals are extremely costly to synthesize or commercially unavailable. There is a variety of experimental equipment and techniques designed to perform phase equilibrium measurements, but such equipment usually require a large volume of the chemical species to undertake measurements. As a result, new techniques and equipment have to be developed to measure phase equilibrium for small volumes (say 20 cm^3) across reasonable temperature and pressure ranges.

This study covers the design of a new apparatus that enables reliable vapour pressure and equilibrium measurements for multiple liquid and vapour phases of small volumes (a maximum of 18 cm^3). These phase equilibria measurements include: vapour-liquid equilibrium (VLE), liquid-liquid equilibrium (LLE) and vapour-liquid-liquid equilibrium (VLLE). The operating temperature of the apparatus ranges from 253 to 473 K and the operating pressure ranges from absolute vacuum to 1600 kPa. The sampling of the phases is accomplished using a Rapid-OnLine-Sampler-Injector (ROLSI^{TM}) that is capable of withdrawing as little as 1µl of sample from each phase (Guilbot et al., 2000). The use of a ROLSI^{TM} also does not disturb the equilibrium under study since approximately only a µl of sample is withdrawn. As an added advantage, a short equilibrium time is generally associated with a small volume apparatus. This enables rapid measurement of multiple phase equilibria.

As part of this study, vapour pressure and phase equilibrium data were measured to test the operation of the newly developed apparatus that include the following systems:

- VLE for 2-methoxy-2-methylpropane + ethyl acetate at 373.17 K
- LLE for methanol + heptane at 350 kPa

- LLE for hexane + acetonitrile at 350 kPa
- VLLE for hexane + acetonitrile at 348.20 K

New experimental vapour pressure and VLE data were also measured for systems of interest to petrochemical companies. These measurements include:

- VLE for methanol + butan-2-one at 383.25, 398.14 and 413.20 K
- VLE for ethanol + butan-2-one at 383.26, 398.23 and 413.21 K
- VLE for ethanol + 2-methoxy-2-methylbutane at 398.25 and 413.19 K
- VLE for ethanol + 2-methylpent-2-ene at 383.20 K

These measurements were undertaken to understand the thermodynamic interactions of light alcohols and carbonyls as part of a number of distillation systems in synthetic fuel processes which are currently not well described. Two of these above mentioned systems include expensive chemicals: 2-methoxy-2-methylbutane and 2-methylpent-2-ene. A quotation obtained from Capital Lab Suppliers CC on 22 April 2010 showed a cost of R5 510 for 500 mL of 2-methoxy-2-methylbutane with purity greater than 97% and R2 605 for 50 mL of 2-methylpent-2-ene with a minimum purity of 98%.

Overall, this study focuses on: the design and development of a new phase equilibrium apparatus for small volumes (a maximum of 18 cm^3), measurement of new vapour pressure and phase equilibria data and thermodynamic modeling of the measured data. Novel features of this apparatus includes: a small equilibrium cell volume (18 cm^3) and a new technique that uses a single movable ROLSI^{TM} for the sampling of equilibrium phases.

La mesure d'équilibre de phase concerne classiquement la mesure de la température, de la pression et des compositions des phases en présence. La littérature fournit les informations nécessaires pour une grande série d'équipements ainsi que sur les techniques disponibles afin de permettre des mesures d'équilibres de phase. La méthode statique est l'une des méthodes les plus utilisées à ce jour pour les équilibres « liquide-vapeur » (ELV) à moyennes et hautes pressions. Elle a donc tout naturellement été au cœur de nos préoccupations pour notre conception et son développement.

Notre revue bibliographique, objet du chapitre 2 est focalisée sur : le matériel de construction de la cellule d'équilibre; les méthodes de régulation de température pour un équilibre de température uniforme autour de la cellule d'équilibre; le dégazage des composés avant leur introduction dans la cellule d'équilibre; les méthodes d'agitation efficaces à l'intérieur des cellules d'équilibre; les méthodes d'échantillonnage des phases liquides et des phases vapeurs et les méthodes de vaporisation et d'homogénéisation des échantillons.

Les cellules d'équilibre sont habituellement construites en acier inoxydable, verre borosilicaté ou saphir dépendant des conditions opératoires (niveau de pression, corrosions possibles etc…). Le saphir est bien connu pour ses propriétés optiques, ses résistances mécanique et chimique. L'acier inoxydable (type 316) est habituellement choisi comme matériau de construction principal pour diverses pièces d'équipement expérimental en raison de ses propriétés mécaniques (résistance en particulier), la facilité à le souder et à l'usiner. Des thermostats à air, (Legret et al., 1981, Galicia-Luna et al., 2000, etc…), ou à azote (Rogers et Prausnitz, 1970), ou des thermostats à eau (Katayama et al., 1975, Wu et al., 2010, etc…) ou encore à huile (Legret et al., 1980, Park et al., 2007, etc…) sont généralement utilisés comme environnement thermique pour la cellule d'équilibre selon la température ambiante requise et les conditions d'utilisation (le nettoyage fréquent de pièces plongées dans un bain d'huile peut s'avérer une contrainte difficile à accepter….). Le chauffage électrique est un autre autres moyen de réaliser l'équilibre thermique (Besserer et Robinson, 1971 ; Konrad et al., 1983 et Corazza et al., 2003). L'équilibre est réalisé dans un temps réduit dans la mesure où le contenu de la cellule d'équilibre est convenablement agité. Parmi les méthodes d'agitation on trouve : l'utilisation d'un barreau magnétique en rotation dans un champ magnétique extérieur (Legret et a.., 1981) ; le bullage de la vapeur au travers du liquide (Outcalt et Lee, 2004), l'utilisation d'un piston commandé par un champ électromagnétique (Gómez-Nieto et Thodos, 1978), l'oscillation de la cellule d'équilibre autour d'un axe horizontal (Huang et autres, 1985) et même l'utilisation des ultrasons (Takagi et al., 2003). Les techniques employées pour prélever les phases à l'équilibre incluent : l'utilisation d'électrovannes pneumatique ou électromagnétique à

action rapide (Figuière et al., 1980) ; une microcellule détachable (Legret et autres, 1981) ; l'utilisation d'un axe percé transversalement agissant comme un tiroir (Rogers et Prausnitz, 1970) ; l'utilisation de capillaires (Wagner et Wichterle, 1987 et Matos et al., 1989) ; une vanne 6 voies pour chromatographie en phase gazeuse (Ramjugernath, 2000) et l'échantillonneur breveté : Rapid-On-Line-Sample-Injector (ROLSI^{TM}) (Guilbot et al., 2000). On trouve dans la littérature beaucoup de procédures pour dégazer les liquides, tels que le chauffage avec reflux de liquide et retrait périodique de phase vapeur, congélation et décongélation sous vide poussé, et aussi sublimation et distillation sous vide. Parmi toutes ces méthodes, Van Ness et Abbott (1978) préfèrent la distillation sous vide qu'ils jugent comme moins pénible et plus rapide.

2

CHAPTER TWO

LITERATURE REVIEW

The measurement of phase equilibrium involves the measurements of temperature, pressure and phase compositions. According to Walas (1985), care must be taken to ensure that the temperature and pressure are measured at the point where equilibrium really exists and that the withdrawal of samples for analysis does not disturb the equilibrium appreciably. It is however practically difficult to obtain experimental data of high accuracy.

Literature indicates a variety of phase equilibrium equipment developments made in order to achieve reliable and appreciably accurate measurements. These include reviews by Hála et al. (1967), Malanowski (1982), Abbott (1986), Schneider (1998), Christov and Dohrn (2002) and Dohrn et al. (2010) to name a few. According to Hála et al. (1967), low pressure vapour-liquid equilibrium (VLE) can be classified into the following categories:

1. Distillation Methods
2. Dynamic Methods
3. Static Methods
4. Flow Methods
5. Dew and Bubble Point Methods

The purpose of this chapter is not to present an exhaustive review of all experimental techniques for phase equilibrium, rather it will focus on the static method for low to moderately high pressure VLE, which is one of the most commonly used methods today. For an excellent review of the other methods in phase equilibrium measurement, the reader is referred to Robinson and Gilliland (1950), Hála et al. (1967), Raal and Mühlbauer (1998), Christov and Dohrn (2002) and Dohrn et al. (2010).

2.1 The Static Method

According to Kolbe and Gmehling (1985), the measurement of VLE using static methods has become increasingly important in recent years, where an important step in this direction was made by Gibbs and Van Ness (1972). The major advantage of the static method is its simplicity. A liquid mixture is charged into an evacuated equilibrium cell immersed in a constant temperature bath and one waits as long as needed until equilibrium is reached. Usually, an internal stirring mechanism is added to the equilibrium cell to promote the establishment of equilibrium in a shorter time.

The static method can be subdivided into analytical methods or the synthetic method. In analytical methods, one or both the liquid and vapour compositions are sampled and analyzed, while in the synthetic method no sampling of the phases is required. This study was concerned with the development of a static analytical apparatus and will therefore focus on this method. Figure 2-1 shows a schematic illustration of the static analytical method. The static synthetic method, on the other hand, has been studied by many researchers which include Gibbs and Van Ness (1972), Aim (1978), Maher and Smith (1979), Kolbe and Gmehling (1985), Rarey and Gmehling (1993), Fischer and Gmehling (1994), Takagi et al. (2003), Franceschi et al. (2004), Outcalt and Lee (2004) and Dohrn et al. (2007) to name a few. The reader is thus referred to the publications mentioned above in regards to the development of a static synthetic apparatus.

For mixtures with more than two components, the information that can be obtained using the static synthetic method is very limited. Furthermore, thermodynamic consistency testing of the data cannot be carried out when the static synthetic method is used (Raal and Mühlbauer, 1998). Hence, the experimental apparatus for the static analytical method has been studied by many other researchers which include: Rigas et al. (1958), Kalra et al. (1978), Ng and Robinson (1978), Figuiere et al. (1980), Guillevic et al. (1983), Zimmerman and Keller (1989), Mühlbauer and Raal (1991), Laursen et al. (2002), Secuianu et al. (2003) and Garmroodi et al. (2004) to name a few. The main differences in these studies were the:

- material of construction for the equilibrium cell,
- methods of creating a uniform equilibrium cell temperature,
- methods of agitating the equilibrium cell contents,
- methods of sampling the liquid and vapour phases,
- methods of vapourising and homogenizing the samples,
- method of in-situ analysis of the liquid and vapour phases,

- and the degassing of components prior to measurements.

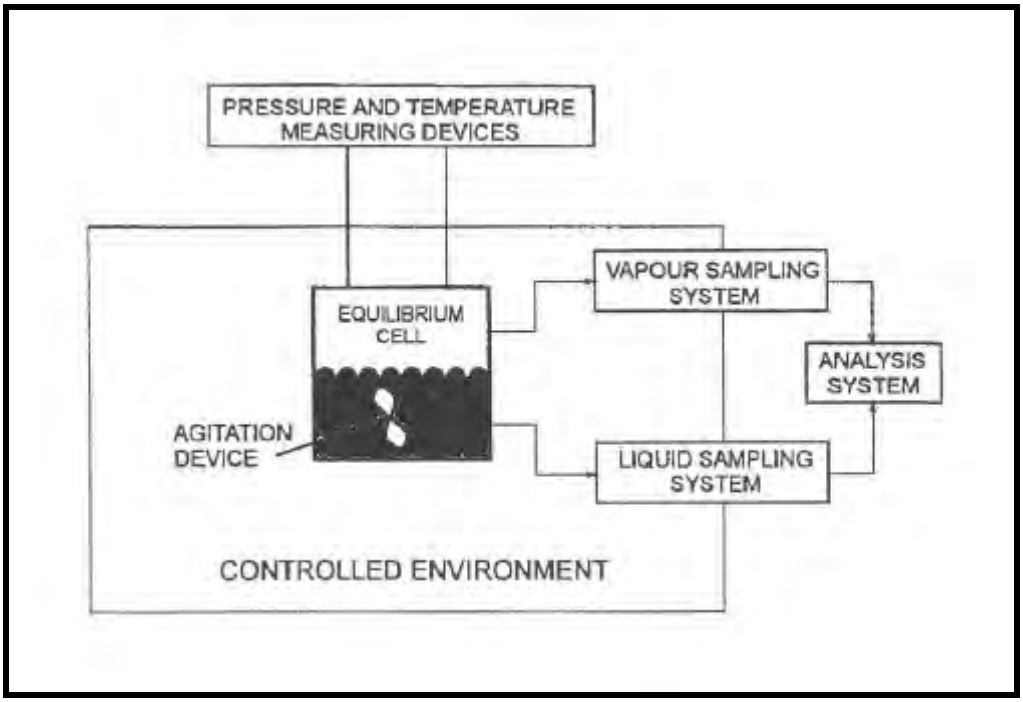

Figure 2-1: Schematic illustration of the static analytical method (Raal and Mühlbauer, 1998).

The above mentioned points can be classified into three main features; cell design, sampling techniques and degassing of components. These features will now be discussed in detail as they form the core for the development of the new experimental apparatus for this study.

Several researchers have also produced semi-micro apparatus. These include: Wichterle and Hála (1963), Wichterle and Boublíková (1969) and Raal and Mühlbauer (1998). The apparatus of Wichterle and Hála (1963) was embedded in a small glass vessel with a jacket that utilized water as the thermal fluid. The apparatus was connected to a glass stopcock which facilitated the supply of carrier gas to a gas chromatograph. Essentially, 2 cm^3 of a liquid mixture (per experimental point) of known composition was introduced into equilibrium cell and stirred and the vapour space was filled with the carrier gas. No pressure measurement or degassing was attempted for this apparatus and hence the apparatus was limited to only isothermal x-y data. This apparatus was later modified by Wichterle and Boublíková (1969) who replaced the simple stopcock with an eight-way stopcock to trap a larger sample of the vapour. Wichterle and Boublíková (1969) reported the use of 3 cm^3 of liquid chemicals per experimental point. However, pressure measurement and degassing were still not catered for. Raal and Mühlbauer (1998) incorporated some of these design features to develop a better semi-micro apparatus that could account for pressure measurement, effective vapor recirculation and degassing. This

apparatus relies on vapour recirculation for the attainment of equilibrium. Furthermore, the apparatus cannot be used for moderate or high pressures but limited to low pressures.

2.2 Cell Design

Literature describes a variety of equipment, where each is designed for a specific application as the design of a "universal" phase equilibrium apparatus for all temperatures, pressures and chemical nature is an impossible task. Over the years, there has been good progress made on broadening existing notions for equipment development with new ideas formed for new applications/purposes. The designs depend on experimental conditions, e.g. temperature and pressure, and on the physical properties of the components studied, which include corrosiveness, density, viscosity, toxicity, etc. It is rather difficult and even unprofitable to propose an apparatus that could be used indiscriminately. Instead, the design of a new apparatus should be as simple as possible without compromising the quality of the data to be measured.

2.2.1 Material of Construction

Over the number of years, researchers have used various materials to construct the equilibrium cell, which is the heart of the apparatus. Some of the most commonly used materials include; stainless steel (Figuiere et al., 1980), chromium-nickel-molybdenum steel (Reiff et al., 1987), duran glass (Holldorff and Knapp, 1988), manganese steel (Ashcroft et al., 1983), brass (Zabaloy et al., 1994) and sapphire (Ng et al., 1985). The choice of material depends on several factors, most of which are already mentioned above. Apart from these factors, visual observation of the cell in operation is also considered important. This importance is evident where the phase separation needs to be viewed prior to sampling especially if a single movable sampling device is employed.

Strength and chemical resistance properties of the material must also be considered. Sapphire is well-known as a strong and tough optical material that also offers excellent chemical resistance (General Ruby and Sapphire Company). In addition to the material of construction properties for the equilibrium cell, the strength and chemical resistance properties for the material of construction of the various equipment parts also used to design the phase equilibrium apparatus must be carefully considered. Stainless steel (SS) is known to succumb to pitting and crevice corrosion in warm chloride environments, however, the addition of 2% molybdenum to 304 SS to produce 316 SS offers a significant increase in resistance to pitting (Fontana and Greene, 1967). Another remarkable property of 316 SS is its mechanical strength (such as high tensile and yield strength) and the ability to retain these properties for long periods of time under

extreme high or low temperatures (Sinnott, 2005). The 316 SS material also has very good welding and machining properties making it suitable to use in the construction of various equipment parts. Hence, 316 SS is usually chosen as the principal material of construction for the various parts in the design of a phase equilibrium apparatus.

2.2.2 Thermal Environment

For isothermal measurements, it is essential to ensure that the equilibrium cell is housed in a temperature controlled environment. To achieve this, researchers used different types of temperature controlled environments; air bath (Legret et al., 1981 and Galicia-Luna et al., 2000), nitrogen bath (Rogers and Prausnitz, 1970), water bath (Katayama et al., 1975 and Wu et al., 2010) and oil bath (Legret et al., 1980 and Park et al., 2007). These baths are usually lined with various materials. These include; aluminum (Ng and Robinson, 1978), copper (Konrad et al., 1983) or jackets. Researchers also use a variation of the above mentioned thermostats e.g. a two-stage water bath thermostat was used by Aim (1978), were an internal thermostat served as a thermal capacity to smooth temperature fluctuations.

Ng and Robinson (1978) used an entirely different approach by making use of a 25 mm thick aluminum shroud containing eight vertically mounted and uniformly spaced pencil-type 250 W electrical heaters, to maintain the equilibrium cell temperature. Other researchers who used electrical heating include Besserer and Robinson (1971), Konrad et al. (1983) and Corazza et al. (2003) were in each case thermostatting jackets were electrically heated to maintain the equilibrium temperature. Besserer and Robinson (1971) were able to control the equilibrium temperature to within 0.5 K of the set-point by making use of a thermocouple proportional-band temperature controller. This temperature controller controlled the heaters in the aluminum shroud which was placed over the ends of the equilibrium cell. Konrad et al. (1983) was able to reduce the axial temperature gradients to smaller than 0.2 K by making use of additional head and bottom heaters whilst Corazza et al. (2003) report a temperature accuracy of 0.1 K.

On the other hand, Outcalt and Lee (2004) made use of fluid circulation in conjunction with computer-controlled electric heating to control the temperature of the system, where the equilibrium cell was housed within an aluminum block (see Figure 2-2). The fluid circulation provided a rough temperature control were flow channels were bored through the sides of the aluminum block and six thin-film heaters were used for the fine temperature control. The outside of the aluminum block was also covered with insulation.

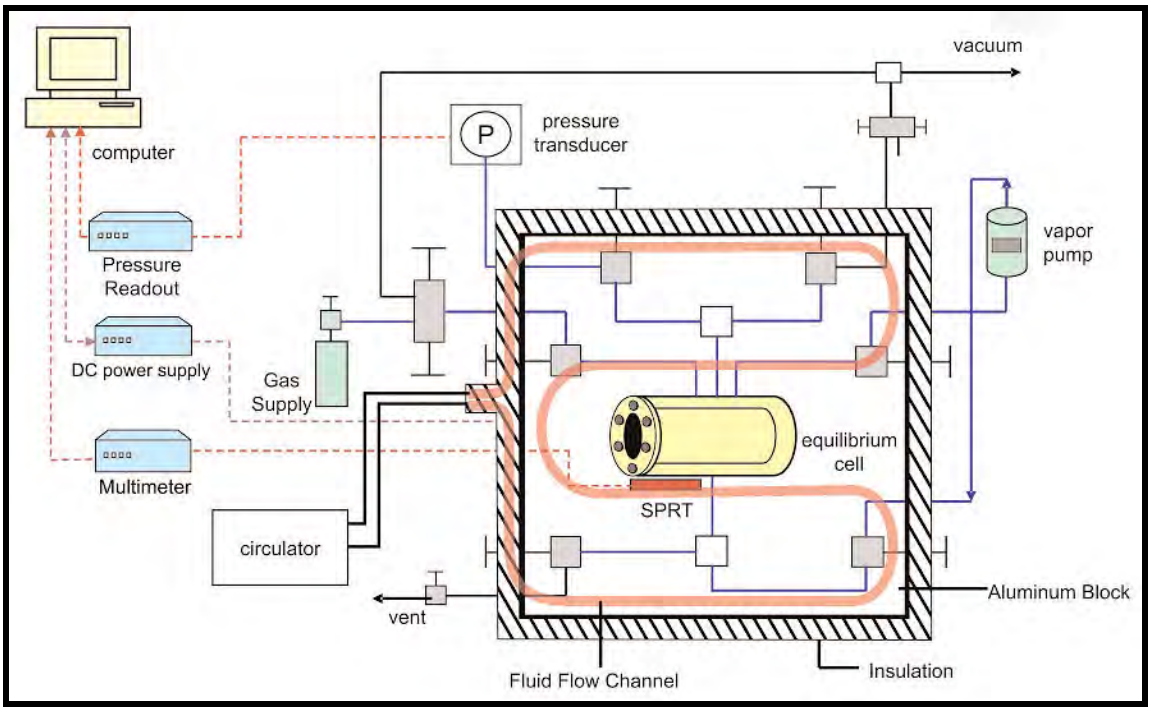

Figure 2-2: Schematic of the experimental apparatus of Outcalt and Lee (2004).

The presence of temperature gradients can lead to considerable error on sample representativity. Naidoo (2004) notes some points with regards to temperature gradients:

- The measurement of temperature at different points within the bath and in the walls of the equilibrium cell allows one to detect temperature gradients.
- The occurrence of local hot or cold spots should be avoided. These local hot or cold spots can occur when energy is exchanged directly from a heater or cooler to the equilibrium cell. The use of stirrers in liquid baths and deflection shields in air or nitrogen baths can help in the prevention of these local spots.
- Conductive paths to and from the equilibrium cell, such as fittings, attachments or sampling devices must be avoided. This problem can be overcome by placing the fittings and attachments within the temperature regulated bath in addition to the equilibrium cell.
- Insulation should be used in-between the inner and outer lining of baths to minimize heat exchange with the surrounding environment. Fibrefrax Duraback and polyurethane foam are typically used for this purpose.
- A large thermal capacity assists to smooth temperature fluctuations.

2.2.3 Agitation of Cell Contents

An internal stirring mechanism is usually added to the equilibrium cell to promote the establishment of equilibrium in a shorter time. Literature reports various methods available for the agitation of the equilibrium cell contents. The most common method employed makes use of internal magnetic stirrers. Kalra and Robinson (1975) made use of a Teflon-coated magnetic stirrer in the equilibrium cell that was driven by a magnetic pile externally mounted to the equilibrium cell. The magnetic pile was made-up of three magnets encased in an aluminum housing and mounted on a variable speed DC motor. Kalra and Robinson (1975) reported that equilibrium between the phases was achieved in 0.5 – 2 hours which was dependant on the conditions and the mixture being studied. Ng and Robinson (1978), Nakayama et al. (1987) and Galicia-Luna et al. (2000) also used similar agitation methods.

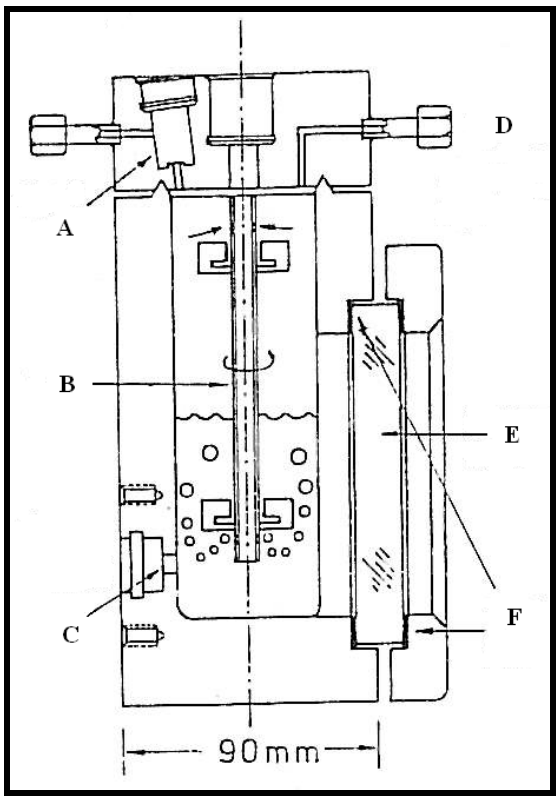

Figure 2-3: Equilibrium cell and agitator of Bae et al. (1981).
A: charge valve; B: agitator; C: liquid withdrawal position; D: fitting to pressure measurement system; E: glass window; F: Teflon packing.

Figuiere et al. (1980), Legret et al. (1981), Guillevic et al. (1983) and Konrad et al. (1983) also made use of an internal stirrer to aid the mixing of phases. However in this case the magnetic stirrers were rotated in an orientable magnetic field that was induced by coils located outside the equilibrium cell. Legret et al. (1981) reported a pressure equilibration time of 10 minutes. On

the other hand, Secuianu et al. (2003) made use of a variable speed stirrer with impellers mounted into the equilibrium cell.

Interestingly, Bae et al. (1981) made use of a unique magnetically driven internally vaned impeller mounted on a hollow shaft to achieve mixing of the equilibrium cell phases. Vapour entered the small holes on the upper part of the shaft then descended down the hollow shaft and finally dispersed into the underlying liquid phase (see Figure 2-3). On the other hand, Huang et al. (1985) made use of another unconventional technique to mix the cell contents by external oscillating movement of the equilibrium cell assembly (see Figure 2-4).

Other researchers such as Gómez-Nieto and Thodos (1978) made use of a piston device to assist in the mixing of the phases. A magnetic agitator was actuated by an electromagnetic field which was generated externally near the top of the equilibrium cell. The magnetic agitator consisted of a thin hollow iron cylinder that was forced to rise into the vapour phase and then fall into the liquid phase once every 30 s controlled by the magnetic field. Measurements first required at least 8 hours to reach thermal equilibrium with an air-bath and once agitation was achieved, the system was then allowed up to 2 hours to ensure that the system pressure achieved equilibrium. Ashcroft et al. (1983) achieved agitation by mechanically rocking the equilibrium cell for approximately 3 hours. Their design consisted of swivel joints for oil and mercury lines leading to the equilibrium cell to enable continuous rotation (see Figure 2-5).

Outcalt and Lee (2004) made use of a vapour circulation pump to bubble the vapour through the liquid phase in order to achieve mixing (see Figure 2-2). The piston of the pump was a magnet that was controlled by pulsing power to a solenoid that was wound around the outside of the pump shaft.

Takagi et al. (2003) used an acoustic interferometer that achieves mixing by means of ultrasonic speed for bubble point pressure measurements (see Figure 2-6). A "sing-around" technique operated at 2 MHz was employed to create the ultrasonic speed.

Conclusively, whatever the method used, it is important to achieve homogeneity inside the cell.

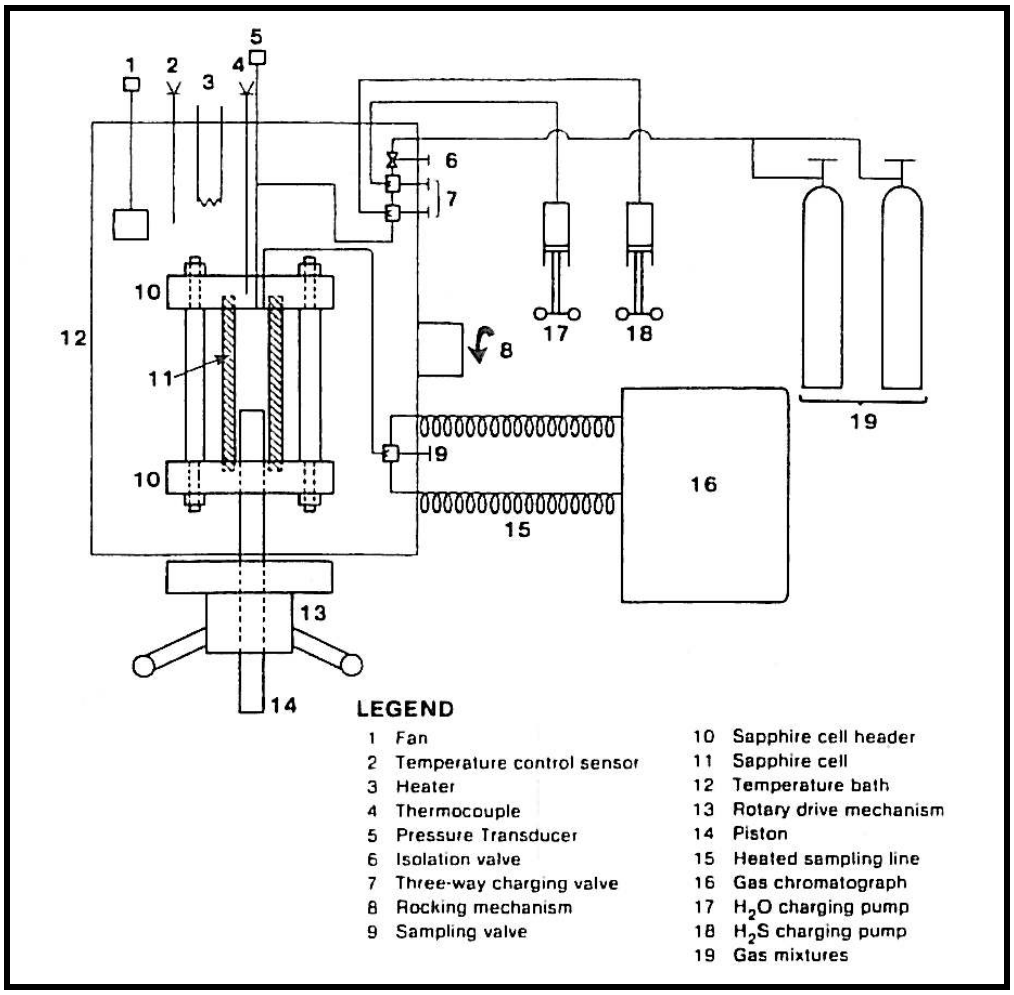

Figure 2-4: Schematic illustration of the equilibrium cell and auxillary equipment of Huang et al. (1985).

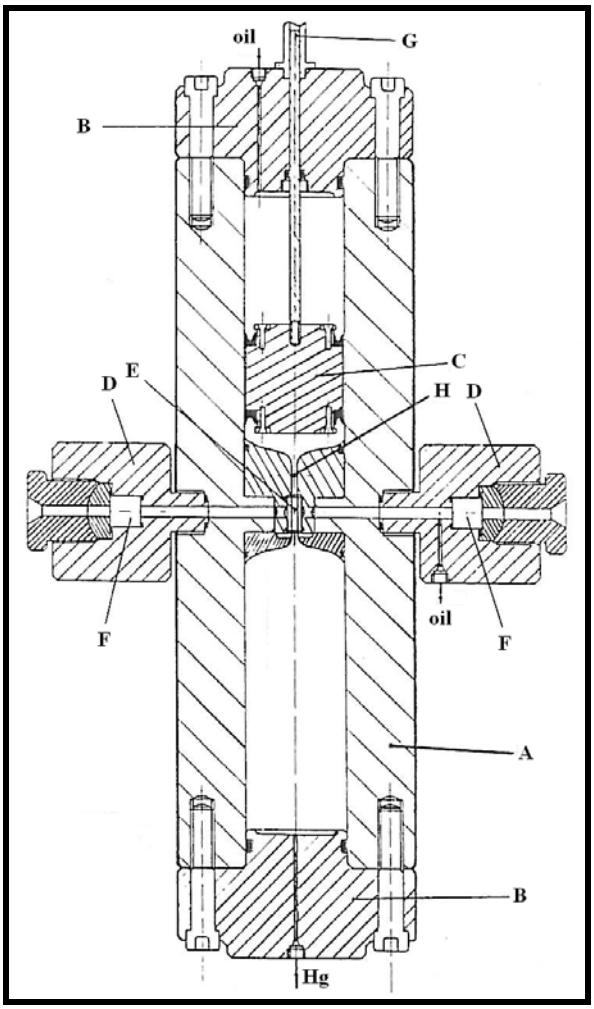

Figure 2-5: Equilibrium cell of Ashcroft et al. (1983).

A: cell body; B: end caps; C: piston; D: window assemblies; E: glass capillary; F: toughened glass windows; G: piston indicating rod; H: sampling valve.

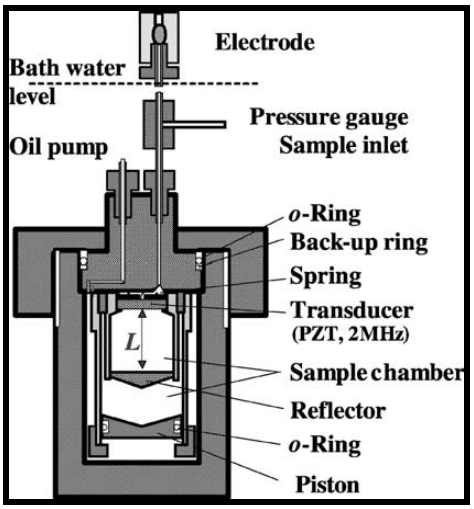

Figure 2-6: Schematic of the acoustic interferometer used for bubble point pressure measurements by Takagi et al. (2003).

2.3 Sampling Techniques

The limit of analytical methods is the technique of analysis itself, which controls the precision that will result for the compositions of the equilibrium phases measured. The sampling technique used has a direct influence on the quality of the results obtained.

Some of the various options available for analyses in relation to analytic methods include:

- Physiochemical methods of analysis, e.g., spectroscopy (Kaiser et al., 1992 and da Cruz Francisco et al., 2004), photometry (Andersen et al., 2001), absorption and fluorescence phenomena (Aizawa et al., 2004), small angle x-ray scattering (Shieh, et al., 2004) and refractive indices. These are some of the methods available for in-situ composition analysis (no sampling required).
- External analyses, where a sampling device for both the liquid and vapour phases is required. The withdrawn samples may be analysed by gas chromatography, mass spectrometry or by titration methods, etc.

The differences in the various methods usually results from the manner in which the samples are taken and how the samples are analysed. It is essential that the sampling procedure does not perturb the equilibrium and that the sample is representative of the studied coexisting phases.

When samples are withdrawn from an equilibrium cell, a change in the volume of the equilibrium cell is experienced. This consequently results in a change of the cell pressure. There are two contributing factors associated with the volume change by sample withdrawal:

1. The size of the withdrawn sample, which is determined by the analytical device employed. Generally, the smaller the size of the sample withdrawn, the smaller the pressure drop.
2. The interior cell volume. The bigger the cell volume, the smaller the pressure drop for a constant sample size.

Hence, an excellent sampling device is one that withdraws the smallest sample volume possible with respect to the interior cell volume. If a mobile sampling device is used, one has to consider the volume displaced by the movement of the sampling device, especially for a small interior cell volume, as this would affect the pressure drop. Furthermore, the sampling device should have the smallest dead volume. Dead volume can cause the thermodynamic condition of the sampled mixture to differ from the thermodynamic equilibrium condition in the cell. This consequently would lead to incorrect determination of phase compositions. To meet these

objectives, and maintain minimal disturbances to equilibrium, several procedures in literature have been proposed. Naidoo (2004) provides a good summary of these procedures:

- Researchers such as Klink et al. (1975) and Mühlbauer (1990) used a large equilibrium cell to dampen the effects of both the withdrawn sample volume and the volume changes associated with the sampling method employed. However, a large equilibrium cell requires an increased consumption of chemicals.
- Figuiere et al. (1980), Danesh and Todd (1990) and Lauret et al. (1994) made use of fast-acting pneumatic or electromagnetic valves, which helped minimize the withdrawn volume of the sample. In addition, measurements were made more rapidly since there was no rotation valve. However, the volumes of the samples taken are not constant, since friction is not completely reproducible. Figure 2-7 shows the equilibrium cell and sampling system of Figuiere et al. (1980).

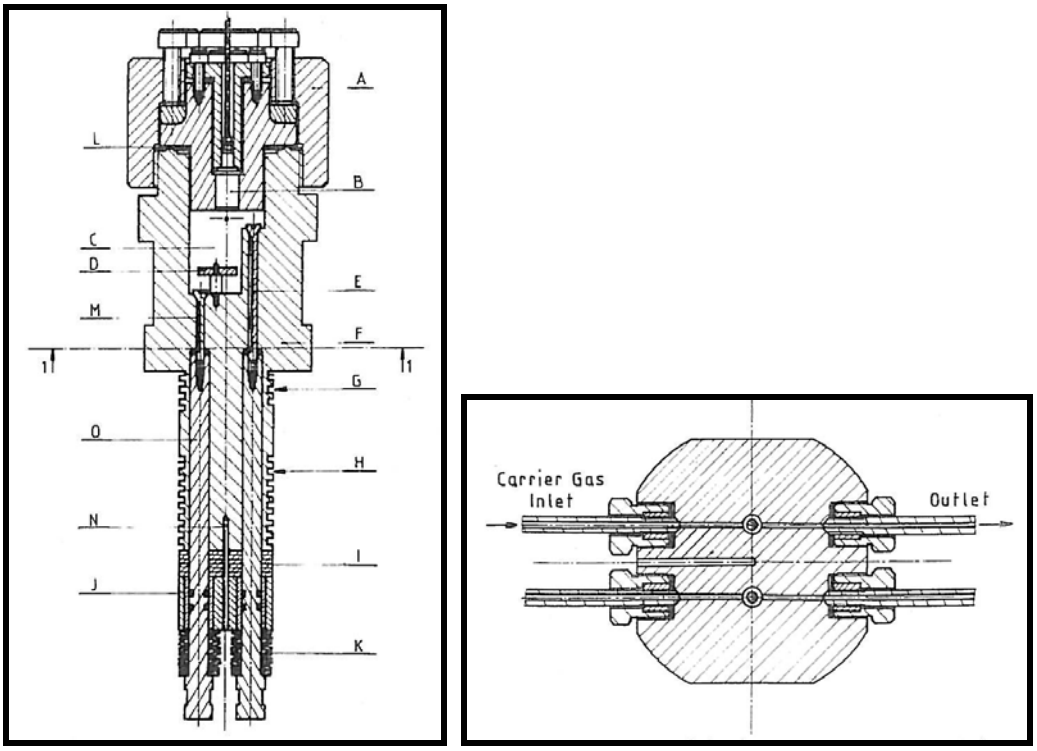

(a) **(b)**

Figure 2-7: (a) Equilibrium cell assembly of Figuiere et al. (1980); (b) carrier gas circulation through the cell to sweep samples (cross section 1-1).

A: cell cap; B: pressure transducer; C: equilibrium compartment; D: magnetic stirrer; E: valve; F: cell body; G: heating resistance place; H: cooling coil space; I: Teflon thermal shield; J: Viton O-ring; K: spring washers; L: copper gasket; M: channel; N: thermocouple well; O: valve pusher.

- Nasir et al. (1981) and Staby and Mollerup (1991) made use of a variable-volume equilibrium cell to compensate for pressure changes.
- Legret et al. (1981) made use of a detachable sampling device or microcell (see Figures 2-8 and 2-9). This helped avoid changes in pressure by taking the sample very close to the equilibrium cell, with practically no dead volume.

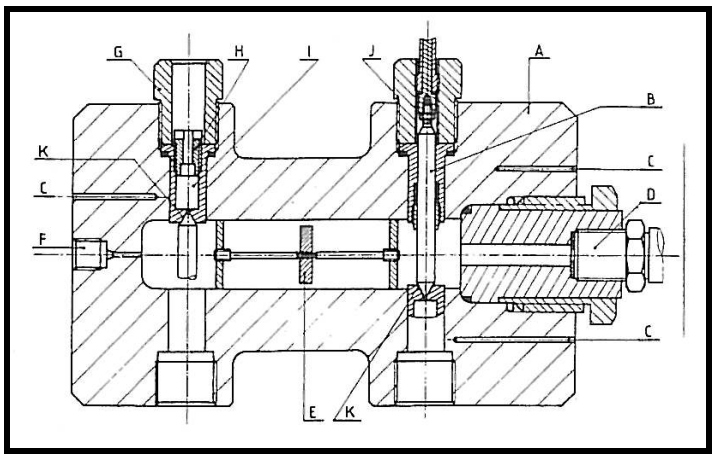

Figure 2-8: Equilibrium cell of Legret et al. (1981).

A: cell body; B: sampling valve with packing joint; C: thermocouple well; D: pressure transducer; E: magnetic stirrer; F: connection to filling circuit; G: microcell bearer fixing-pin; H: microcell set-screw; I: microcell; J: valve fixing pin; K: seat of sampling valve stem.

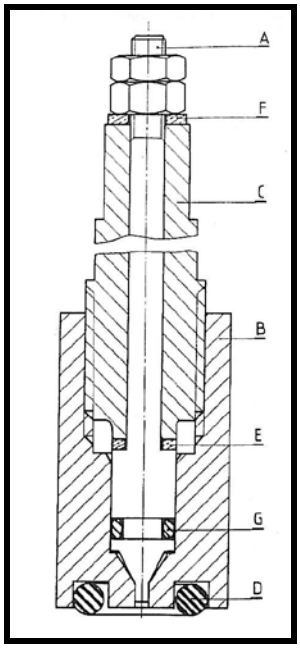

Figure 2-9: Sampling microcell of Legret et al. (1981).

A: stem; B: microcell body; C: driving screw; D,G: joints; E,F: antifriction rings.

- Rogers and Prausnitz (1970) designed an equilibrium cell with pistons moving inside the equilibrium cell (see Figure 2-10). This system is theoretically good as the sample is taken well inside the equilibrium phase and is extracted without a change of pressure. However, it is practically difficult to achieve the necessary tightness of the piston and hence, the rapid wear of the seals makes this technique unreliable.

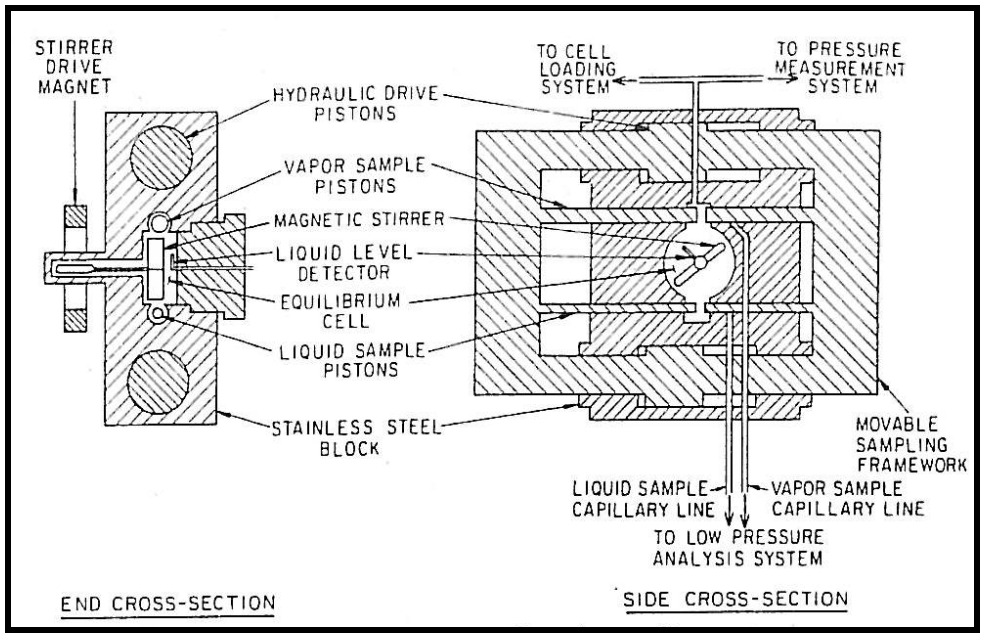

Figure 2-10: Equilibrium cell and sampling system of Rogers and Prausnitz (1970).

- Wagner and Wichterle (1987) and Matos et al. (1989) used capillaries to withdraw small samples. However, according to Brunner et al. (1994), sampling through capillaries can lead to differential vapourisation and scattered result, caused by a pressure drop along the capillary. This effect is more pronounced for mixtures of light and heavy hydrocarbons.
- Ramjugernath (2000) used a novel sampling technique with a six-port gas chromatograph valve (Raal and Mühlbauer, 1998). This technique avoided volume changes by the analytic device as the equilibrium sample was continuously circulated (by impeller induced flow) through the port's loops. Since the sample loop was isolated, there was no change in interior conditions despite the sample withdrawal.
- Galicia-Luna et al. (2000) made use of a compressed air-monitored sampler injector which consisted of a movable capillary adjusted by a differential screw. Samples less than 1 mg were withdrawn. The injector contained an expansion

chamber which was heated by a heating resistance in order to rapidly vapourise liquid samples for good chromatographic analyses.

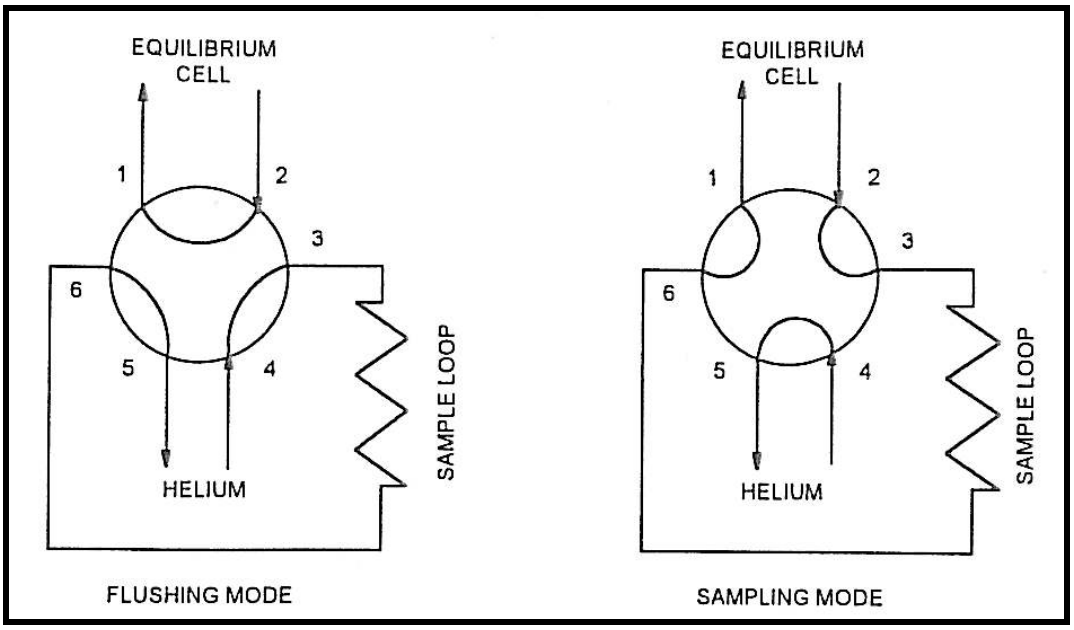

Figure 2-11: Sampling configuration of the six-port gas chromatograph valve used by Ramjugernath (2000) (Raal and Mühlbauer, 1998).

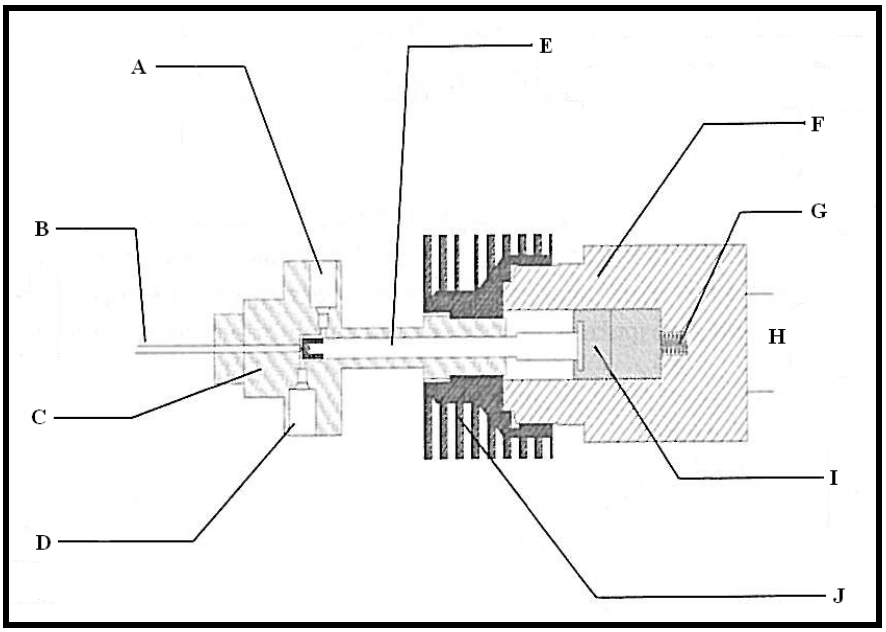

Figure 2-12: Electromagnetic version of the ROLSI™ (ROLSI™ Evolution IV). A: carrier gas inlet; B: capillary; C: body; D: carrier gas outlet; E: moving part set in motion by the electromagnet; F: electromagnet; G: return spring; H: power supply coupled with a timer; I: soft iron core; J: cooling fins.

- Baba-Ahmed et al. (1999) and Guilbot et al. (2000) made use of a Rapid-On-Line-Sample-Injector (ROLSI™). The ROLSI™ allows for measurements up to 1000 bar and 850 K, for corrosive chemicals and samples from 1μg to a few mg (Richon, 2003). The sampler used by Galicia-Luna et al. (2000) is a pneumatic sampler of the ROLSI™. Of recent an electromagnetic version of the ROLSI™ has been developed (ROLSI™ Evolution IV). The electromagnetic version of the ROLSI™ is shown in Figure 2-12. Sampling with the electromagnetic version is achieved by prompting the electromagnet which attracts the moving part and generates a break in the seal between the fixed capillary and the moving part. The size of the samples withdrawn, under given pressure and temperature conditions, is directly proportional to the seal-breaking time. This time can be controlled by means of a timer coupled with the electromagnet's power supply.

2.4 Degassing of Components

Degassing is the removal of highly volatile components (or dissolved gases) from a relatively non-volatile liquid. According to Aim (1978), degassing is crucial as the presence of residual gases dissolved in the investigated solution may lead to large errors in pressure determination. Hence, degassing cannot be ignored as its omission may result in measured pressures that will not correspond to the expected mixture. This is evident especially at low pressures and low volatile component concentrations, as the dissolved gases may compete with the more volatile component in the liquid phase.

Degassing can be achieved either in-situ or external to the equilibrium cell. Literature indicates many procedures for degassing liquids, such as sl iquid refluxing with periodic vapour withdrawal, alternate freezing and pumping to high vacuum, vacuum sublimation and vacuum distillation. Of all these methods, Van Ness and Abbott (1978) found that vacuum distillation is least tedious and requires the least amount of time. According to Van Ness and Abbott (1978), when a flask containing a certain thoroughly degassed liquid is rapidly inverted, a sharp metallic *click* is heard. Van Ness and Abbott (1978) presume this results from a sudden collapse of trapped vapour under the liquid head. However, Van Ness and Abbott (1978) also mention that a positive result from a *click test* is evidently sufficient but not necessary evidence of thorough degassing. Fischer and Gmehling (1994) used the vacuum distillation method of Van Ness and Abbott (1978) but found that without further separation, less volatile impurities are enriched in the degassed liquid in the reboiler. Fischer and Gmehling (1994) therefore developed a modified

vacuum distillation degassing unit that allowed chemical reactions to be carried out before degassing and the desired compound to be separated by further distillation after degassing.

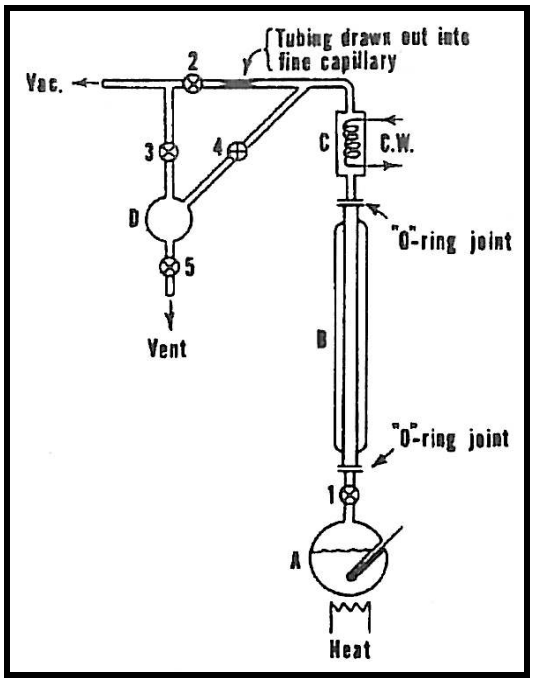

Figure 2-13: Schematic of the degassing apparatus of Van Ness and Abbott (1978). A: still pot; B: rectifying column; C: condenser; D: surge vessel.

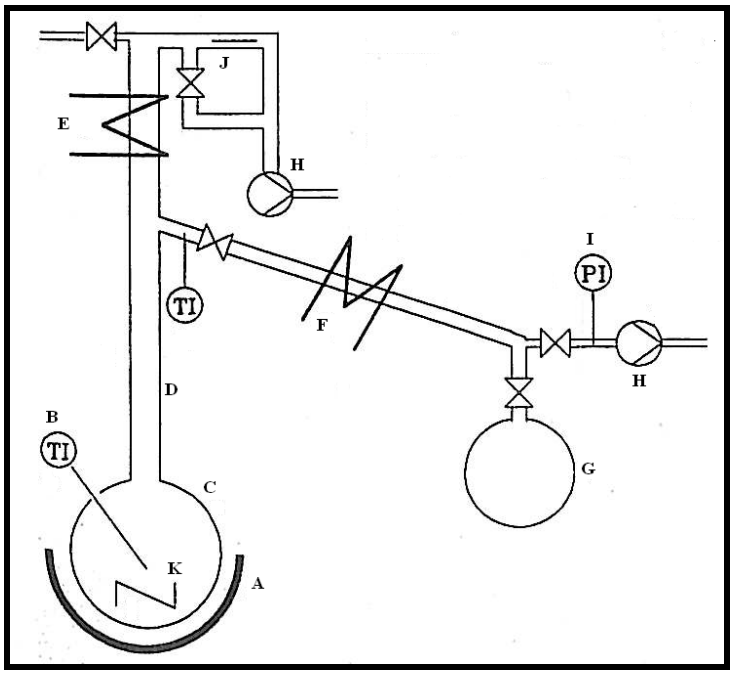

Figure 2-14: Purification and degassing apparatus of Fischer and Gmehling (1994). A: heater; B: thermometer; C: bulb; D: Vigreux column; E: reflux condenser; F: Liebig condenser; G: bulb for pure and degassed product; H: vacuum pump; I: vacuum indicator; J: capillary; K: stirrer.

Il y a différents types d'équilibres de phases, toutefois les trois les plus courants sont: les équilibres ″liquide-vapeur″ (ELV), équilibres ″liquide-liquide″ (ELL) et équilibres ″liquide-vapeur-liquide″ (ELLV). L'équilibre de phases thermodynamique implique que la température, la pression, le potentiel chimique (fugacité) de chaque constituant sont identiques dans chaque phase. La fugacité de mélange contient un coefficient qui exprime la non-idéalité dans le mélange. Dans le cas des équilibres ″liquide-vapeur″, le coefficient de fugacité peut être employé pour décrire la non-idéalité des phases liquide et vapeur. La fugacité de mélange en phase liquide pourrait également être décrite par un coefficient d'activité qui lui aussi tient compte de la non- idéalité en phase liquide.

Les calculs des équilibres de phase font appel à l'utilisation de modèles thermodynamiques. Les deux méthodes les plus utilisées pour la régression des données d'équilibres ″liquide-vapeur″ (ELV) sont les méthodes directes et combinées. La méthode directe se sert d'une même équation d'état (EdE), parmi bon nombre d' équations cubiques, pour calculer les coefficients de fugacité pour chacune des phases, phase liquide et phase vapeur. De telles équations incluent l'EdE de Soave-Redlich-Kwong et l'EdE de Peng-Robinson. Ces équations peuvent s 'appliquer à des composés polaires et non polaires et offrir des résultats satisfaisants. La méthode directe exige l'emploi d'une règle de mélange afin de représenter au mieux les propriétés de mélange. La règle de mélange la plus utilisée est celle de Wong et Sandler (1992).

En ce qui concerne la méthode combinée, on fait appel à deux modèles pour une représentation séparée des phases liquide et vapeur. Une EdE est employée pour représenter la non-idéalité en phase vapeur tandis qu' un modèle de solution liquide (utilisation du coefficient d' activité) est employé pour représenter le non-idéalité en phase liquide. Souvent dans la méthode combinée on fait appel à l'EdE du viriel (avec des corrélations pour calculer les coefficients du viriel) pour tenir compte de la non-idéalité en phase vapeur. Les modèles de solutions liquides avec des expressions pour les coefficients d'activité de phase incluent : le modèle de Tsuboka-Katayama-Wilson (TK-Wilson), Le modèle ″Non-Random Two Liquids″ (NRTL) et le modèle ″Universal Quasi-Chemical″ (UNIQUAC). Ces modèles sont basés sur la théorie de composition locale et offrent des résultats satisfaisants pour des travaux de VLE et de LLE régression de données ELV et ELL de systèmes fortement non-idéaux.

Quand toutes les températures, pressions et compositions dans chacune de s phases ont été déterminées expérimentalement pour un équilibre de phase, ces données peuvent et doivent être examinées pour s 'assurer de leur cohérence thermodynamique. La méthode du test par « point »

exige que la déviation moyenne absolue ne dépasse pas 0.01 pour la fraction molaire en phase vapeur et que la dispersion (erreurs sur la fraction molaire en phase vapeur (Δy_1) en fonction de la fraction molaire en vapeur (y_1)) soit centrée sur zéro. Le test appelé « direct » se sert de l'équation de Gibbs-Duhem d'une part et des résidus sur les coefficients d'activité des composants binaires. Cet essai exige que les résidus des rapports des coefficients d'activité soient dispersés de manière équilibrée autour de zéro dans un graphique en fonction de la fraction molaire en phase liquid (x_1). Ce test fait appel également comme critère quantitatif de l'index d'uniformité élaboré par Van Ness (1995).

3

CHAPTER THREE

THERMODYNAMIC FUNDAMENTALS AND PRINCIPLES

Thermodynamic data on chemical compounds and their mixtures play an important role for phase separation processes in chemical industries as they are needed for efficient design and operation of chemical processing plants. Phase equilibrium is of special interest in chemical engineering as this type of data forms the basis for the design and optimization of separation processes such as distillation and extraction, which involve phase contacting. The separation of mixtures by phase contacting operations is made possible since the equilibrium compositions of two phases are usually very different from one another (Prausnitz et al., 1999).

In chemical industries, separation processes generally occur for multi-component systems. Hence in order to design and optimize such separation processes one requires the information of multi-component phase equilibrium properties. However, obtaining multi-component phase equilibrium properties by measurements is generally difficult and commonly impractical. Raal and Mühlbauer (1998) mention that multi-component phase equilibrium properties can be predicted from the measurement of binary phase equilibrium data, which include vapour-liquid equilibrium (VLE) and liquid-liquid equilibrium (LLE). This involves the theoretical treatment of binary phase equilibrium data to calculate such variables as temperature, pressure and Gibbs excess energy and also to enable extrapolation and interpolation to experimentally difficult conditions. The use of chemical thermodynamics enables one to perform such tasks.

This chapter attempts to provide a review of the thermodynamic fundamentals and principles required to undertake theoretical treatment of phase equilibrium data obtained from measurements. This involves a discussion on the evaluation of the fugacity and activity coefficients together with the analysis, regression and correlation of the experimental data. The two most well known methods of VLE data regression viz. the $\gamma - \Phi$ (combined) method and $\Phi - \Phi$ (direct) method are also

examined along with the associated activity coefficient models and equations of state. The chapter finally discusses some thermodynamic consistency tests carried out on the experimental VLE data. Walas (1985) and Raal and Mühlbauer (1998) offer a more detailed discussion on thermodynamic fundamentals and the reader is referred to such texts for further information.

3.1 Fugacity and Fugacity Coefficients

Smith et al. (2001) state that equilibrium is a static condition where no changes occur in the macroscopic properties of the system with time and that in engineering practice, the assumption of equilibrium is considered justified when it leads to results of satisfactory accuracy. The criterion for phase equilibrium is outlined in Appendix A, where the chemical potential (μ_i) serves as the fundamental criterion for phase equilibrium. However, chemical potential is defined in relation to quantities that are immeasurable where absolute values are unknown. This therefore implies that the chemical potential has no absolute values. G. N. Lewis introduced a quantity known as fugacity (f_i), with units of pressure, which could be related to chemical potential:

$$\overline{G_i} = \Gamma_i(T) + RT \ln f_i \tag{3-1}$$

where $\Gamma_i(T)$ is the integration constant at temperature T (Smith et al., 2001).

The partial molar Gibbs energy is defined as:

$$\overline{G_i} = \left[\frac{\partial(nG)}{\partial n_i}\right]_{T,P,n_j} \tag{3-2}$$

Using Equation (A-6) for the definition of chemical potential implies:

$$\mu_i = \overline{G_i} \tag{3-3}$$

Now comparison of Equations (3-1) and (3-3) shows the following relation of chemical potential and fugacity:

$$\mu_i = \Gamma_i(T) + RT \ln f_i \tag{3-4}$$

Substitution of Equation (3-4) into Equation (A-14) for a closed system at equilibrium with all phases present at the same temperature results in:

$$f_i^{\alpha} = f_i^{\beta} = ... = f_i^{\pi} \tag{3-5}$$

for $i = 1, 2, \ldots, N$.

The following equation holds for an ideal gas:

$$G_i^{ig} = \Gamma_i(T) + RT \ln P \tag{3-6}$$

with $\Gamma_i(T)$ being the same integration constant as in Equation (3-1) at temperature T. The theory of fugacity for a real fluid is given by:

$$G_i = \Gamma_i(T) + RT \ln f_i \tag{3-7}$$

Subtracting Equation (3-6) from Equation (3-7) at constant temperature and pressure:

$$G_i - G_i^{ig} = RT \ln \frac{f_i}{P} \tag{3-8}$$

The left-hand side of Equation (3-8) is defined as the residual Gibbs energy (G^R) and the ratio f_i / P is termed the fugacity coefficient of component i, symbolized as ϕ_i. Equations (3-6) to (3-8) are only applicable to pure species. An equation similar to Equation (3-4) can also be written for a species in solution:

$$\mu_i = \Gamma_i(T) + RT \ln \hat{f}_i \tag{3-9}$$

where $\hat{f}_i$ is the fugacity of species i in solution. Similar to Equation (3-5):

$$\hat{f}_i^{\alpha} = \hat{f}_i^{\beta} = ... = \hat{f}_i^{\pi} \tag{3-10}$$

where α, β and π denote phases. In terms of VLE, Equation (3-10) becomes:

$$\hat{f}_i^v = \hat{f}_i^l \tag{3-11}$$

where i = 1, 2, …, N and v and l denote vapour and liquid phases respectively. The relation of the vapour and liquid fugacities to measurable quantities such as temperature, pressure and composition is achieved by extending the definition of the fugacity coefficient to include the fugacity coefficient of species i in solution ($\hat{\phi}_i$) and another dimensionless variable, γ_i, known as the activity coefficient of species i in solution. The activity coefficient is discussed in Section 3.2. For binary VLE, the relation is described by Equations (3-12) and (3-13):

$$\hat{f}_i^v = y_i \hat{\phi}_i P \tag{3-12}$$

$$\hat{f}_i^l = x_i \gamma_i f_i \tag{3-13}$$

where x_i and y_i are the liquid and vapour compositions respectively of species i. If one considers a phase change of a pure fluid from a saturated liquid to a saturated vapour at saturated pressure and temperature, the following relation can be found as a result of Equation (3-5):

$$f_i^v = f_i^l = f_i^{sat} \tag{3-14}$$

where f_i^{sat} is the saturated fugacity of species i. The saturated fugacity coefficient of pure fluid species i (ϕ_i^{sat}) at saturated pressure is:

$$\phi_i^{sat} = \frac{f_i^{sat}}{P_i^{sat}} \tag{3-15}$$

This therefore leads to:

$$\phi_i^v = \phi_i^l = \phi_i^{sat} \tag{3-16}$$

When Equation (3-7) is differentiated, one obtains:

$$dG_i = RTd \ln f_i \tag{3-17}$$

Using the property relation for Gibbs energy, $dG = VdP - SdT$, for a species i in solution at constant composition and temperature yields:

$$dG_i = V_i dP \tag{3-18}$$

Equations (3-17) and (3-18) are then used to eliminate dG_i:

$$d \ln f_i = \frac{V_i}{RT} dP \tag{3-19}$$

Integrating Equation (3-19) from the initial state of saturated liquid to a final state of compressed liquid at constant pressure (P), results in:

$$\ln \frac{f_i}{f_i^{sat}} = \frac{1}{RT} \int_{P_i^{sat}}^{P} V_i dP \tag{3-20}$$

where V_i is the liquid molar volume of species i which is considered a weak function of pressure for temperatures much lower than the critical temperature (T_c). Therefore, V_i can be assumed approximately constant at the saturated liquid molar volume (V_i^l). Evaluation of the integral in Equation (3-20) yields:

$$\ln \frac{f_i}{f_i^{sat}} = \frac{V_i^l \left(P - P_i^{sat}\right)}{RT} \tag{3-21}$$

Using Equation (3-15) to eliminate f_i^{sat}, results in:

$$f_i = \phi_i^{sat} P_i^{sat} \exp\left[\frac{V_i^l \left(P - P_i^{sat}\right)}{RT}\right] \tag{3-22}$$

The exponential term in Equation (3-22) is known as the Poynting correction factor. This factor provides the correction for the liquid phase fugacity from the vapour pressure of species *i* to the system pressure. The combination of Equations (3-12), (3-13) and (3-22) results in:

$$y_i \Phi_i P = x_i \gamma_i P_i^{sat} \tag{3-23}$$

where

$$\Phi_i = \frac{\hat{\phi}_i}{\phi_i^{sat}} \exp\left[\frac{-V_i^l \left(P - P_i^{sat}\right)}{RT}\right] \tag{3-24}$$

The equation proposed by Rackett (1970) can be used to evaluate the saturated liquid molar volume (V_i^l):

$$V_i^l = \left(V_c\right)_i \left(Z_c\right)_i^{\left(1-\left(T_r\right)_i\right)^{0.2857}} \tag{3-25}$$

where Z is the compressibility factor, subscript c indicates the critical point and $\left(T_r\right)_i$ is the reduced temperature defined as $T / \left(T_c\right)_i$.

Equation (3-23) provides a useful relation for the vapour and liquid phases at equilibrium. In the case of an ideal system, the vapour phase is represented by an ideal gas and the liquid phase by an ideal solution. The ideal system is the simplest possible relation for VLE and is commonly known as Raoult's Law (Smith et al., 2001). Equation (3-24) reduces to Raoult's Law when Φ_i and γ_i are both set to a value of one. Smith et al. (2001) mention that the Poynting factor differs from unit by only a few parts per thousand at low to moderate pressures and therefore its omission introduces negligible error. This assumption is reasonable for non-polar components at low pressures but the error becomes significant for mixtures that contain polar or associating components (Prausnitz et al., 1980).

3.1.1 Fugacity Coefficients from the Virial Equation of State

The determination of the fugacity coefficient of a species in solution is made possible by a number of methods available. One such method that has its theoretical basis in statistical mechanics is known as the virial equation of state which is represented by the Taylor series expansion. The virial equation of state can be used at low to moderate pressures to evaluate the fugacity coefficients in order to adequately describe the non-ideality of the vapour phase in VLE. However, the Taylor series expansion is an infinite series and thus cannot be applied to practical calculations. Hence, a truncated form of the virial equation is usually employed where the degree of truncation is controlled by the temperature and pressure. According to Perry and Green (1998), the pressure explicit form of the virial equation of state truncated to the second term is suitable for describing the vapour phase at sub-critical temperatures and pressures up to 15 bar:

$$Z = 1 + \frac{B_{virial} P}{RT} \tag{3-26}$$

where Z is the compressibility factor and is defined as PV/RT. For an ideal gas the compressibility factor equals unity. The nomenclature B_{virial} is known as the second virial coefficient and is a function of temperature and composition (for mixtures). For a mixture, the composition dependence for the second virial coefficient is based on statistical mechanics:

$$B_{mixture} = \sum_i \sum_j y_i y_j B_{ij} \tag{3-27}$$

where y is the vapour mole fraction of a mixture and the subscripts i and j identify the species. B_{ij} is known as the cross virial coefficient that represents both pure and component mixture coefficients and typifies a bimolecular interaction between species i and j with $B_{ij} = B_{ji}$. When the virial equation of state, truncated to the second term for a binary system, is used to describe the vapour phase, the fugacity coefficient (Φ_i) of Equation (3-24) becomes:

$$\Phi_i = \exp\left[\frac{\left(B_{ii} - V_i^l\right)\left(P - P_i^{sat}\right) + 0.5\sum_j \sum_k P y_j y_k \left(2\delta_{ji} - \delta_{jk}\right)}{RT}\right] \tag{3-28}$$

where

$$\delta_{ij} = 2B_{ij} - B_{ii} - B_{jj} \quad and \quad \delta_{jk} = 2B_{jk} - B_{jj} - B_{kk} \tag{3-29}$$

The pure component second virial coefficients (B_{ii}, B_{kk} and B_{jj}) and that for the mixtures (B_{ij}) can be experimentally determined by various techniques. Ramjugernath (2000) discusses one such technique that involves the calculation of volume in a high pressure VLE cell. Dymond and Smith (1980) and Cholinski et al. (1986) have compiled a list of experimental second and third virial coefficients for various gases and some mixtures at specified temperatures. Since the second virial coefficient is dependent on temperature, it is rather difficult to obtain experimental values of the second virial coefficient at desired temperatures. Hence, correlations were developed to enable calculation of the second virial coefficient for both pure components and their mixtures. According to Hayden and O'Connell (1975), the second virial coefficients can be related to the equilibrium constant in a simple way and therefore if a correlation for the second virial coefficient can yield accurate values for substances which associate very strongly (e.g. carboxylic acids), it can be used for all systems.

The correlation proposed by Tsonopoulos (1974) is one of the most widely used correlations for evaluating the second virial coefficients for both pure components and mixtures of non-polar and polar systems. The correlation of Tsonopoulos (1974) also accounts for species (such as water and alcohols) that exhibit hydrogen bonding. For non-polar gases, Tsonopoulos (1974) proposed that:

$$\frac{B_{virial}P_c}{RT_c} = f^{(0)}(T_r) + \omega f^{(1)}(T_r) \tag{3-30}$$

where

$$f^{(0)}(T_r) = 0.1445 - \frac{0.330}{T_r} - \frac{0.1385}{T_r^2} - \frac{0.0121}{T_r^3} - \frac{0.000607}{T_r^8} \tag{3-31}$$

and

$$f^{(1)}(T_r) = 0.0637 + \frac{0.331}{T_r^2} - \frac{0.423}{T_r^3} - \frac{0.008}{T_r^8} \tag{3-32}$$

Polar components however contain a non-zero dipole moment that expresses the effect of electrostatic forces between molecules. Tsonopoulos (1974) therefore proposed an additional parameter in Equation (3-30):

$$\frac{B_{virial}P_c}{RT_c} = f^{(0)}(T_r) + \omega f^{(1)}(T_r) + f^{(2)}(T_r) \tag{3-33}$$

where

$$f^{(2)}(T_r) = \frac{a_t}{T_r^6} \tag{3-34}$$

In the case of components that exhibit hydrogen bonding, the effect of dimerization makes the temperature dependence of the polar effect more complex for the second virial coefficient. Tsonopoulos (1974) therefore proposed a second additional parameter to account for this effect:

$$f^{(2)}(T_r) = \frac{a_t}{T_r^6} + \frac{b_t}{T_r^8} \tag{3-35}$$

The parameters a_t and b_t are functions of the dipole moment and are determined by regression of experimental B_{virial} data for similar compounds. The second virial cross coefficients can be determined using Equations (3-33) to (3-35) but with the following parameters: $(T_c)_{ij}$, $(P_c)_{ij}$, ω_{ij}, $(a_t)_{ij}$ and $(b_t)_{ij}$. The mixing rules as suggested by Tsonopoulos (1974) are used to determine these parameters:

$$(T_c)_{ij} = \sqrt{(T_c)_i (T_c)_j}\left(1 - k_{ij}\right) \tag{3-36}$$

$$(P_c)_{ij} = \frac{4(T_c)_{ij}\left(\left[\frac{(P_c)_i (V_c)_i}{(T_c)_i}\right] + \left[\frac{(P_c)_j (V_c)_j}{(T_c)_j}\right]\right)}{\left((V_c)_i^{1/3} + (V_c)_j^{1/3}\right)^3} \tag{3-37}$$

and

$$\omega_{ij} = \frac{\omega_i + \omega_j}{2} \tag{3-38}$$

The parameter k_{ij} in Equation (3-36) is an empirical binary interaction parameter which is set to a value of zero when species *i* and *j* are very similar in size and chemical nature. When species *i* and *j* are not similar in size or chemical nature, the guidelines of Tarakad and Danner (1977) are used to determine the value of k_{ij}. For polar/non-polar systems, it is assumed that B_{ij} has no polar term and hence $(a_t)_{ij}$ and $(b_t)_{ij}$ are both set to a value of zero. However for polar/polar systems, B_{ij} is found by assuming:

$$(a_t)_{ij} = \frac{(a_t)_i + (a_t)_j}{2} \tag{3-39}$$

$$(b_t)_{ij} = \frac{(b_t)_i + (b_t)_j}{2} \tag{3-40}$$

3.1.2 Fugacity Coefficients from a Cubic Equation of State

A cubic equation of state (EoS) is also commonly used to evaluate fugacity coefficients. The simplest cubic EoS that accounted for deviations from the ideal gas law and based on intermolecular forces was developed by Van der Waals (1873). In his work, Van der Waals (1873) aimed to develop a simple and generalized semi-empirical EoS that accounted for the behaviour of fluids both above and below the critical point. However the parameters in the equation developed by van der Waals (1873) were not temperature dependent and therefore the equation was limited in its application to describe highly non-ideal systems (Anderko, 1990). Numerous modifications were proposed to the van der Waals (1873) EoS but only the modifications developed by Redlich and Kwong (1949) and Soave (1972) were recognized as the most successful. Later Peng and Robinson (1976) also proposed a modification that was widely accepted. Only the equation of Soave (1972) and that of Peng and Robinson (1976) were used in this study and will therefore be further discussed.

3.1.2.1 The Soave-Redlich-Kwong (SRK) Cubic Equation of State

The cubic EoS of Redlich and Kwong (1949) was not able to offer a satisfactory representation of the liquid phase non-ideality. Hence the equation could not be used to perform accurate calculations for VLE. Soave (1972) therefore modified this equation and proposed that:

$$P = \frac{RT}{(V-b)} - \frac{a(T)}{V(V+b)} \tag{3-41}$$

The constant a is related to the intermolecular attraction force of molecules and is considered temperature dependent whilst the constant b accounts for the molecular size of the molecule and is temperature independent. They are determined from the following equations:

$$a_i(T) = a_i\{(T_c)_i\}\alpha_i\{(T_r)_i, \omega_i\} \tag{3-42}$$

$$b_i(T) = b_i(T_c)_i \tag{3-43}$$

where

$$a_i(T_c)_i = 0.42747\frac{R^2(T_c)_i^2}{(P_c)_i} \tag{3-44}$$

$$b_i(T_c)_i = 0.08664\frac{R(T_c)_i}{(P_c)_i} \tag{3-45}$$

$$\alpha_i\{(T_c)_i, \omega_i\} = \left[1 + \kappa_i\left(1 - (T_r)_i^{0.5}\right)\right]^2 \tag{3-46}$$

The parameter κ_i in Equation (3-46) is a constant characteristic of each component. Soave (1972) proposed a correlation of this constant with respect to the acentric factor:

$$\kappa_i = 0.480 + 1.574\omega - 0.176\omega^2 \tag{3-47}$$

In order to assist with computational calculations, Equation (3-41) can also be expressed in terms of the compressibility factor (Z) for a mixture:

$$Z^3 - Z^2 + \left(A_m - B_m - \{B_m\}^2\right) - A_m B_m = 0 \tag{3-48}$$

where

$$A_m = \frac{a_m(T)P}{R^2T^2} \tag{3-49}$$

$$B_m = \frac{b_m P}{RT} \tag{3-50}$$

where a_m and b_m from Equations (3-51) to (3-53) are obtained from mixing rules, which are discussed in Section 3.1.3. However, Soave (1972) employed the following mixing rules:

$$a_m = \sum_i \sum_j z_i z_j a_{ij} \tag{3-51}$$

$$b_m = \sum_i z_i b_i \tag{3-52}$$

where

$$a_{ij} = (1 - k_{ij})(a_i a_j)^{0.5} \tag{3-53}$$

The use of z in Equations (3-51), (3-52) and (3-54) can be used to represent the liquid mole fraction (x) or the vapour mole fraction (y). The parameter k_{ij} is known as the binary interaction parameter that is unique to each binary system and found from the regression of experimental VLE data. It should be noted that $k_{ij} = k_{ji}$.

In the case of a binary system, the largest real root of Equation (3-48) corresponds to the vapour phase compressibility factor whilst the smallest real root corresponds to that of the liquid phase compressibility factor. The fugacity coefficient of species i in a mixture for each phase is then found from:

$$\ln \hat{\phi}_i = \frac{b_i}{b_m}(Z-1) - \ln(Z - B_m) + \frac{A_m}{B_m}\left(\frac{b_i}{b_m} - 2\frac{\sum_{k=1}^{n} z_k a_{ki}}{a_m}\right)\ln\left(1 + \frac{B_m}{Z}\right) \tag{3-54}$$

Usually, more theoretically correct mixing rules such as those by Wong and Sandler (1992) and Twu and Coon (1996) are employed as they offer a greater degree of flexibility and accuracy. The mixing rule of Wong and Sandler (1992) is discussed further in Section 3.1.3.

The SRK EoS offers a better calculation of vapour pressures for several hydrocarbons and correlation of VLE behaviour for systems consisting of non-polar and slightly polar fluids when compared to the Redlich-Kwong EoS. Soave (1993) later modified the temperature dependence on the attraction term in the SRK EoS to incorporate both polar and non-polar fluids in order to improve vapour pressure calculations. However the calculation of liquid phase specific volume with the SRK EoS is considerably larger (as high as 27 %) than literature values (Peng and Robinson, 1976).

3.1.2.2 The Peng-Robinson (PR) Cubic Equation of State

According to Peng and Robinson (1976), there were still some shortcomings with the equation proposed by Redlich and Kwong (1949) and the modification by Soave (1972). One such shortcoming was concerned with the failure to predict satisfactory liquid density values. Peng and Robinson (1976) also aimed to improve the accuracy of the equation near the critical point. The proposed equation of Peng and Robinson (1976) is:

$$P = \frac{RT}{V-b} - \frac{a(T)}{V(V+b)+b(V-b)} \tag{3-55}$$

The constants a and b are the same as described for the SRK EoS except where Equations (3-44), (3-45) and (3-47) were modified as follows:

$$a_i(T_c)_i = 0.45724\frac{R^2(T_c)_i^2}{(P_c)_i} \tag{3-56}$$

$$b_i(T_c)_i = 0.07780\frac{R(T_c)_i}{(P_c)_i} \tag{3-57}$$

$$\kappa_i = 0.37464 + 1.54226\omega_i - 0.26992\omega_i^2 \tag{3-58}$$

The corresponding relation for Equation (3-55) in terms of the compressibility factor for a mixture is:

$$Z^3 - (1 - B_m)Z^2 + (A_m - 3B_m^2 - 2B_m)Z - (A_m B_m - B_m^2 - B_m^3) = 0 \qquad (3\text{-}59)$$

A_m, B_m, a_m, b_m and a_{ij} are the same for the Peng-Robinson (PR) EoS as described for the SRK EoS in Equations (3-49) to (3-53) respectively. Also, in similar manner the largest and smallest real roots of Equation (3-59) correspond to the vapour and liquid compressibility factor respectively. The expression for the fugacity coefficient of species *i* in a mixture becomes:

$$\ln \hat{\phi}_i = \frac{b_i}{b_m}(Z-1) - \ln(Z - B_m) - \frac{A_m}{2\sqrt{2}B_m}\left(\frac{2\sum_k z_k a_{ki}}{a_m} - \frac{b_i}{b_m}\right)\ln\left[\frac{Z + (1+\sqrt{2})B_m}{Z + (1-\sqrt{2})B_m}\right] \qquad (3\text{-}60)$$

The SRK and PR EoS are most widely used in industry since they require only critical properties and acentric parameters for the generalised parameters as input information, a short computation time and they produce reasonably good VLE predictions for hydrocarbon systems. However, the disadvantages of the SRK and PR EoS include poor liquid density calculations, inaccurate generalised parameters for polar and associating fluids which cannot be used for extrapolation, poor phase behaviour correlation for long-chain molecules, inaccurate calculations in the critical region and inaccurate vapour pressure calculations for pressures below 1.3 kPa. Abbott (1979) and Martin (1979) provide a detailed review concerning the shortcomings of traditional forms of cubic EoS.

3.1.2.3 The Alpha Correlation of Mathias and Copeman (1983)

Twu et al. (1991) mentioned that in order for a cubic EoS to accurately correlate phase equilibrium of mixtures, the vapour pressure of the pure components and the properties of the mixture must be accurately predicted. The temperature dependent attraction term, also known as the α function, significantly contributes to the accurate prediction of vapour pressure whilst the mixing rule employed greatly influences the mixture properties. Mathias and Copeman (1983) proposed an α function with adjustable parameters expressed in the form of a series to be used in any cubic EoS. In the literature, researchers such as Kang et al. (2002), Valtz et al. (2002) and Horstmann et al. (2005) have found that truncating the series to three adjustable parameters was sufficient to provide good accuracy. The use of the three adjustable parameters renders the α function more flexible, where these parameters are found from the regression of experimental vapour pressure data. This α

function of Mathias and Copeman (1983) was used in this study with both the SRK and PR EoS and catered for non-polar and polar components:

$$\alpha_i\left\{(T_c)_i,\omega_i\right\}=\left[1+\kappa_1\left(1-\sqrt{(T_r)_i}\right)+\kappa_2\left(1-\sqrt{(T_r)_i}\right)^2+\kappa_3\left(1-\sqrt{(T_r)_i}\right)^3\right]^2 \qquad (3\text{-}61)$$

where κ_1, κ_2 and κ_3 are the adjustable parameters that are unique to each component and are determined from the regression of experimental vapour pressure data. Since the α function can be applied to any EoS, the adjustable parameters would differ from one EoS to another.

3.1.3 Mixing Rules for Cubic Equations of State

Mixing rules are used to accurately represent the phase equilibrium of mixtures when using an EoS to regress VLE data, where it characterizes the interaction of molecules in a mixture. The mixing rules used by Soave (1972) and Peng and Robinson (1976) are known as the van der Waals one-fluid-theory classical mixing rules. Literature shows numerous mixing rules with different classifications that were developed over the years. Raal and Mühlbauer (1998) provides an excellent detailed review of these mixing rules. According to Hernández-Gaduza et al. (2001), the extrapolation of many mixing rules to multi-component mixtures is incoherent due to the invariance problem and the dilution effect. Michelsen and Kistenmacher (1990) noted these shortcomings in their findings as the Michelsen-Kistenmacher-Syndrome. One such mixing rule that did not suffer these shortcomings was the mixing rule of Wong and Sandler (1992) which was also considered in this study. The mixture parameters a_m and b_m from the Wong and Sandler (1992) mixing is found from:

$$\frac{a_m}{RT}=\frac{QD}{(1-D)} \qquad (3\text{-}62)$$

$$b_m=\frac{Q}{(1-D)} \qquad (3\text{-}63)$$

where Q and D are defined as:

$$Q = \sum_i \sum_j x_i x_j \left(b - \frac{a}{RT} \right)_{ij} \tag{3-64}$$

$$D = \sum_i x_i \frac{a_i}{b_i RT} + \frac{A_\infty^E}{cRT} \tag{3-65}$$

and A_∞^E is the excess Helmholtz free energy calculated at infinite pressure. The mixing rule also makes use of the partial molar derivatives of a_m and b_m with respective to the number of moles to evaluate the fugacity coefficients obtained from an EoS:

$$\frac{1}{RT}\left(\frac{1}{n} \frac{\partial n^2 a_m}{\partial n_i} \right) = D \frac{\partial n b_m}{\partial n_i} + b_m \frac{\partial n D}{\partial n_i} \tag{3-66}$$

$$\frac{\partial n b_m}{\partial n_i} = \frac{1}{(1-D)}\left(\frac{1}{n} \frac{\partial n^2 Q}{\partial n_i} \right) - \frac{Q}{(1-D)^2}\left(1 - \frac{\partial n D}{\partial n_i} \right) \tag{3-67}$$

and the corresponding partial derivatives of Q and D are given by:

$$\left(\frac{1}{n} \frac{\partial n^2 Q}{\partial n_i} \right) = 2 \sum_j x_j \left(b - \frac{a}{RT} \right)_{ij} \tag{3-68}$$

$$\frac{\partial n D}{\partial n_i} = \frac{a_i}{b_i RT} + \frac{\ln \gamma_i^\infty}{c} \tag{3-69}$$

and

$$\ln \gamma_i^\infty = \frac{1}{RT} \frac{\partial n A_\infty^E}{\partial n_i} \tag{3-70}$$

The parameter c is dependent on the EoS used. Equations (3-71a) and (3-71b) show the value of c used in the SRK and PR EoS respectively:

$$c = -\ln(2) \tag{3-71a}$$

$$c = \frac{1}{\sqrt{2}} \ln\left(\sqrt{2} - 1\right) \tag{3-71b}$$

Wong and Sandler (1992) made use of the excess Helmholtz free energy instead of the excess Gibbs free energy as the former is much less pressure dependent and thus the correct behaviour was obtained at both low and infinite pressure. In this study the NRTL activity coefficient model (discussed in Section 3.2.1.2) was used to describe the excess Helmholtz free energy at infinite pressure and the infinite dilution activity coefficients ($\ln \gamma_i^{\infty}$):

$$\frac{A_{\infty}^{E}}{RT} = \sum_i x_i \left(\frac{\sum_j x_j \tau_{ji} g_{ji}}{\sum_k x_k g_{ki}} \right) \tag{3-72}$$

$$\ln \gamma_i^{\infty} = \frac{\sum_j x_j \tau_{ji} g_{ji}}{\sum_k x_k g_{ki}} + \sum_j \frac{x_j g_{ij}}{\sum_k x_k g_{ki}} \left(\tau_{ij} - \frac{\sum_l x_l \tau_{lj} g_{lj}}{\sum_k x_k g_{kj}} \right) \tag{3-73}$$

Equation (3-64) is calculated with the aid of the following:

$$\left(b - \frac{a}{RT}\right)_{ij} = \frac{\left(b_i - \frac{a_i}{RT}\right) + \left(b_j - \frac{a_j}{RT}\right)}{2} \left(1 - k_{ij}\right) \tag{3-74}$$

Experimental binary VLE data are regressed to obtain the binary interaction parameter k_{ij}.

3.2 Activity and Activity Coefficient

The activity coefficient was introduced earlier in Section 3.1 as a factor that accounts for the non-ideality of the liquid phase in VLE. For the activity coefficient to be completely defined, the standard-state fugacity must be specified (Prausnitz et al., 1980). The standard-state fugacity of species *i* is taken as the fugacity of species *i* at the same temperature as that of the mixture and at some specified pressure and composition. According to Gess et al. (1991) the concept of excess properties must be introduced in order to obtain some physical sense of the activity coefficient. The

excess property is defined as the difference between the actual property value and that of an ideal solution at the same temperature, pressure and composition. The activity coefficient for species *i* is:

$$\gamma_i = \frac{\hat{f}_i}{x_i f_i} \tag{3-75}$$

and in terms of the Gibbs energy is:

$$\overline{G}_i = \Gamma_i(T) + RT \ln \hat{f}_i \tag{3-76}$$

The ideal solution behaviour can be adequately represented by the Lewis/Randall rule (Smith et al., 2001):

$$\hat{f}_i^{id} = x_i f_i \tag{3-77}$$

Equation (3-76) written for an ideal solution is:

$$\overline{G}_i^{id} = \Gamma_i(T) + RT \ln x_i f_i \tag{3-78}$$

Using the excess property definition for Equations (3-76) and (3-78):

$$\overline{G}_i^E = RT \ln \gamma_i \tag{3-79}$$

Van Ness (1959) derived the fundamental excess-property relation to show the inter-relation and significance of various excess thermodynamic properties:

$$d\left(\frac{nG^E}{RT}\right) = \frac{nV^E}{RT} dP - \frac{nH^E}{RT^2} dT + \sum_i \frac{\overline{G}_i^E}{RT} dn_i \tag{3-80}$$

The combination of Equations (3-79) and (3-80) provides an alternative form of the fundamental excess property relation in terms of the activity coefficient:

$$d\left(\frac{nG^E}{RT}\right) = \frac{nV^E}{RT}dP - \frac{nH^E}{RT^2}dT + \sum_i \ln\gamma_i dn_i \tag{3-81}$$

Inspection of Equations (3-80) and (3-81) show that:

$$\ln\gamma_i = \left[\frac{\partial\left(nG^E/RT\right)}{\partial n_i}\right]_{P,T,n_j} \tag{3-82}$$

For a binary system and using the properties of a partial molar quantity:

$$\ln\gamma_1 = \frac{G^E}{RT} + \frac{x_2 d\left(G^E/RT\right)}{dx_1} \tag{3-83}$$

$$\ln\gamma_2 = \frac{G^E}{RT} + \frac{x_1 d\left(G^E/RT\right)}{dx_2} \tag{3-84}$$

The partial molar property of G^E/RT is $\ln\gamma_i$, therefore:

$$\frac{G^E}{RT} = \sum_i x_i \ln\gamma_i \tag{3-85}$$

Properties such as V^E, H^E and γ_i may all be accessed experimentally thus rendering the excess property equations quite useful. It should also be noted that the molar excess Gibbs energy is a function of measurable system properties; temperature, pressure and composition. The excess properties are related to the activity coefficient by the Gibbs-Duhem equation:

$$\sum_i x_i d\ln\gamma_i = \frac{\overline{V}_i^E}{RT}dP - \frac{\overline{H}_i^E}{RT^2}dT \tag{3-86}$$

and at constant pressure and temperature, Equation (3-85) becomes:

$$\sum_i x_i d\ln\gamma_i = 0 \tag{3-87}$$

The Gibbs-Duhem equation is the basis used for thermodynamic consistency testing of VLE data.

3.2.1 Liquid Phase Activity Coefficient Models

The liquid phase activity coefficient models are used to account for the non-ideality of the liquid phase in phase equilibrium calculations. The models are generally functions of liquid compositions, expressed as mole fractions, volume fractions or molecular surface fractions and temperature (Walas, 1985). Usually the volume or molecular surface fractions are used when molecules differ substantially in size and chemical nature. The simplest liquid phase activity model is the two-suffix Margules equation (Smith et al., 2001). Over the years, many researchers have proposed numerous liquid phase activity coefficient models to improve representation of the liquid phase non-ideality. Some of these models which have received much attention include: the TK-Wilson (Tsuboka-Katayama-Wilson), NRTL (Non-Random Two Liquid) and modified UNIQUAC (UNIversal QUAsi-Chemical) models. These models were considered in this study and expressed in the form of excess Gibbs energy as a function of liquid mole fractions and temperature. The activity coefficients were then calculated for each component using Equation (3-82).

3.2.1.1 The Tsuboka-Katayama-Wilson (TK-Wilson) Equation

The TK-Wilson equation is a modification of the equation developed by Wilson (1964). Wilson (1964) based his equation on the concept of local composition which occurs within a liquid solution. According to Smith et al. (2001), models which are based on this concept are presumed to account for short-range order and non-random molecular orientations that result from differences in molecular size and intermolecular forces. Prausnitz et al. (1999) found that the Wilson equation appeared to provide a good representation for a wide range of miscible mixtures, particularly for solutions of polar or associating components in non-polar solvents. The Wilson equation can also be readily generalized to multi-component systems without introducing further parameters other than that of the binary constituents. However, there were two major disadvantages with the Wilson equation. One was that the equation could not predict liquid immiscibility and hence could not be used to represent systems that displayed immiscibility. Secondly, the equation could not be used for systems which showed a maximum or minimum when the natural logarithms of the activity coefficients was plotted against the liquid mole fraction. Therefore Tsuboka and Katayama (1975) modified the Wilson equation to meet these shortcomings. The modification was based on an excess

energy equation with the Wilson's local volume fractions and the Gibbs-Helmholtz correlation. The TK-Wilson equation for a binary system is expressed as:

$$\frac{G^E}{RT} = x_1 \ln \frac{x_1 + V_2^l x_2 / V_1^l}{x_1 + \Lambda_{12} x_2} + x_2 \ln \frac{V_1^l x_1 / V_2^l + x_2}{\Lambda_{21} x_1 + x_2} \tag{3-88}$$

where

$$\Lambda_{12} = \frac{V_2^l}{V_1^l} \exp\left(-\frac{\lambda_{12}}{RT} \right) \tag{3-89}$$

$$\Lambda_{21} = \frac{V_1^l}{V_2^l} \exp\left(-\frac{\lambda_{21}}{RT} \right) \tag{3-90}$$

and

$$\lambda_{12} = a_{12} - a_{11} \tag{3-91}$$

$$\lambda_{21} = a_{21} - a_{22} \tag{3-92}$$

The parameters λ_{12} and λ_{21} are the adjustable parameters for the TK-Wilson equation. The corresponding activity coefficients are given as:

$$\ln \gamma_1 = \ln \frac{x_1 + V_2^l x_2 / V_1^l}{x_1 + \Lambda_{12} x_2} + (\beta - \beta_v) x_2 \tag{3-93}$$

$$\ln \gamma_2 = \ln \frac{x_2 + V_1^l x_1 / V_2^l}{x_2 + \Lambda_{21} x_1} - (\beta - \beta_v) x_1 \tag{3-94}$$

where

$$\beta = \frac{\Lambda_{12}}{x_1 + \Lambda_{12} x_2} - \frac{\Lambda_{21}}{\Lambda_{21} x_1 + x_2} \tag{3-95}$$

$$\beta_v = \frac{V_2^l / V_1^l}{x_1 + V_2^l x_2 / V_1^l} - \frac{V_1^l / V_2^l}{x_2 + V_1^l x_1 / V_2^l} \tag{3-96}$$

The Wilson and TK-Wilson equations are generally in very good agreement when the molar volume ratios V_i^l / V_j^l are close to unity. Care must be taken when using the regressed VLE parameters of TK-Wilson to predict LLE as the latter is very sensitive to the parameters (Walas, 1985).

3.2.1.2 The NRTL (Non-Random Two Liquid) Equation

The NRTL equation proposed by Renon and Prausnitz (1968) was based on the local composition model as well as the two-liquid model of Scott (1956) together with an assumption of non-randomness similar to that used by Wilson (1964). The NRTL equation has a major advantage when compared to the original Wilson equation in that both partially miscible and completely miscible systems could be satisfactorily represented. Like the TK-Wilson equation, the NRTL equation is applicable to multi-component mixtures with only the binary parameters. Moreover the NRTL equation can be applied to highly non-ideal systems to yield a good representation of phase equilibrium (Raal and Mühlbauer, 1998). For a binary system, the NRTL equation is:

$$\frac{G^E}{RT} = x_1 x_2 \left[\frac{\tau_{21} G_{21}}{x_1 + G_{21} x_2} + \frac{\tau_{21} G_{12}}{G_{12} x_1 + x_2} \right] \tag{3-97}$$

where

$$G_{12} = \exp\left(-\alpha_{12} \tau_{12}\right) \tag{3-98}$$

$$G_{21} = \exp\left(-\alpha_{21} \tau_{21}\right) \tag{3-99}$$

$$\tau_{12} = \frac{g_{12} - g_{22}}{RT} \tag{3-100}$$

$$\tau_{21} = \frac{g_{21} - g_{11}}{RT} \tag{3-101}$$

The corresponding activity coefficients are given by:

$$\ln \gamma_1 = x_2^2 \left[\tau_{21} \left(\frac{G_{21}}{x_1 + x_2 G_{21}} \right)^2 + \left(\frac{\tau_{12} G_{12}}{(x_2 + x_1 G_{12})^2} \right) \right] \quad (3\text{-}102)$$

$$\ln \gamma_2 = x_1^2 \left[\tau_{12} \left(\frac{G_{12}}{x_2 + x_1 G_{12}} \right)^2 + \left(\frac{\tau_{21} G_{21}}{(x_1 + x_2 G_{21})^2} \right) \right] \quad (3\text{-}103)$$

The NRTL equation consists of the following adjustable parameters: $(g_{12} - g_{22})$, $(g_{21} - g_{11})$, α_{12} and α_{21}. The $(g_{12} - g_{22})$ and $(g_{21} - g_{11})$ parameters represent the interaction between species components 1 and 2. The parameters α_{12} and α_{21} are characteristic of the randomness of the mixture where a value of zero indicates that the mixture is completely random. Renon and Prausnitz (1986) note that $\alpha_{12} = \alpha_{21}$ and provide guidelines for suitable values for α_{12}. However, over the years many researchers have found that the guidelines provided by Renon and Prausnitz (1986) were too restrictive and that values of α_{12} outside these guidelines gave better predictions for phase equilibrium. Walas (1985) notes that if an estimate for α_{12} has to be made; it should be 0.3 for non-aqueous mixtures and about 0.4 for aqueous organic mixtures. On the other hand, Raal and Mühlbauer (1998) have found these suggestions to be inconclusive and mentions that a suitable value for α_{12} should be found from the reduction of experimental data.

The NRTL model can provide very good representation of highly non-ideal systems especially for partially miscible systems and can accurately represent systems which show a maximum or minimum when the natural logarithms of the activity coefficients is plotted against the liquid mole fraction (Walas, 1985). However in the range of very low molar concentrations, the NRTL model is inferior to the Wilson model in treating strongly asymmetric systems (Vetere, 2000). In his study, Vetere (2000) provides an explanation for this behaviour and a simple modification of the NRTL model incorporating molar volume ratios.

The NRTL model has been successfully used to model similar VLE systems to those that were investigated in this study. Wen and Tu (2007) and Martínez et al. (2008) reported that the NRTL model was capable of correlating data for the ethanol + butan-2-one system. Arce et al. (1996, 1997, and 1998) have also reported satisfactory modeling with the NRTL model for the ethanol + 2-methoxy-2-methylbutane system.

3.2.1.3 The Modified UNIQUAC (UNIversal QUAsi-Chemical) Equation

Abrams and Prausnitz (1975) semi-theoretically developed the UNIQUAC equation using the two-liquid model and the theory of local composition. The proposed equation was made up of two parts: a combinatorial part to account for the differences in the size and shape of the molecules and the residual part to account for the intermolecular interactions between the molecules. Anderson and Prausnitz (1978) later modified the UNIQUAC equation to obtain better agreement for systems containing water or lower alcohols by determining optimum values for the surface interaction parameter (q') using a variety of systems containing water and/or alcohols. Similar to the TK-Wilson and NRTL equations, the modified UNIQUAC equation can also be readily extended to multi-component mixtures in terms of the binary parameters only. The modified UNIQUAC equation can also be used to represent systems that exhibit partial miscibility for phase equilibrium. The modified UNIQUAC equation for a binary system is presented as:

$$\frac{G^E}{RT} = x_1\left[\ln\frac{\Phi_1^*}{x_1} + \frac{q_1 z}{2}\ln\frac{\theta_1}{\Phi_1^*} - q_1'\ln\left(\theta_1' + \theta_2'\tau_{21}\right)\right] + x_2\left[\ln\frac{\Phi_2^*}{x_2} + \frac{q_2 z}{2}\ln\frac{\theta_2}{\Phi_2^*} - q_2'\ln\left(\theta_1'\tau_{12} + \theta_2'\right)\right] \tag{3-104}$$

where z is the co-ordination number that is usually set to a value of ten. The volume fraction, Φ^*, and the area fractions θ and θ' are found from:

$$\Phi_i^* = \frac{r_i x_i}{\sum_{j=1}^{2} r_j x_j} \tag{3-105}$$

$$\theta_i = \frac{q_i x_i}{\sum_{j=1}^{2} q_j x_j} \tag{3-106}$$

$$\theta_i' = \frac{q_i' x_i}{\sum_{j=1}^{2} q_j' x_j} \tag{3-107}$$

The parameter r is a pure component volume parameter that accounts for the size of the molecules, whilst the parameters q accounts for the geometric external surface of the molecules and q' for the surface of interaction of the molecules. The parameter q' was introduced by Anderson and Prausnitz (1978) to obtain better agreement for systems containing water or lower alcohols. In their work, Anderson and Prausnitz (1978) found that the values of q' were smaller than q, indicative that for alcohols the intermolecular attraction is determined primarily by the OH group. To revert to the original formulation of the UNIQUAC equation, q' is set equal to q. These pure component structural parameters are evaluated from molecular structure contributions for various groups and subgroups and are outlined in Raal and Mühlbauer (1998). The adjustable parameters ($u_{12} - u_{22}$) and ($u_{21} - u_{11}$) are found from:

$$\tau_{12} = \exp\left(-\frac{u_{12} - u_{22}}{RT}\right) \tag{3-108}$$

$$\tau_{21} = \exp\left(-\frac{u_{21} - u_{11}}{RT}\right) \tag{3-109}$$

The corresponding activity coefficients are given by:

$$\begin{aligned}\ln\gamma_1 = {} & \ln\frac{\Phi_1^*}{x_1} + \frac{z}{2}q_1\ln\frac{\theta_1}{\Phi_1^*} + \Phi_2^*\left(l_1 - \frac{r_1}{r_2}l_2\right) \\ & - q_1'\ln\left(\theta_1' + \theta_2'\tau_{21}\right) + \theta_2' q_2'\left(\frac{\tau_{21}}{\theta_1' + \theta_2'\tau_{21}} - \frac{\tau_{12}}{\theta_1'\tau_{12} + \theta_2'}\right)\end{aligned} \tag{3-110}$$

$$\begin{aligned}\ln\gamma_2 = {} & \ln\frac{\Phi_2^*}{x_2} + \frac{z}{2}q_2\ln\frac{\theta_2}{\Phi_2^*} + \Phi_1^*\left(l_2 - \frac{r_2}{r_1}l_1\right) \\ & - q_2'\ln\left(\theta_2' + \theta_1'\tau_{12}\right) + \theta_1' q_1'\left(\frac{\tau_{12}}{\theta_2' + \theta_1'\tau_{12}} - \frac{\tau_{21}}{\theta_2'\tau_{21} + \theta_1'}\right)\end{aligned} \tag{3-111}$$

where

$$l_i = \frac{z}{2}\left(r_i - q_i\right) - \left(r_i - 1\right) \tag{3-112}$$

The UNIQUAC equation is applicable to a wide variety of non-electrolyte liquid mixtures containing polar or non-polar fluids. The main disadvantage of the UNIQUAC equation is its greater algebraic complexity and the need for pure component structural parameters. The modified UNIQUAC equation was considered in this study since systems that contained lower alcohols were measured as part of this study. However, even with its greater algebraic complexity, the UNIQUAC model on average is less satisfactory in correlating VLE data of moderately non-ideal systems when compared to the Wilson and NRTL models (Malanowski and Anderko,1992).

Similar to the NRTL model, the UNIQUAC model was also found to satisfactorily model similar VLE systems to those that were investigated in this study. For the ethanol + butan-2-one system, Ohta et al. (1981), Wen and Tu (2007) and Martínez et al. (2008) achieved satisfactory modeling with the UNIQUAC model. For the ethanol + 2-methoxy-2-methylbutane, Arce et al. (1996, 1997, and 1998) reported that the UNIQUAC model was suitable for such a system.

3.3 Vapour-Liquid Equilibrium (VLE)

Phase diagrams provide a good summary for VLE data. Some of the most commonly used phase diagrams include the *x-y* plot with either a *T-x-y* plot for an isobar or *P-x-y* plot for an isotherm. There are five types that are used to categorize the VLE behaviour of binary systems (Raal and Mühlbauer, 1998). Systems for which all compositions have boiling points between those of the pure components are classified as type *I*. Type *I* is also more commonly known as intermediate-boiling systems. Types *II* and *III* are used to classify systems that contain homogeneous azeotropes, where type *II* describes minimum boiling homogenous azeotropes and type *III* describes maximum boiling homogenous azeotropes. Azeotropes describe a state at which the vapour composition is exactly the same as the liquid composition; hence at this state no phase separation is possible by conventional distillation. A compilation of data for such states is provided by Gmehling and Onken (1977-1982). The type *IV* classification describes systems with partially miscible liquid phases and a single heterogeneous azeotrope. The temperature of the azeotrope provides a sub-classification to type *IV*; (a) the temperature of the azeotrope is below the pure component boiling temperatures or (b) the temperature of the azeotrope is intermediate between the pure component boiling temperatures. The type *V* classification describes systems with partial liquid miscibility and both a homogenous and heterogenous azeotrope which rarely occurs. Of all the classifications, the first three types are the most commonly encountered and are displayed in Figure 3-1.

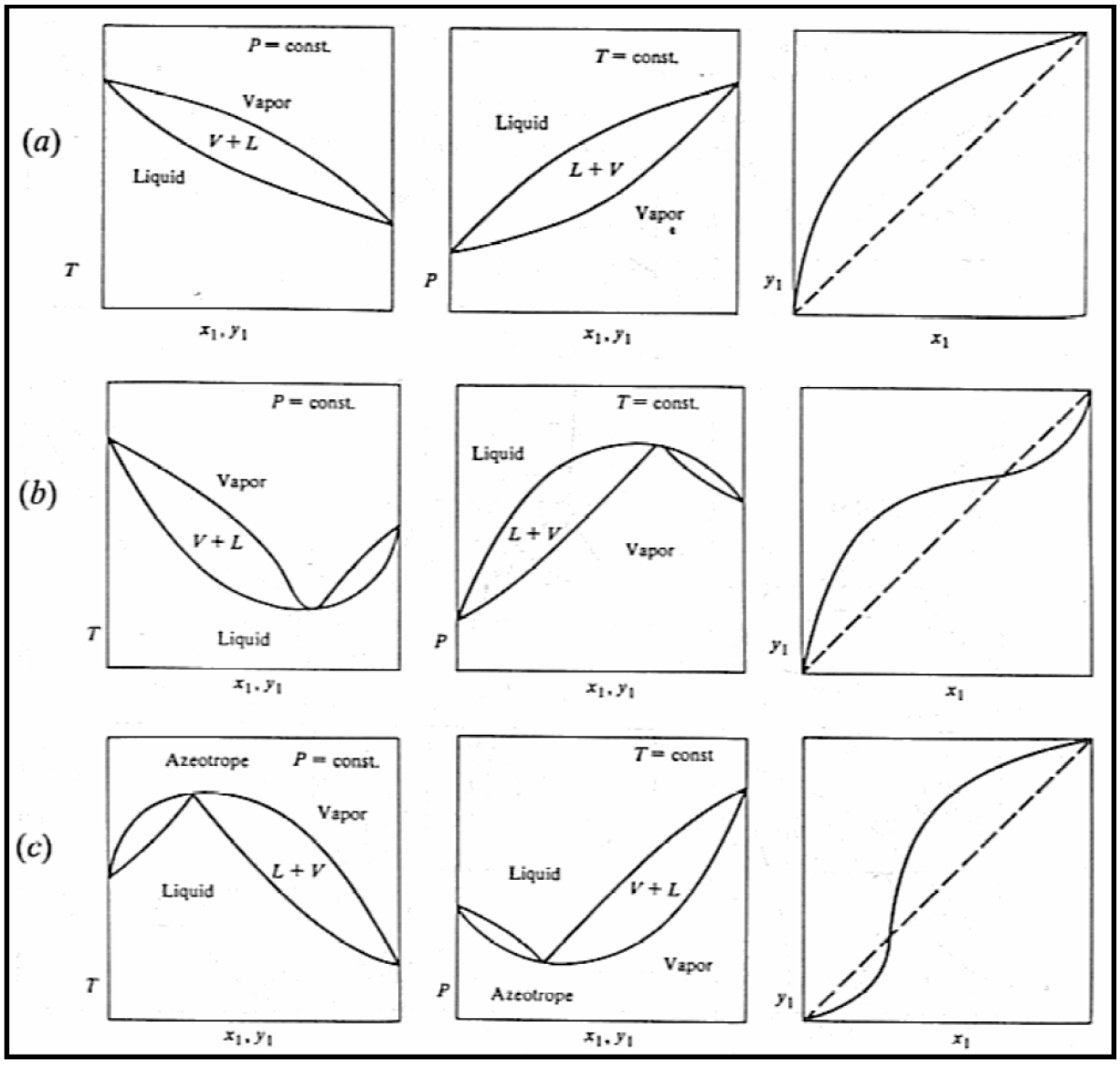

Figure 3-1: The three common types of binary phase diagrams for T-x-y, P-x-y and x-y plots: (a) intermediate-boiling; (b) minimum boiling azeotrope; (c) maximum boiling azeotrope (Raal and Mühlbauer, 1998).

3.3.1 VLE Data Regression

In order to successfully implement a design method for separation processes, quantitative estimates of fluid phase equilibrium are required. Sometimes phase equilibrium data are readily available and thus quantitative estimates can be obtained without much effort. However, in most cases phase equilibrium data are unavailable and thus it becomes rather difficult to make rough estimates on a rational basis. In such cases, predictive models have been developed to assist in the design of

chemical processes. For phase separation processes, these models include the use of cubic equations of state with mixing rules and liquid phase activity coefficient models. Phase equilibrium data are regressed using these models to yield a set of parameters that are unique to each system studied and the model employed. The model parameters are important as it allows prediction of phase equilibrium to experimentally difficult conditions.

The two most widely used methods for the regression of VLE data include: the $\gamma - \Phi$ method or combined method and the $\Phi - \Phi$ method also known as the direct method. In the combined method, the fugacity coefficient from an EoS (such as the virial EoS) is used to describe the non-idealities of the vapour phase whilst an activity coefficient model is used to describe the non-idealities of the liquid phase. For the direct method, the fugacity coefficients from an EoS (such as a cubic EoS) are used to describe the non-idealities in both the vapour and liquid phase where a mixing rule is employed to describe the mixture properties.

For each method, the calculation procedure depends on the nature of the VLE data (isothermal or isobaric). In the case of each experimental point in an isothermal VLE data set, the pressure and vapour composition are calculated by a bubble point pressure computation or the pressure and liquid composition are calculated by a dew point pressure calculation. The computation scheme depends on whether the VLE data are fully determined by the measurement of temperature, pressure, vapour and liquid compositions or partially determined where only one of the phase composition or the overall composition is known. Similarly in the case of each experimental point in an isobaric VLE data set, the temperature and vapour composition are calculated by a bubble point temperature calculation or the temperature and liquid composition are calculated by a dew point temperature calculation. According to Smith et al. (2001), the vapour composition measurements are the most susceptible to error. Therefore the bubble point computation is generally favoured over the dew point computation for a fully determined VLE data set.

The measurement of VLE to obtain a fully determined VLE data set is encouraged by Smith et al. (2001) since this allows for thermodynamic consistency testing to be carried out. In the case where a static analytical apparatus is used to carry out measurements, isothermal VLE data are much more easily measured as opposed to isobaric VLE data. Furthermore, regression of isothermal VLE data is less tedious as the model parameters can be treated as constants since the temperature is constant. These model parameters are known to have strong temperature but weak pressure dependence (Raal and Mühlbauer, 1998). The combined and direct methods are now discussed in greater detail below.

3.3.1.1 The Combined (γ – Φ) Method

This method combines the use of two different equations to regress VLE data, where one equation describes the non-ideality of the vapour phase and the other describes the non-ideality of the liquid phase. In this study, the virial EoS with the second virial coefficient correlation of Tsonopoulos (1974) was used to describe the non-ideality of the vapour phase and an activity coefficient model was used to describe the liquid phase non-ideality. Usually, more than one liquid phase activity coefficient model is used for VLE data regression, as a comparison can be made to check which model fits the experimental data best. For this study, the TK-Wilson, NRTL and modified UNIQUAC liquid phase activity coefficient models (described in Section 3.2.1) were used.

The parameters for the liquid phase activity coefficient models are obtained by using a suitable algorithm to perform the VLE data regression. Since only isothermal binary VLE data were measured in this study, a procedure adapted from Smith et al. (2001) for the regression of an isothermal set of experimental binary VLE data using the combined method follows:

1. The temperature, liquid phase compositions and the pure component properties are selected as inputs for the regression algorithm. A suitable liquid phase activity coefficient model is then chosen.

2. Initial estimates for the parameters of the liquid phase activity coefficient model are then chosen. The activity coefficients are then calculated using Equations (3-83) and (3-84). Initially the vapour phase is assumed ideal and therefore the fugacity coefficients (Φ_i) are initially set to unity to enable an initial calculation of the system pressure. The saturated pressures (P_i^{sat}) are then evaluated from a suitable vapour pressure correlation (such as the extended Antoine or Wagner equation).

3. From the law of mass conservation, $\sum x_i = \sum y_i = 1$. Therefore the system pressure is determined from the manipulation of Equation (3-23):

$$P = \frac{x_1 \gamma_1 P_1^{sat}}{\Phi_1} + \frac{x_2 \gamma_2 P_2^{sat}}{\Phi_2} \qquad (3\text{-}113)$$

4. The vapour mole fractions are then determined from:

$$y_i = \frac{x_i \gamma_i P_i^{sat}}{\Phi_i P} \tag{3-114}$$

5. With the vapour mole fractions calculated, the fugacity coefficients are then evaluated from Equation (3-28) using the correlation of Tsonopoulos (1974) for the second virial coefficients. The system pressure is now recalculated using Equation (3-113) and compared to the previous value:

$$\delta P = \left| P_{new} - P_{old} \right| \tag{3-115}$$

If the difference is within a specified tolerance, the next step is followed; otherwise step 4 is repeated with the new pressure value calculated. Sometimes the specified tolerance is not achieved or divergence occurs in this step. When this occurs, new initial estimates of the model parameters must be chosen in step 1 above.

6. Once all the pressure values for each experimental point of the VLE data set are determined, the model parameters are then optimized by an optimization method with a suitable objective function to yield the best fit to the experimental *P-x* data for the entire composition range.

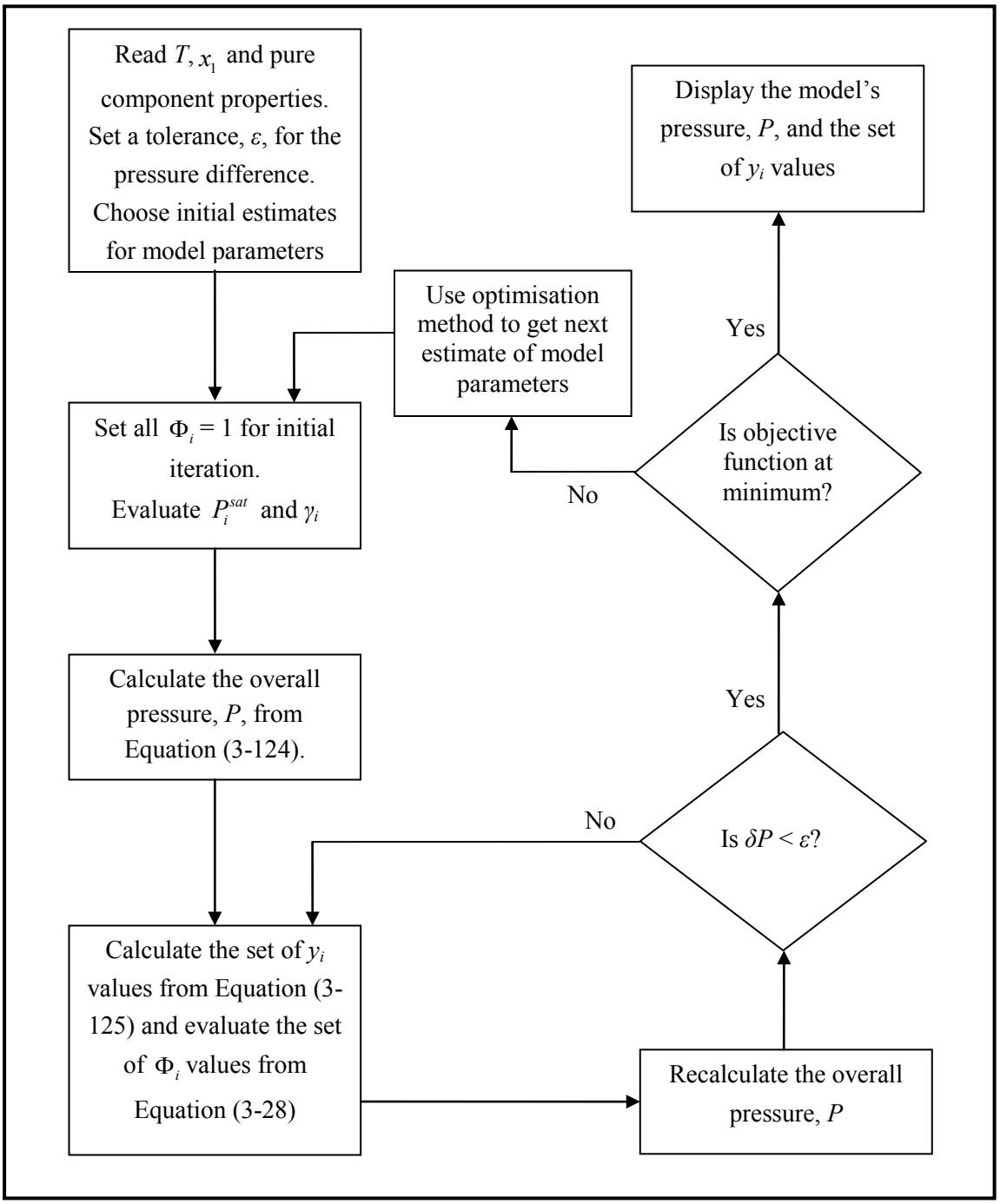

Figure 3-2: Calculation flow diagram for the bubble point pressure procedure of the combined method to obtain the parameters for the liquid phase activity coefficient model (Smith et al., 2001).

The regression algorithm for isobaric VLE data is same as outlined above, except that the temperature is not constant and its variation must be considered. In the sixth step above, an

objective function was required. For this study, the following objective function was used to optimize for the model parameters:

$$F = \sum_{i=1}^{n} \left(\frac{P_{\exp,i} - P_{cal,i}}{P_{\exp,i}} \right) \tag{3-116}$$

Other objective functions are also possible but according to Van Ness et al. (1973), Equation (3-116) is at least as good as any other and is the simplest and direct objective function. According to Van Ness and Abbott (1982), Equation (3-116) is successful in the regression of isothermal VLE data and may also even be superior to any other maximum likelihood method. Optimisation algorithms developed by Marquardt (1963) and Gess et al. (1991) make use of Equation (3-116) for the regression of experimental VLE data. However, software programmes such as MATLAB have built-in algorithms which enable such calculations to be performed with much ease. For this study, the *fminsearch* function in MATLAB which uses the Nelder-Mead simplex method for optimization was employed (Lagarias et al., 1998). The regression procedure for isothermal VLE data is summarized as a calculation flow diagram in Figure 3-2.

3.3.1.2 The Direct (Φ – Φ) Method

This method makes use of a cubic EoS to calculate the fugacity coefficients that describe both the vapour and liquid phase non-idealities. Using Equation (3-11):

$$\hat{f}_i^l = x_i \hat{\phi}_i^l P = \hat{f}_i^v = y_i \hat{\phi}_i^v P \tag{3-117}$$

where the fugacity coefficients are obtained from:

$$\ln \hat{\phi}_i^l = \left(\frac{1}{RT} \right) \int_{V^l}^{\infty} \left[\left(\frac{\partial P}{\partial n_i} \right)_{T,V,n_j} - \frac{RT}{V^l} \right] dV - \ln \left[\frac{PV^l}{n_T RT} \right] \tag{3-118}$$

$$\ln \hat{\phi}_i^v = \left(\frac{1}{RT} \right) \int_{V^v}^{\infty} \left[\left(\frac{\partial P}{\partial n_i} \right)_{T,V,n_j} - \frac{RT}{V^v} \right] dV - \ln \left[\frac{PV^v}{n_T RT} \right] \tag{3-119}$$

where n_T refers to the total number of moles in the system. The terms on the right hand side of the equation are evaluated using a suitable EoS. Often the equilibrium ratio (K_i), defined as the ratio of the vapour composition to the liquid composition, is used to simplify calculations when using the direct method of VLE data regression. Using Equation (3-117):

$$K_i = \frac{y_i}{x_i} = \frac{\hat{\Phi}_i^v}{\hat{\Phi}_i^l} \tag{3-120}$$

Valderrama (2003) notes some of the advantages and disadvantages of cubic equations of state, shown in Table 3-1.

Table 3-1: Advantages and disadvantages of cubic equations of state (Valderrama, 2003).

Advantages	Disadvantages
Equations of state are applicable to both low and high pressure systems.	Actual pressure, volume and temperature data tend to follow a fourth degree equation instead of a cubic equation.
Due to their cubic nature in volume, calculations are relatively simple to perform.	Cubic equations of state cannot represent all properties of a fluid in all different ranges of temperature and pressure.
The equation can be tuned with the adjustable parameters of the temperature attraction (α) function to give accurate values for any volumetric or thermodynamic property for most applications.	Mixing rules used for equations of state are empirical in nature since the interactions between unlike molecules are unknown. This means interaction parameters are usually required. Furthermore, application of mixing rules to complex mixtures might actually require several interaction parameters even with the use of modern mixing rules.
The equations can be easily extended to mixtures by use of mixing rules of any complexity.	

Raal and Mühlbauer (1998) provides a good summary of the challenges associated with using the direct method:

1. The EoS selected must be able to adequately describe both the vapour and liquid phase non-idealities. More importantly, the EoS must be flexible enough to fully describe the pressure, volume and temperature behaviour of a pure substance for both phases in the temperature and pressure range of study.
2. An appropriate mixing rule must be carefully selected to correctly describe the properties of the mixture. Most mixing rules are somewhat empirical in nature and tend to be system specific.
3. If a higher than cubic order EoS is used, care must be taken to locate the appropriate roots for liquid and vapour densities.

The interaction parameters of the mixing rule used are determined from the regression of experimental VLE data. This regression technique is similar to that of the combined method discussed in Section 3.3.1.1 with the same objective function used. Figure 3-3 shows the calculation flow diagram for the regression of isothermal VLE data.

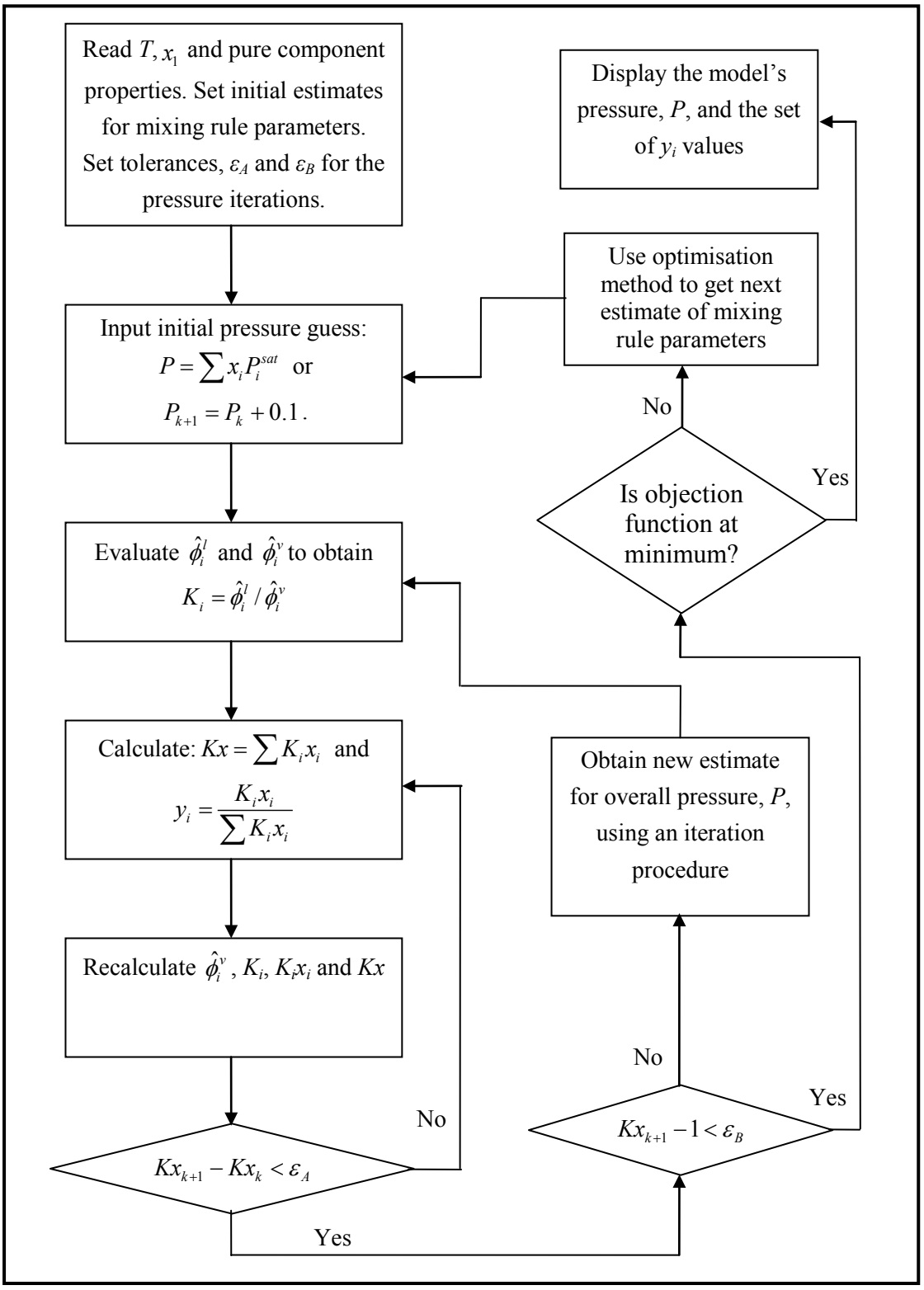

Figure 3-3: Calculation flow diagram for the bubble point pressure iteration for the direct method to obtain parameters for the mixing rule used (Smith et al., 2001).

3.4 Liquid-Liquid Equilibrium (LLE)

Liquid-liquid equilibrium (LLE) is a phenomenon that results when pairs of chemical species are mixed in a certain composition range and allowed to reach thermodynamic equilibrium, do not form a single homogenous phase (Smith et al., 2001). Systems that exhibit LLE form two liquid phases of different compositions. The splitting phenomenon occurs because of a criterion that exits for phase equilibrium in a closed system (Smith et al., 2001). This criterion is satisfied when the Gibbs energy is a minimum with respect to all possible changes at a given temperature and pressure (discussed in more detail in Section 3.4.2). The splitting thus occurs since the system can achieve a lower Gibbs energy by doing so than compared to forming a single homogenous phase.

Temperature has a strong influence on LLE but the effect of pressure is only significant at very high pressures or near the critical point (Walas, 1985). Binary and ternary systems are the two most common types of LLE systems discussed in literature. Binary LLE systems are encountered in an azeotropic distillation column where the condensed distillate forms two liquid phases. A ternary LLE system finds its use in liquid-liquid extraction. Since only binary systems were measured in this study, a short description of binary LLE systems will be presented. The reader is referred to Treybal (1963) and Novák et al. (1987), who discuss ternary LLE systems in detail.

3.4.1 Binary LLE

Phase diagrams for binary LLE systems are simply presented in the form of *T-x-x* diagrams. Some types of binary LLE systems are shown in Figure 3-4. The phase diagram in Figure 3-4 (a) is known as the *island curve* that consists of an upper critical solution temperature (UCST), symbolized as T_U and a lower critical solution temperature (LCST), symbolized as T_L. This type of phase diagram is quite rare and thus seldom encountered as LLE is only possible at temperatures between T_U and T_L. Figure 3-4 (b) shows LLE binary systems that exhibit an UCST only. For this type of systems, the UCST may however not exist if the mixture bubble point is lower than the UCST. Figure 3-4 (c) shows LLE binary systems that exhibit a LCST only. It should be noted that in this case, the LCST may not exist if freezing occurs at a temperature higher than the LCST. Phase diagrams of Figure 3-4 (b) and 3-4 (c) are commonly encountered. The curves of the phase diagrams shown in Figure 3-6 are also known as solubility or binodal curves. For any specific temperature within the solubility curve, A and B denote the equilibrium points with compositions x_1^{α} and x_1^{β} respectively. When the

solubility curve intersects both the bubble and freezing point curves, a fourth type of behaviour is observed (Sørensen et al., 1979 and 1980).

More information on the various types of LLE phase diagrams and on the various types of azeotropes are presented in Appendix F.

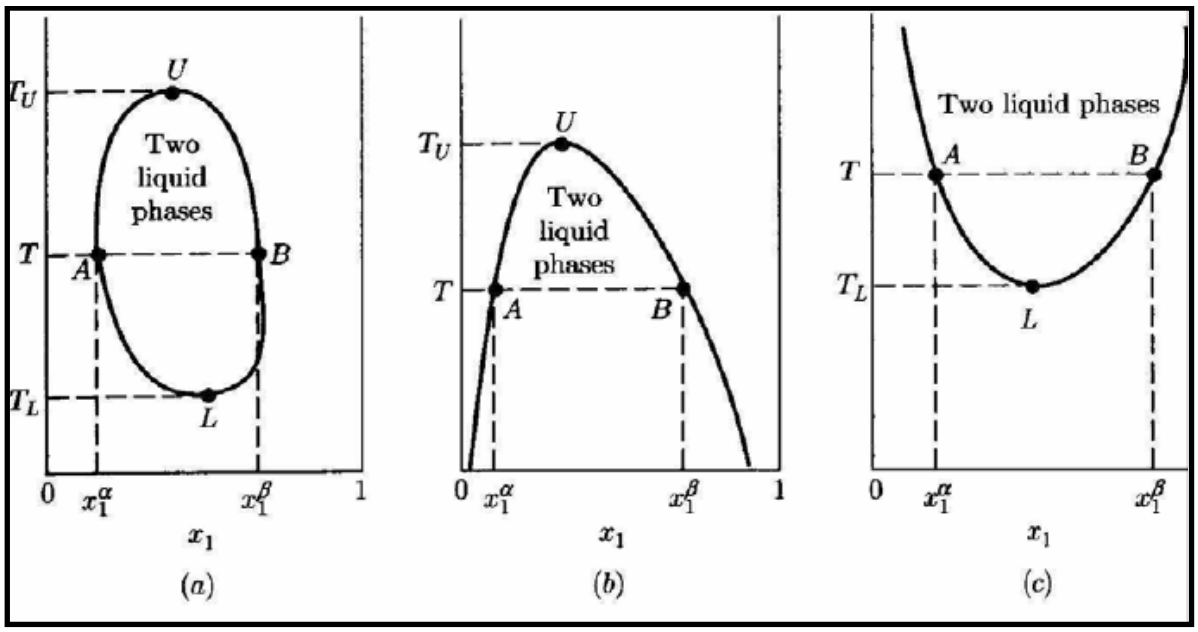

Figure 3-4: Three types of constant pressure binary LLE phase diagrams: (a) an *island curve*, (b) a *convex curve* and (c) a *concave curve*, where *α* and *β* refer to the two liquid phases (Smith et al., 2001).

3.4.2 Theoretical Treatment of LLE

At equilibrium a stable system tends towards achieving a minimum Gibbs energy at a fixed temperature and pressure. The stability criterion indicates that a liquid mixture will split into separate liquid phases if it can lower its Gibbs energy by doing so (Smith et al., 2001). A typical curve showing the Gibbs energy of mixing for a binary partially miscible liquid at constant temperature and pressure is illustrated in Figure 3-5. The Gibbs energy of mixing is defined as $\Delta G = G - \sum_i x_i G_i$, where G is the mixture Gibbs energy and G_i the pure component Gibbs energy.

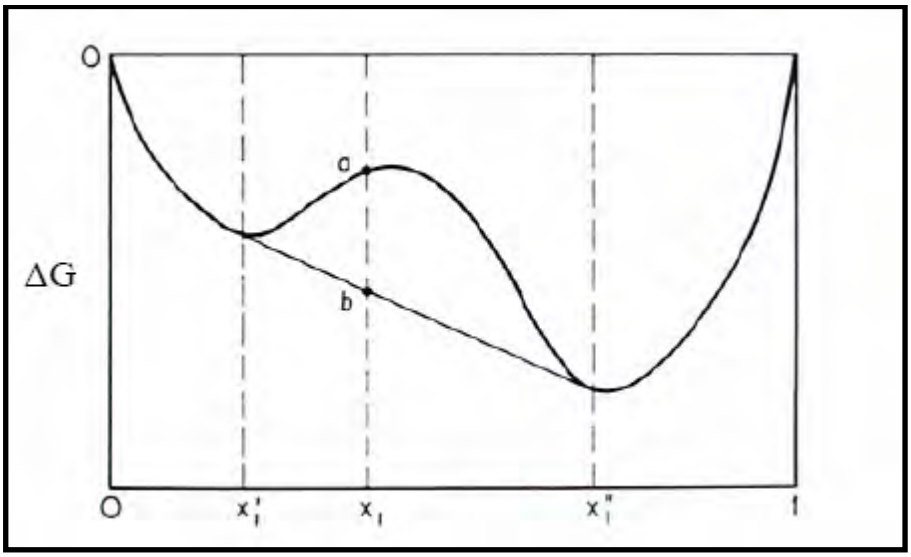

Figure 3-5: Molar Gibbs energy of mixing for a partially miscible binary system at constant temperature and pressure (Prausnitz et al., 1999).

In Figure 3-5, a mixture with composition corresponding to point *a* will split into separate phases with compositions $x_1^{'}$ and $x_1^{''}$ according to the stability criterion. Point *b* represents the molar Gibbs energy change upon mixing and is the lowest possible Gibbs energy that the mixture may attain subject to the conditions of constant pressure, temperature and overall composition x_1.

At constant temperature and pressure, the mathematical interpretation of Figure 3-5 requires that ΔG and its first and second derivatives must be continuous functions of x_1 and that the second derivative must everywhere be positive. Hence for a binary system:

$$\frac{d^2\Delta G}{dx_1^2} > 0 \tag{3-121}$$

The stability requirement in terms of the Gibbs excess energy for a binary system is:

$$\frac{d^2\left(G^E/RT\right)}{dx_1^2} > -\frac{1}{x_1 x_2} \tag{3-122}$$

Application of the phase equilibrium criterion from Equation (3-10) to two liquids phases, noted as α and β, results in:

$$\hat{f}_i^{\alpha} = \hat{f}_i^{\beta} \tag{3-123}$$

Introducing the activity coefficient and considering each pure component as a liquid at the temperature of the system yields:

$$x_i^{\alpha}\gamma_i^{\alpha}f_i^{\alpha} = x_i^{\beta}\gamma_i^{\beta}f_i^{\beta} \tag{3-124}$$

where *i* refers to the component. Equation (3-124) is the fundamental relation for LLE and shows that unlike VLE, the role of the activity coefficients in LLE are the only thermodynamic contribution to an LLE calculation.

3.4.3 Binary LLE Data Regression

For a liquid phase activity coefficient model to be used in LLE regression, it must firstly satisfy the stability criterion. The activity coefficient model of Wilson (1964) is one model that fails to meet the stability criterion and therefore is not able to predict LLE (Smith et al., 2001). However the TK-Wilson equation is able to predict LLE. Unlike the regression of VLE data, the activity coefficient model in LLE data regression is used to represent both liquid phases.

It should also be noted that the direct method, in which an EoS is used, can also be used to regress LLE data. This method however is only applicable for the modeling of high pressure LLE data where the effect of pressure on phase equilibrium cannot be ignored (Walas, 1985 and Raal and Mühlbauer, 1998). The LLE data measured in this study was done at a moderate pressure (350 kPa) and thus the direct method would not have been appropriate for this study. Therefore no further discussion will be made on this method but the reader is referred to Peng et al. (2002) and Ohta et al. (2004) for a detailed discussion.

Raal and Mühlbauer (1998) note that at least two data points for each phase at different temperatures are needed to obtain the temperature dependent parameters of the liquid phase activity model used. Some of the simplest liquid phase activity coefficient models used to represent LLE includes the three-suffix Margules and the Van Laar (1910) models. These models were not considered for this study as they cannot accurately represent LLE data though they are sometimes favoured due to their comparative algebraic simplicity. The liquid phase activity coefficient models discussed in Section 3.2.1 were also considered for the binary LLE regression in this study.

According to Raal and Mühlbauer (1998), activity coefficient models with more than two parameters cannot be used to model solubility data (binary LLE) unless all subsequent parameters are fixed at some trial value/s. This is necessary since having more than 2 parameters as unknown means that there would be more unknown parameters than known equations to solve. Therefore in the case of the NRTL model for binary LLE data, the non-randomness parameter (α_{12}) is fixed to allow calculation of the other two parameters (τ_{12} and τ_{21}). Prausnitz et al. (1999) suggest that the value of α_{12} should be obtained from experimental results of the same class of components as those under study. Due to the algebraic complexity of the TK-Wilson, NRTL and modified UNIQUAC equations, the parameters cannot be determined in a simple manner as compared to the three-suffix Margules or Van Laar (1910) models. Therefore graphs have been published to assist in the computation for the parameters of these models. Walas (1985) however suggests an algorithm for such calculations as well which was subsequently used in this study.

3.5 Vapour-Liquid-Liquid Equilibrium (VLLE)

When the solubility curve that represents LLE intersects the VLE bubble point curve, a phenomenon known as vapour-liquid-liquid equilibrium (VLLE) is obtained. This section will focus on a brief description of binary VLLE and the regression of such data since only binary VLLE data were considered in this study.

From the Gibbs phase rule, only one degree of freedom exists for a binary VLLE system (Smith et al., 2001). Therefore, if the system pressure is specified for a binary system then the temperature and the compositions for all three phases are fixed. Hence for an isobaric binary VLLE system, the state of three phases in equilibrium will necessary occur at one temperature (T^*) when represented on a *T-x-y* phase diagram, as shown in Figure 3-6. Points *C* and *D* in Figure 3-6 represent the two liquid phases in equilibrium with the vapour phase that is represented by point *E*. For this binary VLLE system, if more of either component is added to the system whose overall composition lies between points *C* and *D* together with the three phase equilibrium pressure being maintained, then the Gibbs phase rule necessitates that the temperature and the compositions of the three phases will remain unchanged. However the law of mass conservation must be satisfied to account for the change in the overall composition of the system. This is achieved by the adjustment of the relative amounts of the phases. For temperatures that are above T^* and depending on the overall composition, the system may be a single liquid phase (represented by α or β), a vapour phase (represented as *V*) or a mixture of the two phases (represented as α-*V* or β-*V*). On the other hand, for

temperature below T^*, the system is represented by a mixture of two liquid phases (LLE) or a single liquid phase (either α or β) depending on the overall composition of the system.

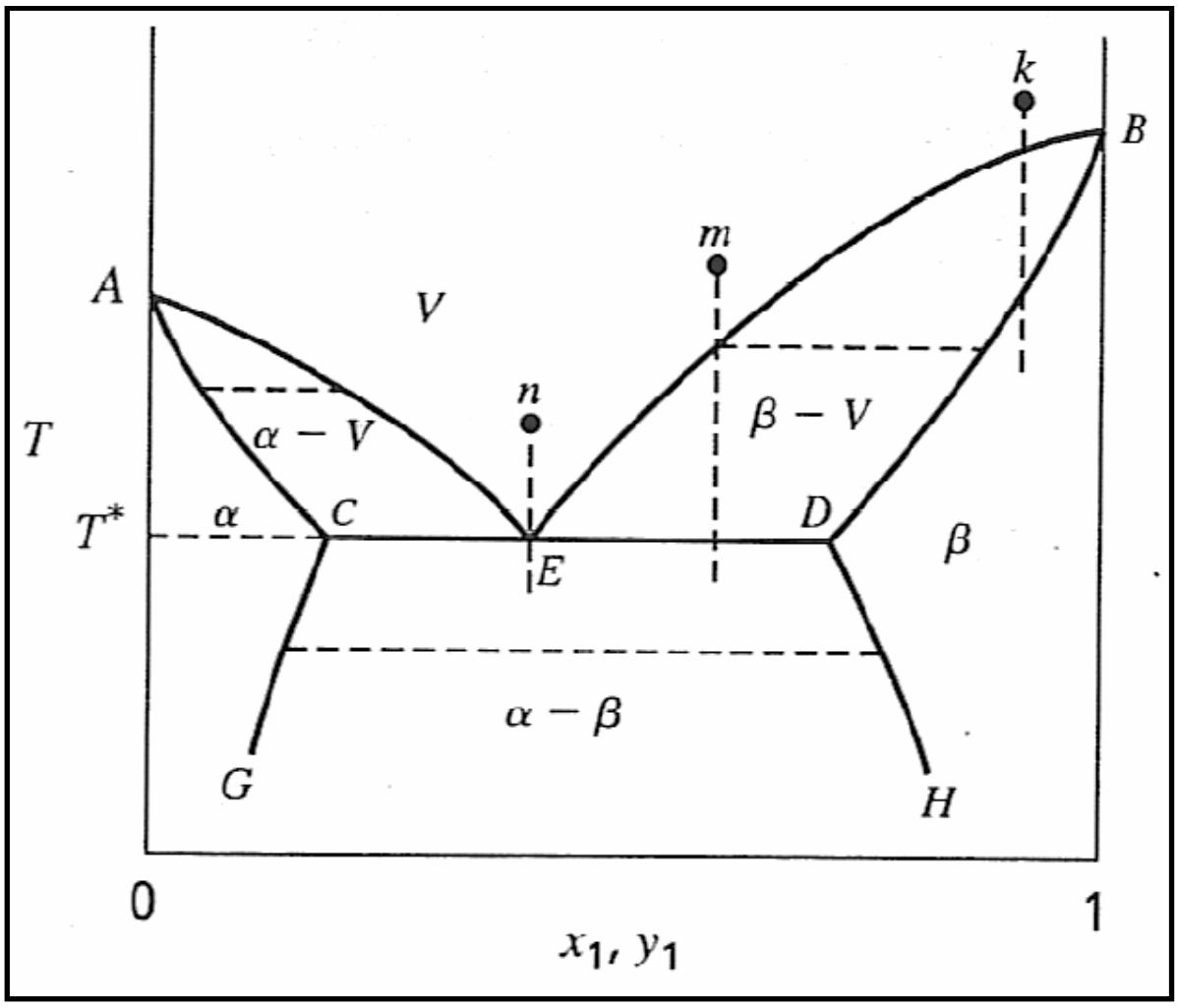

Figure 3-6: A common *T-x-y* diagram at constant pressure for a binary system exhibiting VLLE (Smith et al., 2001).

In similar manner, VLLE can also be measured at a constant temperature as shown by a *P-x-y* phase diagram in Figure 3-7. In this case the pressure (where all three phases exist in equilibrium) is identified as P^*. As mentioned earlier, pressure has a weak influence on the solubility of liquids except at very high pressure near the critical point. Hence in Figure 3-7 for moderate pressures above P^*, the LLE phase boundaries are nearly vertical.

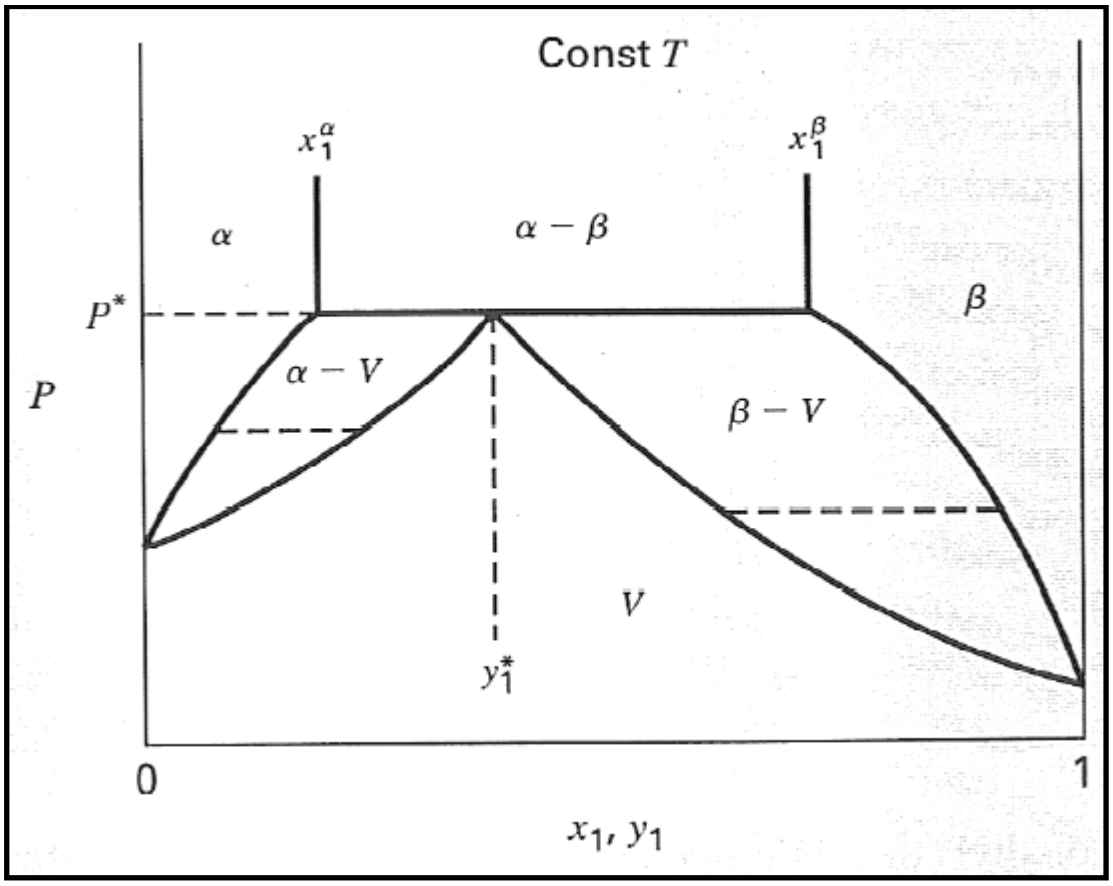

Figure 3-7: A common *P-x-y* diagram at constant temperature for a binary system exhibiting VLLE (Smith et al., 2001).

The regression of VLLE data is carried in a similar manner as outlined for VLE. Using the criterion for phase equilibrium (Equation 3-10) for the point where the two liquid phases (α and β) are in equilibrium with its vapour (V) yields:

$$\hat{f}_i^\alpha = \hat{f}_i^\beta = \hat{f}_i^v \tag{3-125}$$

Elimination of the vapour and liquid fugacities in favour of the fugacity and activity coefficients for a binary system results in:

$$y_1 \Phi_1 P = x_1^\alpha \gamma_1^\alpha P_1^{sat} = x_1^\beta \gamma_1^\beta P_1^{sat} \tag{3-126}$$

$$y_2 \Phi_2 P = x_2^\alpha \gamma_2^\alpha P_2^{sat} = x_2^\beta \gamma_2^\beta P_2^{sat} \tag{3-127}$$

From Equations (3-126) and (3-127), a total of five variables (x_1^{α} , x_1^{β} , y_1, T and P) need to be solved for. From the Gibbs phase rule, when one of the variables is specified (usually either P or T), the other four variables can be solved for.

3.5.1 VLLE Data Regression

Since VLLE is concerned with two liquid phases, any liquid phase activity coefficient model used in the regression of VLLE data must necessarily pass the stability criterion. The regression technique used for VLLE data depends on whether the data are for an isothermal or isobaric system. Walas (1985) provides good guidelines for solving each case using one of two methods:

1. Solve directly the system of equations representing material balances and equilibria between phases.
2. Find the minimum Gibbs energy of the overall mixture. In this case the variables are the amounts and compositions of all the phases and the minimum is constrained subject to the mole fractions summing to unity in each phase.

Regression using an EoS was not considered as this method is only important for high pressure LLE regression. The regression procedure made use of the virial EoS with the second virial coefficient correlation of Tsonopoulos (1974) to account for the vapour phase non-idealities. The TK-Wilson, NRTL and modified UNIQUAC liquid phase activity coefficient models were used to describe the two liquid phase non-idealities.

3.6 Thermodynamic Consistency Tests

With regards to binary VLE data, a system is said to be "over specified" when the temperature, pressure, vapour and liquid compositions are all measured. This "over specification" however enables thermodynamic consistency of the VLE data. Usually the vapour compositions (y_i values) contain the greatest error and therefore thermodynamic consistency tests often focus on the vapour compositions to determine thermodynamic consistency of the VLE data.

Thermodynamic consistency tests are based on the Gibbs-Duhem equation that was introduced in Section 3.2 as Equation (3-86). If VLE data conform to the Gibbs-Duhem equation, then the data are said to be thermodynamically consistent. This subject matter has received much attention in the

literature and thus many adaptations of the of the Gibbs-Duhem equation have been introduced. One of the earliest used thermodynamic consistency tests is the *slope test*. This test compares slopes of curves drawn to fit $\ln\gamma_1$ and $\ln\gamma_2$ vs x_1 graphs. This test was rather tedious and also led to uncertainty (Van Ness, 1995). Thus another test known as the *area test* was introduced as an improvement over the *slope test* (Herington, 1947 and Redlich and Kister, 1948). According to Walas (1985), the *area test* is necessary but insufficient as individual data points that are inconsistent could actually compensate/cancel each other. For example, the pressure is cancelled off and therefore one of the most accurately measured system properties is lost. Hence, the test could actually pass data sets that were inconsistent and also fail data sets that actually were consistent. For this reason the *area test* was not considered for this study but rather two well-known thermodynamic consistency tests were used: the *point test* of Van Ness et al. (1973) and the *direct test* of Van Ness (1995).

One should note that thermodynamic consistency testing cannot be used for VLE data measured with the static synthetic method since the vapour compositions are not measured. Also, LLE data cannot be tested for thermodynamic consistency as well (Raal and Mühlbauer, 1998). This is due to two reasons: firstly, individual activity coefficients cannot be determined directly since the experimental LLE data furnish only a ratio of activity coefficients. Secondly, the LLE data do not extend over a continuous composition range, which is a requirement for thermodynamic consistency testing.

VLLE data however can be tested for thermodynamic consistency with the point test but only for the homogenous (VLE) region. The direct test on the other hand can be applied to the entire composition range.

3.6.1 The Point Test

The *point test* was introduced by Van Ness et al. (1973) as an improvement to the *area test*. Generally the vapour compositions introduce the most error to VLE data measurement and are therefore used to test for thermodynamic consistency. The *point test* simply compares the measured vapour compositions (y_{exp}) to the calculated values (y_{calc}) where the calculated values are determined from data regression using the combined or the direct method. The comparison of the experimental and the calculated values generate residuals, Δy, which gives an indication of the consistency of the VLE data. Hence the *point test* is model dependent. Danner and Gess (1990) provide a quantitative

criterion for the consistency of VLE data by proposing that the absolute average deviation (AAD) should be less than 0.01 for the data to be thermodynamically consistent.

$$AAD = \frac{1}{n}\sum_{i=1}^{n}\left|\Delta y - \Delta\bar{y}\right| \tag{3-128}$$

where n refers to the number of experimental data points, Δy is the difference between the experimental and the calculated value and $\Delta\bar{y}$ is the average difference between the experimental and the calculated value. The AAD is not the only criterion used in the *point test*. The test also requires that a plot of Δy vs y_1 should scatter about zero to indicate thermodynamic consistency.

3.6.2 The Direct Test

The *direct test* was developed by Van Ness (1995) as a direct test of thermodynamic consistency for each point of a VLE data set with respect the Gibbs-Duhem equation itself. The test makes use of the following definitions:

$$\varepsilon_P^* = \frac{V^E}{RT}\frac{dP}{dx_1} \tag{3-129}$$

$$\varepsilon_T^* = \frac{-H^E}{RT^2}\frac{dT}{dx_1} \tag{3-130}$$

where ε_P^* is zero for isobaric data and ε_T^* is zero for isothermal data and consequently only one ε term is required for the derivation of the direct test. Using Equations (3-81) and (3-86) for one mole of liquid phase and with $g = G^E / RT$ results in:

$$\frac{dg}{dx_1} = \ln\frac{\gamma_1}{\gamma_2} + \varepsilon^* \tag{3-131}$$

$$x_1\frac{d\ln\gamma_1}{dx_1} + x_2\frac{d\ln\gamma_2}{dx_1} - \varepsilon^* = 0 \tag{3-132}$$

where ε^* depends on the nature of the VLE data (either isobaric or isothermal). Using Equation (3-85) for a binary system:

$$g = x_1 \ln \gamma_1 + x_2 \ln \gamma_2 \tag{3-133}$$

If the experimental value of g is replaced with g^{exp} and differentiating Equation (3-133) with respect to x_1:

$$\frac{dg^{\exp}}{dx_1} = x_1 \frac{d \ln \gamma_1^{\exp}}{dx_1} + \ln \gamma_1^{\exp} + x_2 \frac{d \ln \gamma_2^{\exp}}{dx_1} - \ln \gamma_2^{\exp} \tag{3-134}$$

which may alternatively be written as:

$$\frac{dg^{\exp}}{dx_1} = \ln \frac{\gamma_1^{\exp}}{\gamma_2^{\exp}} + \varepsilon + x_1 \frac{d \ln \gamma_1^{\exp}}{dx_1} + x_2 \frac{d \ln \gamma_2^{\exp}}{dx_1} - \varepsilon^* \tag{3-135}$$

Subtracting Equation (3-135) from Equation (1-131) and writing it in the terms of residuals ($\delta g = g - g^{exp}$), yields:

$$\frac{d(\delta g)}{dx_1} = \delta \ln \frac{\gamma_1}{\gamma_2} - \left(x_1 \frac{d \ln \gamma_1^{\exp}}{dx_1} + x_2 \frac{d \ln \gamma_2^{\exp}}{dx_1} - \varepsilon^* \right) \tag{3-136}$$

Now if an isothermal or isobaric data set is reduced with $\sum (\delta g)^2$ as the objective function, then the term $d(\delta g) / dx_1$ is effectively zero. Hence:

$$\delta \ln \frac{\gamma_1}{\gamma_2} = x_1 \frac{d \ln \gamma_1^{\exp}}{dx_1} + x_2 \frac{d \ln \gamma_2^{\exp}}{dx_1} - \varepsilon^* \tag{3-137}$$

From the Gibbs-Duhem equation, the right hand side of Equation (3-137) is required to be zero for thermodynamically consistent data and the residual on the left hand side provides a direct measure of deviations from the Gibbs-Duhem equation. The extent to which values of this residual fail to scatter about zero provides a measure of the departure from thermodynamic consistency, which Van Ness (1995) expressed in the form of a consistency index. Table 3-2 shows this consistency index as

a quantitative criterion, where an index of one signifies excellent data and an index of ten very poor data.

Table 3-2: Consistency index for the *direct test* of Van Ness (1995) with the root mean square values (RMSD).

Index	RMSD $\delta\ln(\gamma_1/\gamma_2)$	
1	>0	≤0.025
2	>0.025	≤0.050
3	>0.050	≤0.075
4	>0.075	≤0.100
5	>0.100	≤0.125
6	>0.125	≤0.150
7	>0.150	≤0.175
8	>0.175	≤0.200
9	>0.200	≤0.225
10	>0.225	

Ce chapitre fournit les informations détaillées sur l'appareil récemment développé. La cellule d'équilibre est construite autour d'un cylindre en saphir, acheté auprès de Rayotek Scientific Inc., ce cylindre a un volume interne d'environ 17.4 cm^3. Le saphir a été choisi en raison de ses propriétés optiques, et de résistance à la fois mécanique et chimique. L'acier inoxydable (type 316) est employé comme matériau principal pour construire les diverses pièces de l'équipement à cause de sa résistance mécanique et chimique, de son usinage facile et de ses caractéristiques favorables de soudage. La version mobile de l'échantillonneur électromagnétique : « Rapid On Line Sampling Injector » ROLSI™ est utilisée pour échantillonner à divers niveaux dans la cellule d'équilibre chacune des phases en équilibre, une nouvelle technique d'échantillonnage est également développée pour limiter la perturbation de pression dans la cellule d'équilibre quand un échantillonneur ROLSI™ mobile est employé. La technique se sert d'un doigt métallique dans un arrangement qui maintient un volume constant dans la cellule d'équilibre pendant le prélèvement. L'homogénéisation du contenu de la cellule d'équilibre est réalisée au moyen d'un agitateur magnétique revêtu de téflon qui est activé par un aimant extérieurement entrainé par un moteur. Un bain d'huile permet la régulation thermique de la cellule d'équilibre pour les mesures à hautes températures entreprises dans cette étude. La cellule d'équilibre est maintenue dans une position fixe alors qu'un élévateur mécanique sert à immerger la cellule d'équilibre dans son environnement thermique. La température de la cellule d'équilibre est mesurée à l'aide de deux sondes REB modèles Pt100 de classe A avec bulbe en céramique. L'une des sondes est placée en haut et l'autre au fond de la cellule d'équilibre. Les deux sondes ont une précision de 0.05 K dans le domaine 298 à 355 K et une précision de 0.07 K dans le domaine 355+ à 465 K.

La pression dans la cellule d'équilibre est mesurée à l'aide du capteur de pression absolue 0 – 1 bar, modèle P-10 de WIKA pour des pressions sous-atmosphériques et à l'aide du capteur de pression absolue 0 – 16 bar, modèle P-10 de WIKA des 0 - 16 pour les pressions supérieures. Le capteur « basse pression » a une précision de 0.02 kPa pour une gamme de 5 à 99 kPa, tandis que l'autre a une précision de 0.9 kPa pour une gamme de 97 à 1313 kPa. Les acquisitions numériques sont obtenues avec le boitier d'acquisition 34970A de Agilent.

La composition chimique de chaque phase à l'équilibre est déterminée en utilisant un chromatographe phase gazeuse modèle 2014 de Shimadzu possédant un détecteur à conductivité thermique, étalonné. Des cartouches chauffantes et du fil nichrome sont employés pour le chauffage électrique pour éviter tout point froid sur les lignes de transferts des échantillons. Avant toute mesure, chaque produit chimique est dégazé suivant la méthode de distillation sous vide de

Van N ess e t A bbott (1978) m oyennant l'emploi d' une c olonne de fractionnement de type « Vigreux ».

4

CHAPTER FOUR

EQUIPMENT DESCRIPTION

In order to successfully design an experimental apparatus, one has to carefully consider the objective of the design together with the factors that constrain the design. According to Sinnott (2005), these constraints can either be fixed, invariable or due to physical laws. It could also be restricted by government regulations and standards whilst other constraints are less strict to allow the designer flexibility to achieve the best design. Usually the design of an experimental apparatus is not entirely novel but builds on existing designs with minor changes. The Thermodynamics Research Unit within the University of KwaZulu-Natal has over the past 25 years successfully developed many phase equilibrium equipment designs covering both static and dynamic equipment. However, all of these equipments require rather large amounts of chemicals (on average 120 cm^3) in order to carry out phase equilibrium measurements. Chemical companies/industries often find it expensive to physically synthesize large volumes of high purity chemicals. In light of this, phase equilibrium measurements on these equipment would prove rather costly as large quantities of chemicals would be required to complete phase equilibrium measurements. Therefore, the main objective of this study was to successfully design, develop and commission a new static analytical apparatus capable of carrying out both vapour pressure and phase equilibrium of multiple liquid and vapour phases for small volumes of chemicals (less than 20 cm^3). As mentioned previously, Laugier and Richon (1986) state that there is no equipment capable of measurement for all operating conditions and physical properties of chemicals.

The equipment for this study would allow for an operating temperature range from 253 to 473 K and an operating pressure range from absolute vacuum to 1600 kPa. This chapter focuses on the following experimental features:

- Description of the equilibrium cell and its housing
- Sampling technique and assembly
- Method of agitation within the equilibrium cell
- Isothermal environment for the equilibrium cell
- Temperature and pressure measurement
- Composition analysis
- Data logging
- Degassing apparatus
- Compression device for cell loading
- Safety features
- Overview

4.1 Description of the Equilibrium Cell and its Housing

The equilibrium cell, which is the heart of the experimental equipment used in this study, was constructed around a sapphire cylinder. The optical properties of sapphire make it suitable to view phase separation within the cell which is important prior to sampling. "*Apart from its optical properties useful within its transmission range, sapphire is by far the strongest, toughest and chemically resistant material available. It can also be used at far higher temperatures and pressures than most optical materials. Sapphire also has a high thermal conductivity despite its extreme electrical non-conductivity"* (General Ruby and Sapphire Company). The sapphire cell was constructed by and purchased from Rayotek Scientific Inc., with the following dimensions: 35.60 mm (±0.05 mm) outer diameter, 17.80 mm (±0.10 mm) internal diameter and 70.00 mm height. This results in an approximate internal volume of 17.4 cm^3 for the equilibrium cell.

The equilibrium cell was enclosed within two 316 stainless steel (316 SS) flanges of 15 mm thickness and 110 mm diameter each, by three evenly distributed 316 SS spacer rods of 10 mm diameter. The properties of 316 SS make it desirable to use in many industrial applications. One of the remarkable properties of this material is its mechanical strength (such as high tensile and yield strength) and the ability to retain these properties for long periods of time under extreme high or low temperatures (Sinnott, 2005). Apart from its mechanical strength properties, 316 SS is also more attractively known for its corrosion resistance and is thus widely used for many laboratory applications. Stainless steel is known to succumb to pitting and crevice corrosion in warm chloride environments, however, the addition of 2% molybdenum to 304 SS to produce 316 SS offers a

significant increase in resistance to pitting (Fontana and Greene, 1967). Furthermore, no such chloride environments were used in this study. The 316 SS material also has very good welding and machining properties making it suitable to use in the construction of various equipment parts. Economically, 316 SS is considered a medium cost material when compared to carbon steel (low cost) and titanium (high cost). Hence considering all these key factors, 316 SS was thus chosen as the principal material of construction for this study.

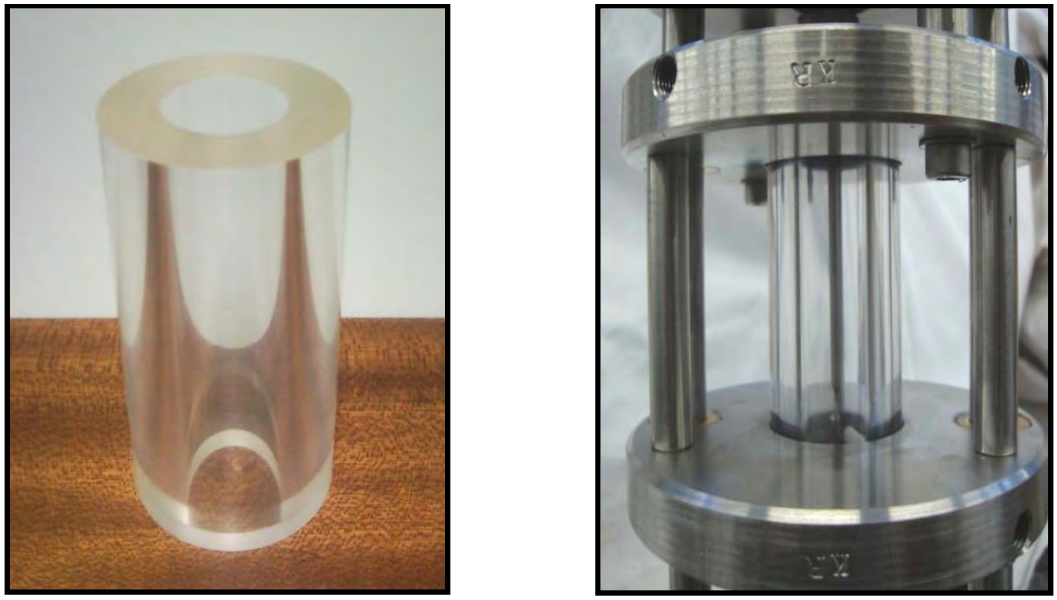

(a) **(b)**

Photograph 4-1: (a) The sapphire equilibrium cell and (b) the cell housed within two 316 stainless steel flanges.

In order to prevent leaks within the equilibrium cell, two O-rings are used at each end of the cell to provide a seal for the equilibrium cell. At each end of the cell, one of the O-rings (19 mm internal diameter) is situated in a groove to provide a seal from the bottom/top whilst the other O-ring (35 mm internal diameter) is situated in a groove on the near bottom/top side of the cell to provide an extra seal against leaks (see Photograph 4-2). The material of the O-rings depends on the nature of the chemicals used to carry out phase equilibrium measurements. For systems explicitly containing alcohols, ketones, esters and ethers, Ethylene Propylene Diene Monomer (EPDM) O-rings were used whilst perfluoroelastomer O-rings were used for systems containing (in addition to the above mentioned groups) alkanes, alkenes and nitriles as it has good compatibility with a wider range of chemical functional groups.

Photograph 4-2: The O-rings in the upper 316 stainless steel flange that seal the equilibrium cell.

The upper 316 SS flange of the equilibrium cell contains the following on its side:

i) 1 × 6 mm diameter hole machined in such a manner that it narrows to a 3 mm diameter upon entry into the equilibrium cell. This is used for the feed line with a $^{1}/_{8}$ inch OD SS pipe fitting.

ii) 1 × 6 mm diameter hole also machined in such a manner that it narrows to a 3 mm diameter upon entry into the equilibrium cell. This is used for the pressure measurement line with a $^{1}/_{8}$ inch OD SS pipe fitting.

iii) 1 × 6 mm diameter hole with a depth of 30 mm to accommodate a heater cartridge.

iv) 2 × 6 mm diameter holes with a depth of 30 mm each to accommodate two temperature probes (explained further in Section 4.5).

The top of the upper 316 SS flange contains a 16 mm diameter hole with M16 threads and 2 mm pitch to cater for the sampling device used (explained in more detail in Section 4.2).

The lower 316 SS flange of the equilibrium cell contains the following:

i) 1 × 6 mm diameter hole machined in such a manner that it narrows to a 3 mm diameter upon entry into the equilibrium cell. This is used for the drain line with a $^{1}/_{8}$ inch OD SS pipe fitting.

ii) 1 × 6 mm diameter hole with a depth of 30 mm to accommodate a temperature probe.

To minimize dead volume, the feed and drain valves are located as close as possible to the equilibrium cell and the connecting line from the equilibrium cell to the pressure transmitters are kept to a minimum. The WIKA model P-10 pressure transmitters for this study contain negligible dead volume. Thus the total dead volume is estimated at 0.9 cm^3.

4.2 Sampling Technique and Assembly

For this study, the accurate composition analysis of equilibrium phases is achieved using an electromagnetic version Rapid-On-Line-Sampler-Injector (ROLSI™) (Guilbot et al., 2000). A schematic diagram of the ROLSI™ was shown earlier as Figure 2-12 in Chapter 2. To promote versatility for the measurement of multiple liquid and vapour phases in equilibrium, a single ROLSI™ is utilized. This means that the ROLSI™ must be mobile within the equilibrium cell to sample all phases. Since the interior volume of the equilibrium cell is small (approximately 17.4 cm^3), it is anticipated that the movement of the ROLSI™ within the equilibrium cell causes an appreciable change in volume and hence a change of pressure during sampling. To counter this shortcoming, a novel technique is designed for sampling. In order to keep the volume within the equilibrium cell constant during sampling, the volume displaced by the capillary of the ROLSI™ must be compensated for by a similar mechanism. To achieve this, a 316 SS dowel with similar dimensions to that of the capillary of the ROLSI™ is operated from the bottom of the cell. The idea centered on creating an arrangement such that when the capillary of the ROLSI™ moved within the equilibrium cell during sampling, the 316 SS dowel would simultaneously move in the same direction thereby keeping the volume within the equilibrium cell constant. This concept was discussed with the supervisor, Prof. D. Ramjugernath.

The ROLSI™ is mounted on a 316 SS flange of 15 mm thickness and 110 mm diameter with a 45 mm diameter cutaway in the center for the base of the ROLSI™. The capillary of the ROLSI™ enters into the equilibrium cell via a 16 mm diameter hole with M16 threads and 2 mm pitch from the upper flange of the equilibrium cell. To provide a seal at the entry point of the capillary of the ROLSI™ into the equilibrium cell, Techtron HVP polyphenylene sulfide (Techtron HVP PPS) is used as a sealant. Techtron HVP PPS offers extreme wear resistance as well as resistance to a wide variety of organic and inorganic chemicals. Furthermore, Techtron HVP PPS has a maximum allowable operating temperature of 493 K and preserves excellent dimensional stability despite temperature variation and chemical attack (Professional Plastics).

Extra sealing is provided by using a perfluoroelastomer O-ring on top of the Teflon sealant with a stainless steel washer that is tightly sealed with a nut. Three spacer 316 SS rods of 10 mm diameter and 155 mm length each were used to attach the flange on which the ROLSI™ base was mounted to another 110 mm diameter and 15 mm thick 316 SS flange (upper flange of the ROLSI™) to maintain a fixed height for the ROLSI™. The ROLSI™ is made movable by use of a 170 mm

length shaft with M16 threads and 2 mm pitch, attached from the upper flange of the ROLSI™ to a 316 SS turn-dial. Two 316 SS guide rods of 12 mm diameter and 250 mm length are used to connect the upper flange of the equilibrium cell to the base flange (110 mm diameter and 28 mm thickness) of the turn-dial. The shaft contains a slot where a pin is fitted to act as a guide mechanism to prevent misalignment of the arrangement. The operation of the turn-dial with this set of connections moves the upper flange of the ROLSI™. This causes the lower flange of the ROLSI™ to simultaneously move (due to the spacer rods between the flanges), thereby moving the capillary of the ROLSI™ within the equilibrium cell (see Figure 4-1).

The challenge remained to simultaneously move the 316 SS dowel with the capillary of the ROLSI™. This is achieved by using two 316 SS guide rods of 12 mm diameter and 200 mm length to attach the flange on which the ROLSI™ is mounted to another 316 SS flange (110 mm diameter and 15 mm thickness) where the 316 SS dowel is mounted (directly below the equilibrium cell). Hence, when the capillary of the ROLSI™ moves within the equilibrium cell, the 316 SS dowel moves in the same direction thereby maintaining a constant volume within the equilibrium cell. The 316 SS dowel enters the equilibrium cell via a 16 mm diameter hole with M16 threads and 2 mm pitch from the bottom flange of the equilibrium cell. The method of sealing is the same to that of the ROLSI™ capillary (explained above).

4.3 Method of Agitation within the Equilibrium Cell

Agitation within the equilibrium cell promotes the establishment of thermodynamic equilibrium in a shorter time. The most common method of agitation used by researchers (as discussed in Chapter 2) makes use of a magnetic stirrer driven by a magnet via a motor. Usually the magnetic stirrer is placed within the equilibrium cell and is agitated from the bottom of the cell. This same concept is employed in this study. However, since the space below the equilibrium cell is already utilized for the metallic dowel arrangement for the sampling mechanism, an alternate positioning for the magnet and motor must be found. This is achieved by mounting a bracket for the motor on the bottom 316 SS flange of the equilibrium cell to support the motor. The motor is positioned such that it is always above the liquid level of the bath when the cell is immersed into the liquid bath. The magnet for stirring is positioned at the side of the equilibrium cell and linked to the motor by a pulley mechanism using a stainless steel chain to prevent slippage. The motor, driven by a DC power supply, allows the magnetic stirrer within the equilibrium cell to rotate near the bottom of the equilibrium cell. A schematic of the assembly set-up is shown in Figure 4-1.

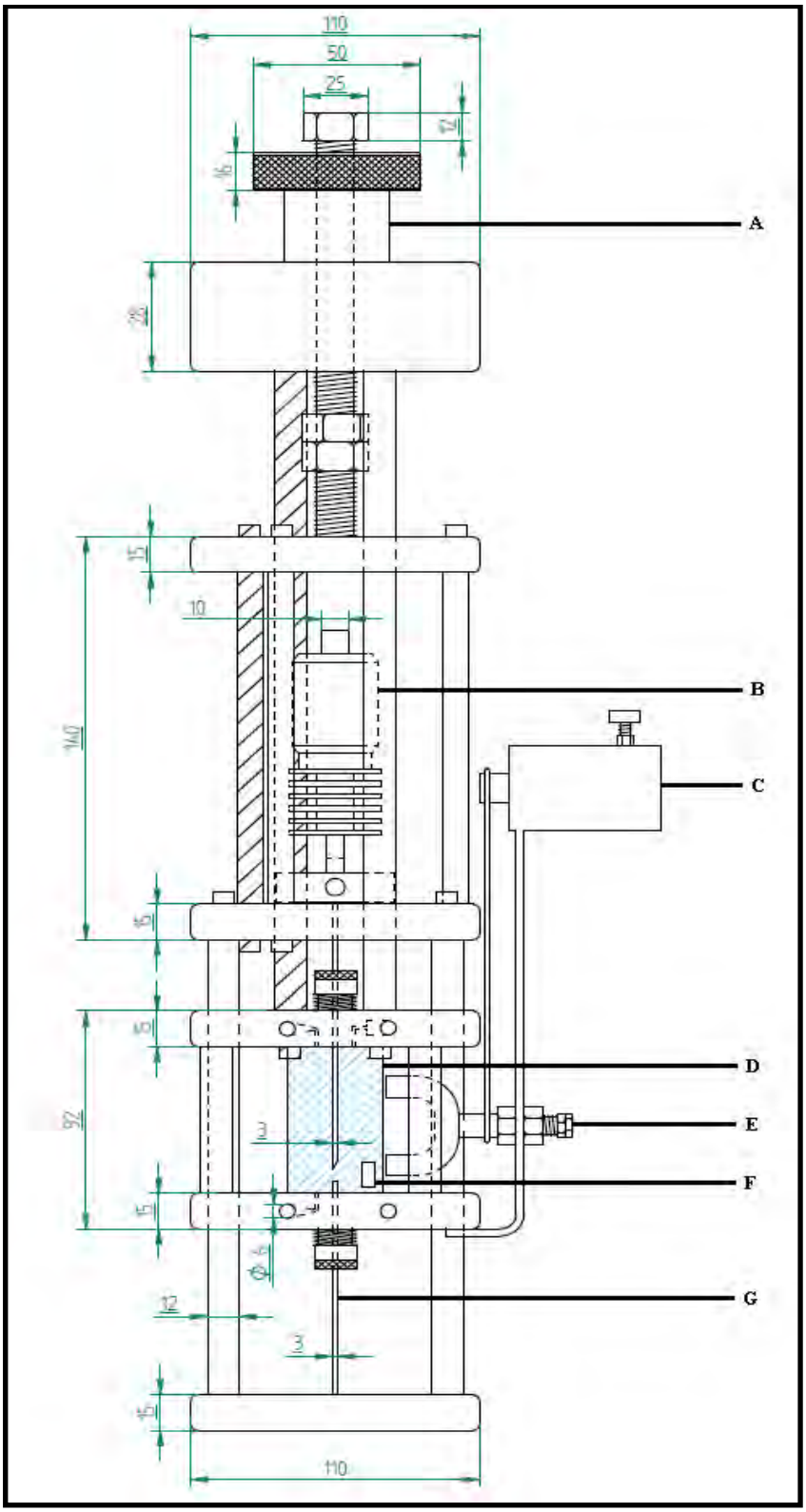

Figure 4-1: Schematic of the equilibrium cell assembly.

A: turn-dial; B: ROLSI™; C: motor for stirrer; D: equilibrium cell; E: stirrer assembly; F: magnetic stirrer; G: metallic dowel.

When compared to conventional stirring at the bottom of the equilibrium cell, the proposed arrangement of stirring provides efficient stirring and did not seem to have an adverse effect on the thermodynamic equilibrium time. From experimental observations, an average of 40 minutes is required for the system to reach thermodynamic equilibrium. A system is said to be at thermodynamic equilibrium when the system temperature and pressure are constant within experimental uncertainties for at least 15 minutes and the vapour and liquid samples withdrawn with the ROLSI™ for at least 5 samples are constant within experimental uncertainties.

4.4 Isothermal Environment for the Equilibrium Cell

Gas (e.g. air and nitrogen) and liquid (e.g. water and oil) baths are the two most common thermal environments used by researchers (as discussed in Chapter 2). Liquid baths are favoured as it avoids the long times required for thermal stability when compared to gas baths. The bath used in this study is custom-made with the following dimensions: 545 mm length, 340 mm width and 280 mm depth for the exterior cover and 485 mm length, 300 mm width and 260 mm depth for the interior lining. The exterior cover is made from 0.8 mm galvanized steel and the interior lining made from 304 type stainless steel. Fiberfrax is used as the insulation material between the interior lining and the exterior cover of the bath since it offers high temperature stability and low thermal conductivity (Slumpys). The bath is custom-made specifically for the depth in order to cater for the complete submersion of the equilibrium cell into the liquid of the bath.

Since the experimental work carried out in this study was to be done at high temperatures, silicone oil is chosen as the heating medium for the thermal environment. Silicon oil (SI-044) is a water-clear silicone fluid with a wide viscosity range. This would thus enable observation during experiments. Other important features of silicone oil include: *little change in physical properties over a wide temperature range, the fluid can be used from 233 to 553 K, it has a low surface tension so the fluid wets clean surfaces and it also has low toxicity* (Power Chemical Corporation).

In order to immerse the equilibrium cell into the oil, the equilibrium cell assembly is held at a fixed position on an iron framework and a mechanical jack is used to lift the oil bath. The iron framework is also used as a guide for the oil bath in order to prevent it from falling over. Removing the cell from the oil bath is accomplished by simply using the mechanical jack to lower the oil bath. Photograph 4-3 shows the iron framework and the two positions of the oil bath.

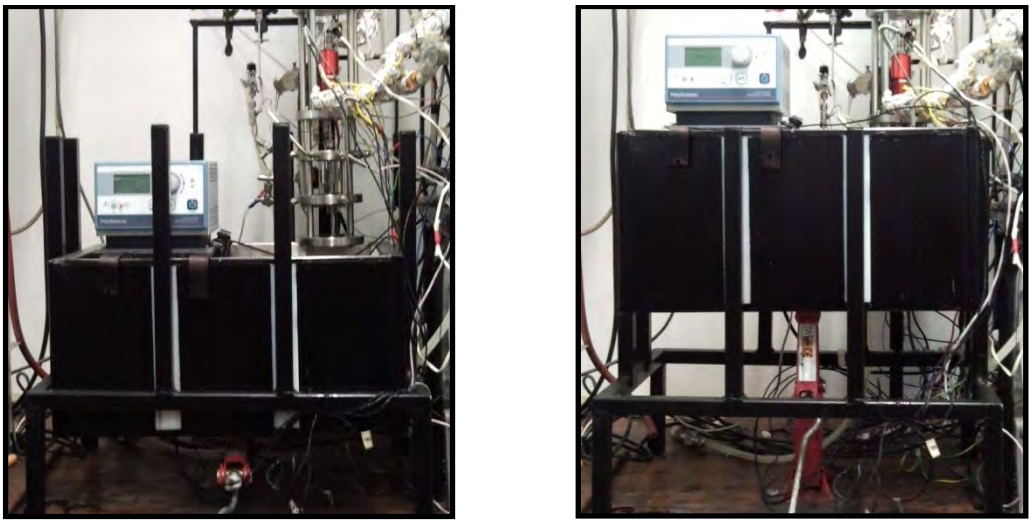

(a) **(b)**

Photograph 4-3: The iron framework for the oil bath and fixed position of the equilibrium cell with the mechanical jack used to (a) lower the oil bath and (b) to raise the oil bath.

In order to minimize heat leaks and conductive paths, the equilibrium cell is immersed within the oil bath such that at least 40 mm of liquid is above the upper 316 S S flange of the equilibrium cell. Since the top of the oil bath could not be covered with a lid, odd pieces of galvanized steel were wrapped in fiberfrax and aluminum foil and carefully placed on top of the oil bath to form a cover-lid for the oil bath to help minimize heat losses to the environment. However for higher temperatures, these provisions alone did not prove to be sufficient. This was evident from the temperature of the upper 316 SS flange of the equilibrium cell being approximately 0.7 K lower than the temperature of the lower 316 SS flange of the equilibrium cell for a temperature setting of 373 K. To overcome this, a 6 mm diameter and 30 mm hole is drilled into the upper 316 SS flange of the equilibrium cell to accommodate, a 3 mm diameter and 190 mm length with a 90 ^{o} bend 70 mm from the tip, heater cartridge with 100 W power rating. The heater cartridge is powered by an ACDC 1kVA voltage regulator model TDGC2. Another 6 mm diameter and 30 mm hole is drilled into the upper 316 S S flange of the equilibrium cell to accommodate a WIKA model REB Pt100 with class A ceramic bulb type sensor temperature probe, of $^{1}/_{8}$ inch diameter and 40 mm length. The temperature reading of this probe is controlled by a Shinko ACS – 13A digital indicating controller. The temperature probe is calibrated using the WIKA CTB 9100 temperature calibration unit. The precision of the temperature probe is within 0.04 K error for a temperature range of 303 to 465 K. The calibration graph is presented in Appendix C as Figures C-9 and C-10. This arrangement compensates for heat losses to the environment and conductive paths (parts of the cell assembly that protrude out of the oil bath).

4.5 Temperature and Pressure Measurement

4.5.1 Temperature Measurement

The bath temperature is controlled using a Polyscience model 7312 programmable temperature controller capable of maintaining temperature stability to within 0.02 K. Statistically, this implies a standard deviation of 0.01 K. The temperature measurement of the equilibrium cell is taken via the temperature measurement of the two 316 SS flanges that encased the equilibrium cell. A hole of 6 mm diameter and 30 mm depth is drilled into each of the 316 SS flanges to accommodate for the temperature measurement. Two WIKA model REB Pt100 with class A ceramic bulb type sensor temperature probes, one of $^{1}/_{8}$ inch diameter and 270 mm length with a 90 ^{o} bend 70 mm from the tip, is used for the lower 316 SS flange and the other of $^{1}/_{8}$ inch diameter and 190 mm length with a 90 ^{o} bend 70 mm from the tip, is used for the upper 316 SS flange. The temperature probes are connected to a 34970A Agilent data acquisition unit through which the temperatures are read and logged via a computer. All the temperature probes are calibrated using the WIKA CTB 9100 temperature calibration unit. The overall (calibration and repeatability) precision of the temperature probes for the upper and lower 316 SS flanges of the equilibrium cell are within 0.05 K error for a temperature range of 298 to 355 K and 0.07 K error for a temperature range of 354 to 465 K. The calibration graphs are presented in Appendix C as Figures C-1 to C-8.

4.5.2 Pressure Measurement

To obtain the pressure readings, two pressure transmitters are used for greater precision as opposed to one. For sub-atmospheric pressure readings, a 0 – 100 kPa absolute WIKA model P-10 pressure transmitter is used, whilst for moderate pressure readings, a 0 – 1600 kPa absolute WIKA model P-10 pressure transmitter is used. The pressure transmitters are connected to the equilibrium cell by a single entry point via the upper 316 SS flange using $^{1}/_{8}$ inch OD stainless steel piping and connected to each other by using a stainless steel T-piece. Two ¼ inch stainless steel ball valves are used to manipulate whether one or both of the pressure transmitters would read the pressure within the equilibrium cell. To prevent damage to the low pressure transmitter, the stainless steel ball valve that leads to the low pressure transmitter is closed when the pressure within the equilibrium cell is higher than atmospheric pressure.

To avoid temperature disturbances on the pressure readings, both the low and high pressure transmitters are kept at a constant temperature of 313 K. This is achieved by encasing each pressure

transmitter within separate aluminum blocks that are each heated with two 6 mm diameter and 36 mm length 100 W heater cartridges, powered by an ACDC 1kVA voltage regulator model TDGC2. The temperature in each aluminum block is measured with a 3 mm diameter and 20 mm length class A, 3-wire Pt 100 simplex 316 SS temperature probe and controlled by a Shinko ACS – 13A digital indicating controller. The temperature probes are calibrated using the WIKA CTB 9100 temperature calibration unit.

The low pressure transmitter is calibrated using the WIKA CPH 6000 pressure calibration unit with a WIKA CCP 30 hand test pump and a 0 – 1 bar absolute WIKA CPT 6000 standard pressure transmitter. The moderate pressure transmitter is internally calibrated by measuring the vapour pressure of ethanol and comparing it to literature (Reid et al., 1988). The ethanol literature vapour pressure of Reid et al. (1988) also serves as verification for the low pressure transmitter calibration. The pressure transmitters are also connected to the same 34970A Agilent data acquisition unit as the temperature probes for the equilibrium cell through which the pressures are read and logged via a computer.

The precision for the temperature probes of the low and moderate pressure transmitter aluminum blocks are within 0.02 K error and 0.01 K error respectively for a temperature range of 298 to 371 K. The overall (calibration and repeatability) precision for the low pressure transmitter was within 0.02 kPa error for a pressure range of 5 to 99 kPa and that for the high pressure transmitter was within 0.9 kPa error for a pressure range of 97 to 1313 kPa. The calibration graphs are presented in Appendix C from Figures C-25 to C-28.

4.6 Composition Analysis

The equilibrium phase samples in this study are analyzed by gas chromatography using a Shimadzu 2014 gas chromatograph (GC) which is fitted with a thermal conductivity detector (TCD). A 0.32 mm ID, 30 m length and 0.25 μm film thickness crosslinked 5 % PH ME silicone Hewlett Packard 5 (HP5) capillary column is used for the analysis with helium as the carrier gas. A TCD is used to detect the presence of water as an impurity. The GC Solutions software package is used to convert the output signal from the GC to a peak area signal and perform integration. The calibration of the TCD is then used to determine the phase composition of the samples.

A single ROLSI™ is used to sample vapour and liquid equilibrium phases. The ROLSI™ contains a differential screw that is used to adjust the path of the ROLSI™ stem, closing the end of the capillary. This path controls the pressure drop at the capillary exit and hence the amount of sample withdrawn in a given opening time, monitored by a Crouzet TOP 948 electronic timer. A 6 mm diameter and 42 mm length heater cartridge of 200 W power rating is used to heat the expansion chamber of the ROLSI™. This is done to completely vapourise the liquid samples rapidly for good chromatographic analysis. The heater cartridge in the expansion chamber of the ROLSI™ is heated by use of an ACDC 1kVA voltage regulator model TDGC2. The temperature within the expansion chamber is measured with a 1.5 mm by 2 mm class A, 3-wire Pt 100 surface element and controlled by a Shinko ACS – 13A digital indicating controller. The surface element is calibrated using the WIKA CTB 9100 temperature calibration unit. The precision of the surface element is within 0.04 K error for a temperature range of 330 to 465 K. The calibration graph is presented in Appendix C as Figures C-15 and C-16.

The ROLSI™ is connected to the GC via a 6-port GC sampling valve and $^{1}/_{16}$ inch OD stainless steel lines. This 6-port valve is the same type used by Ramjugernath (2000) as discussed in Chapter 2. The 6-port GC sampling valve is manufactured by Shimadzu to withstand high temperatures and pressures. The 6-port GC sampling valve enables the withdrawn sample to be swept by the carrier gas and taken to the GC for analysis. This allows the calibration procedure of the GC to be carried out separately thus preventing all the $^{1}/_{16}$ inch OD stainless steel lines from becoming contaminated. The 6-port GC sampling valve is also necessary to carry out sampling for sub-atmospheric measurements. This is necessary since for sub-atmospheric pressures within the equilibrium cell, samples cannot be withdrawn with the ROLSI™ unless the pressure in the ROLSI™ sample circuit is lower (close to absolute vacuum) than the pressure in the equilibrium cell. Thus to enable the vacuum in the ROLSI™ sample circuit, the 6-port GC sampling valve is used in connection with the vacuum pump. However during trial runs of this set-up, the GC displayed a peak with an unusually large tailing effect when the 6-port GC sampling valve was switched. This was most probably due to insufficient sealing in the ROLSI™ for sub-atmospheric operation. This could not be corrected timeously for the study and hence no sub-atmospheric vapour-liquid equilibrium measurements were carried out.

Figure 4-2 shows the two positions of the GC sampling valve. Position A is known as the *flushing* mode, where the $^{1}/_{16}$ inch stainless steel lines and the GC sampling valve are "flushed" from any contaminants by vacuum using a two-stage Edwards RV3 vacuum pump. The vacuum created in

position A also would have enabled sampling during low pressure measurements. It is also used when GC calibrations are carried out. Position B is known as the *sampling* mode, where the sample that is withdrawn from the equilibrium cell by the ROLSI™ is swept by the carrier gas to the GC. The experimental procedures are explained in detail in Chapter 5.

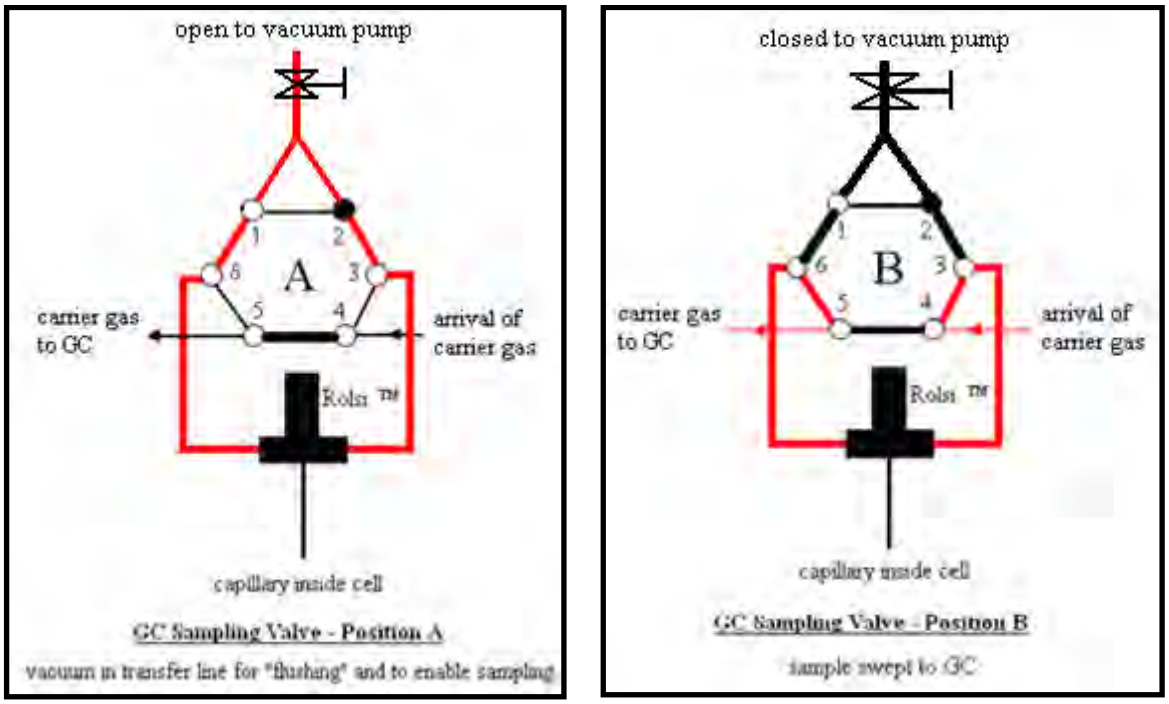

(a) **(b)**

Figure 4-2: Positions of the GC sampling valve during operation for (a) "flushing" and (b) sampling.

Partial condensation of the samples within these lines results in an incorrect determination of the sample composition. Hence in order to prevent this, nichrome wire in an insulation sleeve is carefully wrapped around these lines to avoid any cold points. The nichrome wire is powered by an ACDC 1 kVA voltage regulator model TDGC2. The temperature of the stainless steel lines is measured with a 3 mm diameter and 20 mm length class A, 3-wire Pt 100 simplex 316 SS temperature probe and controlled by a Shinko ACS – 13A digital indicating controller. The temperature probes are calibrated using the WIKA CTB 9100 temperature calibration unit and the temperature of the line is controlled by a Shinko ACS – 13A digital indicating controller. To ensure that there is no partial condensation within the GC sampling valve, the valve is mounted onto an aluminum block that is heated using two 6 mm diameter and 36 mm length 100 W heater cartridges, powered by an ACDC 1kVA voltage regulator model TDGC2. The temperature of the aluminum

block is measured with a 3 mm diameter and 20 mm length class A, 3-wire Pt 100 simplex 316 SS temperature probe and controlled by a Shinko ACS – 13A digital indicating controller.

4.7 Data Logging

The temperatures of the upper and lower 316 SS flanges of the equilibrium cell and the readings from the pressure transmitters are all logged using the 34970A Agilent data acquisition unit. The software allows the user to log the data continuously for a specified time interval between each data point, e.g. the data can be logged every 2 seconds for 100 data points. Once the data has been logged and stored, it can be easily exported to a Microsoft® Excel spreadsheet.

The GC Solutions software is used to convert the output signal from the GC to a peak area signal and perform integration. The calibration of the GC TCD is then used to determine the phase composition of the samples. The user-interface of the 34970A Agilent data acquisition unit and GC Solutions software are shown in Appendix D.

4.8 Degassing Apparatus

The vacuum distillation method of Van Ness and Abbott (1978) is employed in this study. The method made use of boiling the liquid to be degassed in a MRC heating mantle under vacuum followed by distillation with a Vigreux fractionating column. The distillate is then passed through a total condenser where the distillate is returned to the boiling flask, while the highly volatile components (or dissolved gases) are drawn through a fine capillary after escaping the total condenser. The pressure of the degassing apparatus is monitored with a stainless steel vacuum pressure gauge inserted in the vacuum tubing that leads to the apparatus. The total condenser used in this study makes use of a spiral coil and jacket and is shown schematically in Figure 4-3 (a).

The action of boiling is not usually a bubbling process but rather one that occurs by surface evaporation (Van Ness and Abbott, 1978). The Vigreux fractionating column assists in separating the dissolved gases from the liquid by using a condensation-vapourisation cycle. According to Van Ness and Abbott (1978), when a flask containing a certain thoroughly degassed liquid is rapidly inverted, a sharp *metallic click* is heard that presumably results from a sudden collapse of trapped vapour under the liquid head. However, Van Ness and Abbott (1978) also mention that a positive

result from a *click test* is evidently sufficient but not necessary evidence of thorough degassing. Figure 4-7 (b) shows the schematic of the degassing apparatus used in this study.

The boiling flask, Vigreux fractionating column, total condenser and the fitting for the fine capillary are all constructed of glassware, made by a glassblower Mr. P. Siegling, based in Durban, South Africa. Ethanol is used as the cooling medium through the condenser, where a Polyscience KR80A chiller is used to cool the temperature of the ethanol in a liquid bath. The temperature of the ethanol is maintained as low as 253 K by using a Polyscience model PN7306A12E temperature controller. The temperature controller also consists of a liquid pump and is thus used to circulate the ethanol through the total condenser.

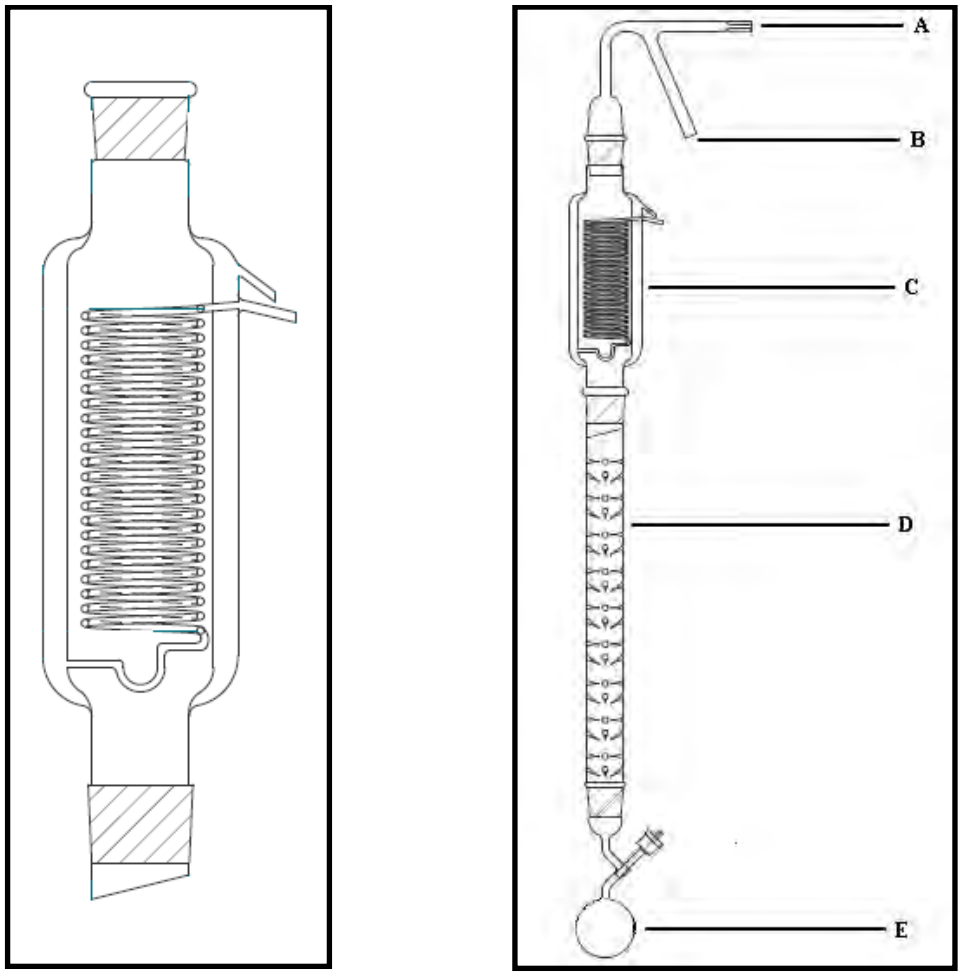

(a) **(b)**

Figure 4-3: Schematic of the (a) total condenser and (b) the degassing unit assembly. A: fine capillary tube to vacuum; B: fitting for air vent; C: total condenser; D: Vigreux fractionating column; E: boiling flask.

4.9 Compression Device for Cell Loading

The equilibrium cell can be initially charged by making use of vacuum and the effect of gravity. However during binary phase equilibrium measurements, each progressive data point is obtained by the addition of the degassed liquids for one of the components. The driving force for the method of addition is pressure. Hence, a compression device is needed to carefully add more of the degassed liquid into the cell. The compression device used in this study is constructed from 316 SS. The main body of the compression device has an OD of 140 mm, ID of 25 mm and length of 135 mm. The piston used to compress the liquid is also made of 316 SS with a diameter of 25 mm and length of 33 mm. Therefore when the piston is fully depressed, the internal volume of the compression device is approximately 50 cm^3. The piston is attached to a shaft of 260 mm length with M16 threads and 2 mm pitch. To indicate the position of the piston within the compression device, a stainless steel rod of 3 mm diameter and 100 mm length is welded onto the piston. Two 316 SS spacer rods of 10 mm diameter and 100 mm length are used to connect the main body of the compression device to a turn-dial. The shaft passes through the turn-dial and contains a slot where a pin is fitted to act as a guide mechanism to prevent misalignment of the arrangement.

Each end of the main body of the compression device contains a cover-lid that is attached to the main body of the compression device by 6 high tensile, 8 mm steel caphead screws. Each cover-lid contains an O-ring to provide an excellent seal. The piston also contains grooves for an O-ring at each end to provide a tight seal. The material of the O-ring is dependent on the nature of chemical used. For alcohols, ketones, esters and ethers, EPDM O-rings are used whilst perfluoroelastomer O-rings are used for alkanes, alkenes and nitriles as it has good compatibility with a wider range of chemical functional groups. A $^1/_8$ inch stainless steel needle valve is attached to one of the cover-lids via an 8 mm diameter hole to control the entry and exit flow of the degassed liquid. The cover-lid and piston are shown in Photograph 4-4. Figure 4-4 shows a schematic of the compression device.

To ensure that the pressure within the compression device is higher than the pressure within the equilibrium cell, a stainless steel gauge pressure (-1 to 25 bar) is inserted into the feed line of the equilibrium cell. The compression device is connected to the equilibrium cell via a three-way stainless steel valve, with the feed line being the common line. The third connection of the three-way valve leads to the vacuum pump. The procedure for charging the equilibrium cell with the compression device is explained in detail in Chapter 5.

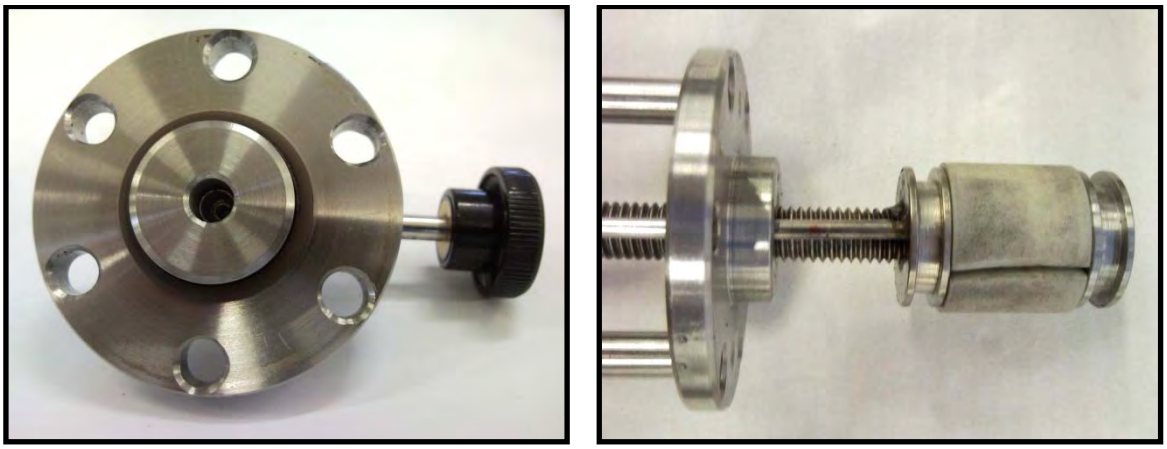

(a) **(b)**

Photograph 4-4: The compression device (a) cover-lid and (b) piston assembly.

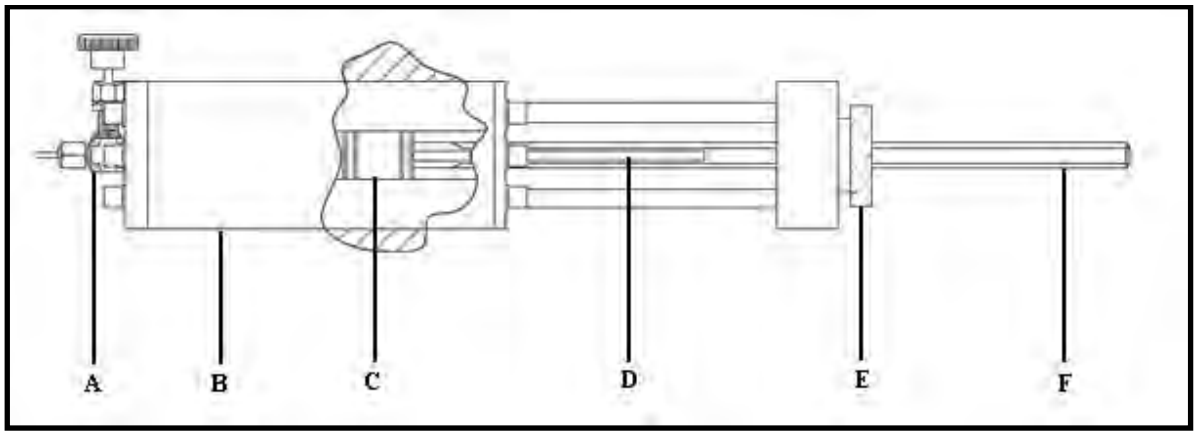

Figure 4-4: Schematic of the compression device.
A: stainless steel needle valve; B: cell body of the compression device; C: piston; D: level indicator for piston; E: turn-dial; F: shaft.

4.10 Safety Features

The process of carrying out experimental work in a laboratory environment necessitates the practice of safety pr ecautions. Most safety precautions are considered in the design of an experimental apparatus. For this study, the following safety precautions were considered:

- The design calculations were done considering a + 100 % over design safety factor. Examples of this include: wall thickness of the equilibrium cell, wall thickness of the auxiliary apparatus, etc.
- A safety relief valve is installed on the line before the pressure transmitters to prevent damage. Furthermore, the pressure transmitters had a 150 % over-pressure safety feature.
- A safety relief valve is also installed in the transfer line where the carrier gas flows from the GC to the GC sampling valve, to prevent a sudden increase of pressure into the GC. The relief valve is strategically placed in this position to avoid any dead volume that would result when the sample is taken from the ROLSI^{TM} and sent to the GC. Any dead volume would necessarily lead to an incorrect determination of the composition as they can accumulate contaminates.
- The equilibrium cell and the degassing apparatus both made use of a single Edwards RV3 vacuum pump. To prevent vapours from corroding the vacuum pump, a cold trap is used before the vacuum tubing entered the vacuum pump. The cold trap made use of liquid nitrogen to condense and trap the vapours before entering the vacuum pump. The line that contained the exhaust vapours of the vacuum pump are sent to the fume hood.
- The exhaust fans within the laboratory are switched on at all times.
- A Perspex shield is placed in front of the degassing apparatus as a safety precaution in the event of an explosion. This ensures that the shards of glassware would not cause injury.
- The material safety data sheets for the chemical used are made visible near the equipment.
- Since high temperature systems are investigated in this study, thermal gloves are worn to open the feed line to the equilibrium cell.
- All the Shinko ACS – 13A digital indicating controllers are mounted within closed boxes such that only the display faces of the controllers could be viewed. This is done to prevent any liquid (for example from an accidental spill) from entering the controllers and causing damage.
- Standard safety precautions of a laboratory must be adhered to at all times within the laboratory. These include: use of a safety glasses and lab coat, use of correct latex gloves when handling chemicals and closed shoes.

4.11 Overview

The design of the static analytical apparatus involved careful considerations and calculations were the main focus was to ensure reliable phase equilibrium measurements for small volumes of chemicals. This resulted in the development of a novel sampling technique that made use of 316 SS compensation rod. This rod was used to maintain a constant interior volume of the equilibrium cell when the mobile ROLSI™ was used during sampling. Auxiliary equipments were also designed to complement the phase equilibrium measurements. This included the design of a degassing apparatus and compression device. Photograph 4-5 shows the experimental set-up in the laboratory.

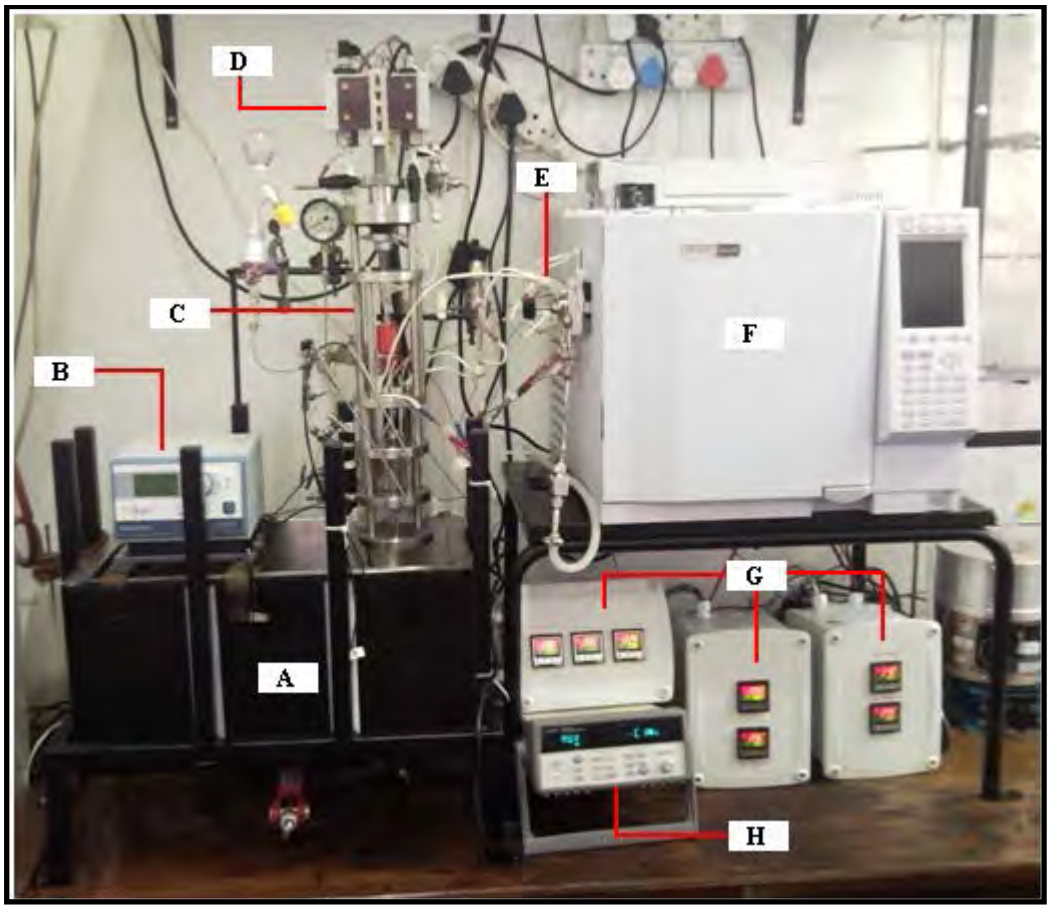

Photograph 4-5: Experimental set-up in the laboratory.

A: oil bath; B: bath temperature controller; C: equilibrium cell assembly; D: pressure transmitters; E: 6-port gas chromatograph sampling valve; F: gas chromatograph; G: Shinko digital temperature controllers; H: data acquisition unit.

Ce chapitre se concentre sur les procédures opérationnelles expérimentales relatives à l'appareil qui vient d'être développé. L'appareillage de dégazage est tout d'abord examiné pour vérifier l'absence de fuites, puis il est nettoyé complètement à l'acétone et mis sous une pression d'environ 5 kPa. De l'éthanol à 253 K est employé au niveau du condensateur pour réduire au maximum les pertes de produit chimique par évaporation. Un dégazage in-situ est préféré lors de l'utilisation de produits chimiques coûteux. Un dispositif de compression a été conçu pour réaliser le transfert du produit chimique dans la cellule d'équilibre en vue des mesures d'équilibres « liquide-vapeur » (ELV). Le dispositif de compression est nettoyé avec de l'éthanol et chargé sous vide par le produit chimique à étudier. Les sondes de la température sont étalonnées au moyen de l'unité d'étalonnage de température : WIKA CTB 9100. Le capteur basse pression est étalonné grâce à l'unité d'étalonnage de pression : WIKA CPH 6000 associée à une presse hydraulique manuelle : CCP 30 de WIKA et au transmetteur de pression standard absolu : 0 - 100 kPa WIKA CPT 6000. Le capteur de pression dit « moyenne pression » a été étalonné par référence à la pression de vapeur de l'éthanol en utilisant les valeurs des tensions de vapeur disponibles dans Reid et al. (1988). Le détecteur du chromatographe en phase gazeuse est étalonné en utilisant la méthode du rapport des surfaces, comme décrit par Raal et Muhlbauer (1998), et ce, pour tous les systèmes en équilibre "liquide-vapeur" mesurés dans cette étude. La méthode de rapport des surfaces évite le problème de la nécessité d'être capable d'injecter des volumes constants et bien définis d'un composant pur. Par contre, c'est la méthode la méthode directe d'injection des composants purs qui a été employée pour l'étalonnage du détecteur du chromatographe en phase gazeuse dans le cas des systèmes non-miscibles étudiés.

Avant d'entreprendre les mesures d'équilibres de phase, l'appareil est complètement testé à la recherche d'éventuelles fuites et nettoyé à l'éthanol. La cellule d'équilibre, garantie sans fuite et propre est alors chargée avec le premier composant. Des mesures de pression de vapeur peuvent alors être faites, après immersion de la cellule d'équilibre dans son environnement thermique, et ce, à chacune des températures désirées.

Pour les mesures à hautes températures, un soin tout particulier est pris pour compenser les pertes de chaleur par conduction et convection dans l'environnement direct en se servant de l'isolation et du chauffage électrique. Les mesures d'ELV sont réalisées de proche en proche par de petites additions du deuxième composant via le dispositif de compression. L'équilibre thermo-dynamique est considéré comme établi quand les valeurs de la température et de la pression sont constantes dans les limites de l'erreur expérimentale durant 30 minutes. Le chauffage électrique de la ligne de

transfert entre la cellule et le chromatographe est activé pour éviter tout risque de condensation partielle. Au moins 5 échantillons de chaque phase sont alors prélevés avec le ROLSI™ mobile et envoyés au chromatographe en phase gazeuse pour analyse afin de tester la répétabilité des résultats compositionnels et estimer leur dispersion. Des mesures d'équilibre (ELL) « liquide-liquide » de binaires sont réalisées après pressurisation à 350 kPa par de l'azote. Le procédé pour des mesures d'ELL est semblable aux mesures d'ELV. Pour des mesures des systèmes binaires en équilibre « liquide-liquide-vapeur » (ELLV), la région à 3 phases est premièrement déterminée comme pour les mesures ELL de binaires puis les régions à deux phases.

5

CHAPTER FIVE

EXPERIMENTAL PROCEDURE

In order to successfully carry out experimental measurements, it is important that the apparatus used be properly operated and calibrated. This is to ensure that variables such as temperature, pressure and composition are accurately measured. This chapter thus focuses on the following sections:

- Preparation and operation of the degassing apparatus
- Preparation and operation of the compression device
- Preparation of the phase equilibrium apparatus
- Calibration procedure for the temperature probes, pressure transmitters and the gas chromatograph (GC) detector
- Operating procedure of the phase equilibrium apparatus for in-situ degassing, vapour pressure, vapour-liquid equilibrium (VLE), liquid-liquid equilibrium (LLE) and vapour-liquid-liquid equilibrium (VLLE) measurements.

This chapter first highlights the preparation and operation of the degassing apparatus and compression device as these equipment are used prior to undertaking phase equilibrium measurements. Emphasis is also placed on the methods of GC detector calibration and phase sampling. The chapter also shows the feasibility of the apparatus by noting the small volume of chemical utilized in each procedure. A schematic of the entire apparatus is presented in Appendix E.

5.1 Degassing Apparatus

5.1.1 Preparation

The vacuum tubing from the degassing apparatus to the Edwards RV3 vacuum pump was firstly checked for any leaks. This involved drawing a vacuum within the degassing unit and isolating the degassing unit overnight. If a significant increase in pressure was observed, other than that of room temperature effects, high vacuum grease was applied to ground glass joints suspected of leaks. Polytetrafluoroethylene (PTFE) tape was used on the stainless steel pipe joints that were suspected of leaking.

5.1.2 Cleaning of the Degassing Apparatus

Cleaning the degassing apparatus was important to remove traces of other chemicals within the apparatus. Before cleaning the degassing apparatus, the Polyscience KR80A chiller was switched on to cool the ethanol in the liquid bath used for the total condenser. The bath temperature controller was set at 253 K. The ethanol was circulated through the total condenser using the built-in liquid pump of the temperature controller. When the temperature of the ethanol was maintained at the set-point (after approximately three hours), cleaning of the degassing apparatus could then begin.

Acetone was used as the cleaning solvent for the degassing apparatus. Approximately 50 cm^3 of acetone was introduced into the boiling flask and the valve of the boiling flask was gently closed. Thereafter the boiling flask was positioned on the heating mantle and carefully inserted into the receiver end of the Vigreux fractionating column assisted with a mechanical jack. High vacuum grease was used to seal the ground glass joint of the boiling flask and the Vigreux fractionating column. The valves of the degassing apparatus and vacuum pump air-vent lines were then closed. Since a common vacuum pump was used for the entire apparatus, all valves for the vacuum tubes leading to equipment other than the degassing apparatus, were closed. The valve for the vacuum tube that led to the degassing apparatus was opened. The glassware for the cold-trap was then cleaned with acetone. A 2 liter insulated flask, that was used as a vessel for the cold-trap fluid (liquid nitrogen), was then filled with liquid nitrogen and the glassware for the cold-trap carefully inserted into the insulated flask.

The vacuum pump was then switched on and the pressure within the degassing unit was monitored from the vacuum pressure gauge. When the pressure within the degassing apparatus stabilized within 1 – 5 kPa, the valve of the boiling flask was partially opened. The heat input from the heating mantle was not necessary as the evaporation of the acetone at such low pressure occurred without any heat input. When the evaporation of the acetone within the degassing apparatus became vigorous, the valve of the vacuum tube that led to the degassing apparatus was partially closed to prevent excess vapours from escaping and entering the vacuum pump. Since the cleaning process occurs at very low pressure, the temperature within the degassing apparatus becomes quite low, resulting in the formation of condensate on the outer glassware. Therefore, absorbent paper was placed around the boiling flask to absorb the condensate that formed on the outer glassware. A time of approximately 10 minutes was allowed for the process of cleaning.

Thereafter, the valve on the vacuum tube that led to the degassing apparatus was closed. The valve of the air-vent line for the vacuum pump was then partially opened before switching the vacuum pump off so that the oil within the vacuum pump would not be "sucked" into the vacuum tubing. The valve of the air-vent line for the degassing apparatus was then slowly opened to release the vacuum within the degassing apparatus. A few minutes were then allowed for the acetone to drip back into the boiling flask. The boiling flask was then disconnected from the Vigreux fractionating column by firstly lowering the position of the heating mantle with the mechanical jack. The acetone in the boiling flask was then discarded into a waste bottle and the remaining acetone within the degassing apparatus was allowed to dry with air. The cleaning procedure was then repeated at least once to ensure the degassing apparatus was thoroughly cleaned.

5.1.3 Operating Procedure of the Degassing Apparatus

The steps followed in the cleaning procedure of the degassing apparatus were also used for the operational procedure. The preparation of the coolant used for the condenser and the cold-trap are as outlined in Section 5.1.2. Approximately 50 cm^3 of the liquid to be degassed was placed into a clean boiling flask and connected to the Vigreux fractionating column with the valve of the boiling flask closed. High vacuum grease was used to seal the ground glass joint of the boiling flask and the Vigreux fractionating column. The valves of the degassing apparatus and vacuum pump air-vent lines were then closed and the valve for the vacuum tube that led to the degassing apparatus was opened. The vacuum pump was then switched on and the pressure within the degassing unit was monitored from the vacuum gauge pressure. When the pressure within the degassing apparatus

stabilized within 1 – 5 kPa, the valve of the boiling flask was not opened as in the cleaning procedure but remained closed for approximately 15 minutes to ensure that the degassing apparatus was free of any acetone residue following the cleaning procedure. This allowed any acetone residue to be vapourised from the degassing apparatus. Once this was done, the valve of the boiling flask was then partially opened.

In order to minimize loss of the degassed chemical due to evaporation, the valve of the boiling flask and that of the vacuum tube that led to the degassing apparatus were partially opened instead of being fully opened. Furthermore a total condenser was used with the temperature of the cooling fluid kept at 253 K. The estimated chemical loss due to evaporation was approximately 3 cm^3 (approximately 6 % of total volume), which is an acceptable loss. Expensive chemicals were degassed in-situ (outlined in Section 5.3.3.1).

The heat input from the heating mantle was dependent on the nature of the chemical degassed. For chemicals such as methanol, ethanol, hexane, 2-methoxy-2-methylpropane, ethyl acetate, butan-2-one and acetonitrile used in this study, no heat input from the heating mantle was necessary as the evaporation of the chemicals occurred without any heat input. The formation of condensate on the outer glassware was also noticed for the degassing of all above mentioned chemicals. However, for higher boiling chemicals such as heptane that was used in this study, the heating mantle was kept at a constant temperature of 303 K. Each chemical was allowed to degas for approximately 4 hours. Once this time had elapsed, the valve of the boiling flask was then closed. Thereafter, the valve for the vacuum tube that led to the degassing apparatus was closed. The valve on the air-vent line for the vacuum pump was then partially opened before switching the vacuum pump off. The valve on the air-vent line to the degassing apparatus was then slowly opened to release the vacuum within the degassing apparatus. The boiling flask was then disconnected from the Vigreux fractionating column by firstly lowering the position of the heating mantle with the mechanical jack. The *click test* of Van Ness and Abbott (1978) was then done to check if sufficient degassing was achieved. This involved rapidly inverting the boiling flask to hear a for a *metallic click* sound that presumably results from a sudden collapse of trapped vapour under the liquid head. According to Van Ness and Abbott (1978), the *metallic click* sound for some chemicals can only be heard when the temperature of the degassed liquid is sufficiently low. However for all the chemicals used in this study, the *click test* of Van Ness and Abbott (1978) was positive when tested immediately after degassing.

5.2 Compression Device

5.2.1 Preparation and Cleaning

The compression device was firstly checked for any leaks. High pressure nitrogen from a cylinder was charged into the compression device to a pressure of 3 000 kPa. The device was then left overnight to monitor any decrease in the pressure reading. If a significant decrease in pressure was observed, other than that of room temperature effects, a soapy solution was applied to joints suspected of leaking. A leak at a joint was confirmed by the presence of bubbles. When leaks were detected at the connection point of the cover-lid with the cell body, the cover-lid was opened and the O-rings were examined and replaced if they were found to be damaged. When a leak was detected at the connection point of the needle valve to the cover-lid, the needle valve was removed and the threaded hole in the cover-lid was cleaned. The needle valve was then replaced and sealed using a high strength thread-locker. The connection lines to the compression device were also examined using high pressure and a soapy solution. Were a leak was detected on these connection points, PTFE tape was used on the ferrule of these connections.

Ethanol was used as the cleaning solvent for the compression device. The cover-lid at each end of the compression device was firstly removed. Ethanol was then flushed into the cell body and needle valve of the compression device. The piston was also cleaned with ethanol. Whilst disassembled, the O-rings of the cover-lids and the piston were also examined and replaced if they were found to be damaged. Compressed air was then used to dry the compression device. The compression device was then reassembled and the pressure leak test as explained above was carried out. Vacuum was then used for approximately 30 minutes to flash off any residue ethanol from the compression device prior to use.

5.2.2 Charging the Compression Device

The compression device was charged with the degassed liquid by making use of gravity and vacuum. Figure 5-1 shows the schematic of the set-up for charging the compression device. The compression device is held in an upright position (as shown in Figure 5-1) by using a laboratory stand and clamps. The compression device and the boiling flask were connected to a single stainless steel three-way valve by using a $^{1}/_{8}$ inch stainless steel piping. A special fitting was made to connect the boiling flask to the $^{1}/_{8}$ inch stainless steel pipe. The stainless steel piping that connected the compression device to the three-way valve was used as the common line. The boiling flask, which

contained the degassed liquid, was inverted and then connected to the three-way valve. The boiling flask was held in an upright position by using clamps and a laboratory stand.

Before charging the compression device with the degassed liquid, all the connection lines were thoroughly cleaned with ethanol and checked for leaks. To remove any ethanol residue that was left behind from cleaning, the compression device (in a fully depressed position) together with the connecting line was opened to the vacuum pump via the three-way valve for approximately 30 minutes to evaporate the residue ethanol. This procedure was also done for the connecting line of the boiling flask and the three-way valve. The compression device, connecting lines and valves were also heated with a heating gun during the vacuum procedure to assist the drying process. No actual analysis was done to ensure that all the residue ethanol was removed as it was assumed that 30 minutes with vacuum and heat was sufficient to remove any residual ethanol.

The compression device was ensured to be in the fully depressed position. Using the arrangement as shown in Figure 5-1 and with the vacuum pump switched on, the three-way valve was switched to the vacuum line until the pressure within the compression device was as close as possible to absolute vacuum. When this was achieved, the needle valve of the compression device was closed. The three-way valve was then switched from the vacuum line position to the position that leads to the boiling flask for a few seconds and then back to the vacuum line position. This was done several times to remove the air that was present in the line that connected the boiling flask to the compression device. Once it was assumed that no air was present in this connecting line, the three-way valve was finally positioned to the line that leads to the boiling flask.

The valve of the boiling flask was then carefully opened to allow the degassed liquid to flow into the compression device. The needle valve of the compression device was then fully opened to receive the degassed liquid into the compression device. Since the pressure within the boiling flask and the compression device are as close as possible to absolute vacuum, the degassed liquid moves from the boiling flask to the compression device due to the effect of gravity and is rather slow. To speed up this process, the boiling flask was gently heated with a temperature gun to cause a pressure differential. Once the compression device was almost full with approximately 45 cm^3 of degassed liquid, the valve of the boiling flask and the needle valve were closed. To ensure that no air was present in the compression device, the three-way valve was switched to the vacuum line position and the needle valve partially opened for a few seconds to dispel any air that could have entered the compression device.

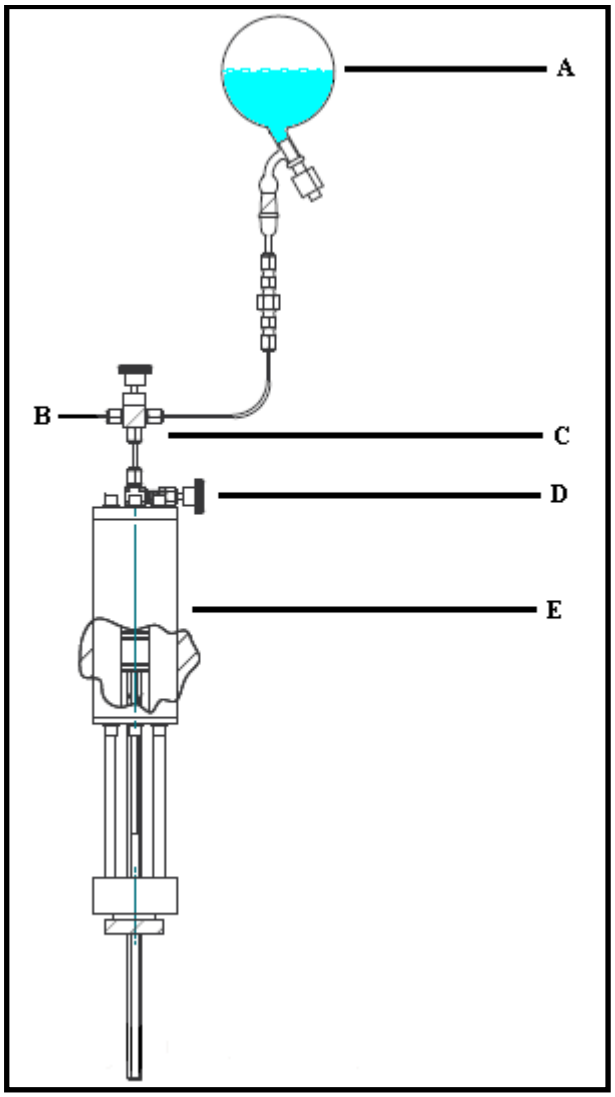

Figure 5-1: Schematic of the set-up for charging the compression device.
A: boiling flask with degassed liquid; B: tube that leads to vacuum pump; C: three-way valve; D: needle valve; E: cell body of compression device.

5.3 Phase Equilibrium Apparatus

5.3.1 Preparation

5.3.1.1 Leak Detection

To detect for any leaks, the equilibrium cell was charged with high pressure nitrogen at 1500 kPa, then isolated and left overnight to monitor any decrease in the pressure reading. If a significant decrease in pressure was observed, other than that of room temperature effects, a soapy solution was applied to joints suspected of leaking. A leak at a joint was confirmed by the presence of bubbles.

All the connecting lines to and from the equilibrium cell were also checked for leaks using high pressure and a soapy solution. If a leak was detected between the upper or lower 316 SS flange of the equilibrium cell, the assembly was dismantled to examine the O-rings within the equilibrium cell and were replaced if they were damaged. If leaks were detected on the ROLSI™ connection nut situated on top of the upper 316 S S flange of the equilibrium cell or the connection nut for the metallic dowel situated below the lower 316 S S flange of the equilibrium cell, the O-ring was examined and replaced if damaged. If leaks were detected on the connection points on the $^{1}/_{8}$ inch stainless steel lines to and from the equilibrium cell, PTFE tape was used on the ferrule of these connections.

Leaks were also checked on the $^{1}/_{16}$ inch stainless steel sampling lines that connected the ROLSI™ to the 6-port gas chromatograph (GC) valve and the GC. This was achieved by switching the 6-port GC valve to the *sampling* position and using the GC carrier gas. The connections in these lines were then tested for leaks with a soapy solution. Any leaks found on these connections were also prevented using PTFE tape on the ferrule of these connections.

5.3.1.2 Cleaning the Equilibrium Cell

The equilibrium cell was always cleaned prior to undertaking any experimental measurements. Ethanol was used as the cleaning solvent. Initially, the $^{1}/_{8}$ inch stainless steel lines that connected the equilibrium cell to the pressure transmitters were heated and maintained at 373 K. It was also ensured the stainless steel ball valves connected on these lines were opened to both the low and high pressure transmitters. The three-way valve of the feed line to the equilibrium cell was switched to the vacuum position, were the common line of this three-way valve was the line that led to the equilibrium cell. This caused the pressure within the equilibrium cell to decrease as close as possible to absolute vacuum (0.05 kPa). Once this was achieved, the needle valve of the feed line was then closed and the three-way valve was then switched to the “charge” position. Approximately 15 cm^3 of ethanol was then charged into the equilibrium cell by using a syringe with a fitting attached to the three-way valve and slowly opening the needle valve of the feed line. When the equilibrium cell was charged, the needle valve of the feed line was then closed. The temperature controller of the oil bath was then set to 323 K and the equilibrium cell was immersed into the oil bath by raising the oil bath with the mechanical jack. The magnetic stirrer was then activated.

The equilibrium cell was left in this condition for approximately 30 minutes for cleaning. Thereafter, the bath temperature controller was switched off, the magnetic stirrer was deactivated and the oil bath was lowered with the mechanical jack. The equilibrium cell was then left to cool for approximately one hour. Once the equilibrium cell had cooled, the ethanol was drained from the equilibrium cell using compressed air to create a pressure differential. This was achieved by ensuring the three-way valve was switched to the "charge" position and connected to the compressed air line. Before the compressed air was charged into the equilibrium cell, it was ensured that the stainless steel valve for the low pressure transmitter was closed. The compressed air was then charged into the equilibrium cell by slowly opening the needle valve on the feed line. The pressure within the equilibrium cell was monitored with the moderate pressure transmitter and a value of approximately 3 bars was maintained in the equilibrium cell. The needle valve for the drain line on the equilibrium cell was then slowly opened and the ethanol was received into a beaker and discarded into a waste bottle. The compressed air line was then disconnected from the apparatus and the entire cleaning procedure was repeated at least once to ensure that the equilibrium cell was thoroughly cleaned. Once the cleaning process was completed, the equilibrium cell was left open to the atmosphere via the needle valves on the feed and drain lines to dry the residue ethanol within the equilibrium cell. Occasionally, compressed air was used to speed up the drying process. To ensure trace amounts of the ethanol were removed, the equilibrium cell was evacuated with the aid of the vacuum pump for approximately 30 minutes. Samples were taken from the equilibrium cell to the GC for analysis to ensure that there was no residual ethanol present.

The sampling lines were also cleaned by heating these lines and maintaining the temperature at 473 K. When the temperature of these lines was reached, the carrier gas (helium) was used to flush these lines. The lines were then evacuated for approximately 30 minutes with the aid of the vacuum pump. The flushing and evacuation procedure was repeated at least once to ensure the sample lines did not contain any trace amount of impurities. As a measure to check that the sample lines did not contain any trace impurities, the sample lines were flushed with the carrier gas and a sample was sent to the GC for analysis. If a peak was found to appear on the GC software, the entire cleaning process for the sampling lines was repeated until no such peaks for the trace impurities were found to appear on the GC chromatograph.

5.3.2 Calibration

5.3.2.1 Temperature Probe Calibration

All the temperature probes used for this study were calibrated using the WIKA CTB 9100 temperature calibration unit. The calibration unit makes use of silicone oil (SI 40) as the fluid medium within the bath. The standard temperature probe for the WIKA CTB 9100 temperature calibration unit was calibrated by WIKA with an accuracy of 0.02 K. The results of the calibration are all presented in Appendix C, Figures C-1 to C-24.

5.3.2.2 Pressure Transmitter Calibration

The 0 – 100 kPa absolute WIKA model P-10 pressure transmitter was used for reading sub-atmospheric pressure. This low pressure transmitter was calibrated using the WIKA CPH 6000 pressure calibration unit with a WIKA CCP 30 hand test pump and 0 – 100 kPa absolute WIKA CPT 6000 standard pressure transmitter. The WIKA CPT 6000 standard pressure transmitter was calibrated by WIKA with an accuracy of 0.02 kPa.

The 0 – 1600 kPa absolute WIKA model P-10 pressure transmitter was used for reading moderate to high pressure. This high pressure transmitter was internally calibrated using the ethanol literature vapour pressure of Reid et al. (1988). This was done to avoid any time lapse as the WIKA CPH 6000 high pressure calibration unit with a WIKA PCS 250 hand pump and 0 – 250000 kPa absolute WIKA CPT 6000 standard pressure transmitter was sent to the manufacturer for repairs. When the unit was received after repairs, it still displayed severe fluctuations and thus could not be used with confidence. This calibration was only carried out after the temperature calibration was done as the calibrated temperature readings were needed to determine the literature vapour pressure of Reid et al. (1988), which was used as a standard. The certified purity of ethanol as stated by the supplier is reported in Table 6-1 of Chapter 6 together with GC tests and refractive index verifications.

The ethanol was initially degassed following the procedure as outlined Section 5.1.3 above and charged into the equilibrium cell following the procedure outlined in Section 5.3.3.2. Before charging the equilibrium cell with the degassed liquid from the boiling flask, the equilibrium cell and all the connection lines were thoroughly cleaned with ethanol and checked for leaks. To remove any ethanol residue that was left behind from cleaning, the equilibrium cell and lines were evacuated with the aid of the vacuum pump via the three-way valve for approximately 20 minutes.

Once the equilibrium cell was charged, the oil bath was then raised to immerse the equilibrium cell into the oil. With the degassed ethanol in the equilibrium cell, the temperature controller of the oil bath was set to a desired value and time was allowed for equilibrium to be reached within the equilibrium cell. Equilibrium within the equilibrium cell was deemed established when the temperature of the 316 SS flanges of the equilibrium cell and the pressure within the equilibrium cell remained constant within experimental uncertainty. The 34970A Agilent data acquisition unit was used to log the temperature and pressure readings for 200 data points with 2 s interval between each data point. This was done for different temperature settings on the oil bath temperature controller that ranged from 350 to 436 K. The ethanol literature vapour pressure of Reid et al. (1988) was used as the standard pressure for the calibration and also served as verification for the low pressure transmitter calibration. The results of the pressure calibration are all presented in Appendix C, Figures C-25 to C-28.

5.3.2.3 Gas Chromatograph Calibration

The equilibrium phase samples in this study were analyzed by gas chromatography using a Shimadzu 2014 GC which was fitted with a thermal conductivity detector (TCD). A 0.32 mm ID, 30 m length and 0.25 μm film thickness crosslinked 5 % PH ME silicone Hewlett Packard 5 (HP5) capillary column was used for the analysis with helium as the carrier gas. The GC Solutions software package was used to convert the output signal from the GC to a peak area signal and perform integration. The compositions of the samples were then determined from the GC detector calibration.

The area ratio method outlined by Raal and Mühlbauer (1998) was used to perform the GC detector calibration in this study. The method made use of analyzing standards that were prepared gravimetrically to cover the entire composition range. In general, the peak area obtained from the integration of the peak is proportional to the number of moles that passes the detector of the GC:

$$n_i = A_i^* F_i \tag{5-1}$$

where, n_i is the number of moles of component i, A_i^* is the peak area of component i and F_i is the proportionality constant of component i that is more commonly known as the response factor. The peak area is dependent on the volume of the sample injected into the GC and this volume injected is

often not reproducible. Hence the response factor obtained for the GC calibration can have significant deviations, especially for small volumes of samples injected. Therefore, Raal and Mühlbauer (1998) suggested the use of area ratios. In the case of a binary system:

$$\frac{n_1}{n_2} = \left(\frac{F_1}{F_2}\right)\left(\frac{A_1^*}{A_2^*}\right) = \frac{x_1}{x_2} \tag{5-2}$$

where, subscripts 1and 2 refer to the components and x is the mole fraction. To obtain the response factor ratio (F_1 / F_2) for the dilute region of component 1, the area ratio (A_1^* / A_2^*) was plotted against the mole fraction ratio (x_1 / x_2) for a composition range of 0 to 1 of the mole fraction ratio, where the response factor ratio was equal to the slope of the plot. In similar manner, the response factor ratio (F_2 / F_1) was obtained for the dilute region of component 2. The plots were also extrapolated through the origin, since no peak area should necessarily be observed without a sample being injected. According to Equation (5-2), the response factor ratio should necessarily be constant for a linear plot of area ratio against the mole fraction ratio. If the linearity exists over the entire composition range, then F_1 / F_2 should equal to the inverse of F_2 / F_1 and vice versa. This was used as a check for the linearity of the GC detector calibration.

The area ratio method outlined by Raal and Mühlbauer (1998) was used for the GC calibrations of all the phase equilibrium measurements that were undertaken in this study, except for systems that exhibited immiscibility. Liquid-liquid equilibrium (LLE) and vapour-liquid-liquid equilibrium (VLLE) (which exhibit immiscibility) experimental measurements were undertaken for the hexane + acetonitrile and methanol + heptane systems. For these systems, the direct GC detector calibration method was used, where Equation (5-1) was used for each component instead of Equation (5-2).

Before the GC detector calibrations were undertaken, the carrier gas lines were examined for any leaks. The carrier gas pressure, injector temperature, oven temperature and the TCD temperature were then activated. For each system studied in this work, trial injections were carried out on the GC to optimize the parameters for good peak areas and separation (retention time) of the components.

The injections for the GC detector calibrations were made with the Shimadzu 2014 AOC-20i auto-sampler that used a good quality 10 µl Dynatech SGE liquid syringe. Care was taken to check for blockages, tightness of the piston plunger and needle seal of the liquid syringe. For each injection,

the syringe was rinsed 5 times with acetone (solvent) before a sample was taken and also rinsed 3 times with the sample. This was to ensure that the impurities in the needle of the syringe were removed. The syringe was also flushed 4 times with the sample to remove the entrainment of air bubbles in the syringe. After the sample was injected into the GC, the syringe was rinsed a further 5 times with acetone. The septum for the GC injector was replaced after every 100 injections to avoid errors that would result from leaks.

The samples for the GC detector calibration were prepared in 4 ml vials such that the vials were nearly full with only a very small vapour space. This was done to ensure that the mixture in the sample vial did not evaporate and thus lead to an incorrect composition. Furthermore, the sample vials were kept in icy water to prevent evaporation before being analyzed by the GC. By trial, it was found that 6 µl of the sample was sufficient to perform GC detector calibrations as this was within the range of the volume sampled from the equilibrium cell by the ROLSI™. For each calibration point, at least 5 samples were injected until the average absolute deviation for the peak area ratio (or peak area for the direct calibration) was within 1 % error. The optimized parameters for the GC, together with the calibration results are presented in Appendix C, Figures C-25 to C-45. The response factor ratio (or the response factor for direct calibration) was determined using linear regression. The accuracy of the mole fractions for each system studied is also presented in Appendix C, Table C-5.

5.3.3 Operating Procedures for Phase Equilibrium Measurements

5.3.3.1 In-Situ Degassing

The method of in-situ degassing was only used for expensive chemicals to minimize loss of the chemical. Prior to in-situ degassing, the equilibrium cell and $^1/_8$ inch stainless steel feed line were cleaned as outlined in Section 5.3.1.2. The $^1/_8$ inch stainless steel lines that connected the equilibrium cell to the pressure transmitters were heated and maintained at 373 K. It was also ensured the stainless steel ball valves connected on these lines were opened to both the low and high pressure transmitters. The three-way valve on the feed line to the equilibrium cell was switched to the vacuum position, were the common line of this three-way valve was the line that led to the equilibrium cell. This caused the pressure within the equilibrium cell to decrease as close as possible to absolute vacuum. Once this was achieved, the needle valve on the feed line was then closed and the three-way valve was then switched to the "charge" position. Approximately 8 cm^3 of the chemical to be degassed was then charged into the equilibrium cell by using a syringe with a

fitting attached to the three-way valve and slowly opening the needle valve on the feed line. When the equilibrium cell was charged, the needle valve on the feed line was then closed. The temperature controller of the oil bath was then set to 303 K and the equilibrium cell was immersed into the oil bath. The magnetic stirrer was then activated. The three-way valve was then switched to the vacuum position.

Once the temperature within the oil bath had stabilized, the needle valve on the feed line was then opened for approximately 20 s to vacuum and then closed. After 3 minutes the needle valve on the feed line was again opened to vacuum for approximately 20 s and then closed. This process was repeated for approximately 1 hour. The *click test* of Van Ness and Abbott (1978) could not be performed for in-situ degassing to check if sufficient degassing was achieved. Alternatively, the measurement of vapour pressure for the chemical and comparison to literature was performed as a check for thorough degassing. When a large deviation was observed between the vapour pressure of the degassed chemical and that of literature, the temperature of the oil bath was increased to 313 K and the degassing procedure repeated for a further 30 minutes. At this point the deviation was within experimental error.

5.3.3.2 Vapour Pressure Measurement

To undertake experimental vapour pressure measurement, the chemical was initially degassed following the procedure as outlined in Section 5.1.3. Figure 5-2 shows the schematic of the set-up for charging the equilibrium cell with the degassed liquid from the boiling flask. The boiling flask was inverted and connected to the stainless steel three-way valve by using $^1/_8$ inch stainless steel piping. A special fitting was made to connect the boiling flask to the $^1/_8$ inch stainless steel pipe. The stainless steel piping that connected the equilibrium cell to the three-way valve was used as the common line. The boiling flask, which contained the degassed liquid, was inverted and then connected to the three-way valve.

Before charging the equilibrium cell with the degassed liquid from the boiling flask, the equilibrium cell and all the connection lines were thoroughly cleaned with ethanol and checked for leaks. To remove any ethanol residue that was left behind from cleaning, the equilibrium cell lines were evacuated with the aid of the vacuum pump via the three-way valve for approximately 20 minutes. Using the arrangement as shown in Figure 5-2 and with the vacuum pump switched on, the three-way valve was switched to the vacuum position until the pressure within the equilibrium cell was as

close as possible to absolute vacuum. When this was achieved, the needle valve on the feed line to the equilibrium cell was closed. The three-way valve was then alternated from the vacuum position to the position that leads to the boiling flask for a few seconds and then back to the vacuum position. This was done several times to remove the air that was present in the line that connected the boiling flask to the three-way valve. Once it was assumed that no air was present in this connecting line (read from the pressure gauge), the three-way valve was finally positioned to the line that leads to the boiling flask.

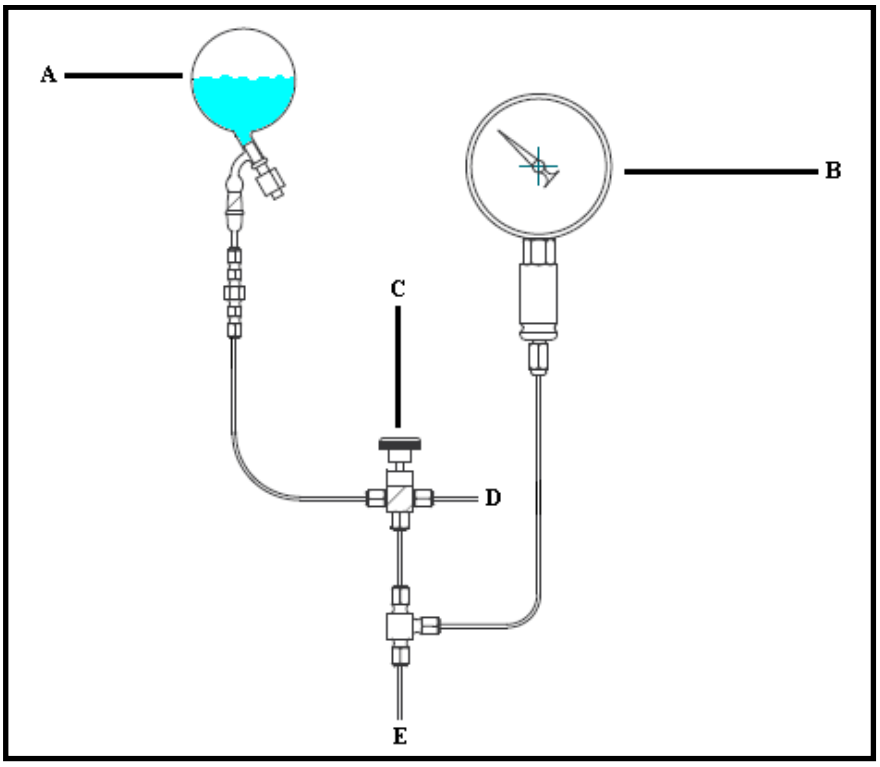

Figure 5-2: Schematic of the set-up for charging the equilibrium cell with degassed liquid from the boiling flask.

A: boiling flask with degassed liquid; B: pressure gauge; C: three-way valve; D: line that leads to the vacuum pump; E: common line of three-way valve that leads to the equilibrium cell.

The valve of the boiling flask was then carefully opened to allow the degassed liquid to flow to the equilibrium cell. The needle valve for the feed line on the equilibrium cell was then fully opened to receive the degassed liquid into the equilibrium cell. Since the pressure within the boiling flask and the equilibrium cell are as close as possible to absolute vacuum, the degassed liquid moves from the

boiling flask to the equilibrium cell due to the effect of gravity and is rather slow. To speed up this process, the boiling flask was gently heated with a temperature gun to cause a pressure differential.

The oil bath was then raised to immerse the equilibrium cell into the oil. With the degassed chemical in the equilibrium cell, the temperature controller of the oil bath was set to a desired value and the system was left to allow for equilibrium to be reached within the equilibrium cell. Equilibrium within the equilibrium cell was deemed established when the temperature of the 316 SS flanges of the equilibrium cell and the pressure within the equilibrium cell displayed a minimum change with time. The criterion used here was a constant temperature and pressure reading within 0.02 K and 0.1 kPa respectively for 30 minutes. The 34970A Agilent data acquisition unit was used to log the temperature and pressure readings for 200 data points with 2 s interval between each data point. This was done for different temperature settings on the oil bath temperature controller.

5.3.3.3 Binary Vapour-Liquid Equilibrium (VLE) Measurement

Before binary vapour-liquid equilibrium (VLE) measurements were undertaken, the equilibrium cell and sampling lines were cleaned as outlined in Section 5.3.1.2. The two components were also thoroughly degassed with the degassing apparatus as outlined in Section 5.1 or in-situ degassing as outlined in Section 5.3.3.1. One of the components was then used to charge the compression device as outlined in Section 5.2.2 whist the other component was used to charge the equilibrium cell as outlined in Section 5.3.3.2 above with only approximately 4 cm^3. In the case were an expensive chemical was used, in-situ degassing was used for this chemical and thus the equilibrium cell was already charged with this component.

Once the equilibrium cell was charged with approximately 4 cm^3 of one component, the needle valve on the feed line was closed and the compression device (charged with the second component) was then fitted to the three-way valve of the equilibrium apparatus feed line using $^1/_8$ inch stainless steel piping as shown in Figure 5-3. The stainless steel piping was initially cleaned with ethanol to remove any contaminants and the residue ethanol was removed via evaporation with the aid of vacuum and heat.

The three-way valve was then switched to the vacuum position to remove any air present in the feed line. Thereafter, the three-way valve was switched to the “charge” position for a few seconds before returning to the vacuum position. This process was repeated until all the air was removed from the

stainless steel line that connected the compression device to the three-way valve on the feed line. Once this was achieved, the thee-way valve was then switched to the "charge" position and the pressure gauge was used to check that the vacuum pressure in the line was as close as possible to absolute vacuum. If leaks were observed, all the fittings were then checked to eliminate the leaks.

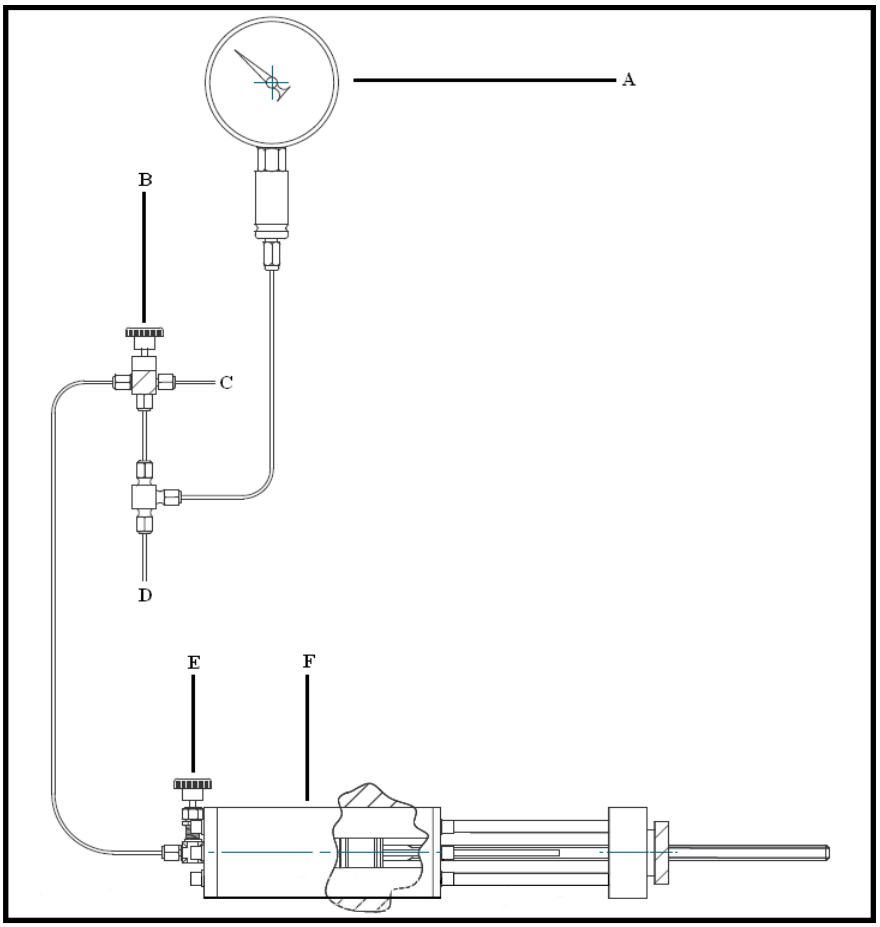

Figure 5-3: Schematic of the set-up for charging the second component into the equilibrium cell.

A: pressure gauge; B: three-way valve; C: line that leads to vacuum pump; D: common line of three-way valve that leads to equilibrium cell; E: needle valve of compression device; F: cell body of compression device.

The turn-dial on the compression device was operated to compress the second liquid component within the compression device until the first instance of resistance was felt. The needle valve on the compression device was then slowly opened to fill the stainless steel lines leading to the needle valve on the feed line of the equilibrium cell with the second component liquid. The turn-dial on the compression device was then operated again to compress the liquid such that its pressure was at

least 1.5 times higher than that of the equilibrium cell, were the pressure gauge was used to check the pressure within the stainless steel lines. The needle valve on the feed line was then partially opened to allow a small amount of the second component liquid into the equilibrium cell before being closed. The ROLSI™ capillary was then positioned in the vapour phase of the equilibrium cell in preparation for sampling using the turn-dial on the equilibrium apparatus. The magnetic stirrer was then activated.

The oil bath was then raised to immerse the equilibrium cell into the oil. The temperature controller of the oil bath was set to the isotherm value and the system was left to equilibrate within the equilibrium cell. The heater cartridge in the upper 316 SS flange of the equilibrium cell was also activated to account for heat losses to the environment and conductive paths. The 34970A Agilent data acquisition unit was then used to log the temperature and pressure readings. Equilibrium within the equilibrium cell was deemed established when the temperature of the 316 SS flanges of the equilibrium cell and the pressure within the equilibrium cell displayed minimum change with time. As with the vapour pressure measurements, the criterion used here was a constant temperature and pressure reading within 0.02 K and 0.1 kPa respectively for 30 minutes.

While equilibrium was being established, the ROLSI™ expansion chamber, sampling lines and the aluminum block for the 6-port GC sampling valve were heated and maintained at a temperature that was 15 K higher than the normal boiling temperature of the less volatile component for the binary system. The 6-port GC sampling valve was also switched to the *flushing* mode. Since all the systems measured in this study were for moderate to high pressures, it was not necessary to switch the 6-port GC valve from this position during sampling as the pressure within the equilibrium cell was always higher than the pressure of the carrier gas in the sampling line. Once equilibrium was established, the 34970A Agilent data acquisition unit was reset to start logging the temperature and pressure readings and the vapour and liquid phases were then ready to be sampled. The magnetic stirrer was also deactivated at this point. By trial it was found that the temperature for the upper 316 SS flange of the equilibrium cell was necessarily needed to be kept at 0.15 K higher than the isotherm value of the system being measured. This was to prevent condensation of the vapour at the tip of the ROLSI™ capillary that would lead to an incorrect value for the vapour composition. The vapour phase was sampled first as this phase required less cleaning time when compared to the liquid phase. The capillary of the ROLSI™ was cleaned by setting a specific opening time on the Crouzet TOP 948 electronic timer. This opening time was found by trial such that the peak areas obtained were within the GC detector calibration range. The Crouzet TOP 948 electronic timer was

also used to set the time between each successive sample. This time was set to the retention time of the first peak. In this way, samples were taken automatically according to the specified times set on the Crouzet TOP 948 electronic timer. The first 3 samples taken were used to clean the capillary of the ROLSI™. Thereafter, at least 5 samples were taken until the absolute average deviation of the composition was within 1 % error.

The turn-dial on the phase equilibrium apparatus was then operated to move the capillary of the ROLSI™ to the liquid phase for sampling. Markings that were made on the 316 SS rods of the phase equilibrium apparatus were used as a guideline to know the position of the ROLSI™ capillary; else the oil bath was lowered to view the equilibrium cell prior to positioning the capillary of the ROLSI™. During this process, the pressure within the equilibrium cell was monitored to check that the pressure was not changing appreciably. Once the capillary of the ROLSI™ was positioned in the liquid phase, the temperature for the upper 316 SS flange of the equilibrium cell was returned to the isotherm value of the system and samples were taken using the Crouzet TOP 948 electronic timer. As in the vapour phase, the opening time for the capillary of the ROLSI™ was found by trial such that the peak areas obtained were within the GC detector calibration range. The first 3 samples taken were used to clean the capillary of the ROLSI™. Thereafter, at least 5 samples were taken until the absolute average deviation of the composition was within 1 % error.

The logging of temperature and pressure readings were then stopped and recorded. The turn-dial on the phase equilibrium apparatus was then operated to return the capillary of the ROLSI™ to the vapour phase within the equilibrium cell. The oil bath was then lowered to view the liquid level in the equilibrium cell. If the liquid level was less than ¾ of the total cell height, then the compression device was used as before to add more of the second component into the equilibrium cell and the entire procedure repeated until the height of the liquid within the equilibrium cell was ¾ that of the cell height. This point was generally reached when the phase equilibrium diagram was half complete. The oil bath was then lowered to drain some of the liquid from the cell via the drain valve of the equilibrium cell such that the level of liquid within the cell was approximately $^1/_5$ that of the height of the equilibrium cell. This was possible since for all systems measured in this study, the pressure within the equilibrium cell was always at a higher value than the atmospheric pressure. The process of draining the equilibrium cell was done as quick as possible as the temperature (and thus the pressure) within the equilibrium cell was constantly decreasing since the equilibrium cell was out of the oil bath. This method saved time for cleaning the equilibrium cell and the amount of chemical used (especially that of the expensive chemical that was initially charged into the

equilibrium cell). Once this was done, the oil bath was then raised to immerse the equilibrium cell within the oil and the procedure continued until the phase equilibrium diagram was completed.

Once the phase equilibrium measurements for the entire composition range was completed, the heat supplied to the ROLSI™ expansion chamber, sampling lines and the aluminum block for the 6-port GC sampling valve were deactivated. The temperature controller for the oil bath was switched off and the equilibrium cell was allowed to cool down before being cleaned.

Overall it was found that only 50 cm^3 of each component was required to carry out GC detector calibrations, degassing, vapour pressure and phase equilibrium measurements for a single isotherm. Were more than one isotherm was measured, only an additional 25 cm^3 of each component was further required per isotherm.

5.3.3.4 Binary Liquid-Liquid Equilibrium (LLE) Measurement

The equilibrium cell and sampling lines were initially cleaned as outlined in Section 5.3.1.2 prior to undertaking liquid-liquid equilibrium (LLE). The two components were also thoroughly degassed with the degassing apparatus as outlined in Section 5.1 or in-situ degassing as outlined in Section 5.3.3.1. One of the components was then used to charge the compression device as outlined in Section 5.2.2 whist the other component was used to charge the equilibrium cell as outlined in Section 5.3.3.2 above with only approximately 6 cm^3. In the case were an expensive chemical was used, in-situ degassing was used for this chemical and thus the equilibrium cell was already charged with this component.

The second component was charged into with the compression device as already outlined in Section 5.3.3.3 above, however approximately 6 cm^3 was charged into the cell instead of a small amount as mentioned in Section 5.3.3.3. The needle valves of the feed line and the compression device were then closed. The stainless steel line connection on the compression device at the three-way valve on the feed line was then carefully removed and the three-way valve was also switched to the vacuum position to remove the excess second component liquid from the feed line. At this point, the pressure within the equilibrium cell was also monitored and the needle valve on the feed line was opened for a few seconds to the vacuum to ensure that no air was present in the equilibrium cell. Thereafter, the needle valve on the feed line was closed and the three-way valve was positioned to the “charge” position. High pressure nitrogen gas was then connected to the “charge” position of the

three-way valve using $^{1}/_{8}$ inch stainless steel piping. With the valve of the high pressure nitrogen gas closed, the three-way valve was then alternated between the vacuum and "charge" position several times to remove all air present in the stainless steel lines before being left in the "charge" positioned. The high pressure nitrogen valve was then slowly opened until the pressure in the stainless steel line was approximately 500 kPa. The needle valve was then partially opened to allow the high pressure nitrogen into the equilibrium cell until the pressure in the equilibrium cell was approximately 350 kPa, were care was taken to ensure that the stainless steel ball valve for the low pressure transmitter was closed. The high pressure nitrogen was used to pressurize the equilibrium cell to enable sampling. The equilibrium composition analysis was in no way compromised since nitrogen, an inert gas, has a very low solubility in liquids used in this study for low to moderately high pressures. Furthermore, liquids are generally incompressible and the phase equilibrium compositions for LLE systems do not significantly change when the pressure is increased from sub-atmospheric pressure to a moderately high pressure.

The magnetic stirrer was activated and the oil bath was then raised to immerse the equilibrium cell into the oil. The temperature controller of the oil bath was set to the isotherm value and the system was left to equilibrate within the equilibrium cell. The heater cartridge in the upper 316 SS flange of the equilibrium cell was also activated to account for heat losses to the environment and conductive paths. The 34970A Agilent data acquisition unit was then used to log the temperature and pressure readings. Equilibrium within the equilibrium cell was deemed established when the temperature of the 316 SS flanges of the equilibrium cell and the pressure within the equilibrium cell did not change with time. If the pressure within the equilibrium cell was below 350 kPa, additional nitrogen was added to the equilibrium cell to maintain a pressure of 350 kPa prior to sampling. The oil bath was also lowered to view the equilibrium cell in order to verify that the position of the capillary for the ROLSI™ was indeed in the upper liquid phase. The mixture was then allowed a few more minutes to reach equilibrium once again.

The procedure for sampling was followed as outlined in Section 5.3.3.3 with the lower liquid phase being sampled first. The logging of temperature and pressure readings were then stopped and recorded. The turn-dial on the phase equilibrium apparatus was then operated to return the capillary of the ROLSI™ to the upper liquid phase within the equilibrium cell. The temperature controller was then set to the next isotherm value and time was allowed for equilibrium to be established. When equilibrium was reached, the procedure for sampling was repeated as before whereby it was ensured that the pressure in the equilibrium cell was maintained at 350 kPa. The entire procedure

was repeated for as many isotherms as were required. Once the phase equilibrium diagram was completed the heat supplied to the ROLSI™ expansion chamber, sampling lines and the aluminum block for the 6-port GC sampling valve were deactivated. The temperature controller for the oil bath was switched off and the equilibrium cell was allowed to cool down before being cleaned.

Overall it was found that only 30 cm^3 of each component was required to carry out GC detector calibrations, degassing, vapour pressure and phase equilibrium measurements.

5.3.3.5 Binary Vapour-Liquid-Liquid Equilibrium (VLLE) Measurement

The equilibrium cell and sampling lines were cleaned as outlined in Section 5.3.1.2. The two components were also thoroughly degassed with the degassing apparatus as outlined in Section 5.1 or in-situ degassing as outlined in Section 5.3.3.1. The experimental phase diagram was completed in the same manner as the binary VLE measurements with the exception of the experimental point of vapour-liquid-liquid equilibrium (VLLE) which was determined first. The procedure for obtaining the VLLE point followed the same procedure to charge the equilibrium cell as described for LLE measurements in Section 5.3.3.4 except that no high pressure nitrogen was charged into the equilibrium cell. Once, the equilibrium cell was charged with both liquid components, the ROLSI™ capillary was then positioned in the vapour phase of the equilibrium cell in preparation for sampling using the turn-dial on the equilibrium apparatus. The magnetic stirrer was then activated.

The procedure for establishing equilibrium and sampling were then followed as outlined in Section 5.3.3.3. However in this case, three samples were analysed starting with the vapour phase. Once the point of VLLE was determined, the turn-dial on the phase equilibrium apparatus was then operated to return the capillary of the ROLSI™ to the vapour phase within the equilibrium cell. The temperature controller for the oil bath was switched off and the equilibrium cell was allowed to cool down before being cleaned.

Thereafter each homogeneous region of the VLLE system was then determined experimentally following the procedure for VLE measurements as outlined in Section 5.3.3.3. Once the phase equilibrium diagram was complete, the heat supplied to the ROLSI™ expansion chamber, sampling lines and the aluminum block for the 6-port GC sampling valve were deactivated. The temperature controller for the oil bath was switched off and the equilibrium cell was allowed to cool before being cleaned.

Overall it was found that only 60 cm^3 of each component was required to carry out GC detector calibrations, degassing, vapour pressure and phase equilibrium measurements for a single isotherm.

Avant d 'entreprendre d es m esures nouvelles d'équilibres d e p hase, l 'appareil qui vi ent d'être développé devait être préalablement testé pour vérifier qu'il est capable de permettre de reproduire des d onnées p récédemment m esurées e t aussi pour examiner les performances de la technique d'échantillonnage originale. Indépendamment de ceci, l'appareil a également été testé pour montrer sa polyvalence dans la mesure des pressions de vapeur, des équilibres « liquide –vapeur » (ELV), des équilibres « liquide-liquide » (ELL) et des équilibres « liquide-liquide-vapeur » (ELLV). Avant utilisation, chacun des produits chimiques a été contrôlé en vue de la vérification de sa pureté. Pour cela ainsi nous avons réalisé des mesures d'indice de réfraction avec le réfractomètre modèle RX 7000α de Atago et des analyses par chromatographie en phase gazeuse. Ces contrôles de pureté ont permis de m ontrer qu'aucune i mpureté n'est p résente en q uantité significative dans l es produits chimiques utilisés po ur cette é tude. L es sy stèmes tests é taient : l'équilibre « liquide –vapeur » (ELV) du m élange 2 m ethoxy-2-méthylpropane + a cétate d'éthyle à 373.1 7 K e t deséquilibres« liquide-liquide » (ELL) concernant l es m élanges m éthanol + heptane et h exane + acétonitrile, tous les deux m esurés à 350 kPa sous p ression d 'azote. C es sy stèmes tests (excepté hexane + acétonitrile) ont servi à établir que l'appareil est bien capable de permettre de mesurer des données fiables d'équilibres de phase. Les valeurs publiées par Bernabe et al. (1988) ontété utilisées pour c omparaison s ur c e s ystéme binaire en équilibre « liquide-liquide ». C ependant c es donn ées obtenues pa r l a m éthode du poi nt de br ouillard ne s ont pa s t rès pr écises et su jettes á d es observations visuelles.

De nouv elles d onnées ex périmentales d 'équilibre d e phase o nt ét é obtenues po ur les sy stèmes suivants :

a) ELV pour le système méthanol + butan-2-one à 383.25, 398.14 et 413.20 K
b) ELV pour le système éthanol + butan-2-one à 383.26, 398.23 et 413.21 K
c) ELV pour le système éthanol + 2 méthoxy-2-méthylbutane à 398.25 et 413.19 K
d) ELV pour le système éthanol + 2 méthylpent-2-ène à 383.20 K
e) ELLV pour le système hexane + acétonitrile à 348.20 K

Le sy stème (a) présente un a zéotrope à 383.25 e t 398.14 K aux e nvirons de x_1 = 0.975 e t 0.98 0 respectivement, mais pas à 413.20 K . Le sy stème (b) présente un a zéotrope à 383.26, 398.2 3 e t 413.21 K respectivement aux environs de x_1 = 0.75, 0.84 et 0.91. Le système (c) présente lui aussi un a zéotrope, c et az éotrope a p our compositions : x_1 = 0.77 0 et 0.78 0 à 398.25 e t 4 13.19 K respectivement. L e système (d) est azéotropique avec la composition x_1 = 0.530. La pr ession d'équilibre triphasique du sy stème (e) a été d éterminée expérimentalement à188.0 k Pa a vec les

compositions suivantes $x_1^I = 0.312$, $x_1^{II} = 0.654$ pour les deux phases liquides et $y_1 = 0.650$ pour la phase vapeur.

6

CHAPTER SIX

EXPERIMENTAL RESULTS

The phase equilibrium apparatus was designed, commissioned and tested by measuring vapour pressure data and three phase equilibrium test systems. These measurements were done to ensure that the apparatus was in correct working order and to test the novel design developed for phase sampling. The test systems included one vapour-liquid equilibrium (VLE) system of 2-methoxy-2-methylpropane + ethyl acetate at 373.17 K and two liquid-liquid equilibrium (LLE) systems of methanol + heptane and hexane + acetonitrile both measured with the aid of high pressure nitrogen at 350 kPa. A vapour-liquid-liquid equilibrium (VLLE) test system of water + butan-1-ol at 383.15 K was also expected to be measured but it was later realized that the polymer used on the stem of the ROLSI^{TM} was not suitable for water. A special stem was needed in order to sample any system that contained water. This special stem was to be ordered from France and the timeframe for receiving it meant that this study would not have been completed timeously.

New experimental phase equilibrium data were also measured for the following systems:

- VLE for methanol + butan-2-one at 383.25, 398.14 and 413.20 K
- VLE for ethanol + butan-2-one at 383.26, 398.23 and 413.21 K
- VLE for ethanol + 2-methoxy-2-methylbutane at 398.25 and 413.19 K
- VLE for ethanol + 2-methylpent-2-ene at 383.20 K
- VLLE for hexane + acetonitrile at 348.20 K

This chapter presents the chemical purity analysis for all the reagents used in this study, together with the results of the vapour pressure measurements, VLE, LLE and VLLE phase equilibrium measurements.

6.1 Chemical Purity

Acetonitrile, butan-2-one, ethanol and methanol were purchased from Merck, while 2-methoxy-2-methylbutane, 2-methoxy-2-methylpropane, 2-methylpent-2-ene, ethyl acetate, heptane and hexane were purchased from Capital Laboratory Suppliers cc.

Table 6-1: Chemical purities and refractive indices for all reagents used in this study.

Reagent	Refractive Index		GC Analysis (Peak Area %)	Min. Purity (Mass %)[f]
	Experimental [a]	Literature [a]		
2-methoxy-2-methylbutane	1.38855	1.3885[b]	99.0	97.0
2-methoxy-2-methylpropane	1.36896	1.36892[c]	99.8	99.8
2-methylpent-2-ene	1.40031	1.4005[d]	99.3	98.0
acetonitrile	1.34388	1.34423[b]	99.9	99.9
butan-2-one	1.37878	1.3788[b]	99.7	99.5
ethanol	1.36180	1.3611[b]	99.6	99.5
ethyl acetate	1.37239	1.3718[e]	99.8	99.8
heptane	1.38782	1.3878[b]	99.7	99.5
hexane	1.37516	1.3751[b]	99.9	99.9
methanol	1.32872	1.3288[b]	99.9	99.9

[a] at 293.15 K, [b] Weast et al. (1984), [c] Aim and Ciprian (1980), [d] Schmitt and Boord (1932), [e] Mcbee and Christman (1955), [f] Stated by supplier

All the reagents used in this study were subjected to a purity check using gas chromatographic analysis with a thermal conductivity detector (TCD) as it is able to pick up non-hydrocarbon impurities as well. It was revealed that no significant impurities were found for all reagents. Hence, all reagents were used without further purification. Each chemical was also subjected to refractive index measurement and compared to literature. The refractive index measurements were made with the Atago refractometer model RX 7000α. The analyses from gas chromatography and refractive index measurements are reported in Table 6-1.

6.2 Experimental Uncertainties

The experimental uncertainties associated with the two temperature probes used to measure the equilibrium temperature and the low and moderate pressure transmitters are reported in Table 6-2. The experimental uncertainty from the gas chromatograph (GC) TCD calibration for the mole fraction composition of each vapour-liquid equilibrium (VLE) system studied is reported in Table 6-3, where calibrations were carried out for dilute regions of each binary pair. All the uncertainty

calculations followed the guidelines outlined by the National Institute of Science and Technology (Taylor et al., 2007). The accuracy of the temperature controller of the oil bath was previously reported as 0.02 °C, thus implying an uncertainty of 0.01 °C. The uncertainty due to the mole number (Δn) of each chemical species was 0.0001 mol, determined from the OHAUS Adventurer™ mass balance used. The standard deviation from the GC TCD calibration can be considered as the uncertainty for the mole fraction, given by the following equation:

$$\Delta x_1 = \sqrt{\left(\frac{dx_1}{dn_1}\right)^2 (\Delta n_1)^2 + \left(\frac{dx_1}{dn_2}\right)^2 (\Delta n_2)^2} \tag{6-1}$$

Table 6-2: Experimental uncertainties for temperature and pressure measurements.

Description	Calibration Uncertainty	Repeatability Uncertainty	Global Uncertainty
equilibrium cell upper 316 SS flange	low range: 0.02 K high range: 0.05 K	low range: 0.05 K high range: 0.05 K	low range: 0.05 K high range: 0.07 K
equilibrium cell lower 316 SS flange	low range: 0.02 K high range: 0.05 K	low range: 0.04 K high range: 0.04 K	low range: 0.05 K high range: 0.07 K
low pressure transmitter	0.003 kPa	0.02 kPa	0.02 kPa
moderate pressure transmitter	0.6 kPa	0.7 kPa	0.9 kPa

Table 6-3: Experimental uncertainties for mole fraction compositions of VLE systems.

System	Calibration Uncertainty for x_1	Repeatability Uncertainty for x_1	Global Uncertainty for x_1
2-methoxy-2-methylpropane (1) + ethyl acetate (2)	dilute region (1): 0.005 dilute region (2): 0.006	dilute region (1): 0.005 dilute region (2): 0.003	dilute region (1): 0.007 dilute region (2): 0.006
methanol (1) + butan-2-one (2)	dilute region (1): 0.004 dilute region (2): 0.003	dilute region (1): 0.002 dilute region (2): 0.003	dilute region (1): 0.004 dilute region (2): 0.004

Table 6-3: Experimental uncertainties for mole fraction compositions of VLE systems (continued).

System	Calibration Uncertainty for x_1	Repeatability Uncertainty for x_1	Global Uncertainty for x_1
ethanol (1) + butan-2-one (2)	dilute region (1): 0.004 dilute region (2): 0.003	dilute region (1): 0.0003 dilute region (2): 0.001	dilute region (1): 0.004 dilute region (2): 0.004
ethanol (1) + 2-methoxy-2-methylbutane (2)	dilute region (1): 0.002 dilute region (2): 0.002	dilute region (1): 0.0005 dilute region (2): 0.001	dilute region (1): 0.002 dilute region (2): 0.002
2-methylpent-2-ene (1) + ethanol (2)	dilute region (1): 0.003 dilute region (2): 0.003	dilute region (1): 0.007 dilute region (2): 0.004	dilute region (1): 0.007 dilute region (2): 0.005

The GC TCD calibrations for the liquid-liquid equilibrium (LLE) systems were achieved using the direct injection method as opposed to the area ratio method of Raal and Mühlbauer (1998) as discussed in Chapter 5. All the calibration equations are reported in Appendix C.

6.3 Vapour Pressure Data

Vapour pressure data were measured for all the reagents used in this study. The data measured were compared to the Wagner equation using the literature data of Reid et al. (1988) and the extended Antoine equation from the property data bank in Aspen Plus (2004). The experimental data were also compared to values obtained using the Redlich-Kwong and the Peng-Robinson equations of state. The comparison to literature data served as a check for thorough degassing of the chemicals. All the experimental vapour pressure data were subjected to least squares regression to obtain parameters for the Wagner and Antoine empirical equations and also the Redlich-Kwong and Peng-Robinson equations of state. The results of the regression are discussed further in Chapter 7. The experimental vapour pressure data are reported in Table 6-4 and presented graphically in Figures 6-1 to 6-5.

Table 6-4: Experimental vapour pressure data.

2-methoxy-2-methylbutane		2-methoxy-2-methylpropane		2-methylpent-2-ene	
T / K	**P / kPa**	**T / K**	**P / kPa**	**T / K**	**P / kPa**
329.35	37.47	312.55	58.77	323.40	56.78
348.37	72.28	317.18	69.83	333.41	79.90
363.33	113.7	324.33	89.53	348.43	129.5
383.23	197.3	333.40	120.4	363.41	198.9
398.18	284.9	343.36	163.5	383.21	329.6
413.16	400.0	353.39	216.7	398.18	465.0
		362.96	280.6	413.13	636.4
		373.15	362.9		
		388.47	517.9		
		402.54	700.3		

acetonitrile		butan-2-one		ethyl acetate	
T / K	**P / kPa**	**T / K**	**P / kPa**	**T / K**	**P / kPa**
305.80	16.8	328.26	42.69	319.59	32.67
314.49	24.27	343.39	74.54	328.83	47.23
328.85	42.62	358.41	121.6	338.36	66.85
338.34	59.50	373.29	187.7	348.36	95.51
348.23	82.77	383.25	245.6	359.37	135.5
367.59	149.6	398.13	358.5	373.16	203.9
384.03	235.0	413.13	506.6	384.57	278.2
398.58	339.5			394.86	361.6
				409.12	507.2

heptane		hexane		methanol	
T / K	**P / kPa**	**T / K**	**P / kPa**	**T / K**	**P / kPa**
303.79	7.96	304.58	26.56	308.17	27.94
323.16	19.06	318.49	46.19	317.86	43.94
343.02	40.77	328.41	65.73	327.90	67.45
363.33	79.18	338.33	90.96	335.68	92.17
388.13	161.2	348.19	123.8	348.20	149.9
399.07	213.6	363.15	188.8	356.18	200.2
410.94	285.7	378.21	279.0	363.20	254.2
		388.77	359.0	373.22	351.6
		400.57	467.5	383.24	480.7
				398.06	732.9
				413.14	1086.0

Table 6-4: Experimental vapour pressure data (continued).

ethanol					
T / K	**P / kPa**	**T / K**	**P / kPa**	**T / K**	**P / kPa**
350.59	97.51	383.90	322.7	415.57	806.9
355.53	119.7	386.47	349.5	418.09	861.6
357.90	130.4	389.40	382.4	420.12	906.9
359.46	138.2	391.81	412.2	422.70	968.1
360.72	145.0	395.15	454.5	425.22	1032.4
362.18	153.2	397.63	489.8	427.17	1085.1
364.57	167.0	400.67	535.0	429.33	1141.9
369.11	196.7	403.14	574.4	431.18	1197.5
372.03	218.0	406.14	624.7	433.16	1255.0
374.87	240.1	408.64	668.4	435.05	1312.7
377.85	265.5	411.14	716.5		
380.61	290.7	413.11	755.1		

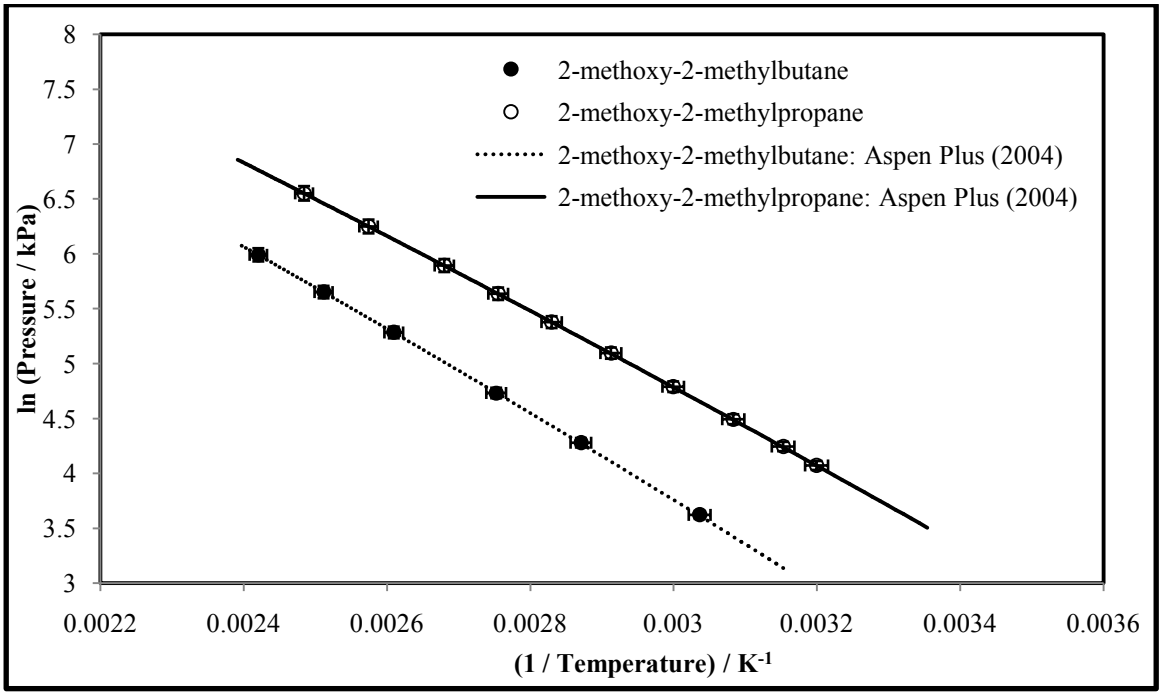

Figure 6-1: Vapour pressure plots for the ethers used in this study, 2-methoxy-2-methylbutane and 2-methoxy-2-methylpropane, compared to literature. Error bars show 1 % error for pressure and 0.5 % error for temperature.

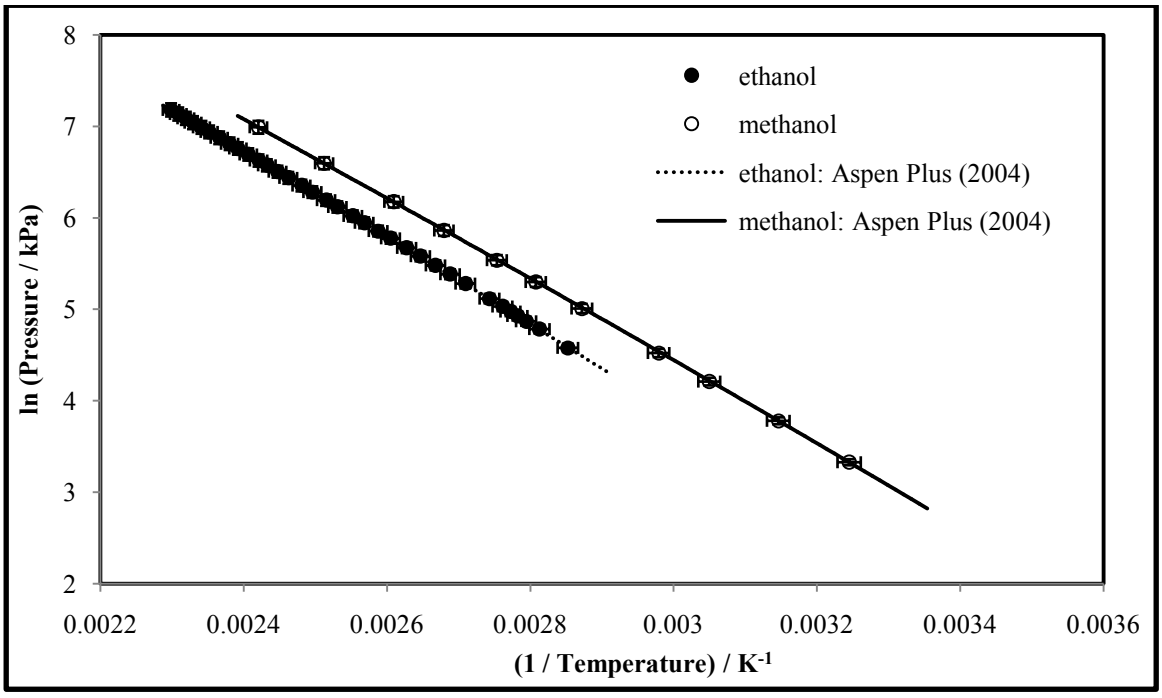

Figure 6-2: Vapour pressure plots for the alcohols used in this study, ethanol and methanol, compared to literature. Error bars show 1 % error for pressure and 0.5 % error for temperature.

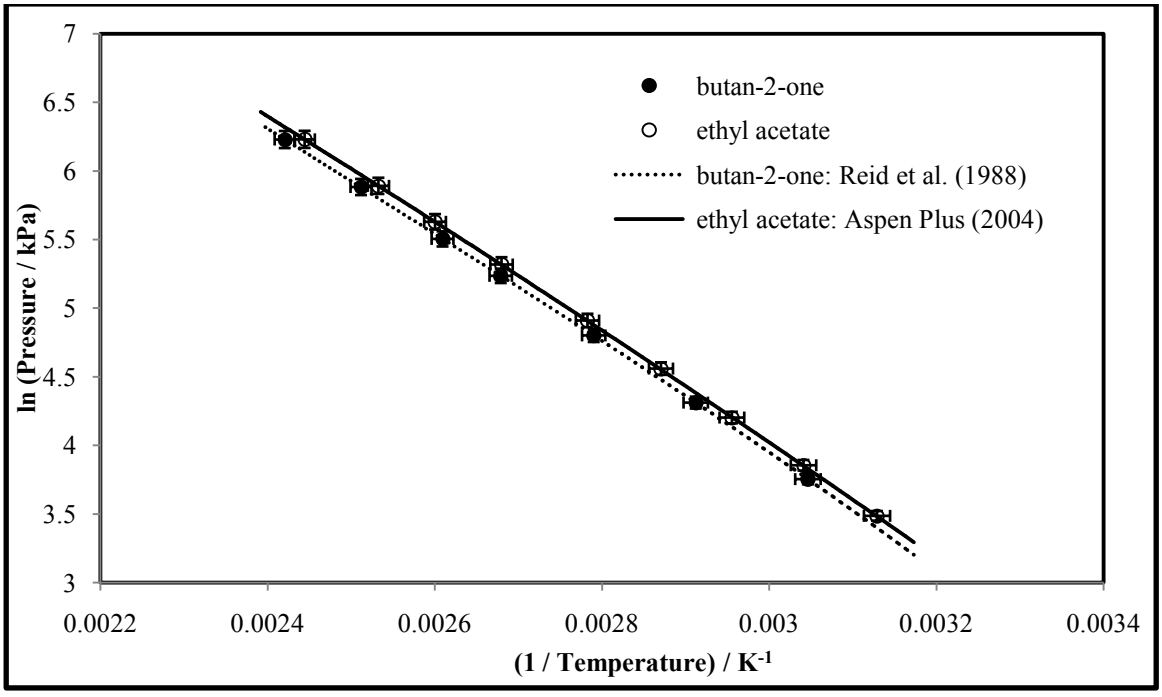

Figure 6-3: Vapour pressure plots for the ketone (butan-2-one) and ester (ethyl acetate) used in this study compared to literature. Error bars show 1 % error for pressure and 0.5 % error for temperature.

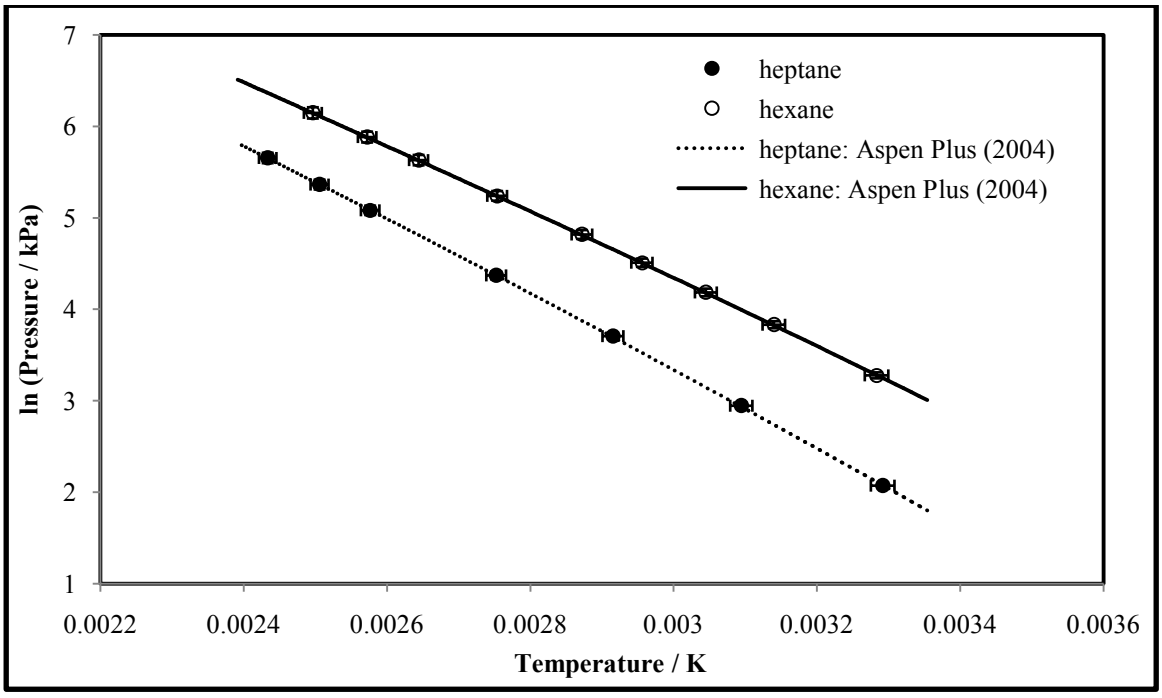

Figure 6-4: Vapour pressure plots for the alkanes used in this study, heptane and hexane, compared to literature. Error bars show 1 % error for pressure and 0.5 % error for temperature.

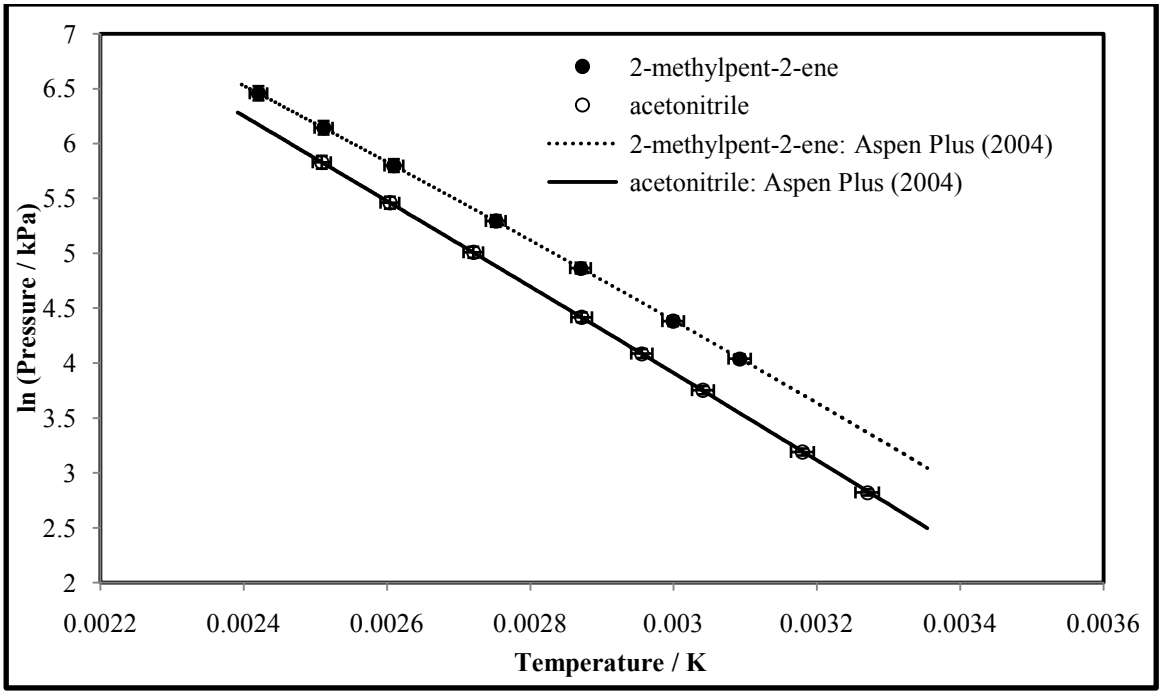

Figure 6-5: Vapour pressure plots for the alkene (2-methylpent-2-ene) and nitrile (acetonitrile) used in this study compared to literature. Error bars show 1 % error for pressure and 0.5 % error for temperature.

6.4 Phase Equilibrium of Test Systems

The Shimadzu 2014 gas chromatograph (GC) was used for the composition analysis of samples for all the test systems undertaken in this study. The GC calibration results and optimized parameters for the GC operation are presented in Appendix C 3. The mole fraction values for each phase sampled were within 1 % error for the average absolute deviation of at least 5 samples taken.

6.4.1 Vapour-Liquid Equilibrium (VLE) Result

6.4.1.1 2-Methoxy-2-Methylpropane (1) + Ethyl Acetate (2)

The literature data of Lee et al. (1997) for the 2-methoxy-2-methylpropane (1) + ethyl acetate (2) system at 373.17 K was used as a test system to demonstrate the capability of the newly developed phase equilibrium apparatus to measure vapour-liquid equilibrium (VLE) data. This literature data set was chosen as the pressure limits were within range for the pressure transmitter used in this study. Furthermore, this literature data set was measured using a reliable technique and according to Lee et al. (1997), the data was found to be thermodynamically consistent. The experimental data measured in this study is reported in Table 6-5 and graphically presented as *x-y* and *P-x-y* plots in Figures 6-6 and 6-7 respectively.

Table 6-5: Experimental vapour-liquid equilibrium data for the 2-methoxy-2-methylpropane (1) + ethyl acetate (2) system at 373.17 K.

P / kPa	x_1	y_1
203.9	0	0
221.2	0.077	0.139
237.7	0.149	0.252
254.3	0.239	0.363
265.4	0.298	0.430
280.2	0.390	0.522
293.5	0.465	0.592
306.5	0.548	0.664
314.1	0.600	0.703
325.9	0.685	0.777
335.5	0.765	0.833
343.6	0.826	0.873
363.3	1	1

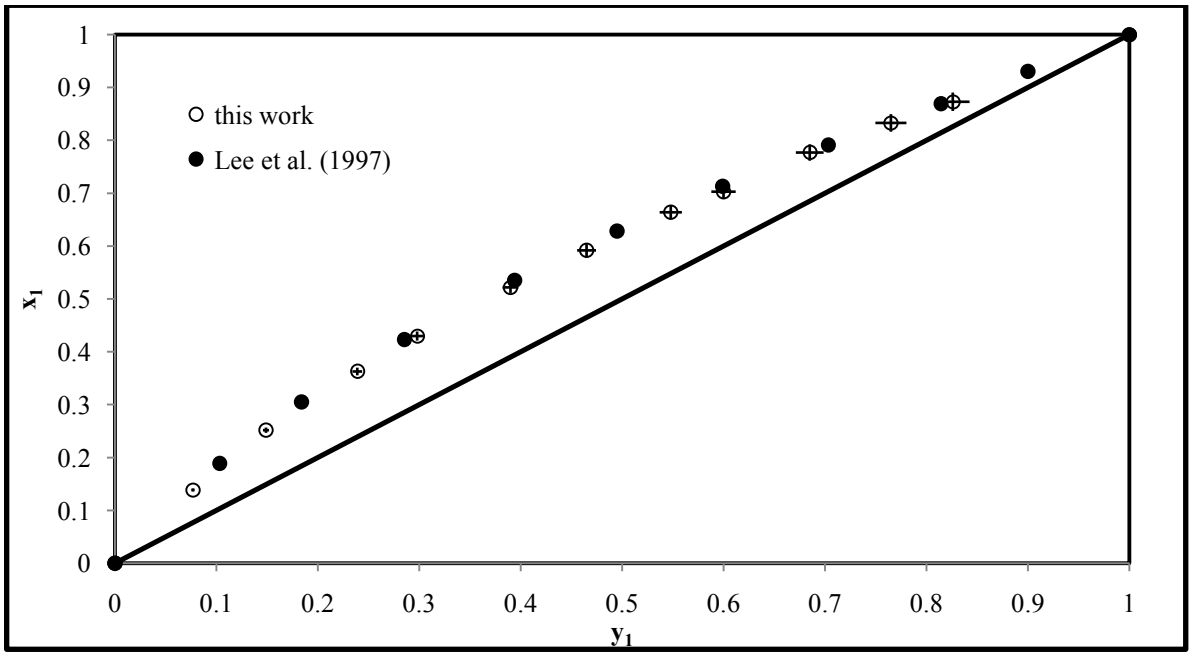

Figure 6-6: The *x-y* plot for the 2-methoxy-2-methylpropane (1) + ethyl acetate (2) system at 373.17 K, error bars show 2% error for x_1 and y_1.

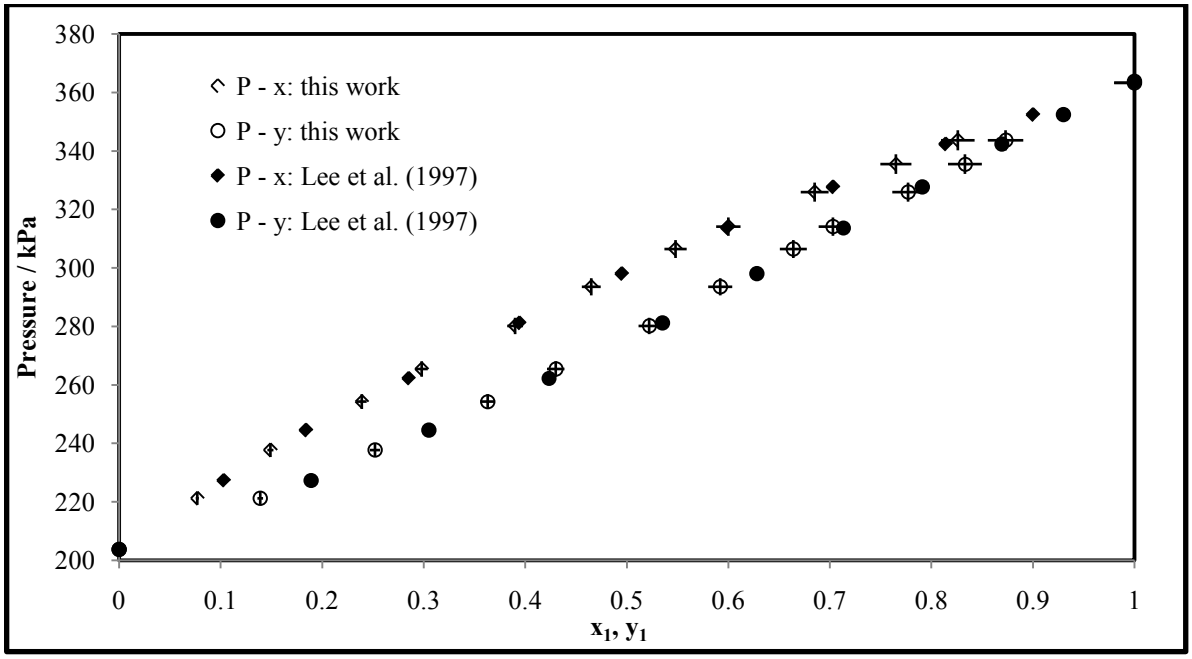

Figure 6-7: The *P-x- y* plot for the 2-methoxy-2-methylpropane (1) + ethyl acetate (2) system at 373.17 K, error bars show 1% error for pressure and 2% error for x_1 and y_1.

6.4.2 Liquid-Liquid Equilibrium (LLE) Results

6.4.2.1 Hexane (1) + Acetonitrile (2)

Two liquid-liquid equilibrium (LLE) systems were measured and compared to literature to show the capability of the newly developed phase equilibrium apparatus to measure LLE data. The first test system of hexane (1) + acetonitrile (2) was measured and compared to the literature data of Bernabe et al. (1988) and Sugi and Katayama (1978). The experimental data measured at 350 kPa in this study are reported in Table 6-6 and graphically presented as a T-x^{I}-x^{II} plot in Figure 6-8.

Table 6-6: Experimental liquid-liquid equilibrium data for the hexane (1) + acetonitrile (2) system at 350 kPa.

	Phase I		Phase II	
T / K	x_1	x_2	x_1	x_2
348.22	0.312	0.688	0.654	0.346
344.43	0.277	0.723	0.729	0.271
337.55	0.221	0.779	0.805	0.195
331.36	0.176	0.824	0.845	0.155
321.94	0.109	0.891	0.889	0.111
313.13	0.062	0.938	0.919	0.081

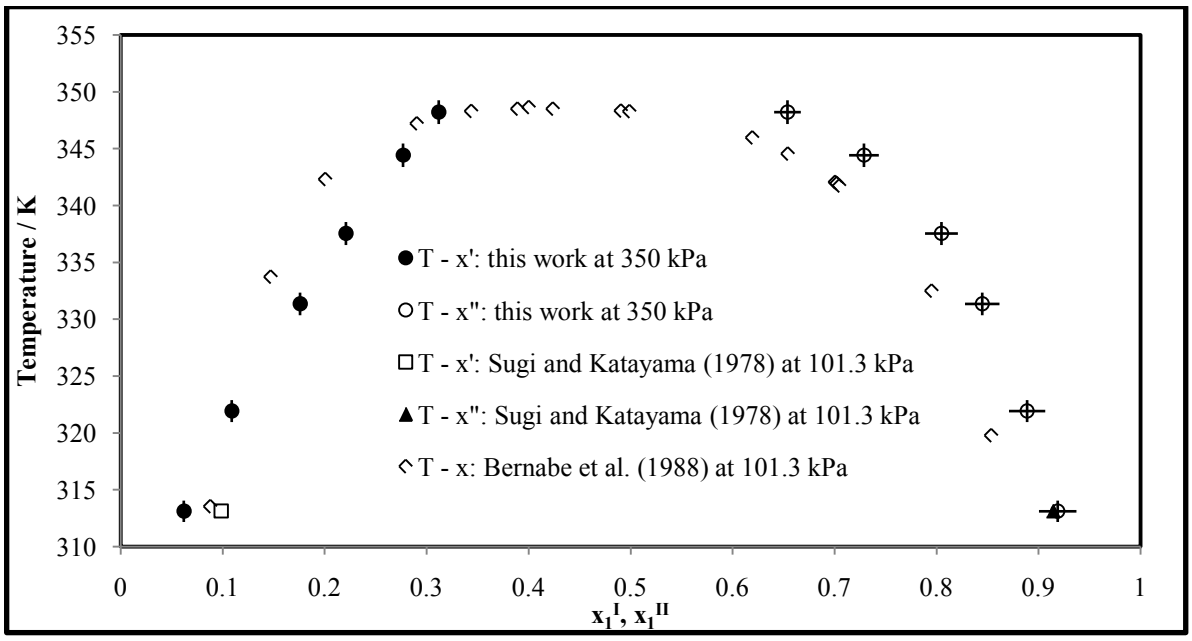

Figure 6-8: The T-x^{I}-x^{II} plot for the hexane (1) + acetonitrile (2) system at 350 kPa, error bars show 0.3% error for temperature and 2% error for x_1^{I} and x_1^{II}.

The data of Sugi and Katayama (1978) was in agreement with the experimental data of this work whereas the data of Bernabe et al. (1988) showed disagreement (discussed further in Section 7.5.1).

6.4.2.2 Methanol (1) + Heptane (2)

The second LLE test system of methanol (1) + heptane (2) was measured to confirm the technique of LLE measurement, since the first LLE test system of hexane (1) + acetonitrile (2) did not compare well to the literature data of Bernabe et al. (1988) (discussed further in Section 7.5.2). This second LLE test system was compared to the literature data of Higashiuchi et al. (1987). The experimental data measured at 350 kPa in this study are reported in Table 6-7 and graphically presented as a T-x^{I}-x^{II} plot in Figure 6-9. Incidentally, Bernabe et al. (1988) also measured data for this system which was shown to be in disagreement with other researchers (see Figure 6-9).

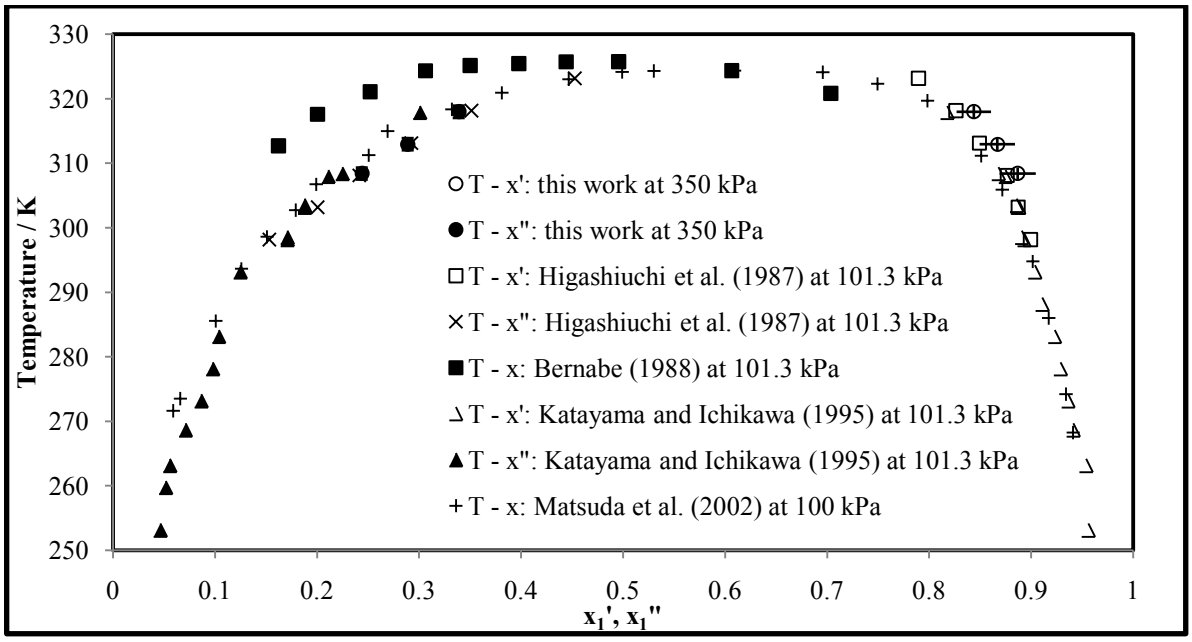

Figure 6-9: The T-x^{I}-x^{II} plot for the methanol (1) + heptane (2) system at 350 kPa, error bars show 0.3% error for temperature and 2% error for x_1^{I} and x_1^{II}.

Table 6-7: Experimental liquid-liquid equilibrium data for the methanol (1) + heptane (2) system at 350 kPa.

	Phase I		Phase II	
T / K	x_1	x_2	x_1	x_2
308.41	0.887	0.113	0.244	0.756
312.96	0.867	0.133	0.289	0.711
317.98	0.844	0.156	0.339	0.661

The experimental data of the test systems showed that the newly developed apparatus was capable of performing vapour pressure and phase equilibrium measurements. The test systems also showed versatility of the apparatus to measure vapour-liquid equilibrium (VLE) and liquid-liquid equilibrium (LLE) data.

6.5 Phase Equilibrium of New Systems

For all the systems, the GC TCD calibration results and optimized parameters for the GC operation are presented in Appendix C3. The mole fraction values for each phase sampled were within 1 % error for the average absolute deviation of at least 5 samples taken. All the new systems experimentally measured in this work have previously not been reported in the open literature.

6.5.1 Vapour-Liquid Equilibrium (VLE)

6.5.1.1 Methanol (1) + Butan-2-one (2)

Data for this system were measured at three temperatures: 383.25, 398.14 and 413.20 K. They are reported in Table 6-8 and graphically presented as *x-y* plots in Figure 6-10 and *P-x-y* plots in Figure 6-11. This system exhibited an azeotrope for the 383.25 and 398.14 K isotherms at approximately x_1 = 0.975 and 0.98 respectively. The experimental data does not however seem to indicate an azeotrope at 413.20 K. The presence of an azeotrope implies that a system is non-ideal and that conventional distillation cannot separate the components into high purity chemicals. Hence alternate forms of distillation should be considered such as pressure-swing distillation or homogeneous or heterogeneous azeotropic distillation.

Table 6-8: Experimental vapour-liquid equilibrium data for the methanol (1) + butan-2-one (2) system.

383.25 K			398.14 K			413.20 K		
P / kPa	**x_1**	**y_1**	**P / kPa**	**x_1**	**y_1**	**P / kPa**	**x_1**	**y_1**
245.6	0	0	358.5	0	0	506.6	0	0
305.9	0.131	0.266	466.3	0.165	0.338	619.8	0.113	0.256
359.3	0.292	0.480	540.7	0.305	0.521	668.0	0.171	0.348
387.0	0.385	0.573	576.7	0.382	0.591	731.7	0.254	0.459
427.1	0.545	0.701	608.0	0.459	0.656	800.6	0.351	0.551
436.4	0.599	0.731	637.0	0.548	0.703	853.5	0.434	0.628
455.3	0.720	0.800	678.7	0.693	0.798	920.2	0.550	0.715
463.5	0.778	0.834	713.2	0.849	0.887	981.1	0.673	0.786
472.1	0.863	0.890	733.7	1	1	1024.6	0.780	0.850
476.3	0.906	0.917				1059.5	0.889	0.914
479.4	0.974	0.975				1086.0	1	1
480.7	1	1						

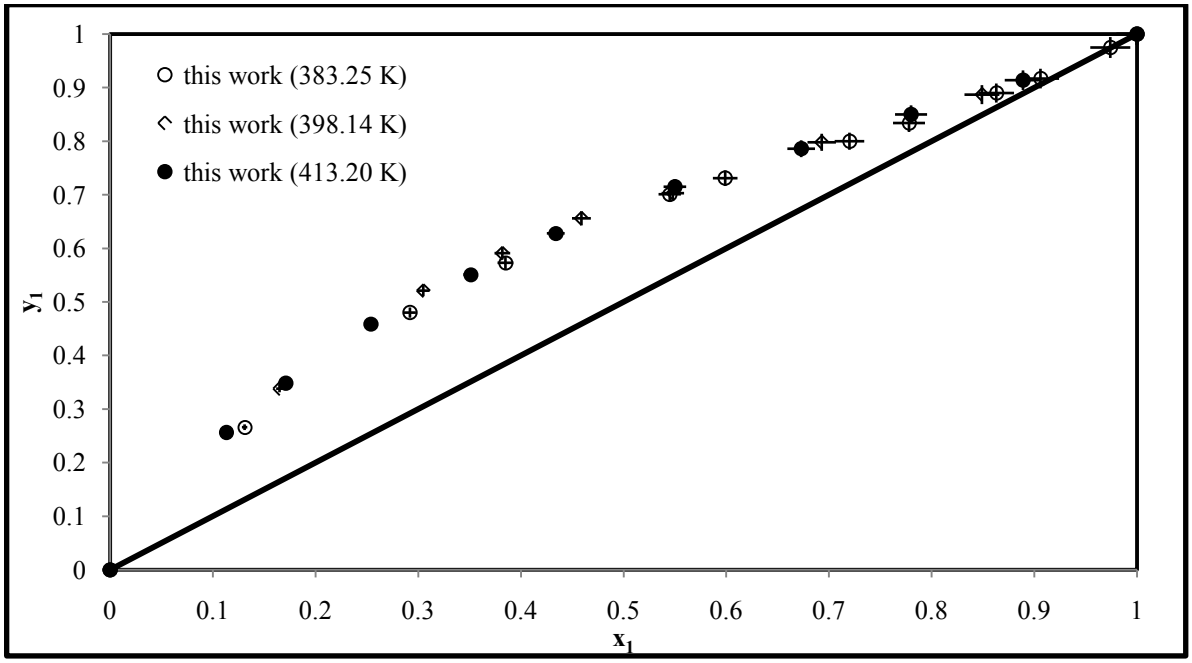

Figure 6-10: The *x-y* plot for the methanol (1) + butan-2-one (2) system, error bars show 2% error for x_1 and y_1.

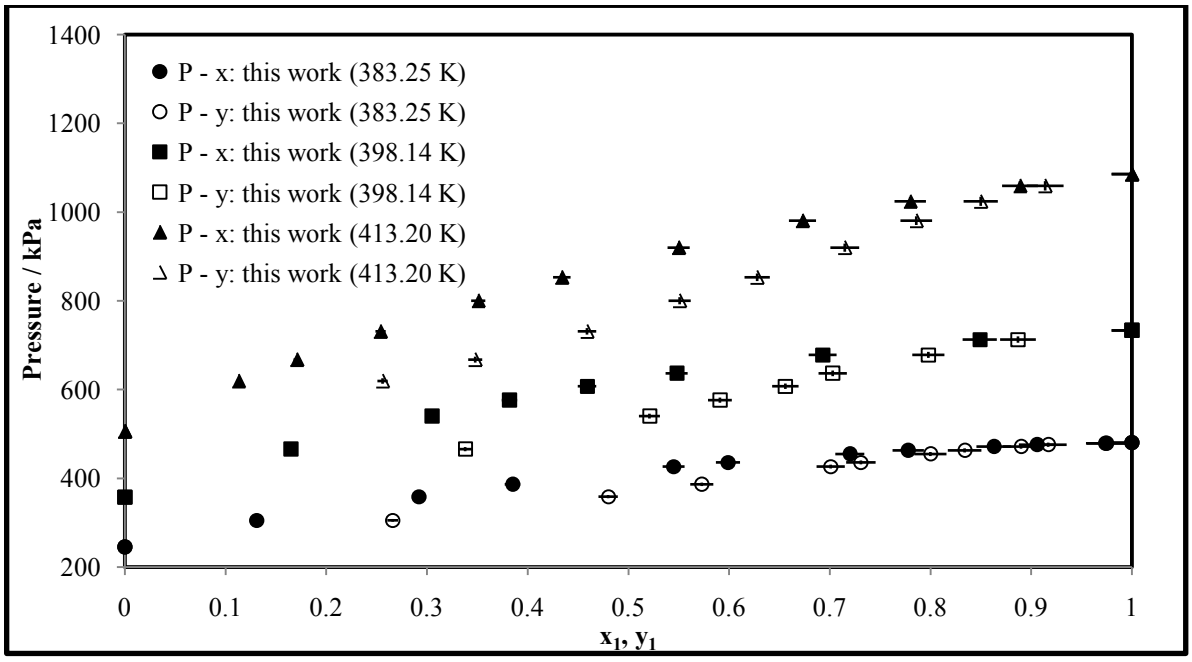

Figure 6-11: The *P-x-y* plot for the methanol (1) + butan-2-one (2) system, error bars show 1% error for pressure and 2% error for x_1 and y_1.

6.5.1.2 Ethanol (1) + Butan-2-one (2)

Data for this system were measured at three temperatures: 383.26, 398.23 and 413.21 K. They are reported in Table 6-9 and graphically presented as *x-y* plots in Figure 6-12 and *P-x-y* plots in Figure 6-13. This system exhibited an azeotrope for the 383.26, 398.23 and 413.21 K isotherms at approximately x_1 = 0.75, 0.84 and 0.91 respectively. Hence as mentioned previously, alternate forms of distillation need to be considered to separate these components into high purity chemicals.

Table 6-9: Experimental vapour-liquid equilibrium data for the ethanol (1) + butan-2-one (2) system.

383.26 K			398.23 K			413.21 K		
P / kPa	**x_1**	**y_1**	**P / kPa**	**x_1**	**y_1**	**P / kPa**	**x_1**	**y_1**
245.6	0	0	358.5	0	0	506.6	0	0
271.6	0.111	0.187	405.6	0.135	0.221	572.6	0.122	0.207
279.8	0.160	0.244	423.5	0.202	0.304	607.7	0.208	0.320
290.3	0.231	0.328	433.9	0.244	0.358	639.5	0.295	0.419
297.9	0.290	0.393	457.4	0.358	0.470	662.7	0.370	0.491
304.5	0.358	0.450	483.3	0.537	0.607	695.7	0.492	0.592
314.0	0.465	0.527	488.4	0.588	0.651	710.2	0.554	0.640
321.8	0.645	0.67	499.3	0.749	0.768	726.7	0.641	0.703
323.1	0.755	0.752	501.4	0.842	0.843	740.7	0.718	0.759
322.0	0.858	0.842	498.3	1	1	753.8	0.835	0.843
315.6	1	1				756.8	0.900	0.903
						758.7	0.916	0.919
						757.0	1	1

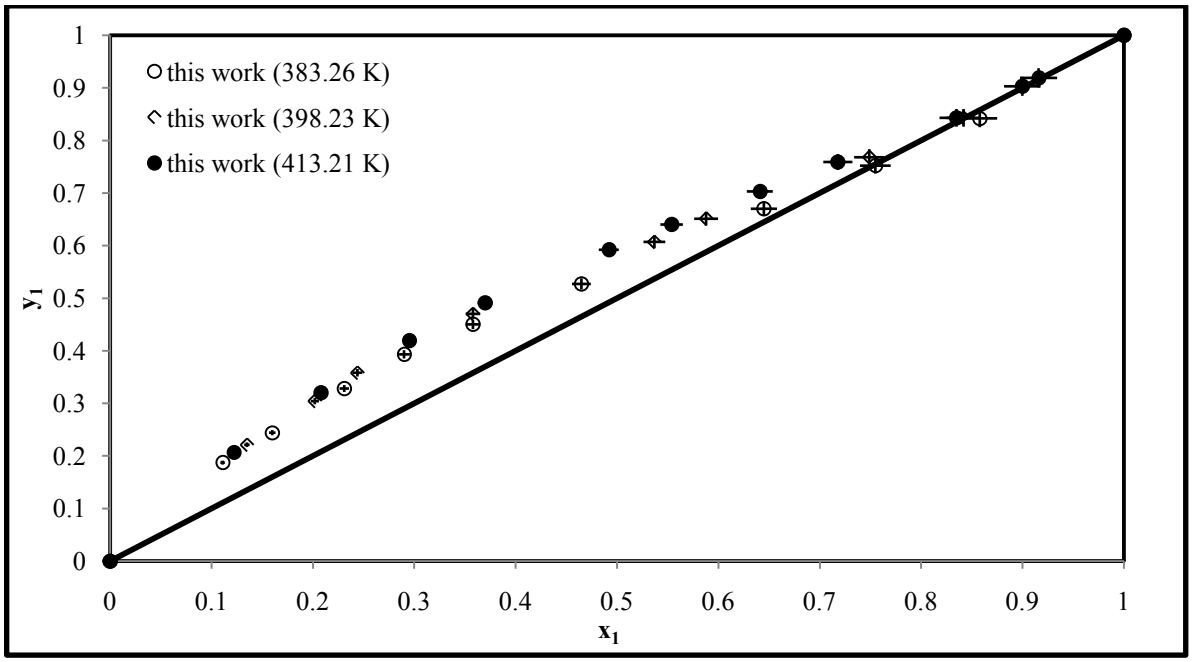

Figure 6-12: The *x-y* plot for the ethanol (1) + butan-2-one (2) system, error bars show 2% error for x_1 and y_1.

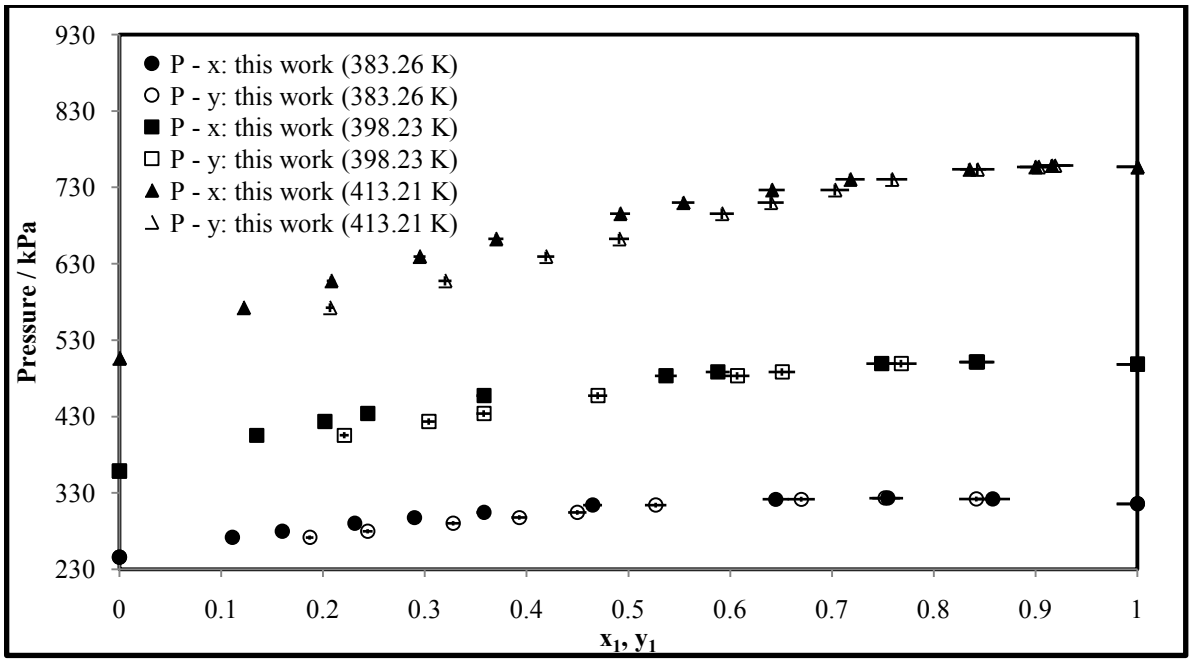

Figure 6-13: The *P-x-y* plot for the ethanol (1) + butan-2-one (2) system, error bars show 1% error for pressure and 2% error for x_1 and y_1.

6.5.1.3 Ethanol (1) + 2-Methoxy-2-Methylbutane (2)

Data for this system were measured at two temperatures: 398.25 and 413.19 K. They are reported in Table 6-10 and graphically presented as *x-y* plots in Figure 6-14 and *P-x-y* plots in Figure 6-15. This system exhibited an azeotrope for both the 398.25 and 413.19 K isotherms at approximately x_1 = 0.77 and 0.78 respectively. Again, alternate forms of conventional distillation should be considered for the separation of these chemicals.

Table 6-10: Experimental vapour-liquid equilibrium data for the ethanol (1) + 2-methoxy-2-methylbutane (2) system.

398.25 K			413.19 K		
P / kPa	**x_1**	**y_1**	**P / kPa**	**x_1**	**y_1**
285.79	0	0	400.03	0	0
307.44	0.026	0.094	453.10	0.044	0.143
322.98	0.049	0.155	501.74	0.090	0.253
364.90	0.110	0.291	557.21	0.150	0.356
409.68	0.190	0.413	605.10	0.213	0.449
460.12	0.318	0.517	662.00	0.303	0.522
496.31	0.453	0.606	707.95	0.400	0.591
512.59	0.547	0.654	736.10	0.479	0.646
528.78	0.732	0.750	771.11	0.622	0.715
529.60	0.769	0.770	782.64	0.691	0.750
526.92	0.855	0.832	790.68	0.783	0.781
523.16	0.895	0.872	779.77	0.936	0.921
517.30	0.935	0.909	757.00	1	1
498.32	1	1			

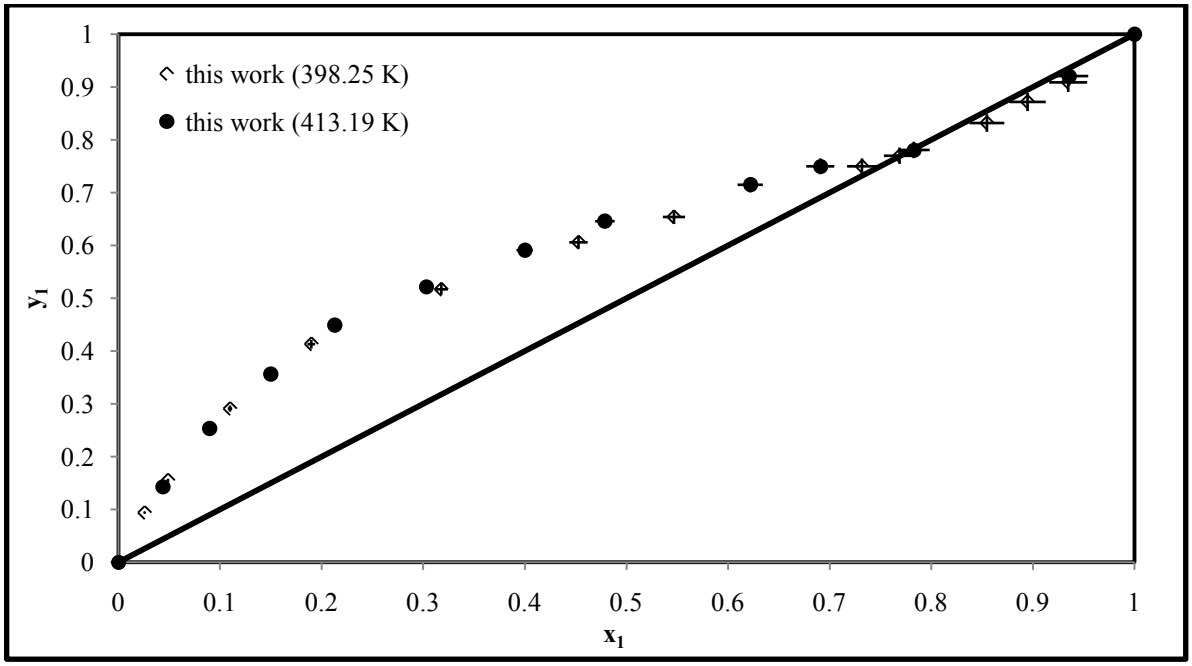

Figure 6-14: The *x-y* plot for the ethanol (1) + 2-methoxy-2-methylbutane (2) system, error bars show 2% error for x_1 and y_1.

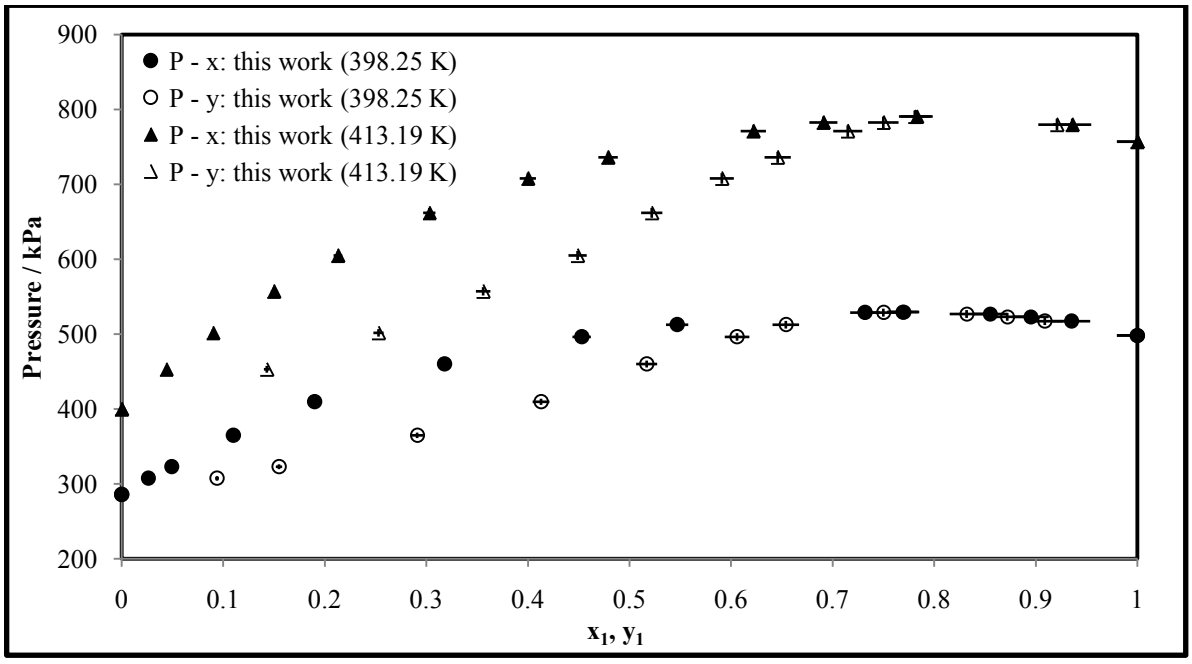

Figure 6-15: The *P-x-y* plot for the ethanol (1) + 2-methoxy-2-methylbutane (2) system, error bars show 1% error for pressure and 2% error for x_1 and y_1.

6.5.1.4 2-Methylpent-2-ene (1) + Ethanol (2)

Data for this system was measured at an isotherm of 383.20 K. The data are reported in Table 6-11 and graphically presented as an *x-y* plot and *P-x-y* plot in Figures 6-16 and 6-17 respectively. This system also exhibited an azeotrope at approximately $x_1 = 0.53$. Once more, alternate forms of conventional distillation should be considered for separation of these chemicals.

Table 6-11: Experimental vapour-liquid equilibrium data for 2-methylpent-2-ene (1) + ethanol (2) at 383.20 K.

P / kPa	x_1	y_1
315.6	0	0
399.9	0.077	0.271
435.3	0.128	0.336
465.1	0.194	0.409
488.2	0.296	0.472
501.1	0.457	0.535
501.0	0.590	0.562
491.9	0.719	0.597
480.1	0.788	0.616
455.0	0.865	0.676
412.8	0.931	0.778
389.8	0.955	0.824
329.6	1	1

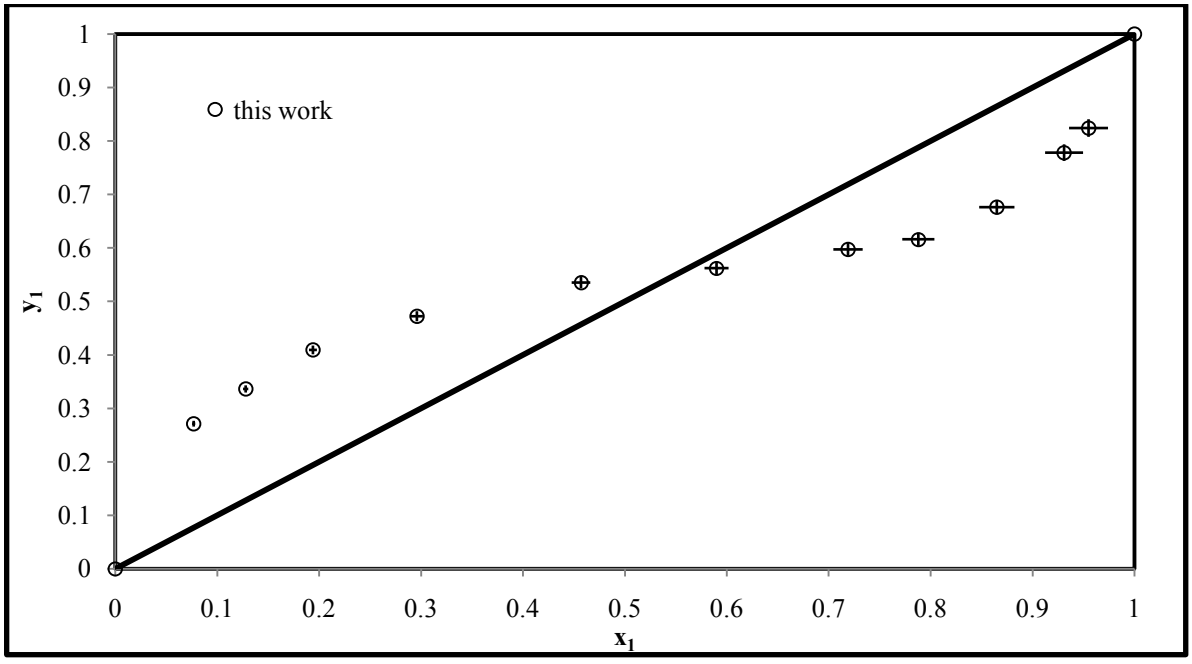

Figure 6-16: The *x-y* plot for the 2-methylpent-2-ene (1) + ethanol (2) system at 383.20 K, error bars show 2% error for x_1 and y_1.

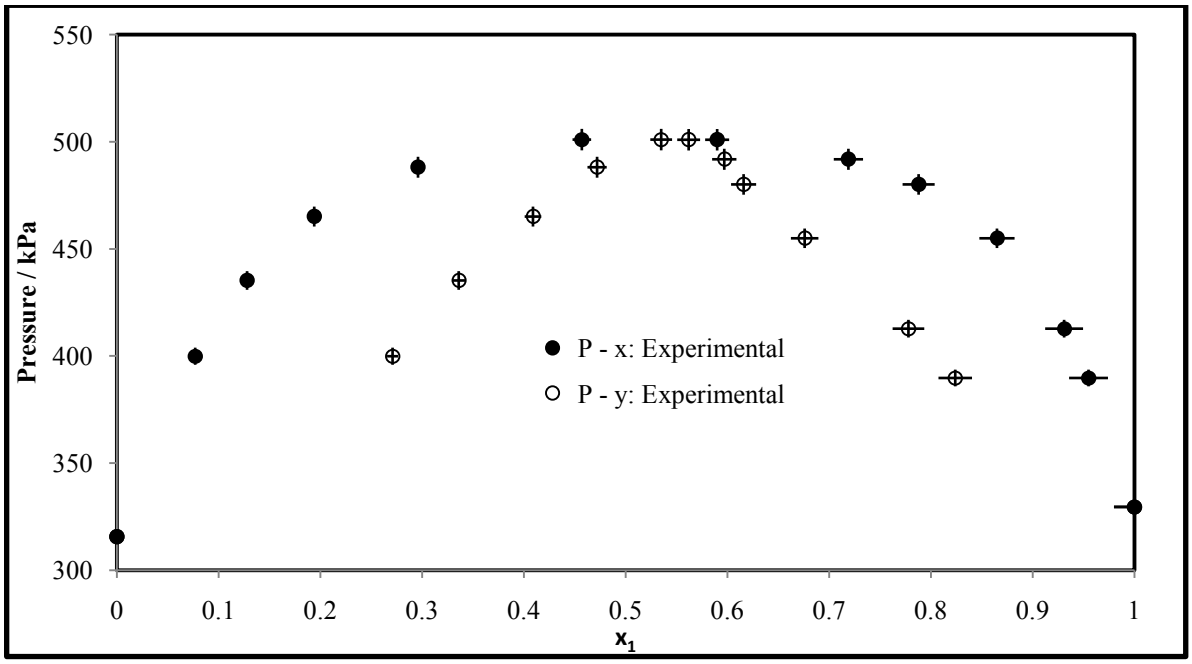

Figure 6-17: The *P-x-y* plot for the 2-methylpent-2-ene (1) + ethanol (2) system at 383.20 K, error bars show 1% error for pressure and 2% error for x_1 and y_1.

6.5.2 Vapour-Liquid-Liquid Equilibrium (VLLE)

6.5.2.1 Hexane (1) + Acetonitrile (2)

The experimental measurement of this system was done to demonstrate that the newly developed apparatus was capable of measuring vapour-liquid-liquid equilibrium (VLLE). Data for this system was measured at 348.20 K. The data are reported in Table 6-12 and graphically presented as a x^I-x^{II}-y plot and P-x^I-x^{II}-y plot in Figures 6-27 and 6-28 respectively.

Table 6-12: Experimental vapour-liquid-liquid equilibrium data for hexane (1) + acetonitrile (2) at 348.20 K.

P / kPa	x_1^I	x_1^{II}	y_1
83.74	0	-	0
138.0	0.042	-	0.475
151.5	0.064	-	0.525
162.5	0.081	-	0.565
171.8	0.099	-	0.595
184.0	0.132	-	0.624
188.0*	0.312*	0.654*	0.650*
184.4	-	0.872	0.674
176.2	-	0.916	0.714
169.1	-	0.934	0.756
156.5	-	0.971	0.815
140.5	-	0.989	0.899
125.3	-	1	1

* Point of VLLE

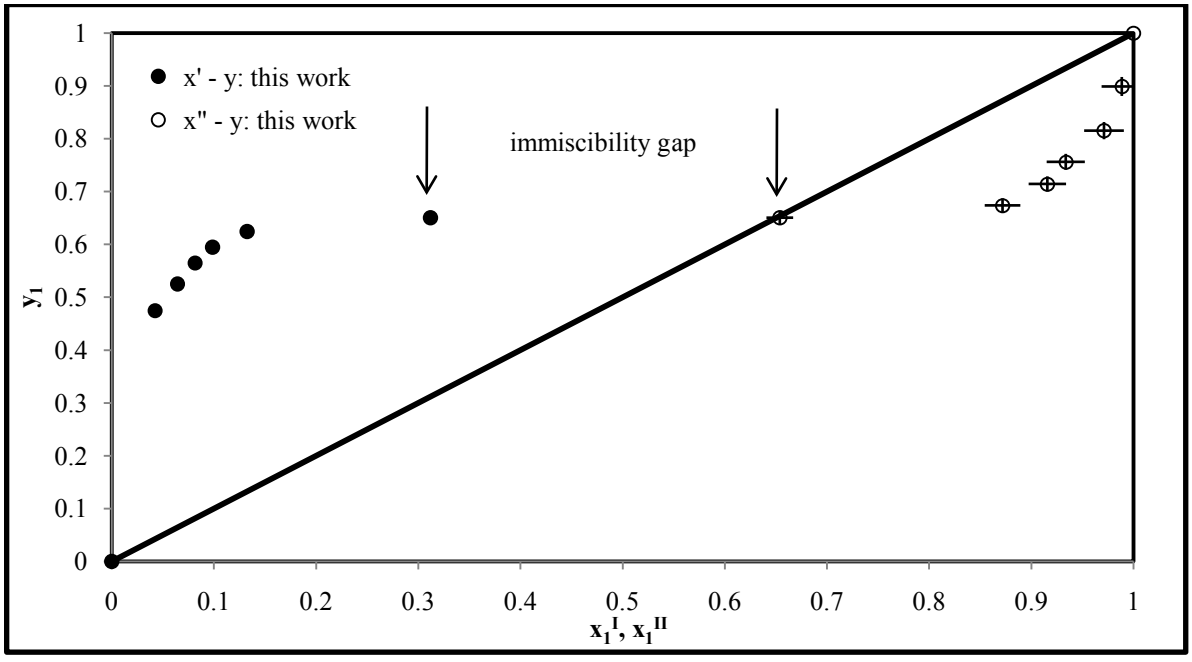

Figure 6-18: The x^I-x^{II}-y plot for the hexane (1) + acetonitrile (2) system at 348.20 K, error bars show 2% error for x_1^I, x_1^{II} and y_1.

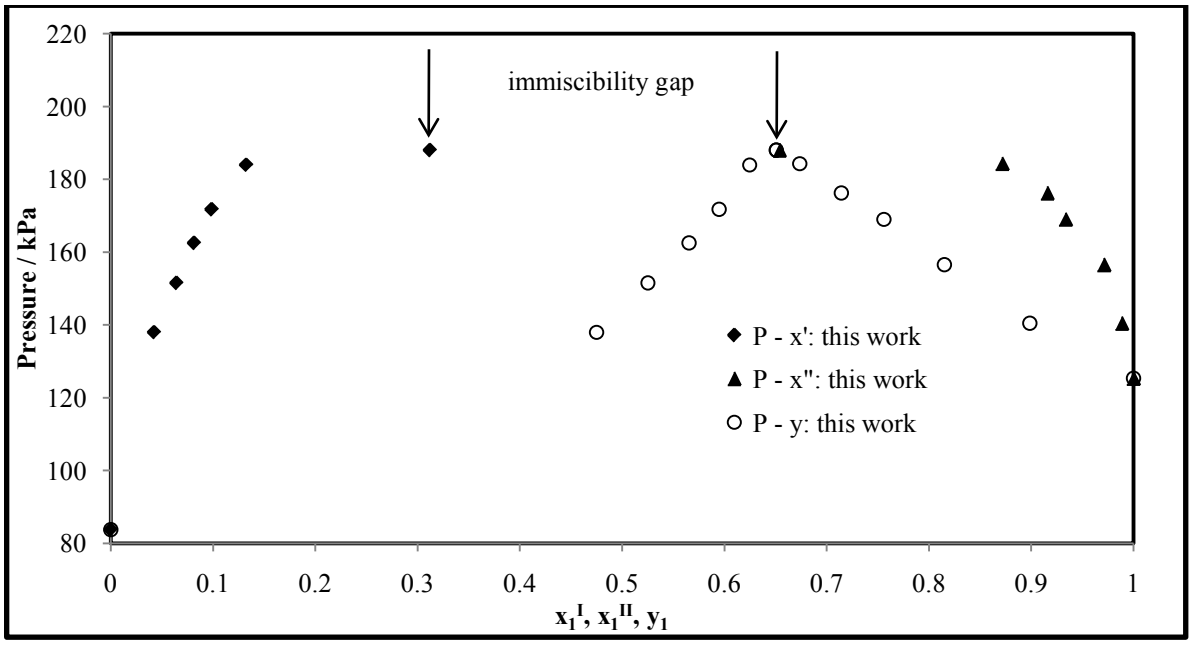

Figure 6-19: The *P-x^{I}-x^{II}-y* plot for the hexane (1) + acetonitrile (2) system at 348.20 K, error bars show 1% error for pressure and 2% error for x_1^{I}, x_1^{II} and y_1.

Toutes les données de tensions de vapeur et d'équilibres de phase mesurées avec l'appareillage récemment développé ont été soumises à une procédure d'analyse de données et discutées. Toutes les données de pression de vapeur se sont révélées thermodynamiquement cohérentes. Elles ont toutes été régressées en utilisant les équations empiriques étendues d'Antoine et de Wagner ainsi que les équations d'état PR et SRK. Des méthodes combinées et directes de régression de données ont été employées pour obtenir les paramètres des modèles associés aux systèmes en équilibres « liquide-vapeur ». Pour les méthodes combinées, la non-idéalité de la phase vapeur a été prise en compte par l'équation du viriel avec un deuxième coefficient du viriel provenant de la corrélation de Tsonopoulos (1974). Le non- idéalité de la phase liquide pour les méthodes combinées a été représentée au moyen des modèles de solutions liquides faisant appel au coefficient d'activité de phase (à savoir TK-Wilson, NRTL et modified UNIQUAC). Quant à la méthode directe, les non-idéalités en phases vapeur et liquide ont été prises en compte par des équations d'état cubique (à savoir celles de Peng et Robinson et de Soave, Redlich et Kwong avec la fonction alpha (α), dépendante de la température, celle de Mathias et Copeman (1983)). Les mêmes modèles de solutions liquides avec coefficient d'activité utilisés dans les méthodes combinées ont été également employés pour régresser des données des systèmes mesurés, en équilibre « liquide-liquide ». Pour montrer la polyvalence de l'appareillage de mesure d'équilibres, des équilibres « liquide-liquide-vapeur » ont été mesurés et les résultats analysés suivant la méthode combinée de régression de données. De façon générale, l'analyse a indiqué que toutes les données expérimentales mesurées ont été modélisées de manière satisfaisante à l'exception de celles d'équilibres « liquide-liquide-vapeur ». Les tests de cohérence thermo-dynamique (*point* and *direct tests)* concernant les données ELV comme élément de l'analyse des données ont été utilisés. Ils ont permis de constater que la majeure partie des données était thermodynamiquement cohérente à l'exception de peu d'entres elles.

7

CHAPTER SEVEN

DATA ANALYSIS AND DISCUSSION

This chapter focuses on the data analysis and discussion thereof for all the experimental results that were presented in Chapter 6 and begins with referencing the pure component properties for all the chemicals used in this study. This chapter also includes the analysis of vapour pressure data using both empirical equations and equations of state, determination of experimental activity coefficients, vapour-liquid equilibrium (VLE) data reduction with the combined and direct methods, liquid-liquid equilibrium (LLE) data reduction for the test systems measured and vapour-liquid-liquid equilibrium (VLLE) data reduction with the combined method. A discussion on thermodynamic consistency testing is also included.

7.1 Pure Component Properties

These properties describe the nature of the chemical and thus play an important role when analyzing thermodynamic data. Thermodynamic models rely on pure component properties to determine the model parameters, which are then used for predictions. Hence, the use of accurate pure component properties is essential for the correct theoretical treatment of phase equilibrium data. The pure component properties of all the chemicals used in this study were taken from the Dortmund Data Bank (2010). These properties include: critical temperature, critical pressure, critical volume and the acentric factor.

The second virial coefficients were evaluated using the correlation of Tsonopoulos (1974) as discussed in Section 3.1.1. This correlation requires the use of two pure component parameters: one to account for the polar effects and another to account for the hydrogen bonding effect. These parameters were taken from the publication of Tsonopoulos (1974) for all of the chemicals used in this study, except for ethyl acetate, 2-methoxy-2-methylbutane and 2-methoxy-2-methylpropane

which were not available. Tsonopoulos (1974) however found a correlation for the polar effect pure component parameter of ethers that required the use of dipole moments. The dipole moments for 2-methoxy-2-methylbutane and 2-methoxy-2-methylpropane were taken from the Dortmund Data Bank (2010) and used with the correlation of Tsonopoulos (1974) to determine the polar effect pure component parameter. Tsonopoulos (1974) also mentioned that these two pure component parameters were determined from the regression of experimental second virial coefficients. Thus the polar effect pure component parameter for ethyl acetate was found from the least squares regression of experimental second virial coefficients using the data presented in Dymond and Smith (1980).

The liquid molar volumes of all the chemicals used in this study were determined from the correlation of Rackett (1970) as discussed in Section 3.1, Equation (3-25). The pure component properties for all the chemicals used in this study are presented in Appendix B.

7.2 Experimental Vapour Pressure Data

Experimental vapour pressure data were measured using the newly developed apparatus (see Chapter 4) for all chemicals used in this study. Apart from verifying the operation of the apparatus, the measurement of experimental vapour pressure also served as a check for thorough degassing of the chemicals. Numerous empirical correlations are available to correlate vapour pressure of chemicals; however the Antoine and Wagner equations are the two most commonly used (Smith et al., 2001). These correlations contain pure component parameters that are valid for a specified temperature range. For this study, a modified Antoine equation known as the extended Antoine equation and the Wagner equation were used to correlate vapour pressure for the combined method of VLE data reduction.

An equation of state (EoS) can also be used to correlate vapour pressure of chemicals. The pure component parameter used in an EoS is dependent on the temperature dependent function (α) utilized. These pure component parameters, from an empirical correlation or EoS, are found by the regression of experimental vapour pressure measurements. For this study, the Soave-Redlich-Kwong (SRK) and Peng-Robinson (PR) equations of state with the temperature dependent function (α) of Mathias and Copeman (1983) were used as thermodynamic models for the direct method of VLE data reduction. In order to improve the accuracy of vapour pressure correlations in VLE data reduction, the pure component parameters from the empirical correlations and the temperature dependent function (α) of Mathias and Copeman (1983) in the SRK or PR EoS were regressed.

7.2.1 Comparison of Experimental and Literature Vapour Pressure

Experimental vapour pressures were measured for all chemicals used in this study and compared to literature values obtained from the extended Antoine equation in Aspen Plus (2004), except for butan-one and methanol. The literature values for butan-2-one and methanol were taken from Reid et al. (1988). Aspen Plus is a simulation software that contains a property data bank and is widely used in universities, research institutes and even in industries. The experimental vapour pressure data were compared to literature and presented graphically in Chapter 6 (Figures 6-1 to 6-5). The comparison of the experimental and literature vapour pressures are presented as deviation plots for all chemicals used in this study in Figures 7-1 to 7-5.

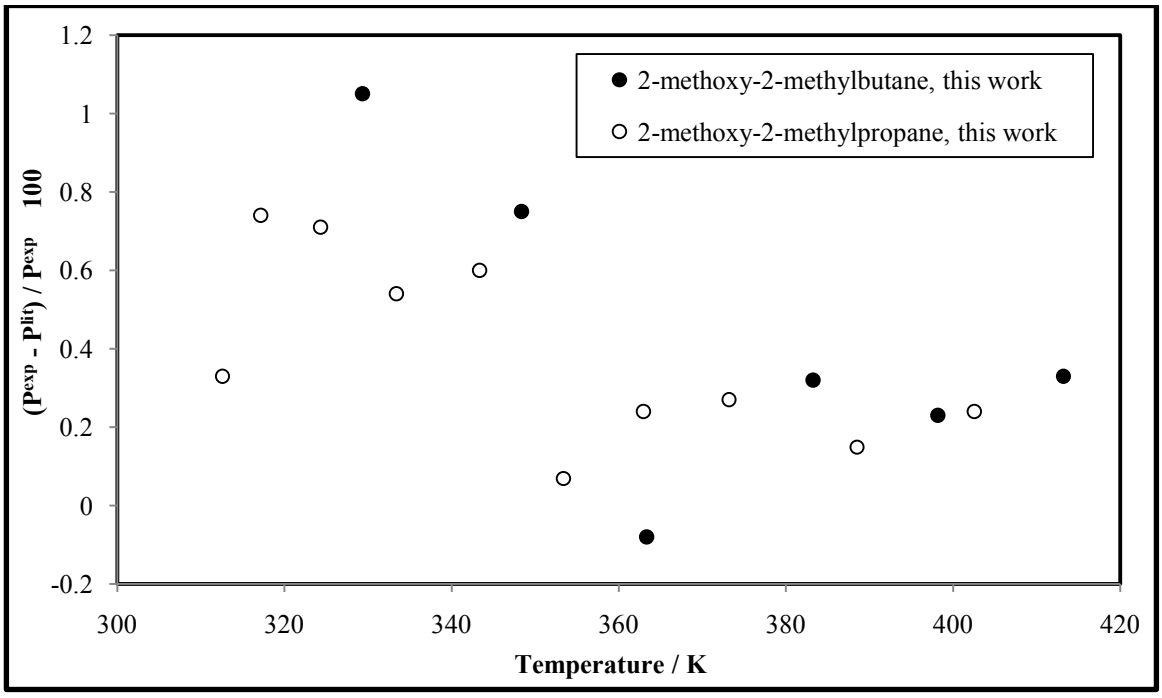

Figure 7-1: Vapour pressure deviation plots for the comparison of experimental data with Aspen Plus (2004) for 2-methoxy-2-methylbutane and 2-methoxy-2-methylpropane.

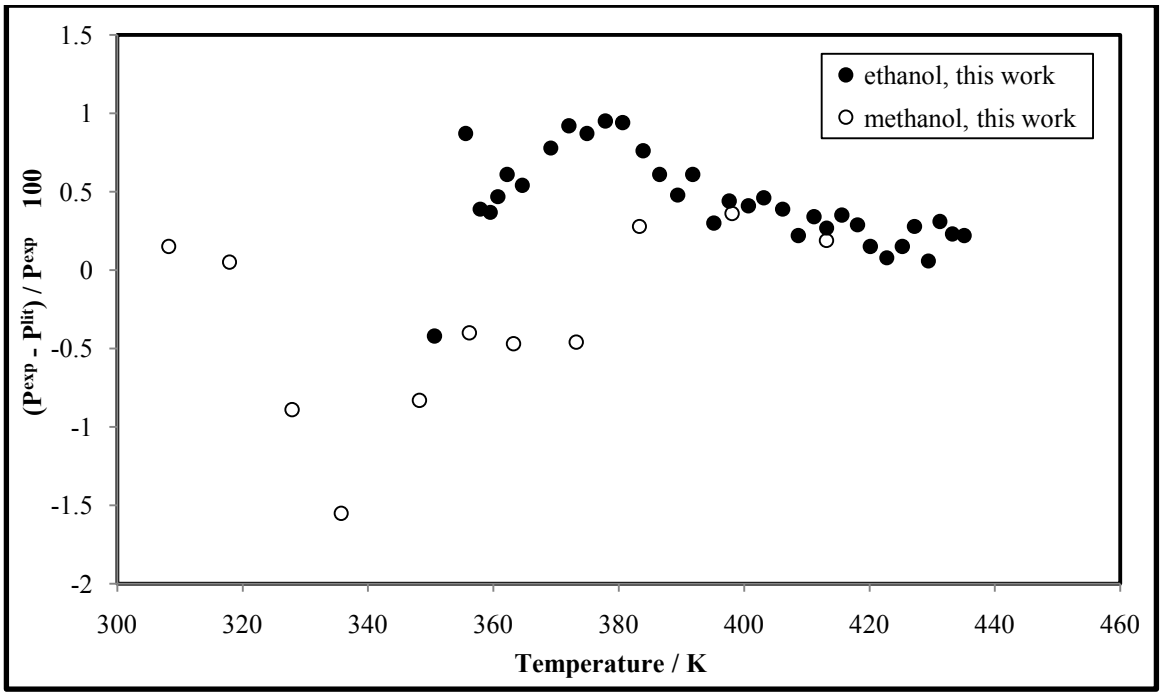

Figure 7-2: Vapour pressure deviation plots for the comparison of experimental data with Aspen Plus (2004) for ethanol and methanol.

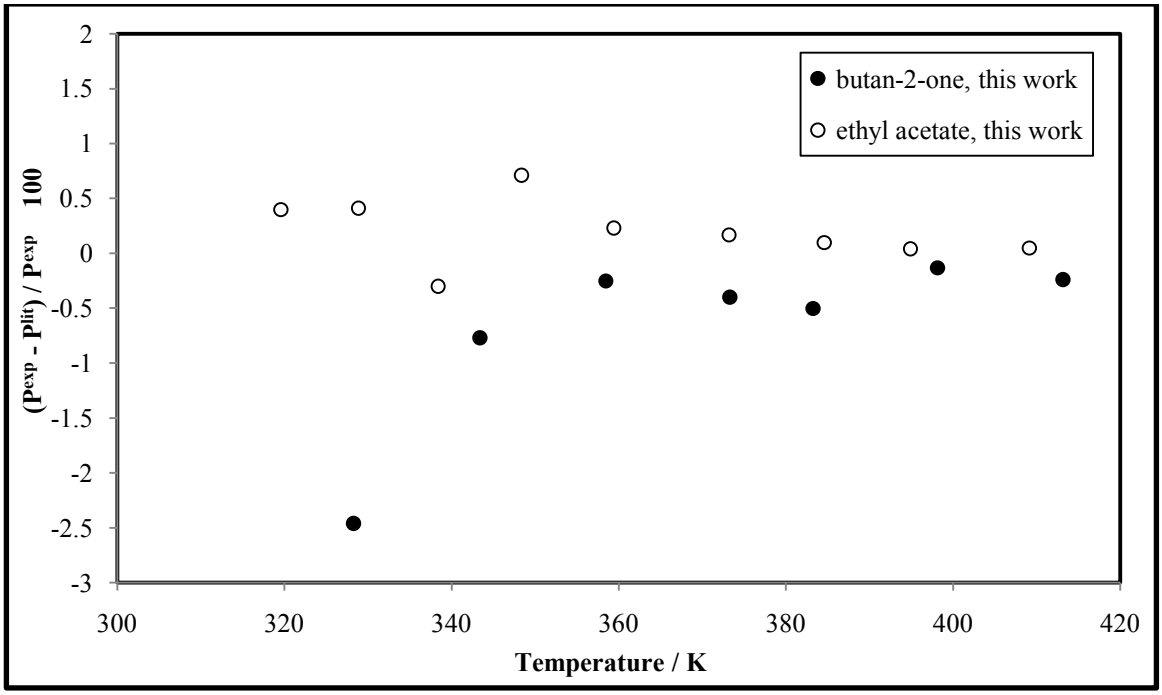

Figure 7-3: Vapour pressure deviation plots for the comparison of experimental data with Reid et al. (1988) for butan-2-one and experimental data with Aspen Plus (2004) for ethyl acetate.

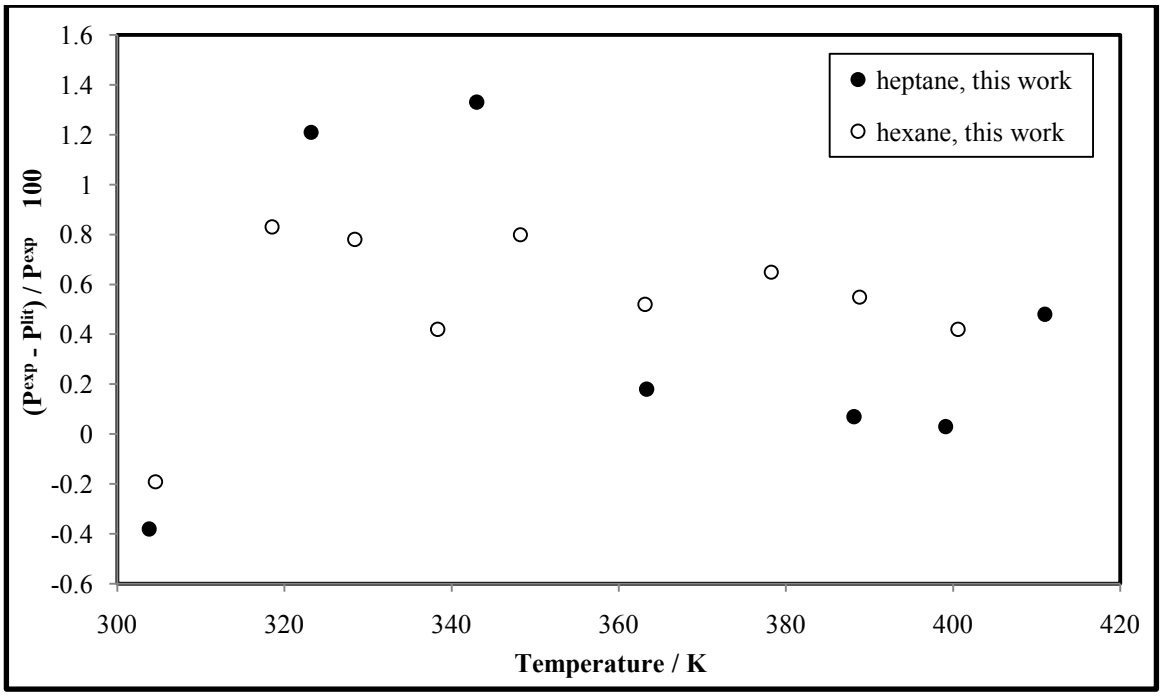

Figure 7-4: Vapour pressure deviation plots for the comparison of experimental data with Aspen Plus (2004) for heptane and hexane.

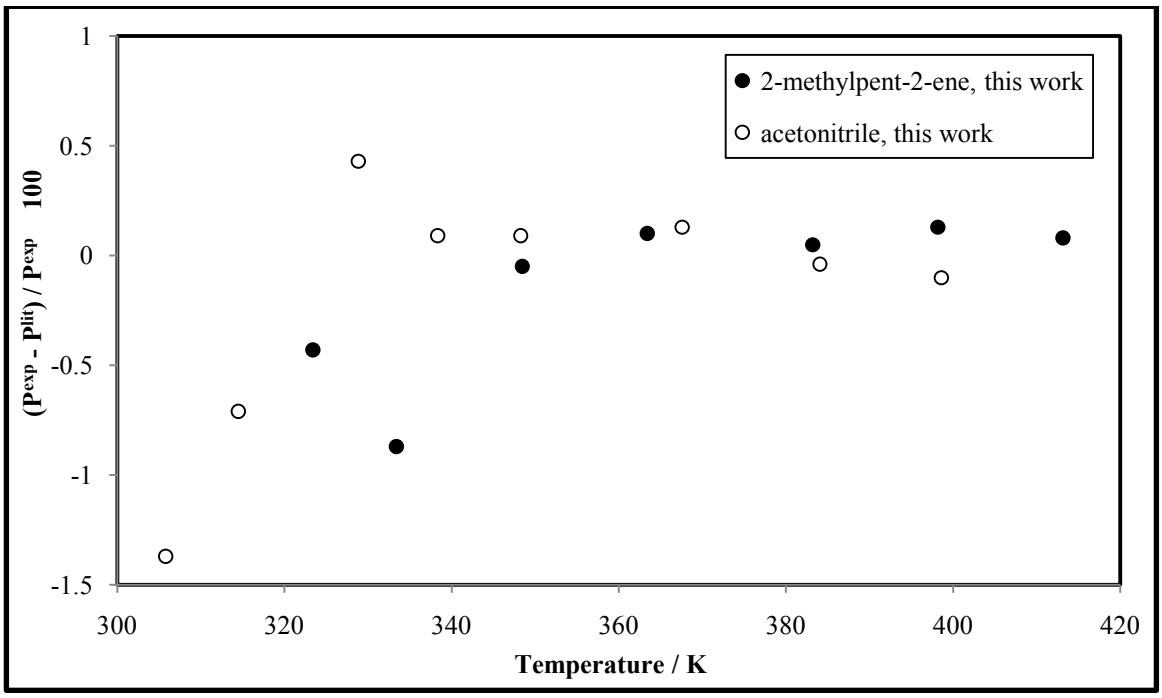

Figure 7-5: Vapour pressure deviation plots for the comparison of experimental data with Aspen Plus (2004) for 2-methylpent-2-ene and acetonitrile.

The experimental and literature values were also compared by determining the average absolute deviations (AAD):

$$AAD = \frac{1}{n}\sum_{i=1}^{n}\left|\Delta P_i\right| \tag{7-1}$$

where n is the number of experimental points and ΔP is the difference between the experimental and literature vapour pressure. The AAD values are reported in Table 7-1.

The deviation plots in Figures 7-1 to 7-5 and the AAD values in Table 7-1 show that the experimental vapour pressure data compares well with literature values for all chemicals except for, ethanol, hexane and methanol. The literature values for butan-2-one and methanol were taken from an alternate source (Reid et al., 1988) for comparison purpose only as large deviations were observed for these chemicals with the literature values from Aspen Plus (2004). In fact literature values for methanol from Reid et al. (1988), Aspen Plus (2004) and the Dortmund Data Bank (2010) all showed significant deviations when compared with each other especially for temperatures greater than 363 K. The scatter observed in the deviation plots was expected since the correlation coefficients in literature sources have most likely been obtained from the regression of experimental measurements.

Table 7-1: Average absolute deviations (AAD) for the vapour pressures.

	AAD	Temperature Range	
Chemical	**/ kPa**	**Min / K**	**Max / K**
2-methoxy-2-methylbutane	0.29	329.35	413.16
2-methoxy-2-methylpropane	0.30	312.55	402.54
2-methylpent-2-ene	0.33	323.40	413.13
acetonitrile	0.16	305.80	398.58
butan-2-one	0.31	328.26	413.13
ethanol	0.76	350.59	435.05
ethyl acetate	0.15	319.59	409.12
heptane	0.35	303.79	410.94
hexane	0.61	304.58	400.57
methanol	0.79	308.17	413.14

7.2.2 Regression using Empirical Correlations

The extended Antoine equation used in this study is of the form (Reid et al., 1988):

$$\ln P = A' + \frac{B'}{T} + C' \ln(T) + D' T^{E'} \tag{7-2}$$

The parameter E' was kept as a constant integer and therefore only the other four parameters were determined from the regression of the experimental data.

The Wagner equation is known as:

$$\ln\left(\frac{P}{P_c}\right) = (1-x')^{-1}\left[A''x' + B''(x')^{1.5} + C''(x')^3 + D''(x')^6\right] \tag{7-3}$$

where:

$$x' = 1 - \frac{T}{T_c} \tag{7-4}$$

For both the extended Antoine and Wagner equations, the pressure is given in kPa and the temperature in Kelvin. The regression algorithm was based on the Nelder-Mead simplex method (Lagarias et al., 1998). Initial estimates of the parameters for the method of regression were taken from Aspen Plus (2004) for the extended Antoine equation and Reid et al. (1988) for the Wagner equation. The objective function used was the least squares deviation of the pressure:

$$F = \sum_{i=1}^{n}\left[(P_i)_{\exp} - (P_i)_{cal}\right]^2 \tag{7-5}$$

where n is the number of experimental points. The pure component parameters from the regression using the extended Antoine and Wagner equations are presented in Tables 7-2 and 7-3 respectively. The root mean squared deviation was used as a measure to compare the regression results of the extended Antoine and Wagner equations:

$$RMSD = \sqrt{\frac{\sum_{i=1}^{n}\left[(P_i)_{\exp} - (P_i)_{cal}\right]^2}{n}} \qquad (7\text{-}6)$$

The RMSD values for both equations indicate a good fit of the experimental vapour pressure data. The comparison of the RMSD values indicates that the extended Antoine equation provides a better fit for 2-methoxy-2-methylbutane, 2-methylpent-2-ene, ethyl acetate and methanol whilst the Wagner equation provides a better fit for 2-methoxy-2-methylpropane, acetonitrile, butan-2-one, ethanol, heptane and hexane. Therefore, each component in the binary VLE data reduction with the combined method made use of the equation that corresponded to the lower RMSD. Overall, the result was not surprising since both equations cater for a greater degree of complexity with each having 4 adjustable parameters.

7.2.3 Regression using Equations of State

The SRK and PR equations of state are the two most widely used cubic equations of state for industrial applications as they require little input information to produce reasonable phase equilibrium predictions. They also generate reasonably good vapor pressure predictions for non-polar components. Since polar components were used in this study, the temperature dependent function (α) of Mathias and Copeman (1983) was used with the SRK and PR equations of state. The temperature dependent function (α) of Mathias and Copeman (1983) has the advantage of introducing a greater degree of complexity by using adjustable parameters to improve vapour pressure predictions and cater for polar components. Furthermore, the temperature dependent function (α) of Mathias and Copeman (1983) can be used in any cubic EoS; however the adjustable parameters would differ for each cubic EoS.

The accuracy of VLE calculations is greatly influenced by the accurate prediction of vapour pressure (Twu et al., 1991). Hence the experimental vapour pressure data were also regressed to determine the parameters of the temperature dependent function (α) of Mathias and Copeman (1983) in order improve vapour pressure predictions. The regression was carried out using the THERMOPACK version 1.10 software program developed by A. Baba Ahmed and C. Coquelet. Equation (7-4) was also used as the objective function. The pure component parameters from the regression using the temperature dependent function (α) of Mathias and Copeman (1983) in the

Table 7-2: Regressed pure component parameters for the extended Antoine equation.

Chemical	A'	B'	C'	D'	E'	RMSD / kPa	Temperature Range Min / K	Max / K
2-methoxy-2-methylbutane	46.3240	-5440.75	-4.5185	1.11E-17	6	0.21	329.35	413.16
2-methoxy-2-methylpropane	64.5687	-5827.53	-7.2921	4.62E-17	6	0.30	312.55	402.54
2-methylpent-2-ene	43.9110	-5084.75	-4.1869	4.28E-07	2	0.27	323.40	413.13
acetonitrile	129.442	-8347.48	-17.6904	2.05E-05	2	0.12	305.80	398.58
butan-2-one	229.959	-12618.75	-33.0512	3.46E-05	2	0.45	328.26	413.13
ethanol	225.4857	-13616.05	-31.6697	2.85E-05	2	0.64	350.59	435.05
ethyl acetate	57.9767	-6137.38	-6.1214	1.43E-17	6	0.24	319.59	409.12
heptane	218.7101	-12135.72	-31.4728	3.49E-05	2	0.16	303.79	410.94
hexane	143.5933	-8724.96	-19.8727	2.14E-05	2	0.27	304.58	400.57
methanol	-24.1119	-3103.80	6.7383	-1.16E-05	2	0.48	308.17	413.14

Table 7-3: Regressed pure component parameters for the Wagner equation.

Chemical	A''	B''	C''	D''	RMSD / kPa	Temperature Range Min / K	Max / K
2-methoxy-2-methylbutane	-7.759	1.994	-3.970	-0.534	0.23	329.35	413.16
2-methoxy-2-methylpropane	-6.922	0.414	-0.603	-19.096	0.28	312.55	402.54
2-methylpent-2-ene	-6.835	1.341	-5.833	12.124	0.31	323.40	413.13
acetonitrile	-6.523	-1.543	3.679	-18.935	0.10	305.80	398.58
butan-2-one	-6.443	-1.846	4.973	-46.097	0.39	328.26	413.13
ethanol	-7.687	-2.170	3.155	-75.194	0.59	350.59	435.05
ethyl acetate	-8.184	2.699	-6.876	7.487	0.25	319.59	409.12
heptane	-5.667	-3.811	6.715	-37.284	0.11	303.79	410.94
hexane	-7.303	0.751	-0.381	-21.089	0.26	304.58	400.57
methanol	-8.901	1.804	-6.193	20.504	0.64	308.17	413.14

SRK and PR equations of state are reported in Tables 7-4 and 7-5 respectively (see Equation (3-61)). The root mean squared deviation, Equation (7-5), was used a measure to compare the regression results from the two equations of state.

The results from the regression indicated a reasonably good fit for the vapour pressure of all chemicals except for 2-methoxy-2-methylpropane with the PR EoS. The high RMSD for ethanol and methanol are due to a wider temperature range. Furthermore, methanol has a steeper gradient for the vapour pressure curve. Overall, the empirical correlations provide a better fit for the vapour pressure. The best fit of the empirical correlations for each component is shown graphically in Figures 7-6 to 7-10.

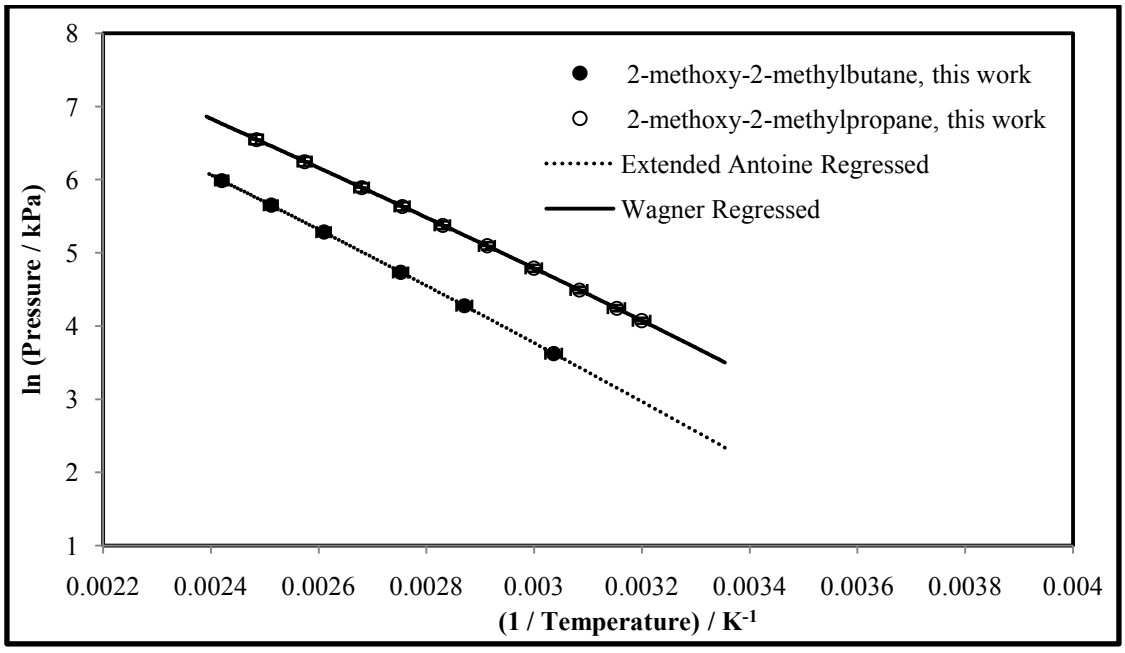

Figure 7-6: Vapour pressure plots for the ethers used in this study, 2-methoxy-2-methylbutane and 2-methoxy-2-methylpropane, with the best fit of the empirical correlations. Error bars show 1 % error for pressure and 0.5 % error for temperature.

Table 7-4: Regressed pure component parameters for the α function of Mathias and Copeman (1983) with the SRK EoS.

Chemical	κ_1	κ_2	κ_3	RMSD / kPa	Temperature Range Min / K	Max / K
2-methoxy-2-methylbutane	1.038	-0.846	1.797	0.29	329.35	413.16
2-methoxy-2-methylpropane	0.948	-0.740	2.138	0.25	312.55	402.54
2-methylpent-2-ene	0.741	0.621	-0.518	0.22	323.40	413.13
acetonitrile	1.103	-1.108	1.500	0.24	305.80	398.58
butan-2-one	1.102	-1.377	3.533	0.44	328.26	413.13
ethanol	1.425	-0.142	0.227	1.00	350.59	435.05
ethyl acetate	1.074	-0.567	1.582	0.26	319.59	409.12
heptane	1.082	-0.815	1.984	0.64	303.79	410.94
hexane	1.070	-1.392	3.395	0.19	304.58	400.57
methanol	1.376	-0.072	-1.756	1.39	308.17	413.14

Table 7-5: Regressed pure component parameters for the α function of Mathias and Copeman (1983) with the PR EoS.

Chemical	κ_1	κ_2	κ_3	RMSD / kPa	Temperature Range Min / K	Max / K
2-methoxy-2-methylbutane	0.862	-0.447	1.214	0.29	329.35	413.16
2-methoxy-2-methylpropane	0.738	0.159	-0.015	1.00	312.55	402.54
2-methylpent-2-ene	0.592	0.831	-0.684	0.19	323.40	413.13
acetonitrile	0.929	-0.739	1.045	0.25	305.80	398.58
butan-2-one	0.924	-0.954	2.877	0.45	328.26	413.13
ethanol	0.592	0.831	-0.684	1.01	350.59	435.05
ethyl acetate	0.882	-0.018	0.560	0.43	319.59	409.12
heptane	0.907	-0.444	1.480	0.65	303.79	410.94
hexane	0.895	-0.979	2.765	0.19	304.58	400.57
methanol	1.173	0.380	-2.338	1.32	308.17	413.14

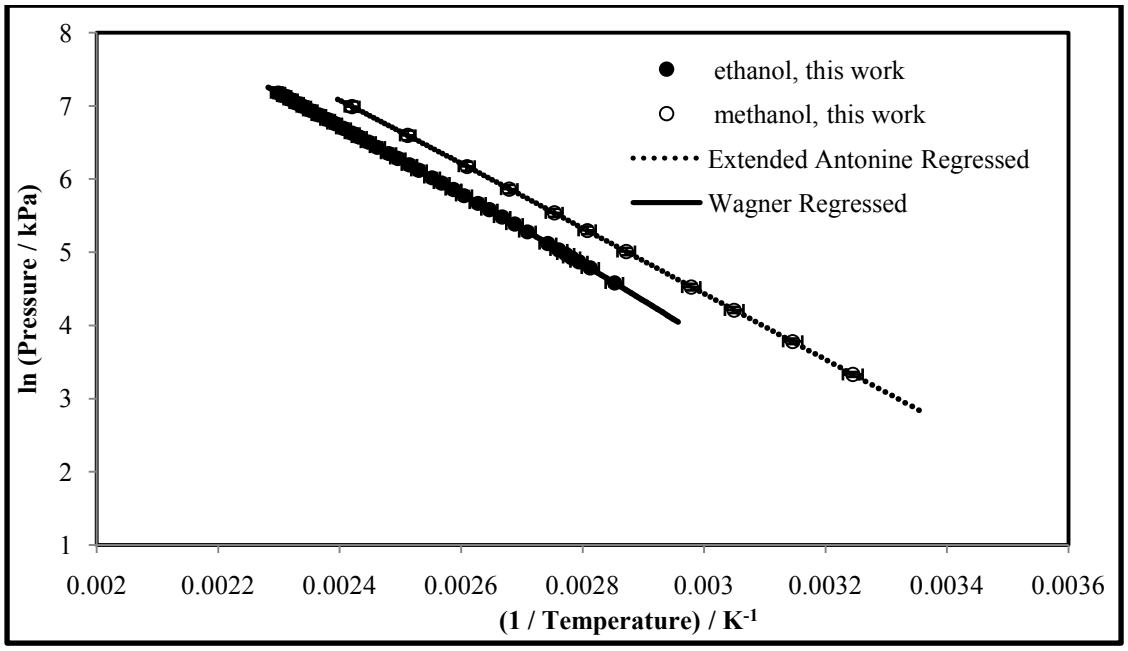

Figure 7-7: Vapour pressure plots for the alcohols used in this study, ethanol and methanol, with the best fit of the empirical correlations. Error bars show 1 % error for pressure and 0.5 % error for temperature.

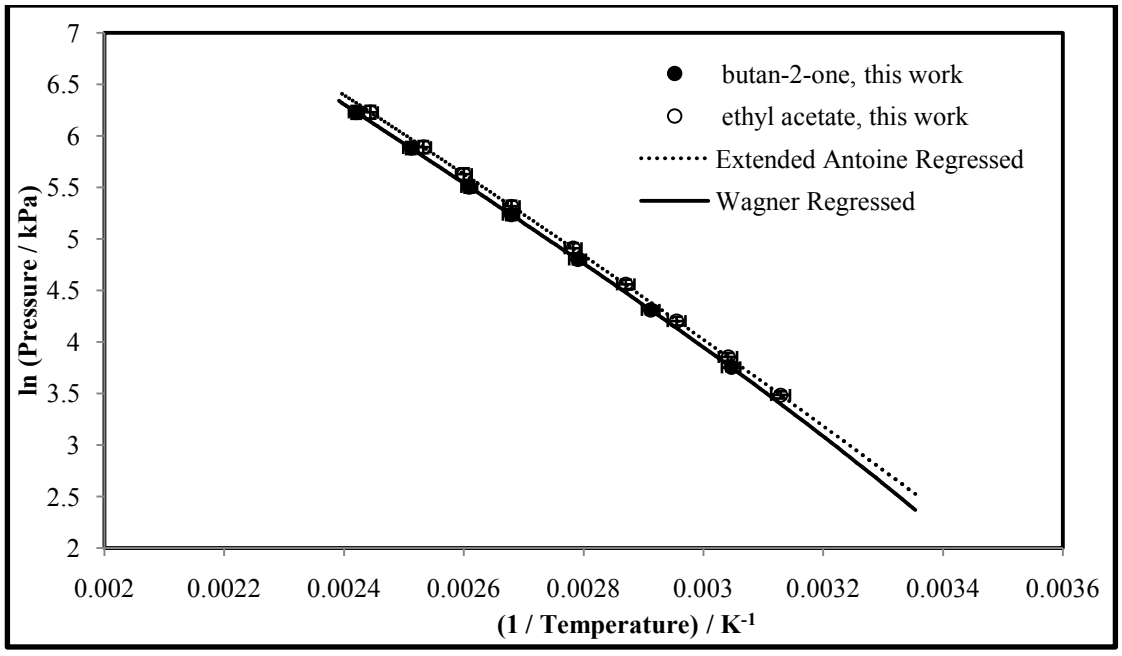

Figure 7-8: Vapour pressure plots for the ketone (butan-2-one) and ester (ethyl acetate) used in this study with the best fit of the empirical correlations. Error bars show 1 % error for pressure and 0.5 % error for temperature.

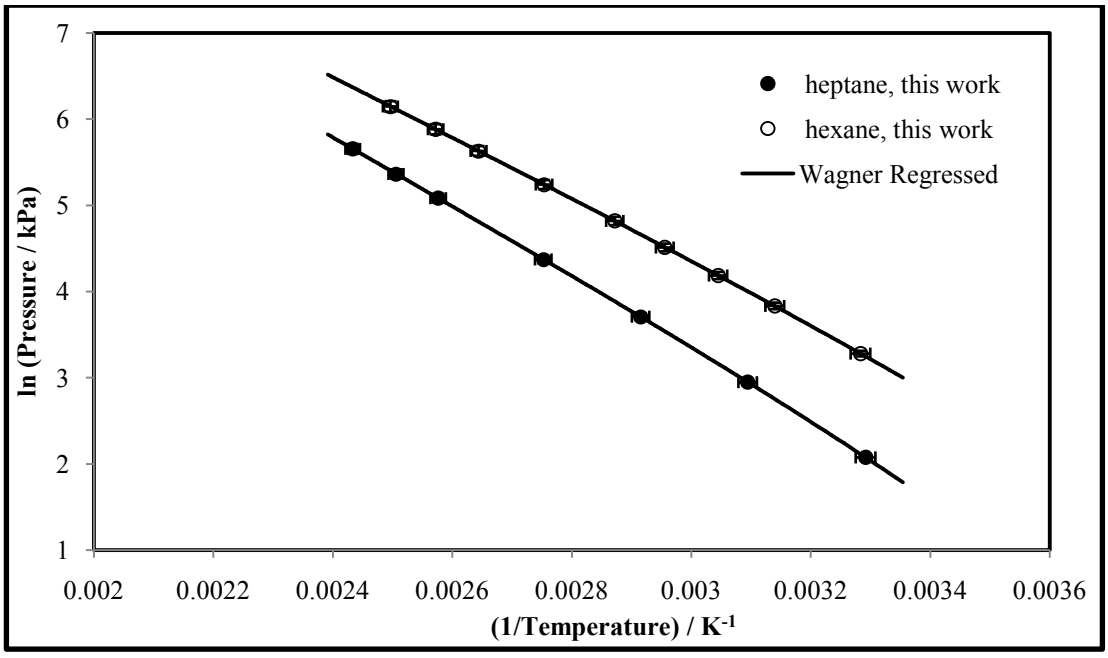

Figure 7-9: Vapour pressure plots for the alkanes used in this study, heptane and hexane, with the best fit of the empirical correlations. Error bars show 1 % error for pressure and 0.5 % error for temperature.

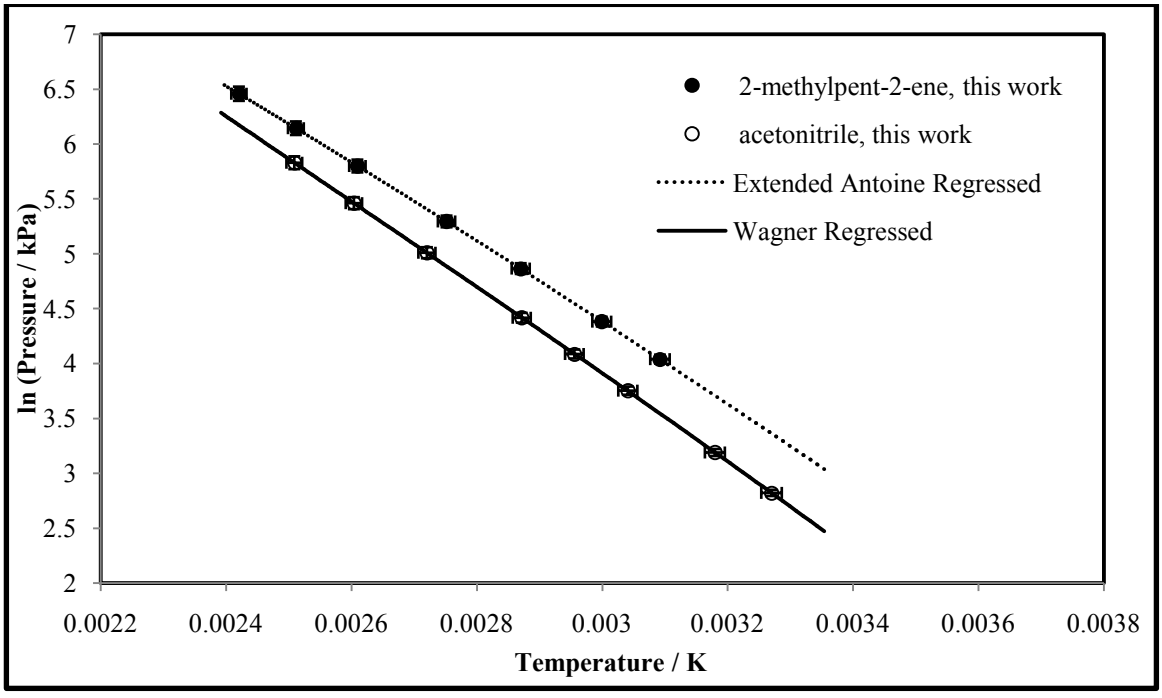

Figure 7-10: Vapour pressure plots for the alkene (2-methylpent-2-ene) and nitrile (acetonitrile) used in this study with the best fit of the empirical correlations. Error bars show 1 % error for pressure and 0.5 % error for temperature.

7.2.4 Thermodynamic Consistency Testing for Vapour Pressure Data

The experimental vapour pressure data were also checked for qualitative thermodynamic consistency using the recommendation of researchers in the Design Institute for Physical Property Data (DIPPR) Compilation Project (Daubert et al., 1990). This basically involved representing the data in the form of a ln P versus (1 / T) plot to visually check for the occurrence of decomposition or polymerization with an increase in temperature. If the plot shows a linear trend, then the data are considered thermodynamically consistent as no decomposition or polymerization would have occurred. However care should be exercised to ensure that a wide temperature range is considered to reach a compelling conclusion. The experimental vapour pressure data presented in Chapter 6 (Figures 6-1 to 6-5) showed a linear trend for all chemicals used in this study and therefore passed the qualitative thermodynamic consistency test within its temperature range. It should however be noted that the quotient of latent heat of vapourization and the vapour phase compressibility factor is assumed independent of temperature within the temperature range studied.

7.3 Experimental Activity Coefficients – VLE/VLLE Systems

The determination of the experimental activity coefficients was possible due to an "over specification" of the system where the temperature, pressure and both liquid and vapour compositions were measured. However, in order to determine the experimental activity coefficients, the vapour phase correction factor (Φ_i) was first evaluated with Equation (3-24). This was achieved by employing the Tsonopoulos (1974) correlation for the second virial coefficients, Equation (3-30), as outlined in Section 3.1.1, using the experimental pressure and vapour composition values. This correlation was chosen as it caters for both polar and non-polar components and provides very good predictions for the second virial coefficients. Furthermore, less input information was required than compared to other correlations such as Hayden and O'Connell (1975).

Once the vapour phase correction factor was evaluated, Equation (3-23) was then used to determine the experimental activity coefficient values. The activity coefficient determined in this manner is termed experimental as only experimental data was used in its evaluation and no thermodynamic model was used to determine the values. The experimental activity coefficients were also required to carry out thermodynamic consistency testing. The experimental activity coefficients for the VLE/VLLE systems studied in this work are reported in Tables 7-6 to 7-11. The comparison of

experimental and calculated activity coefficients are presented in Section 7-4 and the thermodynamic consistency test is presented in Section 7-7.

Table 7-6: Experimental liquid-phase activity coefficients for the 2-methoxy-2-methylpropane (1) + ethyl acetate (2) system at 373.17 K.

x_1	γ_1	γ_2
0.077	1.17	1.01
0.149	1.17	1.02
0.239	1.11	1.03
0.298	1.10	1.04
0.390	1.07	1.06
0.465	1.06	1.08
0.548	1.04	1.10
0.600	1.03	1.13
0.685	1.03	1.12
0.765	1.02	1.16
0.826	1.01	1.22

Table 7-7: Experimental liquid-phase activity coefficients for the methanol (1) + butan-2-one (2) system.

383.25 K			398.14 K			413.20 K		
x_1	γ_1	γ_2	x_1	γ_1	γ_2	x_1	γ_1	γ_2
0.131	1.37	1.04	0.165	1.39	1.01	0.113	1.43	1.00
0.292	1.28	1.05	0.305	1.32	1.01	0.171	1.36	1.01
0.385	1.23	1.07	0.382	1.26	1.03	0.254	1.30	1.01
0.545	1.16	1.12	0.459	1.22	1.05	0.351	1.22	1.05
0.599	1.12	1.17	0.548	1.14	1.14	0.434	1.19	1.07
0.720	1.06	1.31	0.693	1.08	1.22	0.550	1.13	1.11
0.778	1.04	1.40	0.849	1.02	1.48	0.673	1.07	1.23
0.863	1.02	1.55				0.780	1.04	1.35
0.906	1.00	1.72				0.889	1.01	1.60
0.974	1.00	1.91						

Table 7-8: Experimental liquid-phase activity coefficients for the ethanol (1) + butan-2-one (2) system.

383.26 K			398.23 K			413.21 K		
x_1	γ_1	γ_2	x_1	γ_1	γ_2	x_1	γ_1	γ_2
0.111	1.52	1.01	0.135	1.42	1.01	0.122	1.39	1.01
0.160	1.41	1.02	0.202	1.35	1.02	0.208	1.32	1.01
0.231	1.35	1.03	0.244	1.34	1.02	0.295	1.26	1.02
0.290	1.32	1.03	0.358	1.24	1.04	0.370	1.21	1.04
0.358	1.24	1.06	0.537	1.11	1.14	0.492	1.14	1.09
0.465	1.15	1.13	0.588	1.10	1.16	0.554	1.11	1.12
0.645	1.07	1.23	0.749	1.03	1.31	0.641	1.07	1.19
0.755	1.02	1.35	0.842	1.01	1.42	0.718	1.04	1.26
0.858	1.00	1.50				0.835	1.01	1.44
						0.900	1.00	1.50
						0.916	1.01	1.50

Table 7-9: Experimental liquid-phase activity coefficients for the ethanol (1) + 2-methoxy-2-methylbutane (2) system.

398.25 K			413.19 K		
x_1	γ_1	γ_2	x_1	γ_1	γ_2
0.026	2.42	0.99	0.044	2.14	1.00
0.049	2.21	0.99	0.090	2.02	1.01
0.110	2.05	1.00	0.150	1.87	1.02
0.190	1.86	1.01	0.213	1.77	1.02
0.318	1.54	1.10	0.303	1.56	1.08
0.453	1.35	1.21	0.400	1.42	1.15
0.547	1.24	1.33	0.479	1.34	1.19
0.732	1.09	1.69	0.622	1.18	1.39
0.769	1.06	1.81	0.691	1.13	1.52
0.855	1.03	2.11	0.783	1.04	1.92
0.895	1.02	2.22	0.936	1.01	2.40
0.935	1.01	2.54			

Table 7-10: Experimental liquid-phase activity coefficients for the 2-methylpent-2-ene (1) + ethanol (2) system at 383.20 K.

x_1	γ_1	γ_2
0.077	4.34	0.99
0.128	3.48	1.03
0.194	2.94	1.06
0.296	2.31	1.14
0.457	1.72	1.34
0.590	1.40	1.68
0.719	1.20	2.22
0.788	1.10	2.75
0.865	1.05	3.49
0.931	1.02	4.31
0.955	1.00	4.98

Table 7-11: Experimental liquid-phase activity coefficients for the hexane (1) + acetonitrile (2) system at 348.20 K.

x_1	γ_1	γ_2
0.042	12.64	0.87
0.064	10.00	0.88
0.081	9.05	0.88
0.099	8.25	0.88
0.132	6.85	0.90
0.312*	3.07*	1.09*
0.654*	1.47*	2.16*
0.872	1.12	5.36
0.916	1.08	6.91
0.934	1.08	7.27
0.971	1.04	11.92
0.989	1.01	15.09

* Point of VLLE

7.4 Experimental VLE Data Reduction

The reduction of the experimental VLE data was accomplished using the combined method and the direct method which were discussed in detail in Section 3.3.1. In the combined method, the vapour phase correction factor was determined using the virial equation of state where the correlation of Tsonopoulos (1974) was used to evaluate the second virial coefficients. The correlation of Tsonopoulos (1974) was able to cater for non-polar, polar and hydrogen bonding components and combinations thereof. The liquid phase correction factor was determined from three local-composition based liquid phase activity coefficient models viz. the TK-Wilson, NRTL and modified UNIQUAC thermodynamic models. The saturated pressures used in the combined method of VLE data reduction made use of the extended Antoine and Wagner equations, where the equation with a better fit of the experimental vapour pressure data was used for each component.

In the direct method, the two most industrially used equations of state were considered viz. the SRK and PR equations of state. To improve predictions with these equations of state, the temperature dependent function (α) of Mathias and Copeman (1983) was used to replace the originally proposed temperature dependent function in each EoS. This allowed the EoS to become more flexible and cater for both polar and non-polar components, where the regressed adjustable parameters for the temperature dependent function (α) of Mathias and Copeman (1983) were utilized. The direct method also required the use of a mixing rule to account for the interaction of the components in order to accurately model the experimental VLE data. For this purpose, the Wong and Sandler (1992) mixing rule, as discussed in Section 3.1.3, was used. The mixing rule also required the use of an activity coefficient model; hence the NRTL activity coefficient model was used for this purpose. The combinations used for the combined and direct methods are summarized in Tables 7-12 and 7-13 respectively.

Table 7-12: The regression combinations used for the combined method.

Second Virial Coefficient Correlation	Activity Coefficient Model	Abbreviation
Tsonopoulos (1974)	TK-Wilson	TS-TKWILSON
Tsonopoulos (1974)	NRTL	TS-NRTL
Tsonopoulos (1974)	modified UNIQUAC	TS-UNIQUAC

Table 7-13: The regression combinations used for the direct method.

Equation of State	α Correlation	Mixing Rule	Activity Coefficient Model for Mixing Rule	Abbreviation
Soave (1972)	Mathias and Copeman (1983)	Wong and Sandler (1992)	NRTL	SRK-MC-WS-NRTL
Peng and Robinson (1976)	Mathias and Copeman (1983)	Wong and Sandler (1992)	NRTL	PR-MC-WS-NRTL

The regression algorithm for the experimental VLE data reduction for the combined method made use of the Nelder-Mead simplex method (Lagarias et al., 1998). The regression with the direct method was achieved using the THERMOPACK version 1.10 developed by A Baba Ahmed and C. Coquelet. The objective function used for both methods was:

$$F = \left[\sum_{i=1}^{n} \left(\frac{P_{\exp,i} - P_{cal,i}}{P_{\exp,i}} \right)^2 \right] \tag{7-6}$$

Van Ness and Abbott (1982) found that using such an objective function as shown in Equation (7-6) provides a fit that was at least as good as any other and was the most simplest and direct objective function. The regression for the combined method was written in MATLAB as a variety of built-in optimization functions were available for use. The *fminsearch* function, which finds the minimum of an unconstrained multi-variable function, was chosen in this study.

7.4.1 2-Methoxy-2-Methylpropane (1) + Ethyl Acetate (2)

Once the novel apparatus was constructed, test systems were selected to verify that the apparatus was capable of measuring phase equilibrium data and to check the accuracy of the experimental procedure. With regards to VLE, the system of 2-methoxy-2-methylpropane + ethyl acetate at 373.17 K was selected as a test system. This system was chosen since literature data was available within the pressure range of the apparatus and the data were also proven to be thermodynamically consistent (Lee et al., 1997).

The GC TCD calibration for this system is presented in Figures C-25 and C-26 and reported in Table C-5 of Appendix C. The calibrations showed a linear response for both dilute regions of this system. The inverse of the response factor ratio of the 2-methoxy-2-methylpropane dilute region did not differ significantly from the response factor ratio of the ethyl acetate dilute region. This confirmed a linear relationship for the entire composition range. An average response factor ratio was however not used but care was taken to ensure that the correct calibration graph was employed, depending whether the samples were taken in the dilute 2-methoxy-2-methylpropane region or dilute ethyl acetate region. The influence of taking an average response factor ratio would slightly affect the accuracy especially for very dilute regions.

Figures 6-6 and 6-7 show that the experimental data measured compared well with literature data of Lee et al. (1997). However, there were slight deviations in the vapour composition values. Initially when the vapour composition was sampled, there were significant deviations between the experimental data and the literature data of Lee et al. (1997). It was found that these deviations were attributed to a thermal gradient that existed on the upper 316 SS flange of the equilibrium cell due to conductive and convective paths of heat transfer. Hence the capillary of the ROLSI™ was at a slightly lower temperature than compared to the equilibrium temperature. This implied that there was slight condensation of the vapour on the tip of the ROLSI™ capillary thus leading to an incorrect determination of the vapour phase composition. By trial and error, it was found that when the temperature of the upper 316 SS flange of the equilibrium cell was kept at 0.1 K higher than the equilibrium temperature, the condensation of vapour at the tip of the ROLSI™ capillary was prevented.

This test system was also subjected to thermodynamic modeling with the combined and direct methods of VLE data regression. The combined method used the second virial coefficient correlation of Tsonopoulos (1974) to represent the vapour phase non-ideality and the liquid phase non-idealities were represented with NRTL, modified UNIQUAC and TK-Wilson activity coefficient models. Regression of the experimental data showed that the NRTL model (with the α parameter included in the regression) provided the best fit to the experimental data, where the best fit was judged from the lowest root mean square deviation (RMSD) of the pressure and vapour compositions. The parameters from the regression of the experimental data with the combined method are reported in Table 7-14.

As can be seen from the RMSD values for pressure and vapour composition in Table 7-14, the NRTL model offers only a slightly better fit than compared to the other thermodynamic models. The regressed value of the non-randomness parameter (α) is rather large, implying that the local distribution is highly non-random around the centre molecule. Generally, a high value of α is typical of systems that exhibit hydrogen bonding. Although 2-methoxy-2-methylpropane and ethyl acetate do not exhibit hydrogen bonds, they are both polar compounds. Nevertheless, Walas (1985) emphasizes that the parameter α is strictly an empirical factor and does not clearly relate to any mechanism. Indeed this can be seen when α is fixed at a value of 0.3, the regression results show that the NRTL model offers no distinct advantage over the TK-Wilson or modified UNIQUAC models in the representation of this experimental data (see Table 7-13). The TK-Wilson, NRTL (with α fixed at 0.3 during regression) and the modified UNIQUAC models all show large values for the binary interaction parameters. However the NRTL model with α included as a regression parameter showed smaller values for the binary interaction parameters, indicative of the empirical nature of the α parameter. The large value of $\alpha = 3.54$ could also indicate a very organized solution in terms of molecular structure. The *x-y* and *P-x-y* plots for the combined method are presented in Figures 7-11 and 7-12 respectively. The experimental activity coefficients and those calculated by the NRTL model (with $\alpha = 3.54$) are presented in Figure 7-13, which shows that there is considerable deviation. This could possibly be due to errors in the measurement of the vapour compositions (discussed further in thermodynamic consistency testing). The estimated uncertainty on the activity coefficient is 3 %.

Table 7-14: Model parameters (A_{12} and A_{21})[a], root mean square deviations (RMSD) and absolute average deviation (AAD) values for the combined method of the 2-methoxy-2-methylpropane (1) + ethyl acetate (2) system at 373.17 K.

Model	A_{12} J.mol^{-1}	A_{21} J.mol^{-1}	RMSD P / kPa	AAD P / kPa	RMSD y_1	AAD y_1
TS-TKWILSON	-1120	1950	0.57	0.40	0.010	0.008
TS-NRTL ($\alpha = 0.3$)	1512	-602.6	0.58	0.41	0.0010	0.008
TS-NRTL ($\alpha = 3.54$)	688.3	459.1	0.50	0.41	0.009	0.008
TS-UNIQUAC	1134	-745.5	0.58	0.41	0.010	0.008

[a]TKWilson: $A_{12} = a_{12} - a_{22}$ and $A_{21} = a_{21} - a_{11}$; NRTL: $A_{12} = g_{12} - g_{22}$ and $A_{21} = g_{21} - g_{11}$; mod UNIQUAC: $A_{12} = u_{12} - u_{22}$ and $A_{21} = u_{21} - u_{11}$.

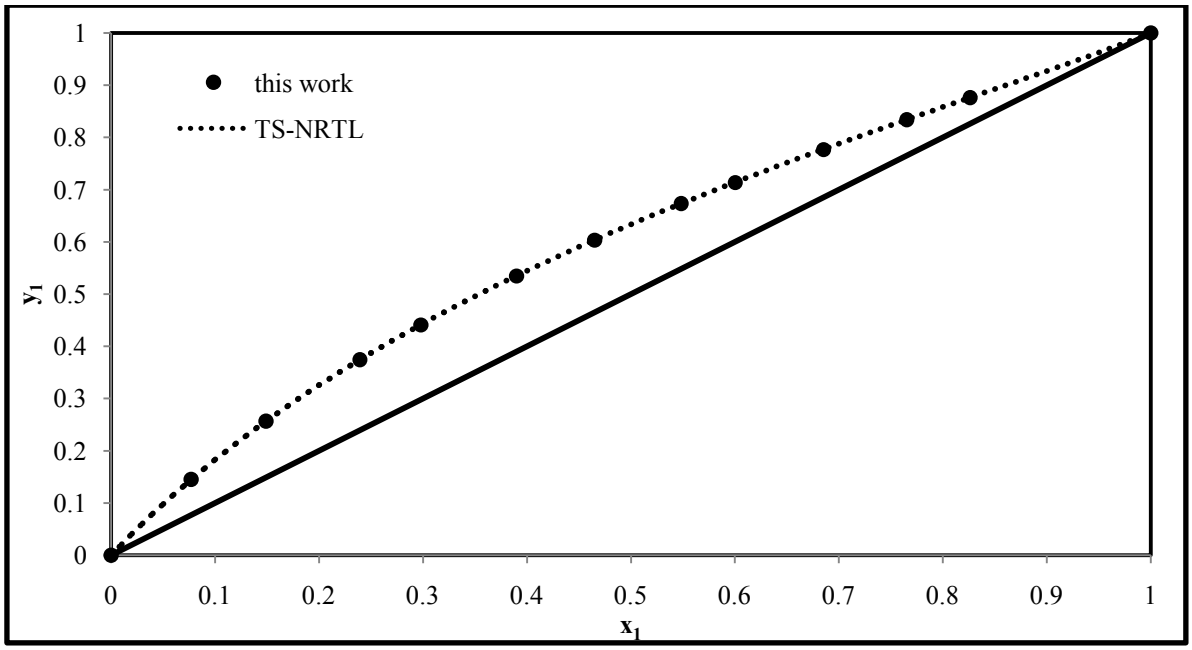

Figure 7-11: Fit of the TS-NRTL model combination to the x-y plot of the methoxy-2-methylpropane (1) + ethyl acetate (2) system at 373.17 K for the combined method.

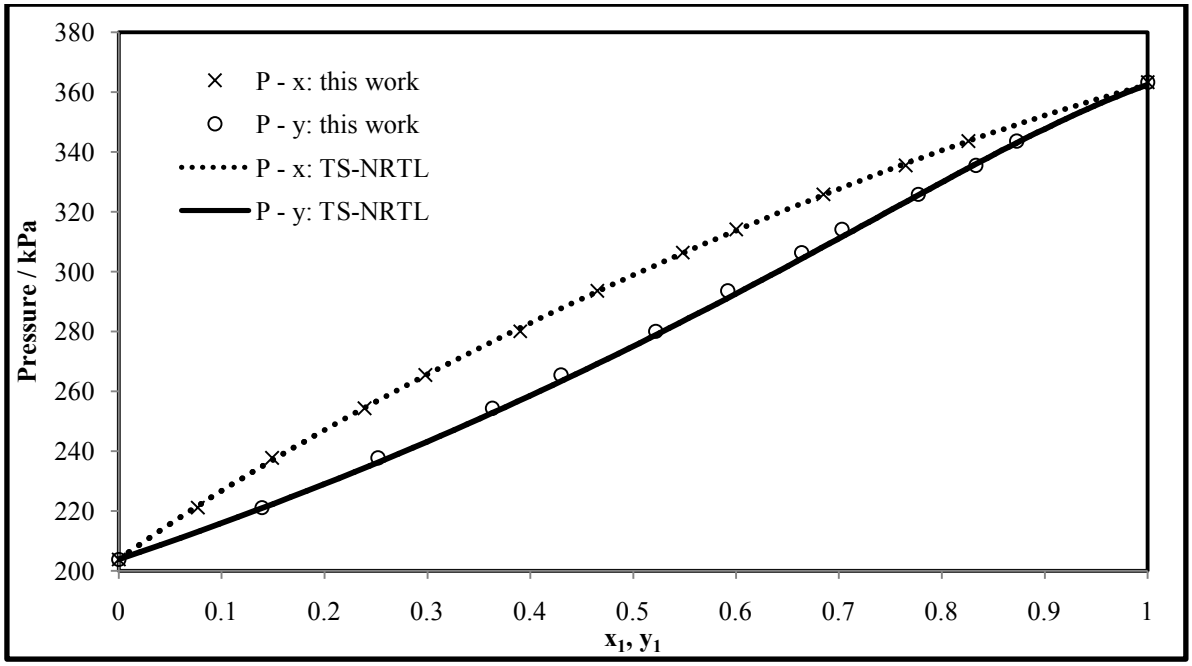

Figure 7-12: Fit of the TS-NRTL model combination to the P-x-y plot of the methoxy-2-methylpropane (1) + ethyl acetate (2) system at 373.17 K for the combined method.

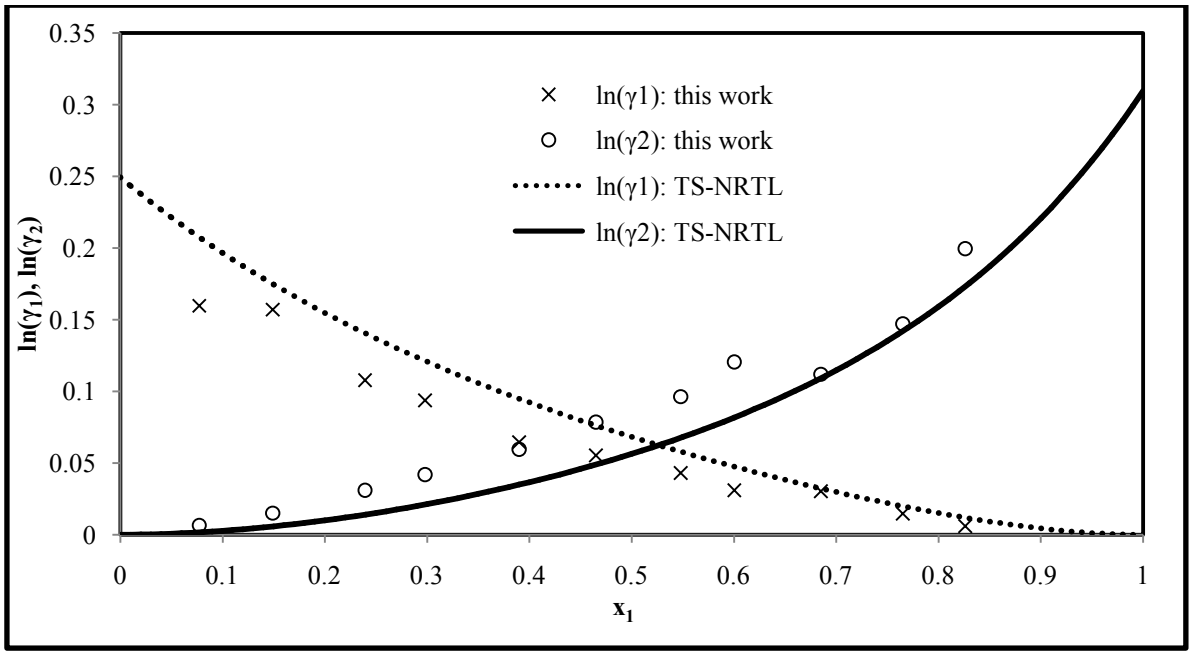

Figure 7-13: Comparison of the experimental activity coefficients and those calculated from the TS-NRTL model combination for the 2-methoxy-2-methylpropane (1) + ethyl acetate (2) system at 373.17 K for the combined method.

The direct method made use of the PR and the SRK equations. For each equation of state (EoS), the α-function of Mathias and Copeman (1983) and the mixing rule of Wong and Sandler (1992) with the NRTL model were used to regress the experimental data. The regression showed that the PR EoS provides a slightly better fit to the experimental data. The parameters from the regression of the experimental data with the direct method are reported in Table 7-15. As can be seen from the RMSD values for pressure and vapour composition in Table 7-15, the PR EoS offers only a slightly better fit than compared to the SRK EoS. The *x-y* and *P-x-y* plots for the combined method are presented in Figures 7-14 and 7-15 respectively.

Table 7-15: Model parameters, root mean square deviations (RMSD) and absolute average deviation (AAD) values for the direct method of the 2-methoxy-2-methylpropane (1) + ethyl acetate (2) system at 373.17 K.

Model	k_{12}	$g_{12} - g_{22}$ J.mol^{-1}	$g_{21} - g_{11}$ J.mol^{-1}	RMSD P / kPa	AAD P / kPa	RMSD y_1	AAD y_1
SRK-MC-WS-NRTL	-0.145	2123	459.6	0.56	0.41	0.006	0.004
PR-MC-WS-NRTL	-0.038	1640	-146.7	0.53	0.40	0.006	0.004

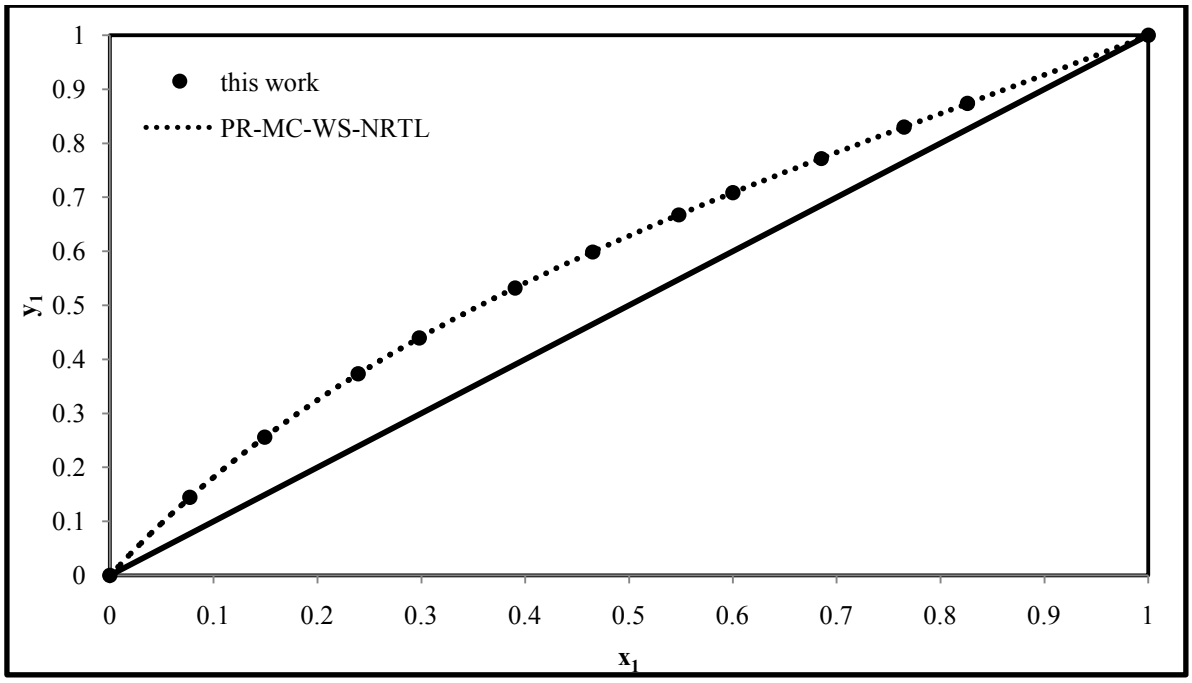

Figure 7-14: Fit of the PR-MC-WS-NRTL model combination to the x-y plot of the 2-methoxy-2-methylpropane (1) + ethyl acetate (2) system at 373.17 K for the direct method.

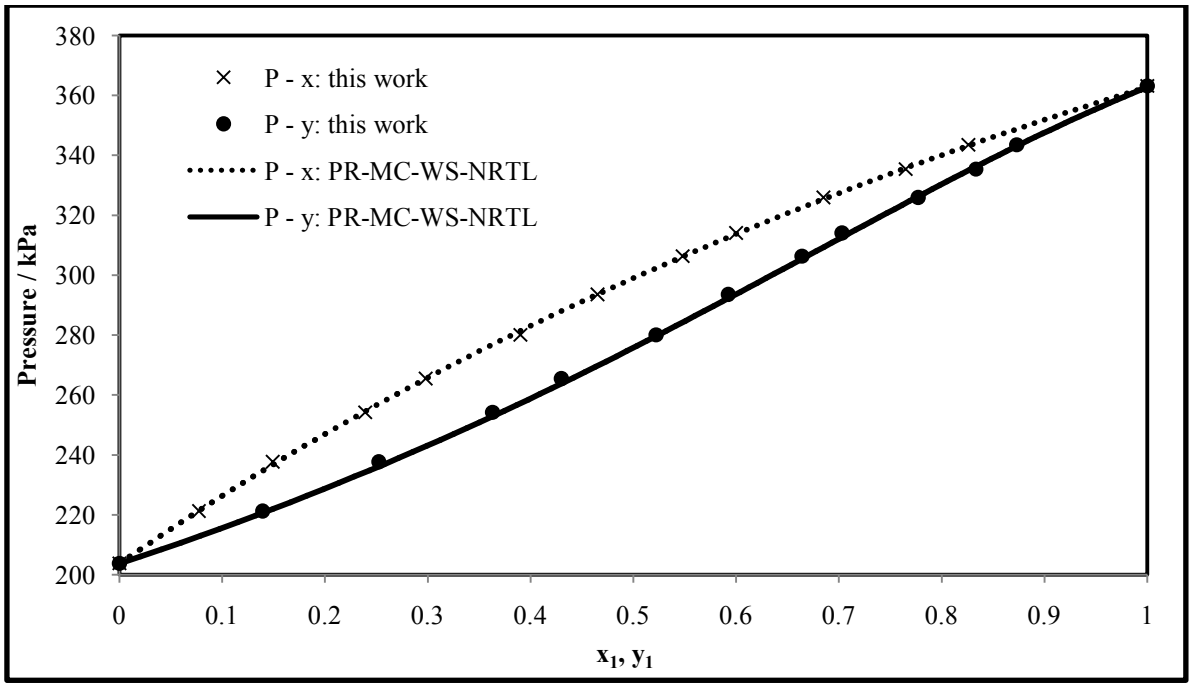

Figure 7-15: Fit of the PR-MC-WS-NRTL model combination to the P-x-y plot of the 2-methoxy-2-methylpropane (1) + ethyl acetate (2) system at 373.17 K for the direct method.

Overall by comparison, the regression results from the direct method show slightly higher values for the pressure RMSD but slightly lower values for the vapour composition RMSD. Thus the thermodynamic models from both methods show good representation of the experimental data.

7.4.2 Methanol (1) + Butan-2-one (2)

This system was one of the systems primarily measured for a South African petrochemical company, where thermodynamic interactions of light alcohols and carbonyls for a number of distillation systems are not well described. This system has also been studied by other researchers such as Britton et al. (1947), Hill and Van Winkle (1952), Privott et al. (1966), Eduljee and Tiwari (1976), Knapp and Doherty (1992) and Lee et al. (1995) to name a few. However, VLE data in the open literature for this system was not experimentally measured at 383.25, 398.14 and 413.20 K. Hence, VLE data measured for this system at these temperatures constitute new experimental data.

The GC TCD calibration for this system is presented in Figures C-28 and C-29 and reported in Table C-5 of Appendix C. The calibrations showed a linear response for both dilute regions of this system. The inverse of the response factor ratio of the methanol dilute region does not differ significantly from the response factor ratio of the butan-2-one dilute region. This confirmed a linear relationship for the entire composition range. An average response factor ratio was however not used but care was taken to ensure that the correct calibration graph was employed, depending whether the samples were taken in the dilute methanol region or dilute butan-2-one region.

The parameters from the regression of the experimental data with the combined method are reported in Table 7-16. Based on the RMSD values, it can be seen that the TK-Wilson model provides a slightly better fit for the system at 383.25 and 413.20 K but the NRTL model (with α being regressed) provided a better fit for the system at 398.14 K. The NRTL model (with α being regressed) seemed to represent the experimental data well for this system at all the isotherms measured, however the TK-Wilson model offered a slightly better fit at 383.25 and 413.20 K. The modified UNIQUAC model on the other hand, was also able to show a good fit of the experimental data at 383.25 and 398.14 K but displayed a large deviation from the experimental data at 413.20 K. The *x-y* plots for 383.25, 398.14 and 413.20 K are shown in Figure 7-16. The *P-x-y* plots for 383.25, 398.14 and 413.20 K are shown in Figure 7-17. The experimental activity coefficients and those calculated by the respective best fit models for the system at 383.25, 398.14 and 413.20 K are presented in Figure 7-18, where it can be seen that temperature has no significant effect on the

activity coefficient. This could be due the excess enthalpy being independent of temperature within the range measured. The estimated uncertainty on the activity coefficient is 3 %.

Table 7-16: Model parameters (A_{12} and A_{21})[a], root mean square deviations (RMSD) and absolute average deviation (AAD) values for the combined method of the methanol (1) + butan-2-one (2) system.

Model	A_{12} J.mol^{-1}	A_{21} J.mol^{-1}	RMSD P / kPa	AAD P / kPa	RMSD y_1	AAD y_1
		383.25 K				
TS-TKWILSON	5679	-4683	0.99	0.81	0.007	0.005
TS-NRTL (α = 0.3)	3072	-883.7	1.07	0.81	0.007	0.005
TS-NRTL (α = 1.45)	1710	752.2	1.00	0.83	0.007	0.005
TS-UNIQUAC	-153.3	1620	1.03	0.80	0.007	0.005
		398.14 K				
TS-TKWILSON	5546	-4711	1.73	1.49	0.009	0.006
TS-NRTL (α = 0.3)	3034	-879.8	0.73	0.68	0.008	0.006
TS-NRTL (α = 0.077)	7779	-5070	0.70	0.63	0.008	0.006
TS-UNIQUAC	-221.8	1718	0.79	0.74	0.008	0.006
		413.20 K				
TS-TKWILSON	6640	-5426	1.09	0.84	0.004	0.004
TS-NRTL (α = 0.3)	3206	-1119	2.28	2.07	0.004	0.003
TS-NRTL (α = 1.89)	1705	771.9	1.30	1.04	0.004	0.004
TS-UNIQUAC	-181.7	1604	2.07	1.86	0.004	0.003

[a]TKWilson: $A_{12} = a_{12} - a_{22}$ and $A_{21} = a_{21} - a_{11}$; NRTL: $A_{12} = g_{12} - g_{22}$ and $A_{21} = g_{21} - g_{11}$; mod UNIQUAC: $A_{12} = u_{12} - u_{22}$ and $A_{21} = u_{21} - u_{11}$.

The system exhibits an azeotrope for the 383.25 and 398.14 K isotherms at approximately x_1 = 0.975 and 0.98 respectively. The experimental data does not however seem to indicate an azeotrope at 413.20 K. Hence, as the temperature increases, the composition of the azeotrope changes such that it becomes richer in the more volatile component. The presence of an azeotrope for this system is not surprising as experimental measurements at lower temperatures and pressure have been previously carried out by researchers such as Britton et al. (1947), Hill and Van Winkle (1952) and Knapp and Doherty (1992) to name a few, who have found that this system exhibits a homogeneous azeotrope. The presence of an azeotrope implies that a system is non-ideal and that conventional distillation cannot separate the components into high purity chemicals. Knapp and Doherty (1992)

explored the use of pressure-swing distillation for separating such a homogeneous azeotropic mixture.

The best fit models for the respective isotherms of this system were also able to show a good representation of the experimental activity coefficients. The experimental activity coefficients were used to carry out the *direct test* for thermodynamic consistency (discussed later).

With regards to the direct method, both the SRK and PR EoS provide a good fit of the experimental data of this system. The PR EoS however provides a marginally better fit at 383.25 and 413.20 K whilst the SRK EoS provided a slightly better fit at 398.14 K. The parameters from the regression of the experimental data with the direct method are reported in Table 7-17. The *x-y* plots for 383.25, 398.14 and 413.20 K are shown in Figure 7-19 and the *P-x-y* plots for 383.25, 398.14 and 413.20 K are shown in Figures 7-20.

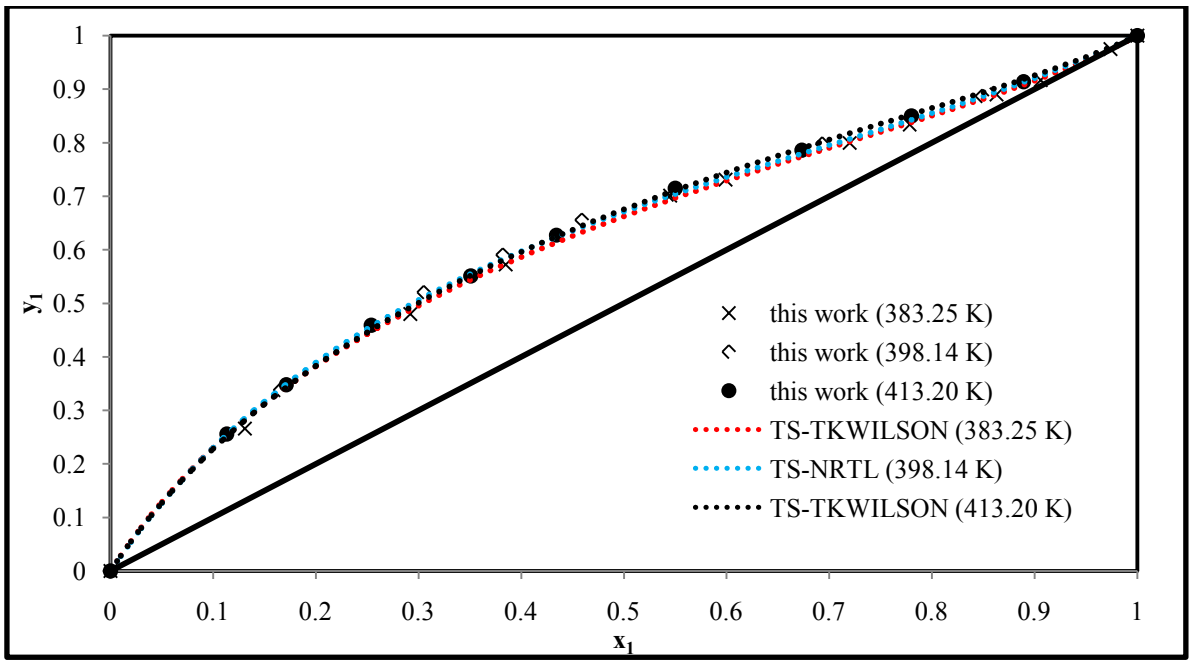

Figure 7-16: Best fit model combination for the x-y plot of the methanol (1) + butan-2-one (2) system with the combined method.

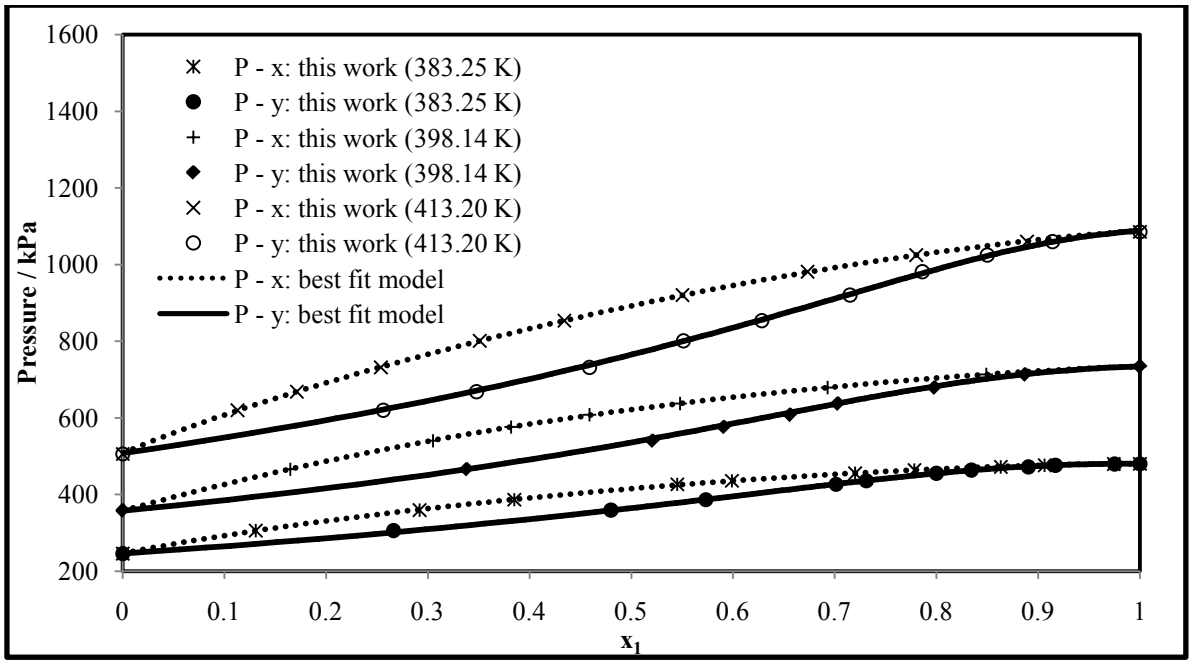

Figure 7-17: Best fit model combination (383.25 K: TS-TKWILSON; 398.14 K: TS-NRTL; 413.20 K: TS-TKWILSON) to the P-x-y plot of the methanol (1) + butan-2-one (2) system with the combined method.

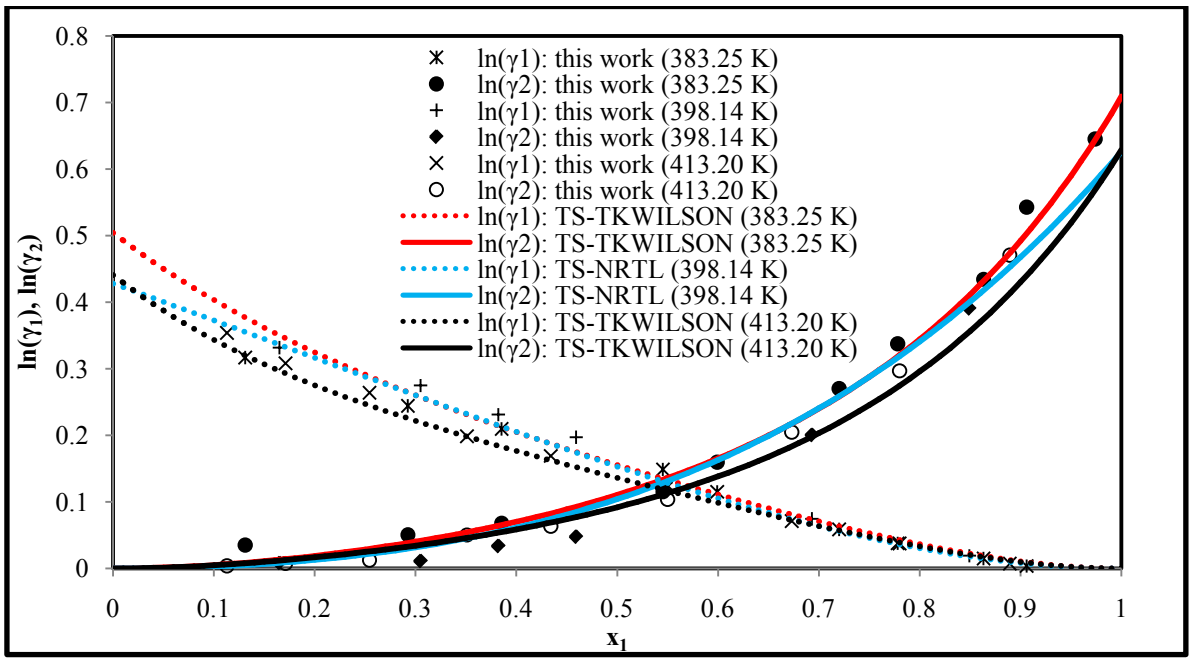

Figure 7-18: Comparison of the experimental activity coefficients and those calculated from the best fit model combination for the methanol (1) + butan-2-one (2) system with the combined method.

Table 7-17: Model parameters, root mean square deviations (RMSD) and absolute average deviation (AAD) values for the direct method applied to the methanol (1) + butan-2-one (2) system.

Model	k_{12}	$g_{12} - g_{22}$ J.mol^{-1}	$g_{21} - g_{11}$ J.mol^{-1}	RMSD P / kPa	AAD P / kPa	RMSD y_1	AAD y_1
			383.25 K				
SRK-MC-WS-NRTL	-0.422	8755	2382	1.04	0.87	0.011	0.008
PR-MC-WS-NRTL	-0.467	9076	2580	1.02	0.86	0.011	0.009
			398.14 K				
SRK-MC-WS-NRTL	0.199	607.8	1213	0.75	0.61	0.012	0.010
PR-MC-WS-NRTL	0.197	630.1	1178	0.85	0.73	0.012	0.010
			413.20 K				
SRK-MC-WS-NRTL	0.289	-3653	6455	1.93	1.00	0.006	0.005
PR-MC-WS-NRTL	0.291	-3677	6466	1.87	0.97	0.007	0.006

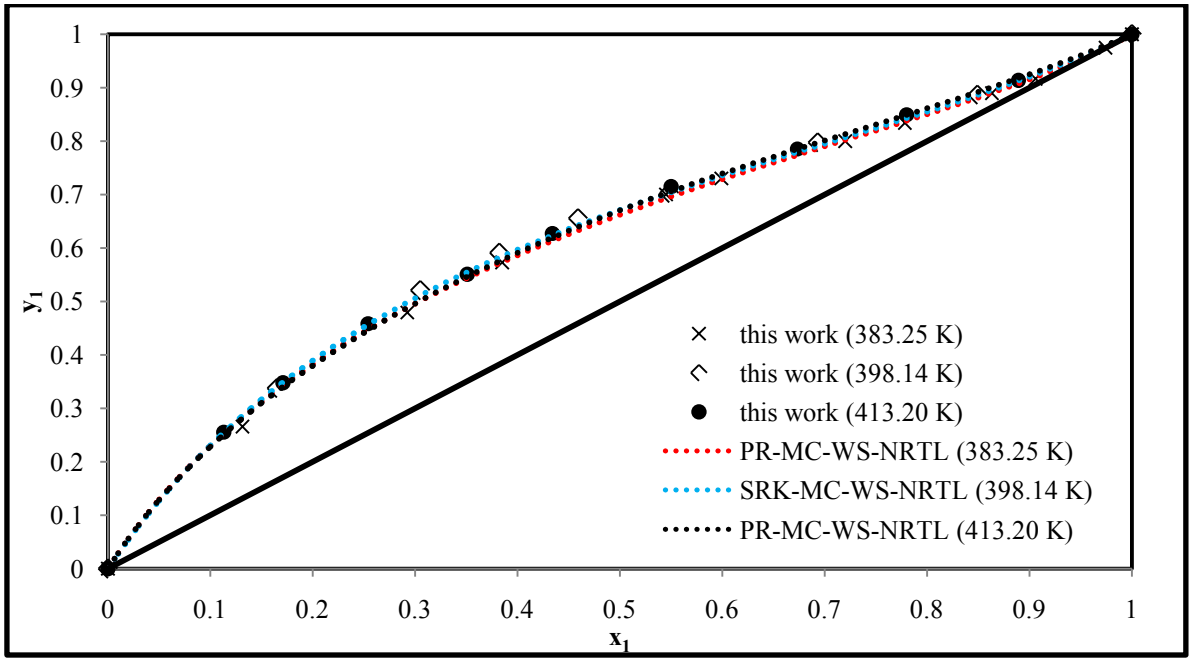

Figure 7-19: Best fit model combination for the x-y plot of the methanol (1) + butan-2-one (2) system with the direct method.

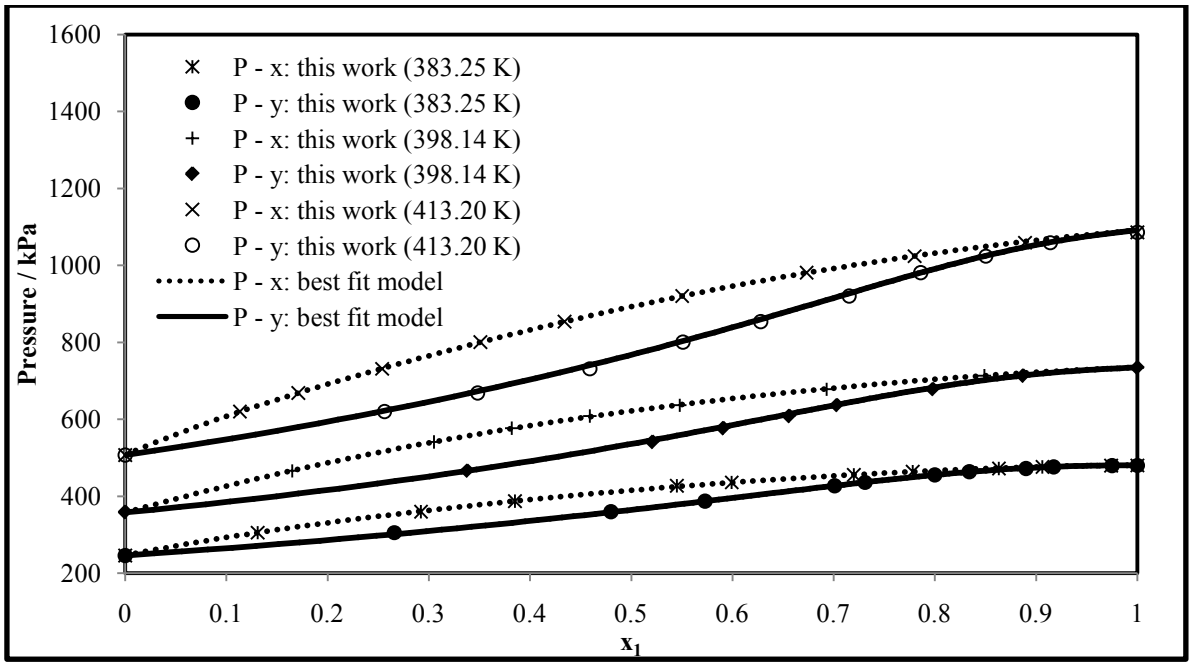

Figure 7-20: Best fit model combination (383.25 K: PR-MC-WS-NRTL; 398.14 K: SRK-MC-WS-NRTL; 413.20 K: PR-MC-WS-NRTL) to the P-x-y plot of the methanol (1) + butan-2-one (2) system with the direct method.

7.4.3 Ethanol (1) + Butan-2-one (2)

This system was a continuation of the work carried out for a South African petrochemical company for another light alcohol viz. ethanol. Experimental data for this binary system at low temperatures and sub-atmospheric pressures were available in the open literature but there were no data for moderate to high pressure ranges (Hellwig and Van Winkle, 1953; Ohta et al., 1981; Arce et al., 1996; Wen and Tu, 2007 and Martínez et al., 2008). Hence the experimental work carried or this system at 383.26, 398.23 and 413.21 K were not previously reported in the open literature and thus constituent as new experimental data.

The GC TCD calibration for this system is presented in Figures C-31 and C-32 and reported in Table C-5 of Appendix C. Similar to the previously discussed system, the calibrations showed a linear response for both dilute regions of this system. The inverse of the response factor ratio of the ethanol dilute region did not differ significantly from the response factor ratio of the butan-2-one dilute region. This confirmed a linear relationship for the entire composition range. As before, an average response factor ratio was however not used but care was taken to ensure that the correct

calibration graph was employed, depending whether the samples were taken in the dilute ethanol region or dilute butan-2-one region.

Table 7-18: Model parameters (A_{12} and A_{21})[a], root mean square deviations (RMSD) and absolute average deviation (AAD) values for the combined method of the ethanol (1) + butan-2-one (2) system.

Model	A_{12} J.mol^{-1}	A_{21} J.mol^{-1}	RMSD P / kPa	AAD P / kPa	RMSD y_1	AAD y_1
		383.26 K				
TS-TKWILSON	2614	-1250	0.39	0.35	0.006	0.005
TS-NRTL (α = 0.3)	484.4	1158	0.38	0.33	0.006	0.005
TS-NRTL (α = 0.044)	-1413	3060	0.38	0.33	0.006	0.005
TS-UNIQUAC	-1770	4325	0.37	0.29	0.005	0.004
		398.23 K				
TS-TKWILSON	2123	-818.1	0.43	0.34	0.005	0.003
TS-NRTL (α = 0.3)	1153	482.3	0.40	0.32	0.005	0.003
TS-NRTL (α = 0.028)	4280	-2609	0.40	0.32	0.005	0.003
TS-UNIQUAC	-1722	4130	0.29	0.23	0.004	0.003
		413.21 K				
TS-TKWILSON	1370	-53.0	1.21	1.04	0.004	0.003
TS-NRTL (α = 0.3)	2185	-474.8	1.26	1.09	0.004	0.003
TS-NRTL (α = 2.06)	1326	872.6	0.64	0.48	0.005	0.004
TS-UNIQUAC	-1574	3677	1.35	1.18	0.003	0.003

[a]TKWilson: $A_{12} = a_{12} - a_{22}$ and $A_{21} = a_{21} - a_{11}$; NRTL: $A_{12} = g_{12} - g_{22}$ and $A_{21} = g_{21} - g_{11}$; mod UNIQUAC: $A_{12} = u_{12} - u_{22}$ and $A_{21} = u_{21} - u_{11}$.

The parameters from the regression of the experimental data with the combined method are reported in Table 7-18. Based on the RMSD values, it can be seen that the modified UNIQUAC model provides the best fit for the system at 383.26 and 398.23 K but the NRTL model (with α being regressed) provided the best fit for the system at 413.21 K. Nevertheless all the liquid phase activity coefficient models provided a reasonable fit to the experimental data for all the isotherms measured. The *x-y* plots are shown in Figure 7-21. The *P-x-y* plots are shown in Figure 7-22. The experimental activity coefficients and those calculated by the respective best fit models for the system are presented in Figure 7-23. Similar to the previous system, it can be seen that temperature has no significant effect on the activity coefficient. This could be due the excess enthalpy being

independent of temperature within the range measured. The estimated uncertainty on the activity coefficient is 3 %.

The system exhibits an azeotrope for the 383.26, 398.23 and 413.21 K isotherms at approximately x_1 = 0.75, 0. 84 a nd 0.91 r espectively, w hich indicates t hat a s t he t emperature increases, the composition of the azeotrope changes such that it becomes richer in the more volatile component. The rapid change in azeotropic composition with temperature most likely indicates the presence of a Bancroft poi nt. W hen t he v apour pressures of t wo separate pure components a re t he s ame, the temperature and pressure at which this occurs is known as t he Bancroft point (Rowlinson, 1969). According t o E lliott a nd Rainwater (2000), the e xistence o f a B ancroft po int c an i ndicate a significant composition dependence o f an az eotropic system. Indeed the literature d ata (Aspen, 2004) for the v apour pr essures o f e thanol a nd but an-2-one i ndicates a Bancroft p oint a t approximately 347. 7 K a nd 86.7 k Pa. The experimental d ata at 383.26, 398 .23 a nd 413.2 1 K measured for this system of ethanol (1) + butan-2-one (2), are all greater than the Bancroft point. The rapid ch ange o f az eotropic c omposition w ith t emperature indicates that t he l ikelihood o f a n azeotrope d iminishes as conditions diverge from the Bancroft point (Elliot and Rainwater, 2000). The p resence o f an az eotrope f or t his sy stem w as al so o bserved at atmospheric p ressure by researchers such as Wen and Tu (2007) and Martínez et al. (2008). As mentioned previously, the presence of an azeotrope implies that a system is non-ideal and that conventional distillation cannot separate t he c omponents i nto hi gh pur ity c hemicals. According t o M artínez e t a l. (2008), a n azeotrope for this system was found to be rather sensitive to pressure and thus the use of pressure-swing distillation would prove to be a useful technique to overcome this azeotropic mixture.

The b est f it m odels f or t he r espective i sotherms o f t his sy stem w ere al so ab le t o sh ow a g ood representation of the experimental activity coefficients. However, the modified UNIQUAC model shows significant deviation in the butan-2-one dilute region for the system at 383.26 and 398.23 K (see Figure 7-17). The experimental activity coefficients were used to carry out the *direct test* for thermodynamic consistency (discussed later).

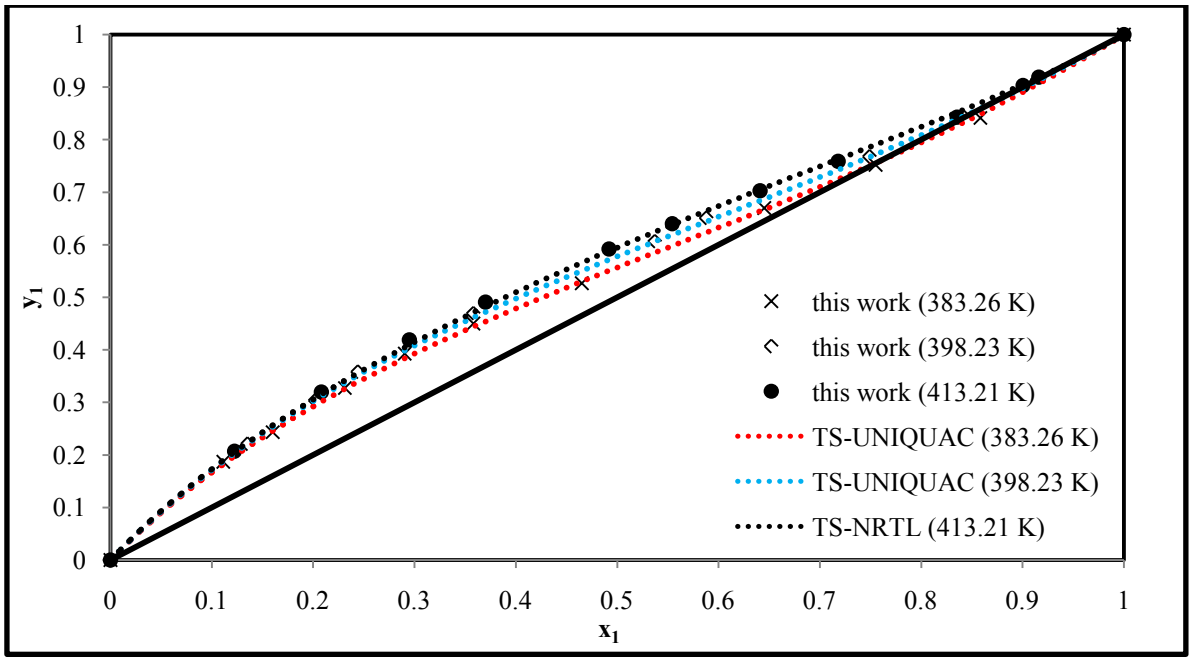

Figure 7-21: Best fit model combination for the x-y plot of the ethanol (1) + butan-2-one (2) system with the combined method.

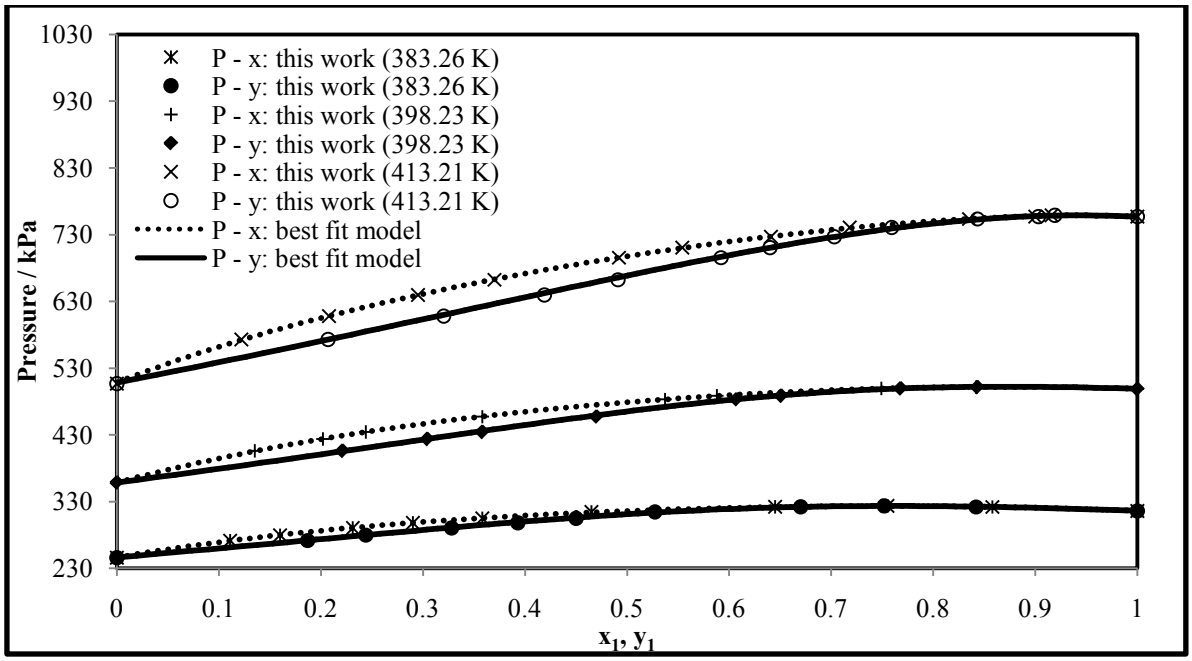

Figure 7-22: Best fit model combination (383.26 K: TS-UNIQUAC; 398.23 K: TS-UNIQUAC; 413.20 K: TS-NRTL) to the P-x-y plot of the ethanol (1) + butan-2-one (2) system with the combined method.

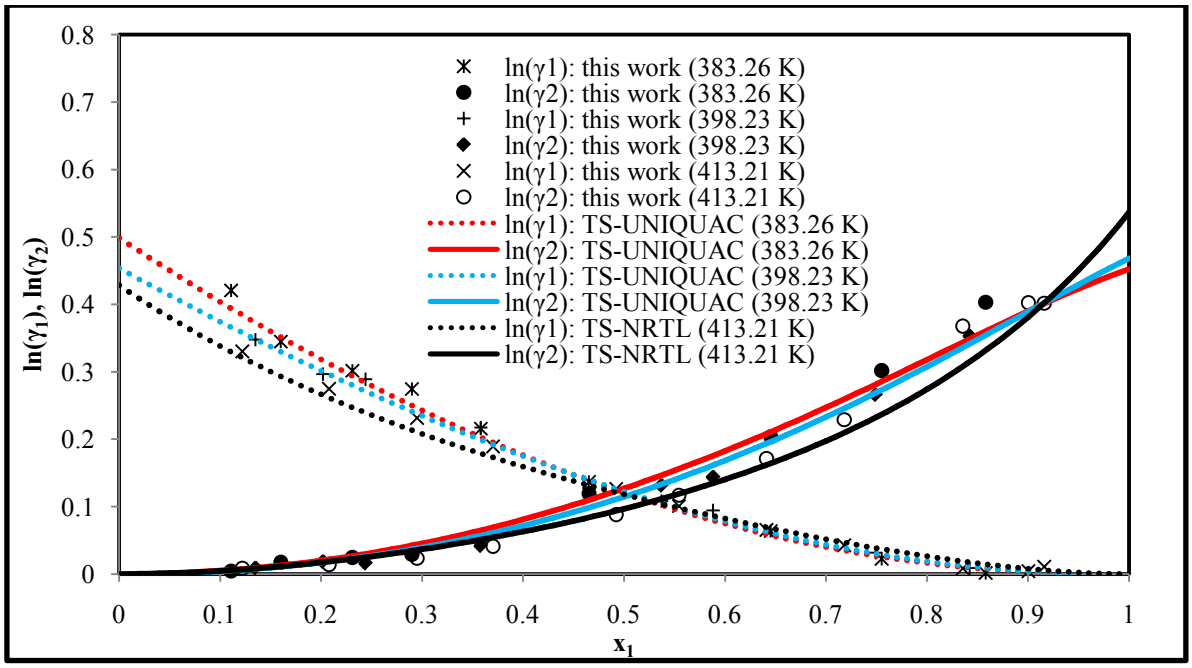

Figure 7-23: Comparison of the experimental activity coefficients and those calculated from the best fit model combination for the ethanol (1) + butan-2-one (2) system with the combined method.

Table 7-19: Model parameters, root mean square deviations (RMSD) and absolute average deviation (AAD) values for the direct method of the ethanol (1) + butan-2-one (2) system.

Model	k_{12}	$g_{12} - g_{22}$ J.mol^{-1}	$g_{21} - g_{11}$ J.mol^{-1}	RMSD P / kPa	AAD P / kPa	RMSD y_1	AAD y_1
			383.26 K				
SRK-MC-WS-NRTL	-0.193	3176	1833	0.38	0.28	0.007	0.006
PR-MC-WS-NRTL	-0.171	2950	1722	0.38	0.28	0.007	0.006
			398.23 K				
SRK-MC-WS-NRTL	-0.521	6555	3314	0.32	0.21	0.012	0.010
PR-MC-WS-NRTL	-0.402	5436	2516	0.33	0.22	0.011	0.009
			413.21 K				
SRK-MC-WS-NRTL	-0.038	2757	736.5	1.07	0.91	0.009	0.007
PR-MC-WS-NRTL	-0.016	2423	687.9	1.11	0.92	0.009	0.007

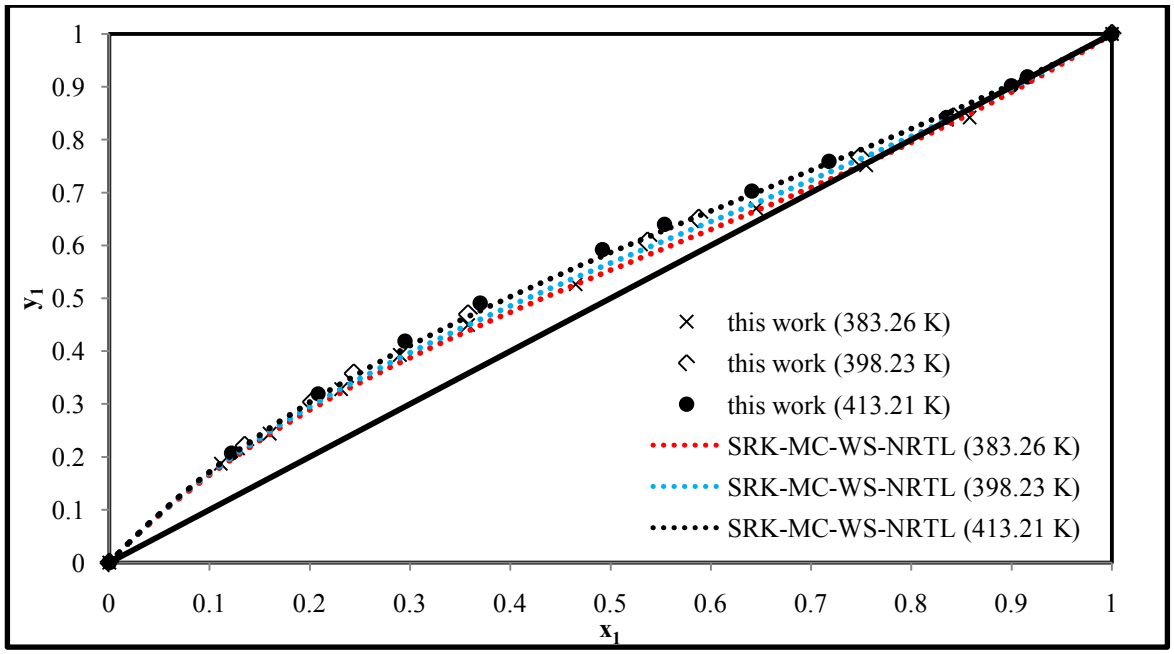

Figure 7-24: Best fit model combination for the x-y plot of the ethanol (1) + butan-2-one (2) system with the direct method.

With regards to the direct method, both the SRK and PR EoS provided a good fit of the experimental data of this system. The SRK EoS however provided a marginally better fit for this system at 398.23 K, whereas at 383.26 and 413 K there is no significant advantage of one EoS to the other. The parameters from the regression of the experimental data with the direct method are reported in Table 7-19. The *x-y* and *P-x-y* plots for 383.26, 398.23 and 413.21 K are shown respectively in Figures 7-24 and 7-25.

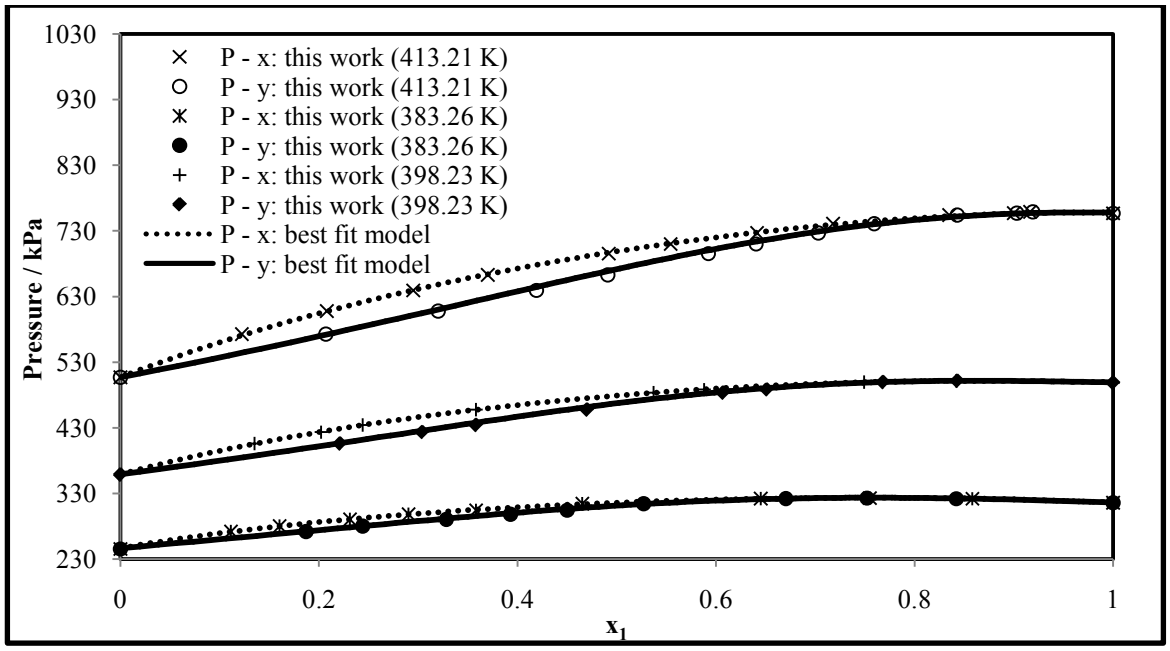

Figure 7-25: Best fit model combination (383.26, 398.23 and 413.21 K: SRK-MC-WS-NRTL) to the P-x-y plot of the ethanol (1) + butan-2-one (2) system with the direct method.

7.4.4 Ethanol (1) + 2-Methoxy-2-Methylbutane (2)

This system was also measured as a continuation of the work carried out for a South African petrochemical company. Over the years 2-methoxy-2-methylbutane has been considered as a fuel oxygenate to increase octane enhancement and oxygen content in gasoline in forming lead-free gasoline (Ignatius et al., 1995). VLE data at 101.32 kPa and physical properties for the ternary mixture of water + ethanol + 2-methoxy-2-methylbutane have been studied by Arce et al. (1997 and 1998). Experimental data for the binary system of ethanol + 2-methoxy-2-methylbutane at 101.32 kPa were available in the open literature but there were no data for moderate to high pressure ranges (Arce et al., 1996). Hence the experimental work carried on this system at 398.25 and 413.19 K was not previously reported in the open literature and thus constituent as new experimental data. It should be noted that 2-methoxy-2-methylbutane is a costly chemical. A quotation obtained from Capital Lab Suppliers cc on 22 April 2010 showed a cost of R5 510 for 500 mL of 2-methoxy-2-methylbutane with purity greater than 97%. As explained in Chapter 5, only approximately 75 cm^3 of each component was needed to carry out GC calibrations, degassing, vapour pressure and VLE measurements for two isotherms.

The GC TCD calibration for this system is presented in Figures C-34 and C-35 and reported in Table C-5 of Appendix C. Similar to the previously discussed systems, the calibrations showed a linear response for both dilute regions of this system. The inverse of the response factor ratio of the ethanol dilute region did not differ significantly from the response factor ratio of the 2-methoxy-2-methylbutane dilute region. This confirmed a linear relationship for the entire composition range. As before, an average response factor ratio was however not used but care was taken to ensure that the correct calibration graph was employed, depending whether the samples were taken in the dilute ethanol region or dilute 2-methoxy-2-methylbutane region.

Table 7-20: Model parameters (A_{12} and A_{21})[a], root mean square deviations (RMSD) and absolute average deviation (AAD) values for the combined method of the ethanol (1) + 2-methoxy-2-methylbutane (2) system.

Model	A_{12} J.mol^{-1}	A_{21} J.mol^{-1}	RMSD P / kPa	AAD P / kPa	RMSD y_1	AAD y_1
		398.25 K				
TS-TKWILSON	3595	-1558	0.86	0.73	0.008	0.007
TS-NRTL (α = 0.3)	3510	188.2	0.59	0.53	0.008	0.007
TS-NRTL (α = 0.083)	7386	-3411	0.56	0.47	0.008	0.007
TS-UNIQUAC	-1535	5825	0.73	0.63	0.007	0.007
		413.19 K				
TS-TKWILSON	3507	-1419	0.340	0.26	0.007	0.005
TS-NRTL (α = 0.3)	3780	32.0	0.65	0.62	0.007	0.005
TS-NRTL (α = 0.55)	3113	908.9	0.32	0.26	0.007	0.005
TS-UNIQUAC	-1566	5894	0.33	0.26	0.007	0.005

[a]TKWilson: $A_{12} = a_{12} - a_{22}$ and $A_{21} = a_{21} - a_{11}$; NRTL: $A_{12} = g_{12} - g_{22}$ and $A_{21} = g_{21} - g_{11}$; mod UNIQUAC: $A_{12} = u_{12} - u_{22}$ and $A_{21} = u_{21} - u_{11}$.

The parameters from the regression of the experimental data with the combined method are reported in Table 7-20. Based on the RMSD values, it can be seen that the NRTL model (with α being regressed) provides the best fit for the system at both 398.25 and 413.19 K. Nevertheless all the liquid phase activity coefficient models provide a reasonable fit to the experimental data for both the isotherms measured. The *x-y* and *P-x-y* plots for 398.25 and 413.19 K are shown respectively in Figures 7-26 and 7-27. The experimental activity coefficients and those calculated by the respective best fit models for the system at 398.25 and 413.19 K are presented in Figure 7-28. Once more this system like the previous two shows that temperature has no significant effect on the activity

coefficient. This could be due the excess enthalpy being independent of temperature within the range measured. The estimated uncertainty on the activity coefficient is 3 %.

The system exhibits an azeotrope for both the 398.25 and 413.19 K isotherms at approximately x_1 = 0.77 and 0. 78 respectively. From the experimental data, one can observe that the azeotropic composition is hardly affected by the 15 K change in temperature between the two isotherms. The presence of an azeotrope for this system was also observed at 101.32 kPa by Arce et al. (1996). As mentioned previously, an azeotrope implies that a system is non-ideal and that conventional distillation cannot separate the components into high purity chemicals. Unlike the previously discussed system of ethanol (1) + butan-2-one (2), pressure-swing distillation cannot be considered for this system of ethanol (1) + 2-methoxy-2-methylbutane (2) since the experimental data suggests that the azeotropic composition hardly changes with a 15 K change of temperature. Therefore, alternative forms of distillation should be considered viz. homogeneous or heterogeneous azeotropic distillation. Such distillation techniques are discussed by Seader and Henley (1998).

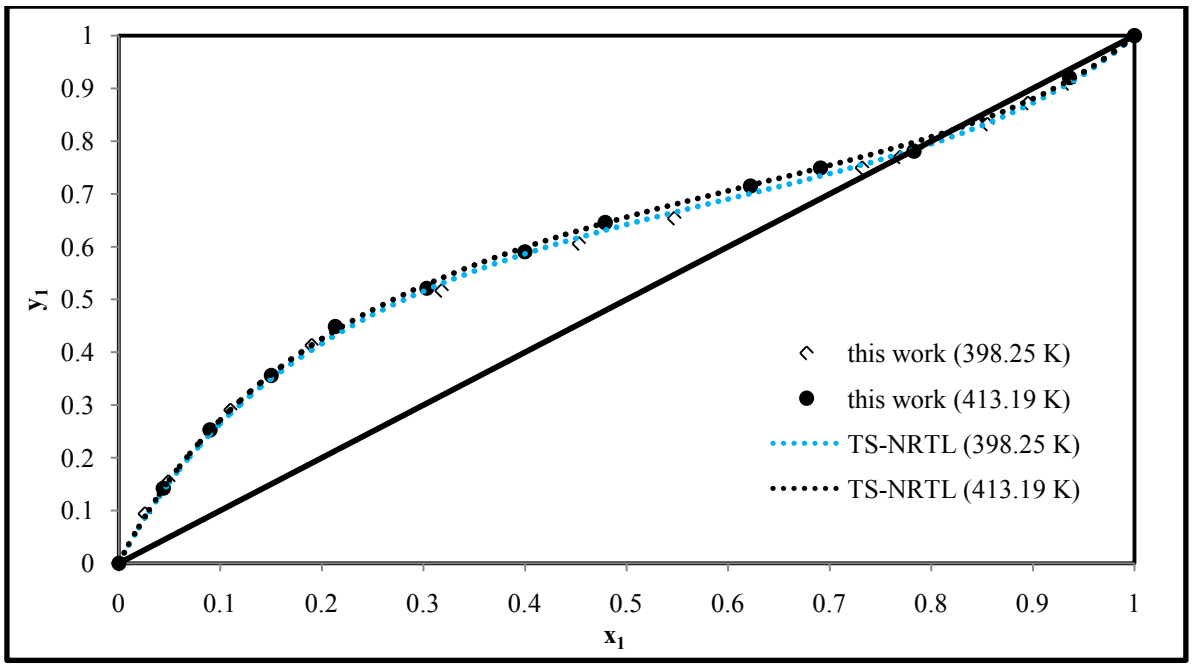

Figure 7-26: Best fit model combination for the x-y plot of the ethanol (1) + 2-methoxy-2-methylbutane (2) system with the combined method.

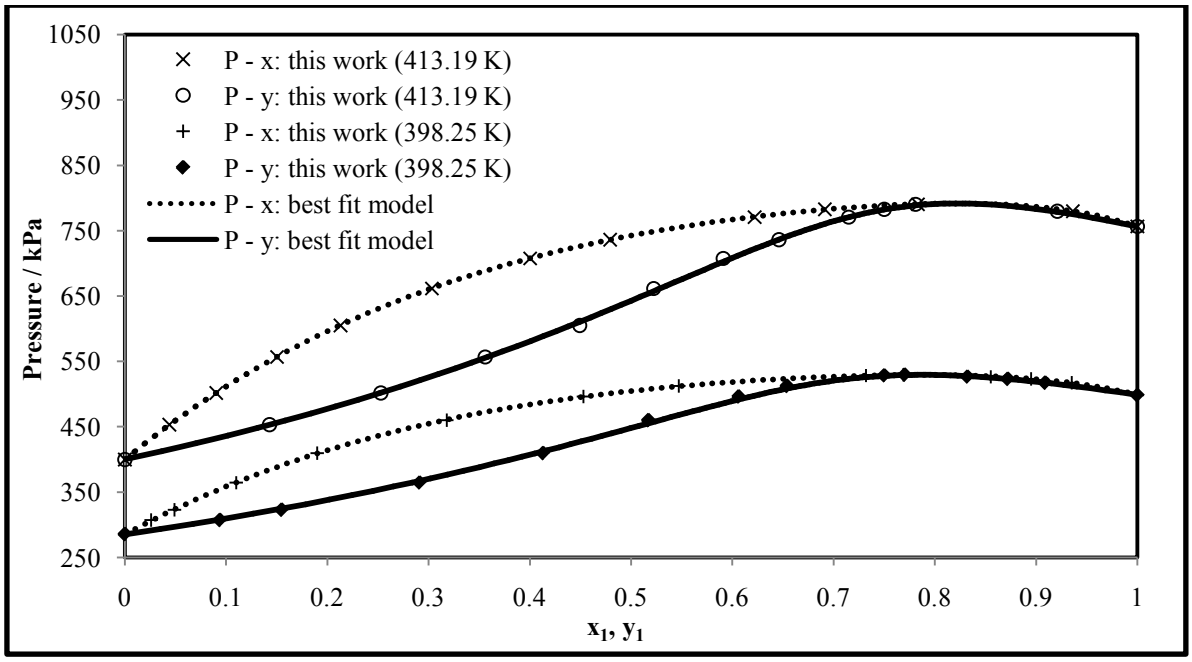

Figure 7-27: Best fit model combination (398.25 and 413.19 K: TS-NRTL) to the P-x-y plot of the ethanol (1) + 2-methoxy-2-methylbutane (2) system with the combined method.

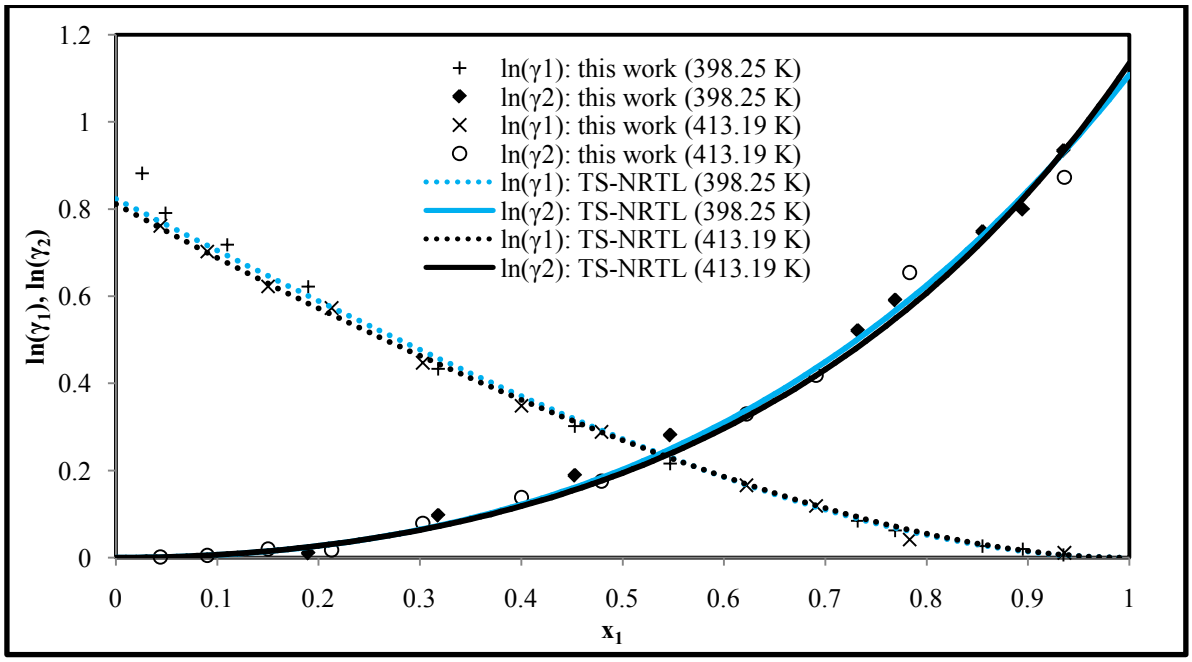

Figure 7-28: Comparison of the experimental activity coefficients and those calculated from the best fit model combination for the ethanol (1) + 2-methoxy-2-methylbutane (2) system with the combined method.

The best fit models for both isotherms of this system were also able to show a good representation of the experimental activity coefficients. The experimental activity coefficients were used to carry out the *direct test* for thermodynamic consistency (discussed later).

Table 7-21: Model parameters, root mean square deviations (RMSD) and absolute average deviation (AAD) values for the direct method of the ethanol (1) + 2-methoxy-2-methylbutane (2) system.

Model	k_{12}	$g_{12} - g_{22}$ J.mol^{-1}	$g_{21} - g_{11}$ J.mol^{-1}	RMSD P / kPa	AAD P / kPa	RMSD y_1	AAD y_1
			398.25 K				
SRK-MC-WS-NRTL	0.306	316.1	2938	0.71	0.62	0.007	0.006
PR-MC-WS-NRTL	0.303	373.9	2859	0.71	0.61	0.007	0.006
			413.19 K				
SRK-MC-WS-NRTL	0.286	984.4	2743	0.52	0.45	0.008	0.006
PR-MC-WS-NRTL	0.282	1021	2672	0.52	0.45	0.008	0.006

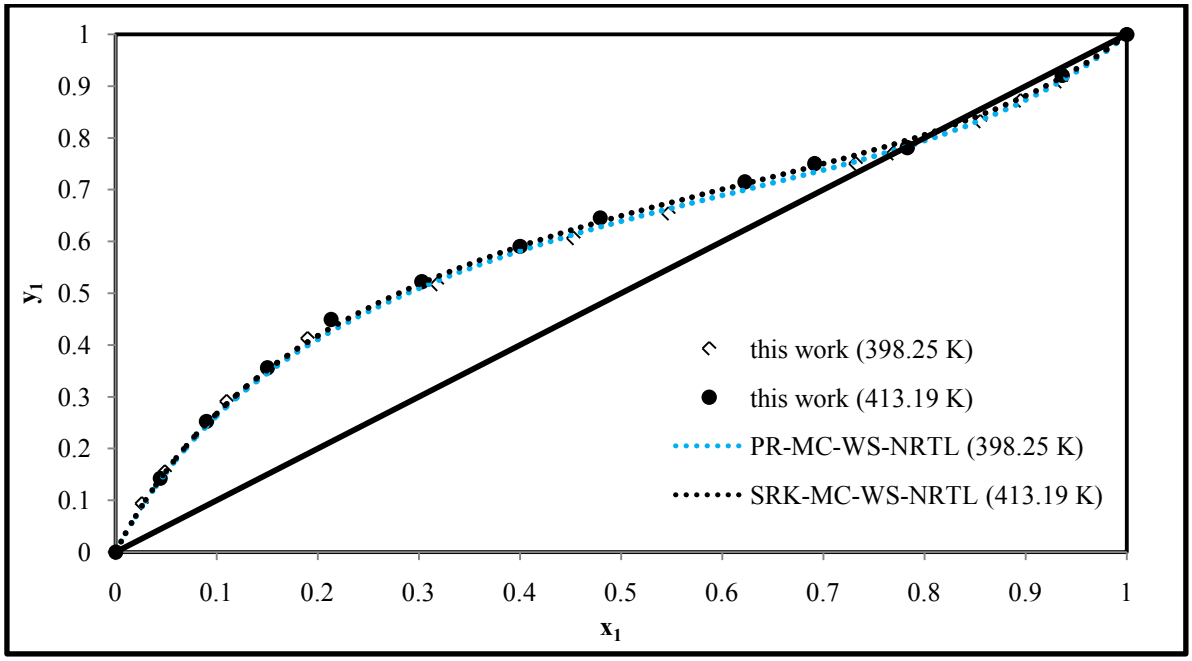

Figure 7-29: Best fit model combination for the x-y plot of the ethanol (1) + 2-methoxy-2-methylbutane (2) system with the direct method.

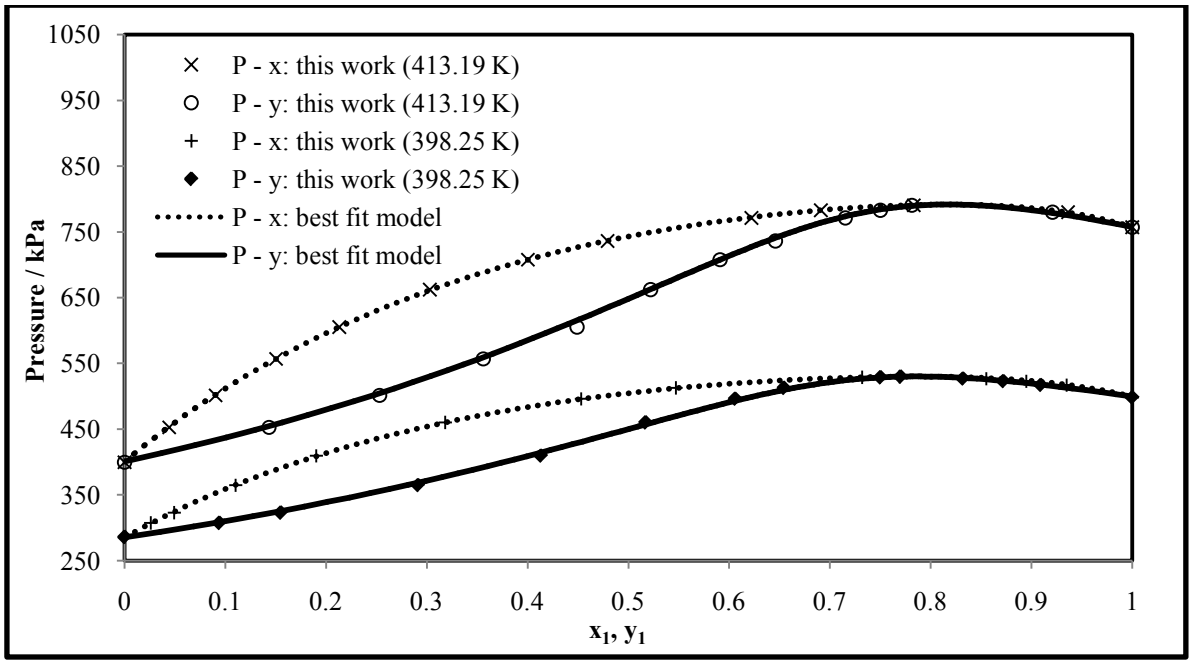

Figure 7-30: Best fit model combination (398.25 K: PR-MC-WS-NRTL and 413.19 K: SRK-MC-WS-NRTL) to the P-x-y plot of the ethanol (1) + 2-methoxy-2-methylbutane (2) system with the direct method.

With regards to the direct method, both the SRK and PR EoS provide a good fit of the experimental data of this system. There is no advantage of one EoS compared to the other at 398.25 K but for the isotherm at 413.19 K, the SRK EoS provides a marginally better fit to the experimental data. The parameters from the regression of the experimental data with the direct method are reported in Table 7-21. The *x-y* plots for 398.25 and 413.19 K are shown in Figure 7-29 and the *P-x-y* plots for 398.25 and 413.19 K are shown in Figure 7-30.

7.4.5 2-Methylpent-2-ene + Ethanol (2)

This system was also measured as a continuation of the work carried out for a South African petrochemical company. The component 2-methylpent-2-ene is best known for its use as a fuel additive (Hodges and Ketley, 2003). Due to 2-methylpent-2-ene being an expensive chemical, there is very little or no reported thermodynamic data for the binary system of 2-methylpent-2-ene (1) + ethanol (2) in the open literature. A quotation obtained from Capital Lab Suppliers cc on 22 April 2010 showed a cost of R2 605 for 50 mL of 2-methylpent-2-ene with a minimum purity of 98%. Hence, the experimental VLE data measured for this system in this study constitutes as new experimental data.

The GC TCD calibration for this system is presented in Figures C-41 and C-42 and reported in Table C-5 of Appendix C. Unlike the previously discussed systems, the calibrations here showed a non-linear response for both dilute regions of this system. A second order polynomial equation was found to adequately describe both dilute regions well. However the calibration curve for the ethanol dilute region showed a more distinctive shape when compared to the calibration curve for the 2-methylpent-2-ene dilute region. Hence, care was taken to ensure that the correct calibration graph was employed, depending on whether the samples were taken in the dilute ethanol region or dilute 2-methylpent-2-ene region.

The parameters from the regression of the experimental data with the combined method are reported in Table 7-22. Based on the RMSD values, it can be seen that the NRTL model (with α being regressed) provides the best fit. The TK-Wilson and modified UNIQUAC models both show significantly larger deviations for pressure. However, the vapour composition deviations are somewhat large but similar for all the liquid phase activity models. Hence the experimental vapour compositions must therefore contain some error. The *x-y* and *P-x-y* plots for this system are shown in Figures 7-31 and 7-32 respectively. The experimental activity coefficients and those calculated by the best fit model are presented in Figure 7-33. The estimated uncertainty on the activity coefficient is 3 %.

Table 7-22: Model parameters (A_{12} and A_{21})[a], root mean square deviations (RMSD) and absolute average deviation (AAD) values for the combined method of the 2-methylpent-2-ene (1) + ethanol (2) system at 383.20 K.

Model	A_{12} J.mol^{-1}	A_{21} J.mol^{-1}	RMSD P / kPa	AAD P / kPa	RMSD y_1	AAD y_1
TS-TKWILSON	-1064	6393	1.40	1.16	0.013	0.011
TS-NRTL (α = 0.3)	3516	2728	0.76	0.59	0.014	0.011
TS-NRTL (α = -0.55)	2051	2406	0.48	0.40	0.013	0.011
TS-UNIQUAC	8674	-1259	2.20	1.85	0.013	0.011

[a]TKWilson: $A_{12} = a_{12} - a_{22}$ and $A_{21} = a_{21} - a_{11}$; NRTL: $A_{12} = g_{12} - g_{22}$ and $A_{21} = g_{21} - g_{11}$; mod UNIQUAC: $A_{12} = u_{12} - u_{22}$ and $A_{21} = u_{21} - u_{11}$.

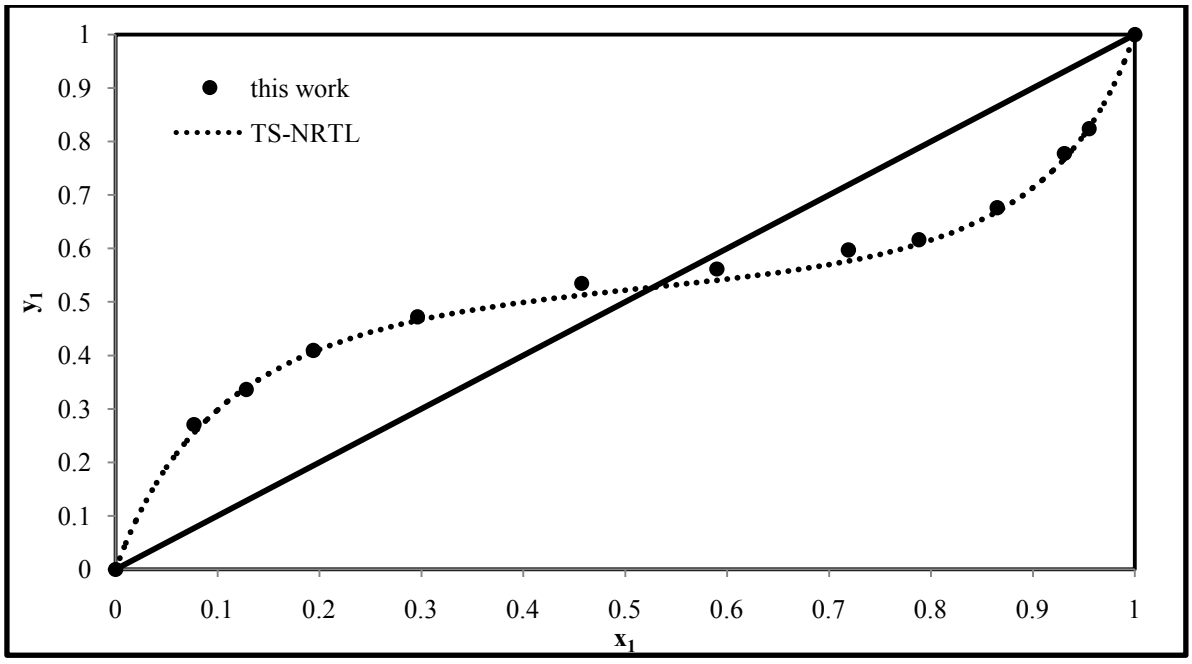

Figure 7-31: Fit of the TS-NRTL model combination to the x-y plot of the 2-methylpent-2-ene (1) + ethanol (2) system at 383.20 K for the combined method.

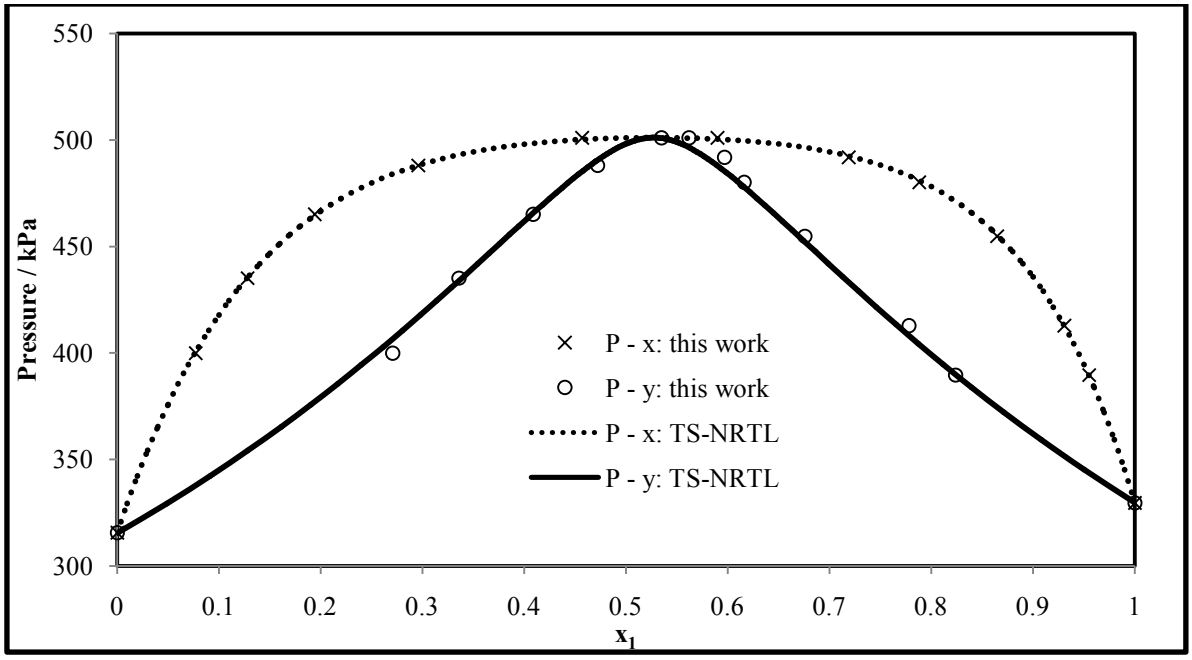

Figure 7-32: Fit of the TS-NRTL model combination to the P-x-y plot of the 2-methylpent-2-ene (1) + ethanol (2) system at 383.20 K for the combined method.

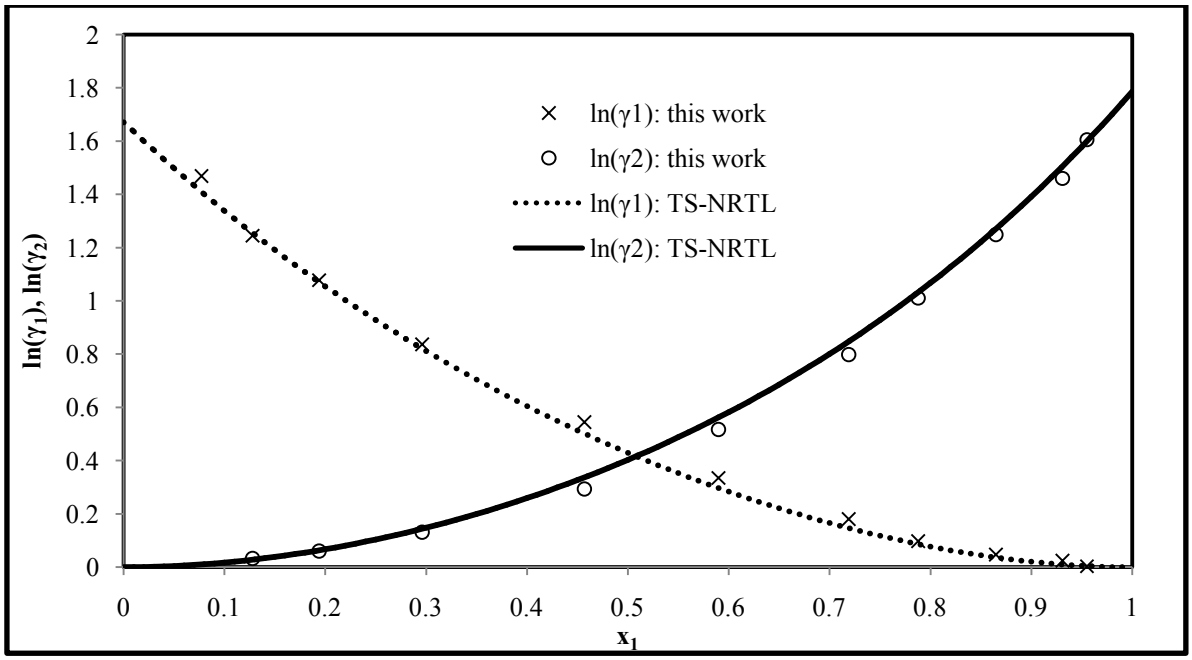

Figure 7-33: Comparison of the experimental activity coefficients and those calculated from the TS-NRTL model combination for the 2-methylpent-2-ene (1) + ethanol (2) system at 383.20 K for the combined method.

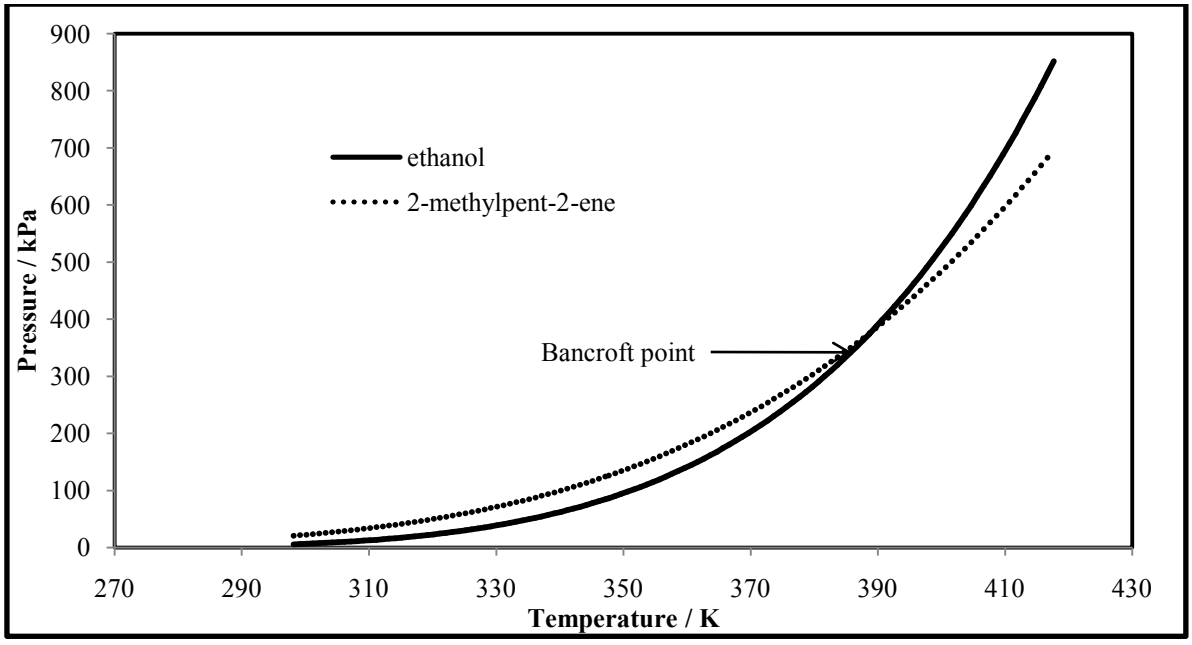

Figure 7-34: Comparison of the vapour pressures of ethanol and 2-methylpent-2-ene showing the Bancroft point.

This system also exhibits an azeotrope at approximately $x_1 = 0.53$. The vapour pressure data for these two components show that they have very close boiling points. The regressed experimental vapour pressure data for these two components studied in this work is shown in Figure 7-34, where the Bancroft point occurs at approximately 389 K and 380 kPa. Due to time constraints and chemical availability, only one isotherm was measured for this system. Hence the effect of temperature on the azeotropic composition could not be studied for this system. Elliott and Rainwater (2000) also mention that the likelihood of an azeotrope diminishes as conditions diverge from the Bancroft point and as a consequence the composition of the azeotrope shifts, increasing the mole fraction of the component whose vapour pressure increases more rapidly with temperature (in this case ethanol). As discussed previously, alternate forms to conventional distillation (such as pressure-swing and homogeneous or heterogeneous azeotropic distillation) must be considered to separate these two components into high purity chemicals.

The best fit model for this system was also able to show good representation of the experimental activity coefficients which were used to carry out the *direct test* for thermodynamic consistency (discussed later).

With regards to the direct method, the PR EoS provided a better fit than the SRK EoS to the experimental data of this system. Similar to the combined method, the models for the direct method also showed considerable deviation for the vapour compositions. The parameters from the regression of the experimental data with the direct method are reported in Table 7-23. The *x-y* and *P-x-y* plots are shown in Figures 7-35 and 7-36.

Table 7-23: Model parameters, root mean square deviations (RMSD) and absolute average deviation (AAD) values for the direct method of the 2-methylpent-2-ene (1) + ethanol (2) system at 383.20 K.

Model	k_{12}	$g_{12} - g_{22}$ J.mol^{-1}	$g_{21} - g_{11}$ J.mol^{-1}	RMSD P / kPa	AAD P / kPa	RMSD y_1	AAD y_1
SRK-MC-WS-NRTL	0.328	6814	939.6	0.78	0.70	0.012	0.009
PR-MC-WS-NRTL	0.315	6643	1111	0.69	0.62	0.012	0.009

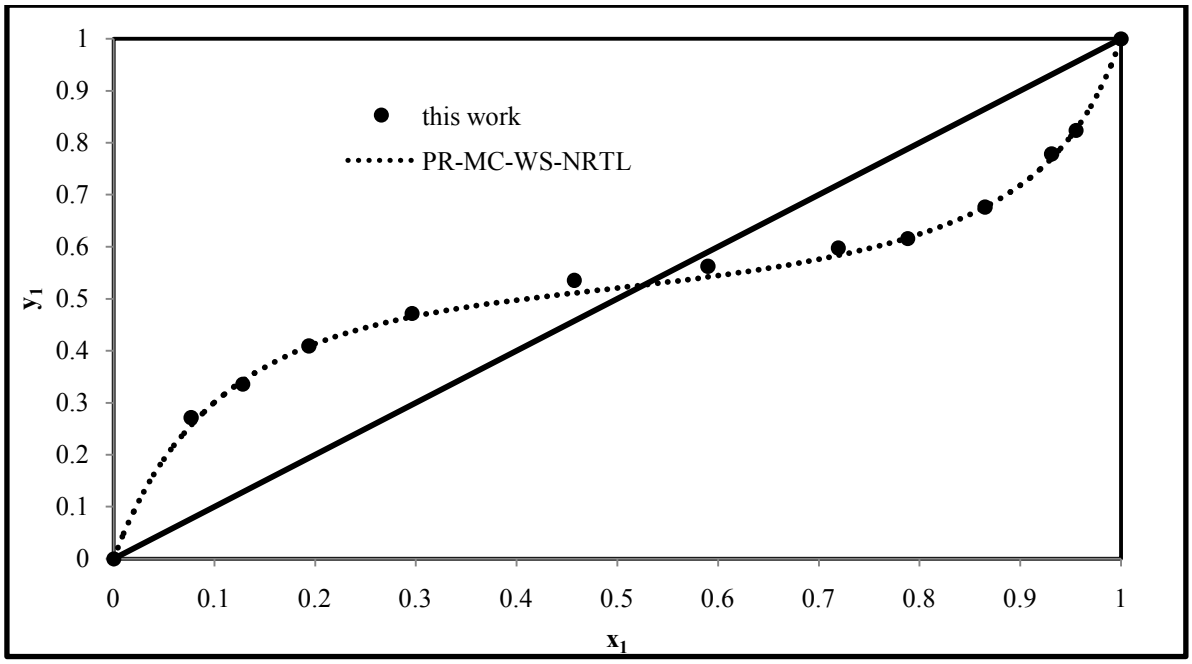

Figure 7-35: Fit of the PR-MC-WS-NRTL model combination to the x-y plot of the 2-methylpent-2-ene (1) + ethanol (2) system at 383.20 K for the direct method.

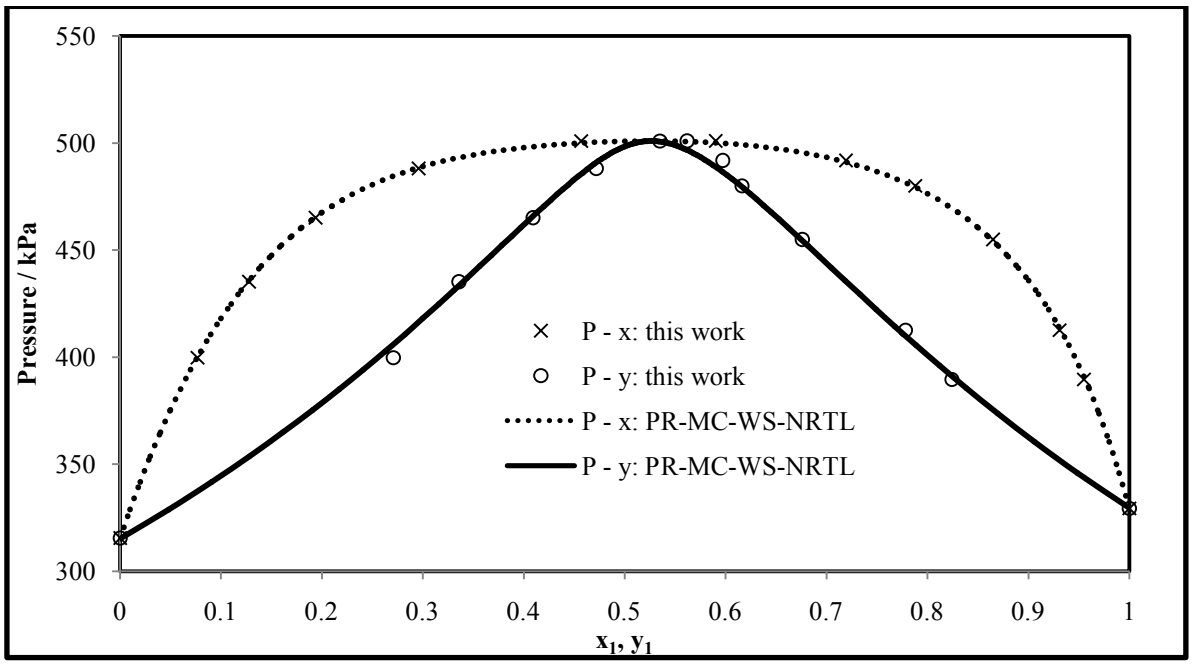

Figure 7-36: Fit of the PR-MC-WS-NRTL model combination to the P-x-y plot of the 2-methylpent-2-ene (1) + ethanol (2) system at 383.20 K for the direct method.

7.5 Experimental LLE Data Reduction

The experimental LLE data measured in this study was to confirm the versatility of the newly developed apparatus. Hence binary systems of LLE data were measured for two systems used as tests: hexane + acetonitrile and methanol + heptane. Binary systems of LLE data are also known as mutual solubility data. Raal and Mühlbauer (1998) mentioned that there is no means for finding the activity coefficients from mutual solubility data but only the ratio of the activity coefficients. Hence, mutual solubility data can only be used to obtain the parameters of a liquid phase activity coefficient model as a function of temperature (usually two parameters per temperature for asymmetric models). The activity coefficient models that were used for VLE data reduction were also used for the LLE data reduction as these models were also capable of representing LLE data. Therefore the experimental mutual solubility data were regressed with the TK-Wilson, NRTL and modified UNIQUAC activity coefficient models. With regards to the NRTL model, the non-randomness parameter (α) was fixed to a value of 0.3.

For both the LLE systems measured in this study, the GC TCD calibration was carried out using the direct calibration method as opposed to the area ratio method. This was done since a suitable solvent for the heterogeneous mixtures could not be found such that the retention time of the solvent peak was different from the binary components. Various available GC columns were also investigated but to no avail.

7.5.1 Hexane (1) + Acetonitrile (2)

This test system was selected since both binary LLE and VLLE data could be measured. In finding such a system, one had to ensure that the pressure values of the VLLE data were above atmospheric pressure to enable the ROLSI^{TM} to sample the respective equilibrium phases. With regards to the binary LLE data, high pressure nitrogen was used to maintain a pressure of 350 kPa in the equilibrium cell to enable sampling with the ROLSI^{TM}, as was outlined in Chapter 5. The experimental data of Bernabe et al. (1988) and Sugi and Katayama (1978) were available for comparison and are shown in Section 6.3.2 of Chapter 6. The data measured in this study showed considerable deviation to that of Bernabe et al. (1988). It should be noted that the data measured by Bernabe et al. (1988) made use of the cloud point method which was rather subjective since the equilibrium point was judged from visual observations. On the other hand, the data of Sugi and Katayama (1978) was in agreement with the data measured in this study for the hexane rich phase.

The GC TCD calibration results are presented in Figures C-44 and C-45 for hexane and acetonitrile respectively and reported in Table C-6 of Appendix C. The model parameters for the LLE data reduction are reported in Table 7-24 and the temperature dependence of the parameters is presented in Figures 7-37 to 7-39. The fitted equations for the model parameters within the temperature range are reported in Table 7-25.

Table 7-24: Model parameters from mutual solubility data for the hexane (1) + acetonitrile (2) system.

	Activity Coefficient Models					
	TK-Wilson		NRTL		mod. UNIQUAC	
Temperature (K)	$a_{12} - a_{22}$ J.mol^{-1}	$a_{21} - a_{11}$ J.mol^{-1}	$g_{12} - g_{22}$ J.mol^{-1}	$g_{21} - g_{11}$ J.mol^{-1}	$u_{12} - u_{22}$ J.mol^{-1}	$u_{21} - u_{11}$ J.mol^{-1}
348.22	-3252	10037	3628	4141	3871	-13.9
344.43	-3309	12669	4047	3931	4518	-225.2
337.55	-3161	12039	4420	3960	4728	-215.5
331.36	-3004	11662	4587	4173	4768	-140.4
321.94	-2550	10611	4767	4822	4730	66.9
313.13	-1797	9756	4966	5690	4647	334.9

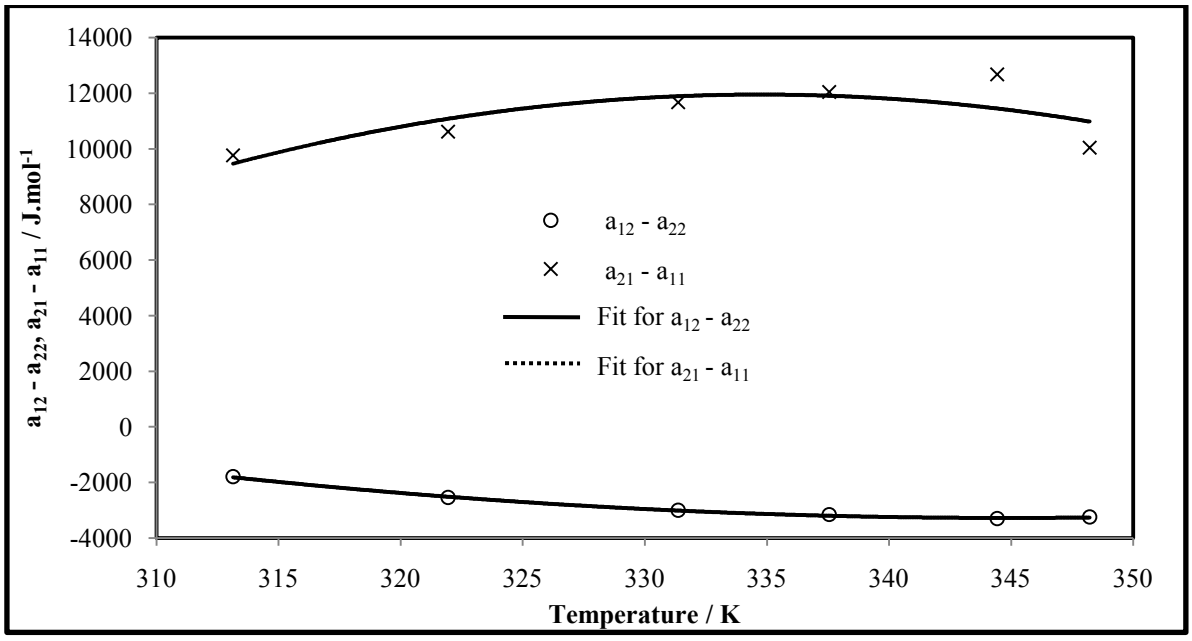

Figure 7-37: Temperature dependence of the TK-Wilson model parameters for the hexane (1) + acetonitrile (2) system.

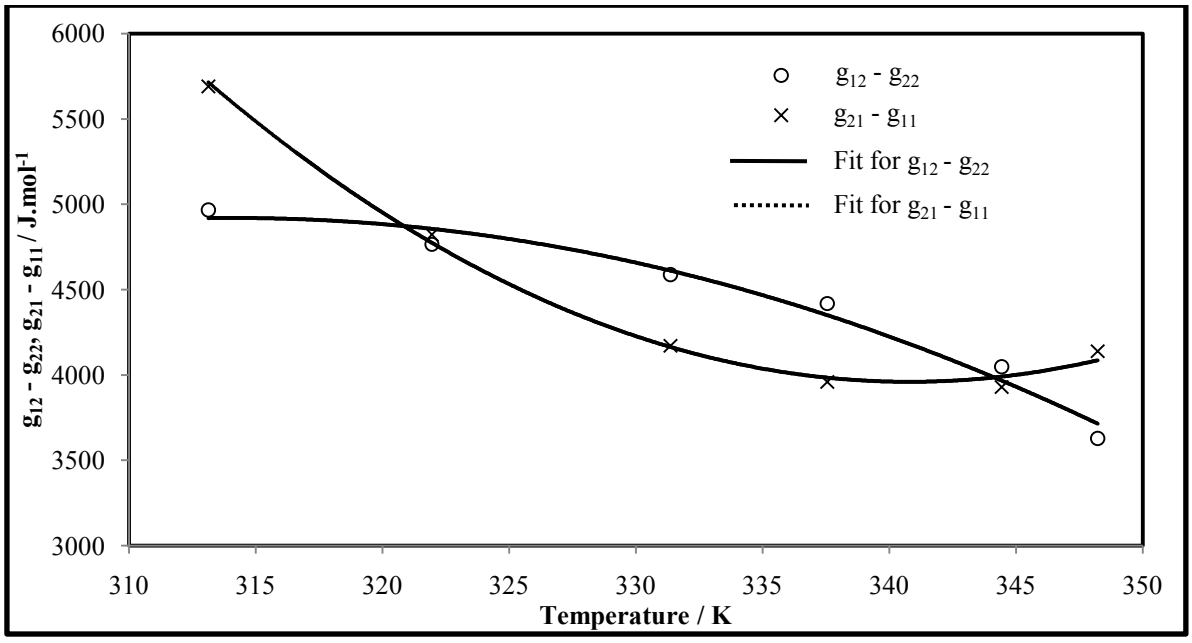

Figure 7-38: Temperature dependence of the NRTL model parameters for the hexane (1) + acetonitrile (2) system.

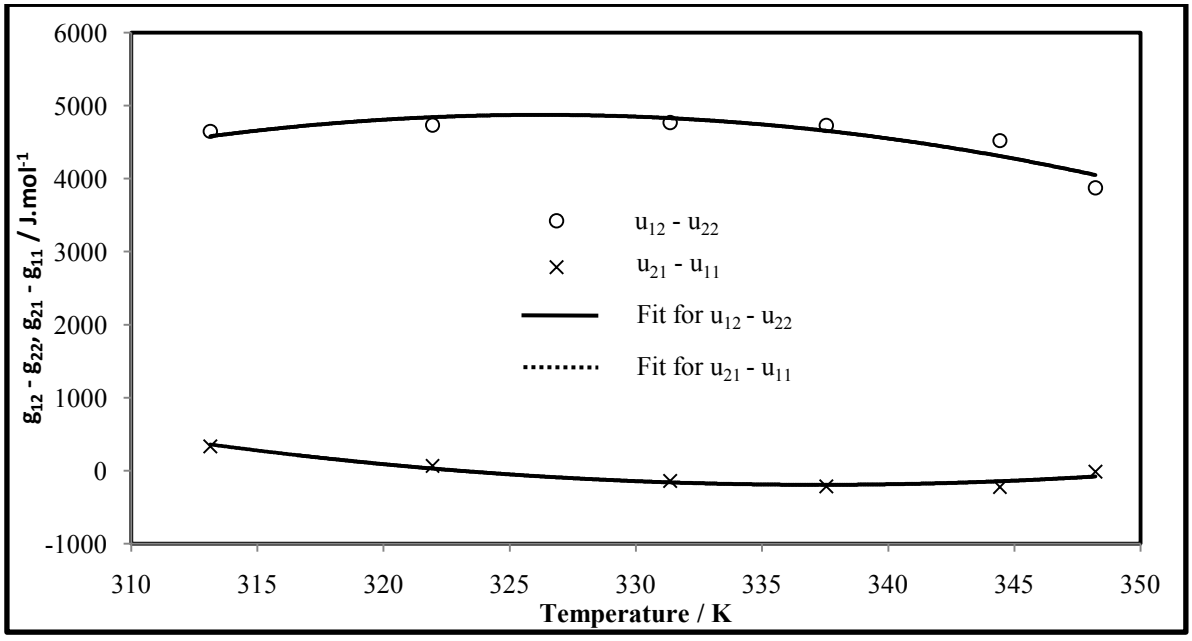

Figure 7-39: Temperature dependence of the modified UNIQUAC model parameters for the hexane (1) + acetonitrile (2) system.

Table 7-25: Fitted equations for the activity coefficient models used in the LLE data reduction for the hexane (1) + acetonitrile (2) system.

Activity Coefficient Model	Fitted Equations	Temperature Range / K
TK-Wilson	$a_{12} - a_{22} = 1.4565T^2 - 1004.48T + 169910$ $a_{21} - a_{11} = -5.3281T^2 + 3566.83T - 584997$	348 to 314
NRTL	$g_{12} - g_{22} = -1.0351T^2 + 650.24T - 97198$ $g_{21} - g_{11} = 2.2924T^2 - 1562.47T + 270202$	348 to 314
Mod. UNIQUAC	$u_{12} - u_{22} = -1.6997T^2 + 1109.02T - 176027$ $u_{21} - u_{11} = 0.9478T^2 - 639.35T + 107620$	348 to 314

The activity coefficient model parameters from the LLE data reduction were satisfactorily fitted with a second order polynomial equation for the temperature range studied. It was clear from Figures 7-31 to 7-33 that the trend of the fitted equations showed considerable deviation to the reduced LLE data. It should be noted however that each mutual solubility data point was reduced individually. Hence such deviations can be explained since there are multiple solutions that can be obtained from each data reduction. However it should be noted that uncertainties in the measurement of the data could also have contributed to the deviations. Therefore care should be exercised when using the fitted equations for predictions outside the temperature range.

7.5.2 Methanol (1) + Heptane (2)

As the experimentally measured LLE data for the hexane + acetonitrile system did not agree to the literature data of Bernabe et al. (1988), a second LLE test system was chosen to consolidate and verify the versatility of the newly developed apparatus to measure LLE data. Hence only a few data points were measured for the methanol + heptane system to accomplish this purpose. The results presented in Section 6.4.2.2 of Chapter 6 showed that the experimental data measured was in agreement with the literature data of Higashiuchi et al. (1987). The comparison of data confirmed that the newly developed apparatus was capable of measuring LLE data.

The GC TCD calibration results are presented in Figures C-43 and C-44 for methanol and heptane respectively and reported in Table C-6 of Appendix C. The model parameters for the LLE data reduction are reported in Table 7-26 and the temperature dependence of the parameters are

presented in Figures 7-40 to 7-42. The fitted equations for the model parameters within the temperature range are reported in Table 7-27.

Table 7-26: Model parameters from mutual solubility data for the methanol (1) + heptane (2) system.

	Activity Coefficient Models					
	TK-Wilson		NRTL		mod. UNIQUAC	
Temperature (K)	$a_{12} - a_{22}$ J.mol^{-1}	$a_{21} - a_{11}$ J.mol^{-1}	$g_{12} - g_{22}$ J.mol^{-1}	$g_{21} - g_{11}$ J.mol^{-1}	$u_{12} - u_{22}$ J.mol^{-1}	$u_{21} - u_{11}$ J.mol^{-1}
308.41	10051	-3399	5292	2882	141.3	4784
312.96	10775	-3546	5260	2655	121.5	4676
317.98	12427	-3680	5251	2457	105.9	4585

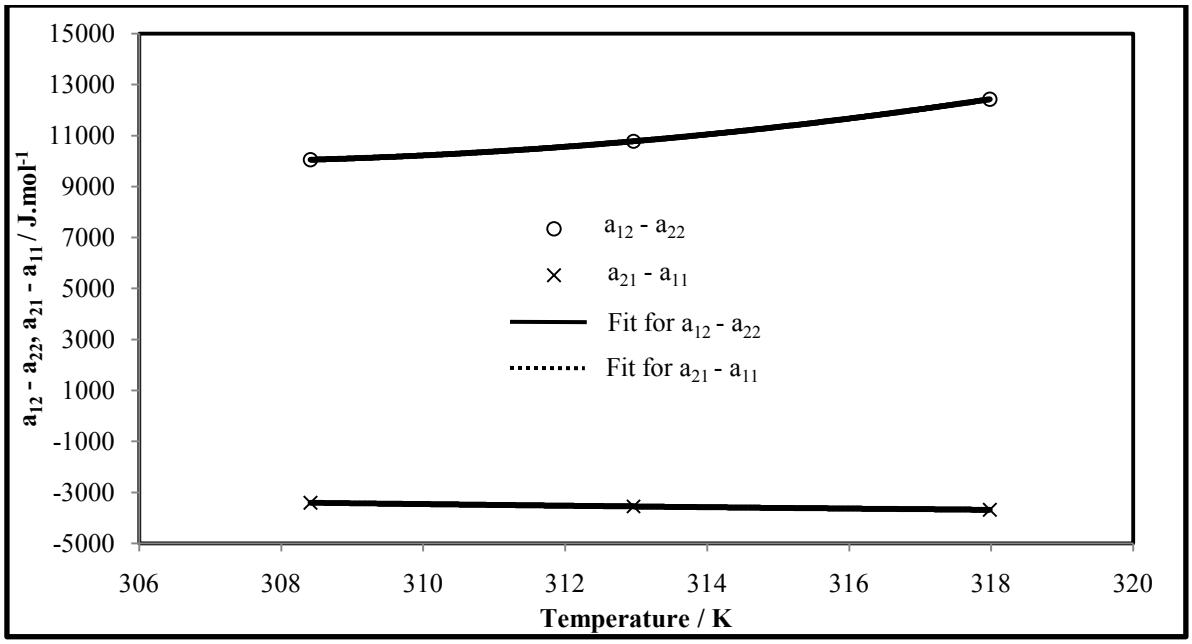

Figure 7-40: Temperature dependence of the TK-Wilson model parameters for the methanol (1) + heptane (2) system.

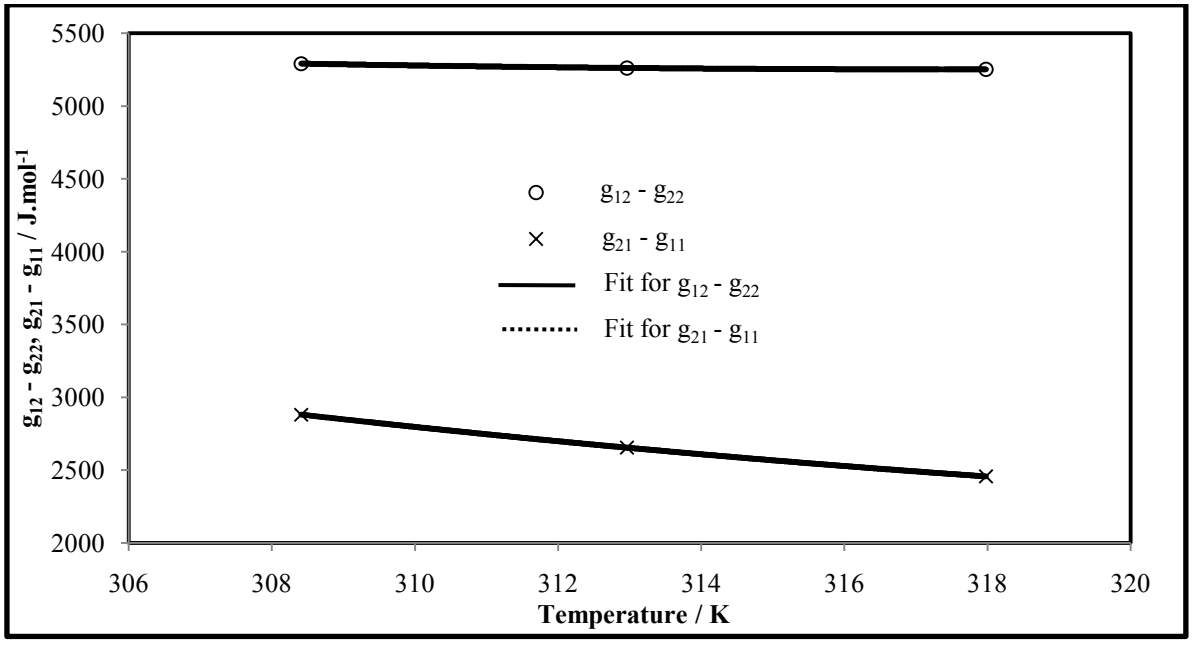

Figure 7-41: Temperature dependence of the NRTL model parameters for the methanol (1) + heptane (2) system.

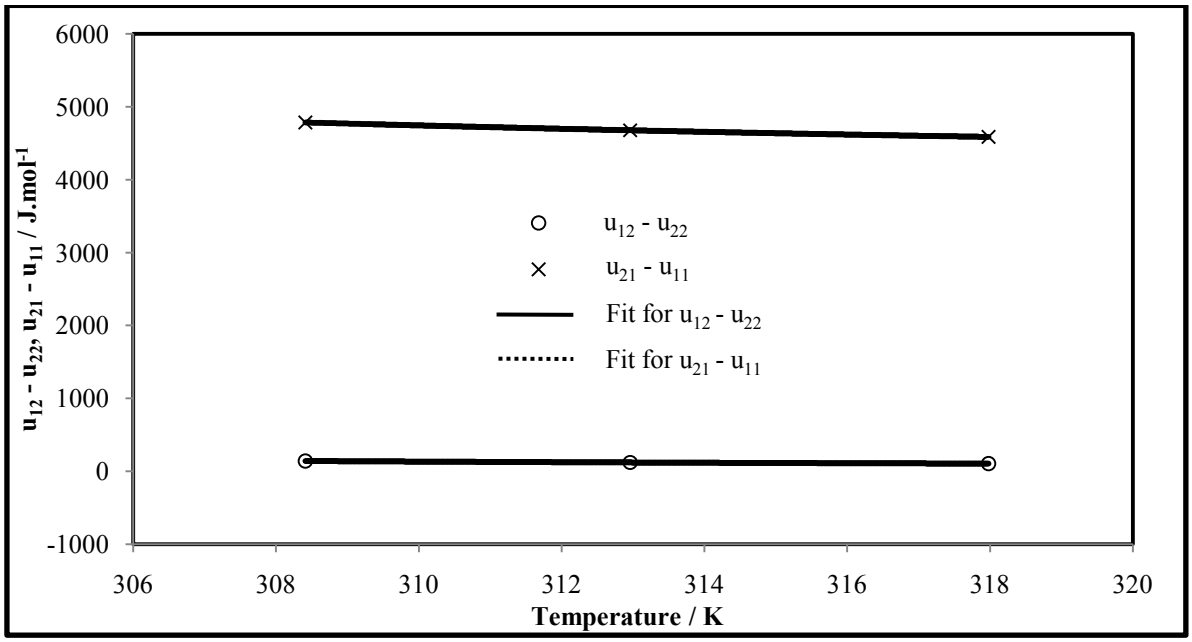

Figure 7-42: Temperature dependence of the modified UNIQUAC parameters for the methanol (1) + heptane (2) system.

Table 7-27: Fitted equations for the activity coefficient models used in the LLE data reduction for the methanol (1) + heptane (2) system.

Activity Coefficient Model	Fitted Equations	Temperature Range / K
TK-Wilson	$a_{12} - a_{22} = 17.748T^2 - 10868.7T + 1.674 \times 10^6$ $a_{21} - a_{11} = 0.577T^2 - 390.9T + 62273$	308 to 318
NRTL	$g_{12} - g_{22} = 0.514T^2 - 326.3T + 57037$ $g_{21} - g_{11} = 1.095T^2 - 730.4T + 12397$	308 to 318
Mod. UNIQUAC	$u_{12} - u_{22} = 0.132T^2 - 86.35T + 14223$ $u_{21} - u_{11} = 0.581T^2 - 384.6T + 68160$	308 to 318

Since only three data points were measured for this system, no conclusive comment on the fitted equations can be made as a second order polynomial equation requires a minimum of three data points for fitting.

7.6 Experimental VLLE Data Reduction

As mentioned previously in Chapter 3, systems that exhibit VLLE behaviour are highly non-ideal. Experimental VLLE data was also measured as part of this study to show versatility of the newly developed apparatus. The measurement of the VLLE point also showed the success of using a single mobile ROLSI™ to sample all three phases. The combined method for data reduction was used for the VLLE system measured in this study.

7.6.1 Hexane (1) + Acetonitrile (2)

As mentioned previously, this system was chosen since VLLE data could be measured at pressures higher than atmospheric to accommodate the use of the ROLSI™. Although there are numerous aqueous systems that exhibit LLE or VLLE behaviour, water was avoided as a component for this study. This was done to avoid damage to the polymer used in the ROLSI™. Although modifications for the polymer were available, this was not included as part of this study due to time constraints. Hence, a suitable non-aqueous VLLE test system within the pressure transmitter range could not be found in literature for data comparison. However, since the system of hexane + acetonitrile met all the conditions for use in the newly developed apparatus, it was therefore chosen as a system to test

the versatility of the apparatus. This also means that the VLLE data for the hexane + acetonitrile at 348.20 K constitutes as a new experimental VLLE data set.

The GC TCD calibration results were already mentioned and discussed previously in Section 7.5.1. The parameters from the regression of the experimental data with the combined method are reported in Table 7-28. Based on the RMSD values, it can be seen that the NRTL model (with α being regressed) and the TK-Wilson models provided the best fit with the latter having only a marginally better RMSD for the pressures. The UNIQUAC model showed a significantly larger value for the pressure RMSD. However, the vapour composition deviations are significantly large but similar for all the liquid phase activity models. Hence the experimental vapour compositions must therefore contain some error or it could mean that the second virial coefficient of Tsonopoulos (1974) could not represent the vapour phase accurately. The *x-y* and *P-x-y* plots for this system are shown in Figures 7-43 and 7-44 respectively.

Table 7-28: Model parameters (A_{12} and A_{21})[a], root mean square deviations (RMSD) and absolute average deviation (AAD) values for the combined method of the hexane (1) + acetonitrile (2) system at 348.20 K.

Model	A_{12} J.mol^{-1}	A_{21} J.mol^{-1}	RMSD P / kPa	AAD P / kPa	RMSD y_1	AAD y_1
TS-TKWILSON	-3664.20	10557.1	2.60	1.95	0.062	0.058
TS-NRTL (α = 0.3)	4555.18	4560.10	5.27	3.67	0.057	0.053
TS-NRTL (α = 0.44)	5873.82	5621.96	2.61	2.12	0.062	0.057
TS-UNIQUAC	4813.50	-78.82	5.48	3.86	0.057	0.053

[a]TKWilson: $A_{12} = a_{12} - a_{22}$ and $A_{21} = a_{21} - a_{11}$; NRTL: $A_{12} = g_{12} - g_{22}$ and $A_{21} = g_{21} - g_{11}$; mod UNIQUAC: $A_{12} = u_{12} - u_{22}$ and $A_{21} = u_{21} - u_{11}$.

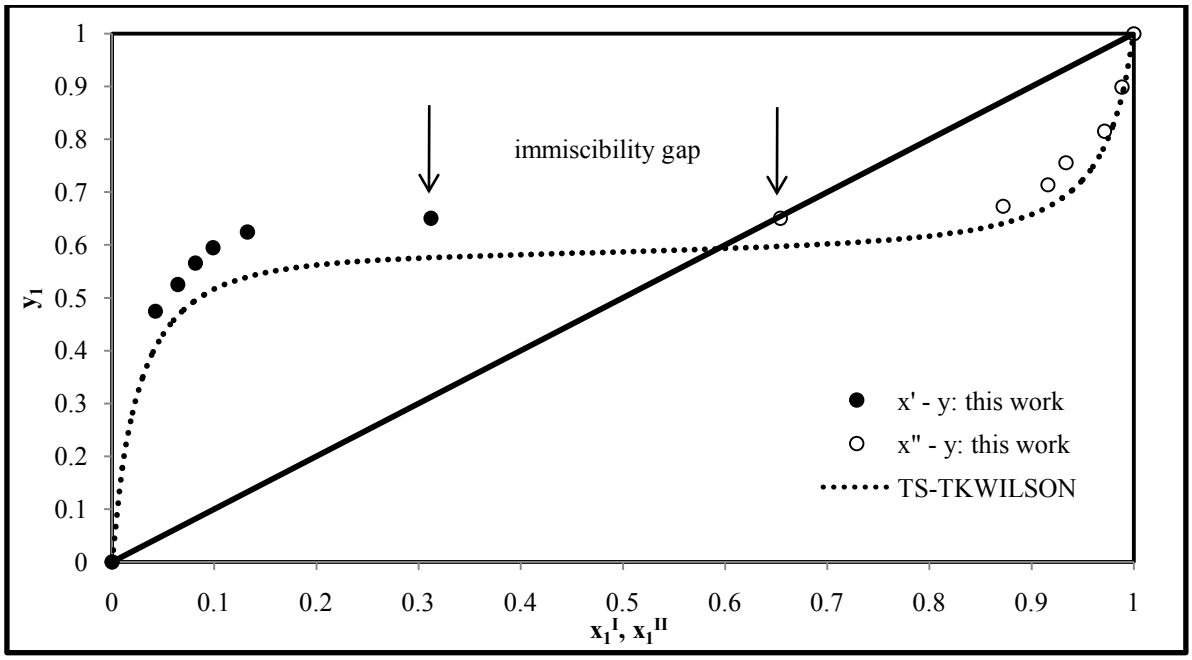

Figure 7-43: Fit of the TS-TKWILSON model combination to the x^I-x^{II}-y plot of the hexane (1) + acetonitrile (2) system at 348.20 K for the combined method.

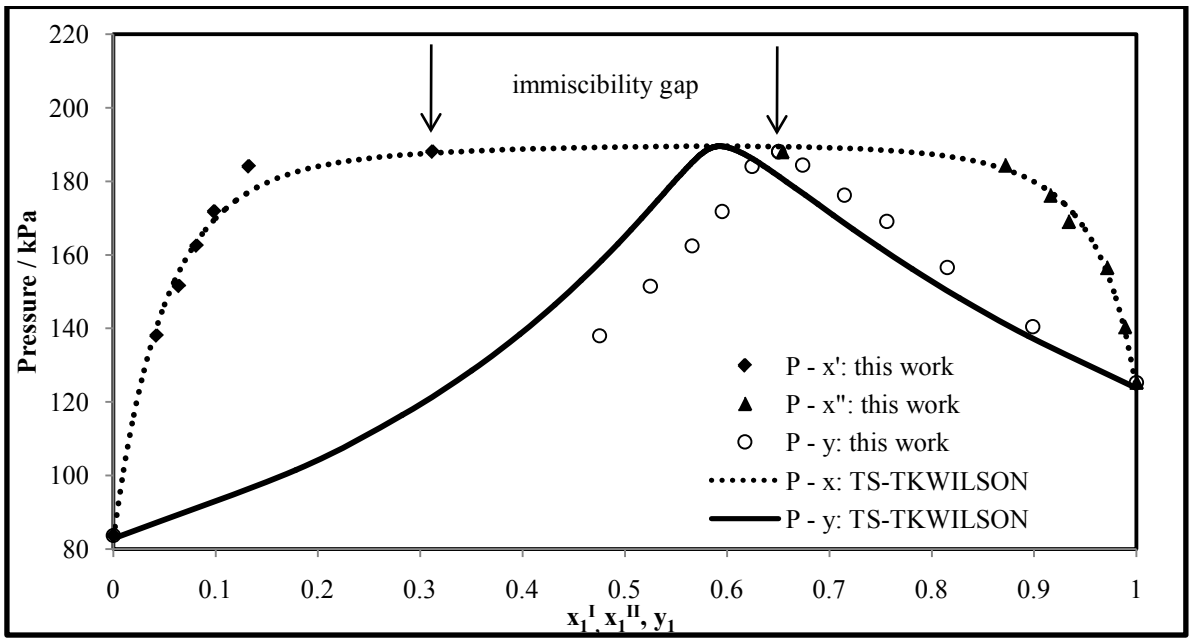

Figure 7-44: Fit of the TS-TKWILSON model combination to the P-x^I-x^{II}-y plot of the hexane (1) + acetonitrile (2) system at 348.20 K for the combined method.

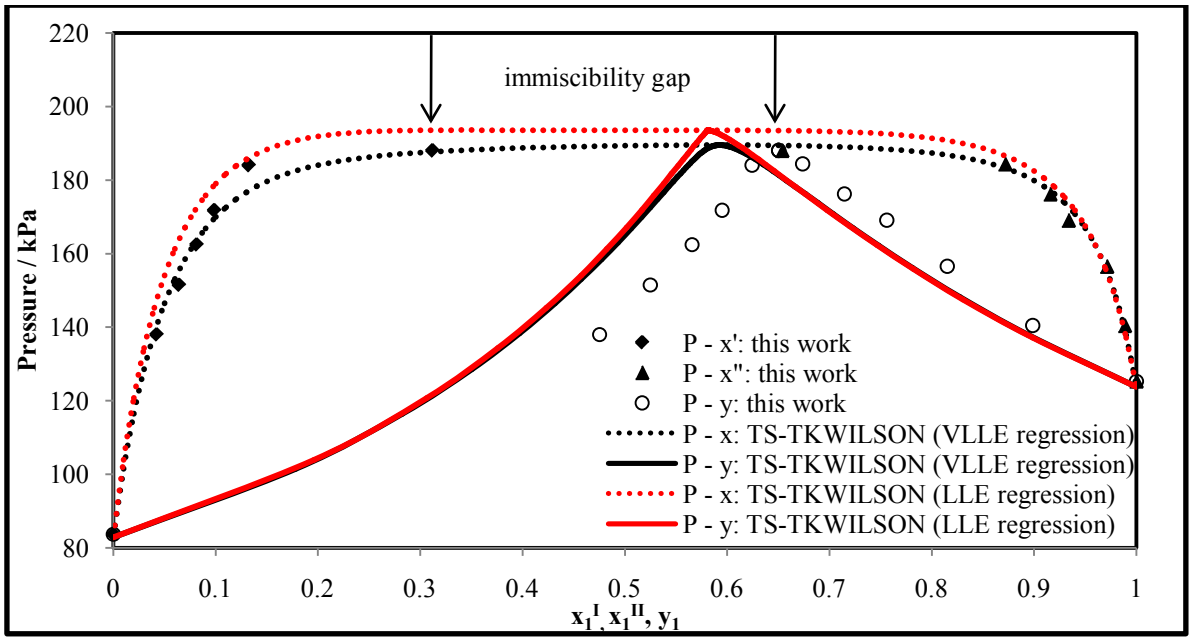

Figure 7-45: Comparison of the P-x^I-x^{II}-y prediction plot using the parameters regressed from LLE and VLLE data with the TK-Wilson model for the hexane (1) + acetonitrile (2) system at 348.20 K.

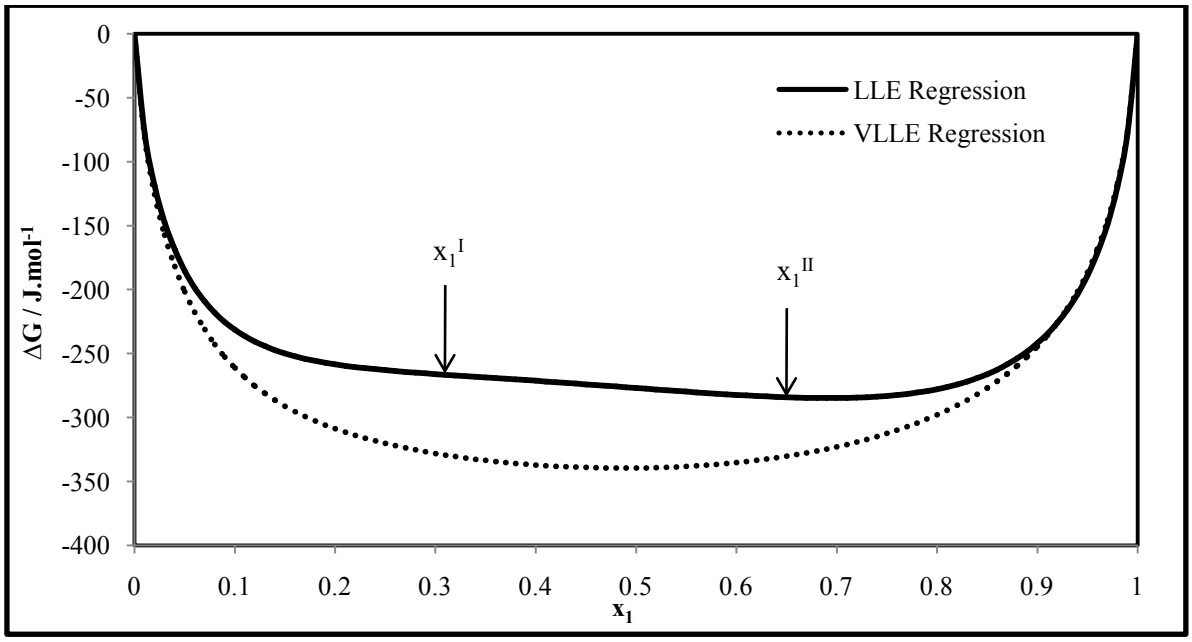

Figure 7-46: Comparison of the molar Gibbs energy of mixing using the parameters regressed from LLE and VLLE data with the TK-Wilson model for the hexane (1) + acetonitrile (2) system at 348.20 K.

All the models used for the VLLE data regression failed to correctly predict the VLLE point. Interestingly though, when the model parameters from the LLE regression at 348.20 K were used to predict the VLLE phase envelope, the results revealed some degree of deviation as shown in Figure 7-45. The deviation was more pronounced for the P-x region and the point of VLLE but the P-y region remained fairly the same. The ΔG plotted against x_1 also verified that the VLLE regression failed to predict the region where the two liquid phases split as shown in Figure 7-46. On the other hand, using the parameters from the regression of the binary LLE data, one cannot clearly identify the regions of phase splitting in Figure 7-46, although the criterion for LLE was satisfied in the regression algorithm.

Interestingly the composition of the vapour phase is extremely close to that of the II liquid phase at the VLLE point. This implies that the obtained azeotrope is thus simultaneously homogeneous and heterogeneous. Therefore this point can be classified as a bi-azeotrope. It should be noted that such a measurement is quite rare.

To determine whether the model prediction or the experimentally measured vapour composition for this system is correct, an experiment using a transparent variable-volume cell can be carried out. This would involve preparing a gaseous mixture of hexane (x_1) + acetonitrile (x_2), say $x_1 = 0.5$, in a variable-volume cell that is kept constant at 348.20 K (in a transparent liquid bath for example). Once this is achieved, the pressure of the cell would then be gradually increased (by use of a piston for example) until the formation of a dewpoint is observed. The pressure at which this occurs is then noted and compared to Figure 7-44. For an overall composition of $x_1 = 0.5$, the experimentally measured VLLE data in Figure 7-44 suggests the dewpoint occurs at approximately 144 kPa. On the other hand for the same overall composition, the model in Figure 7-44 suggests the dewpoint occurs at approximately 164 kPa. Hence by comparison of the pressure obtained from the variable-volume cell experiment and that of Figure 7-44, one can deduce whether the vapour composition given by the model is correct.

7.7 Thermodynamic Consistency Testing for VLE Systems

As mentioned in Section 3.6 of Chapter 3, an "over specification" of VLE data allows for thermodynamic consistency testing to be carried out. The *point test* of Van Ness et al. (1973) and the *direct test* of Van Ness (1995) were used in this study to test the thermodynamic consistency of

the experimental VLE data measured as part of this study. This section will thus focus on the results obtained from each test applied to the experimental VLE data and a discussion thereof.

7.7.1 2-Methoxy-2-Methylpropane (1) + Ethyl Acetate (2)

The values of the average absolute deviation (AAD) for the pressure and vapour composition values for all models are reported in Tables 7-14 and 7-15 for the combined and direct methods respectively. With regards to the *point test*, the NRTL model shows AAD values of 0.41 kPa and 0.008 for the pressure and vapour mole fraction respectively, whilst the PR EoS shows AAD values of 0.40 kPa and 0.004 for the pressure and vapour mole fraction respectively. Since the vapour mole fraction AAD values for both the NRTL model and PR EoS are less than 0.01, one can assume that the *point test* has been partly satisfied. The ΔP and Δy_1 plots are presented in Figures 7-47 and 7-48 respectively. The ΔP plot shows random scattering around the x-axis for both the NRTL model and the PR EoS (a positive indication for the *point test*). However, the Δy_1 plot showed no scattering around the x-axis for the NRTL model but a negative bias whilst the PR EoS shows very poor scattering where only two deviation points are positive and the rest are negative. This is indicative that the point test is subjective to the model employed. Hence, according to the point test, one cannot successfully conclude that the data are thermodynamically consistent as only one of the two conditions has been adequately satisfied.

The *direct test* requires the RMSD value for $\ln(\gamma_1/\gamma_2)$ of the combined method. The results for combined method are reported in Table 7-29. According to Table 3-1, all the models indicate excellent results for thermodynamic consistency as seen by the index values for the *direct test*. However for the NRTL model, Figure 7-49 shows no random scattering about the x-axis for the $\Delta \ln(\gamma_1/\gamma_2)$ plot, which is also a requirement of the *direct test*. Hence, similar to the point test, one cannot successfully conclude that the data are thermodynamically consistent according to the *direct test*. It may well be true that the data are indeed thermodynamically consistent but the models employed render them thermodynamically inconsistent.

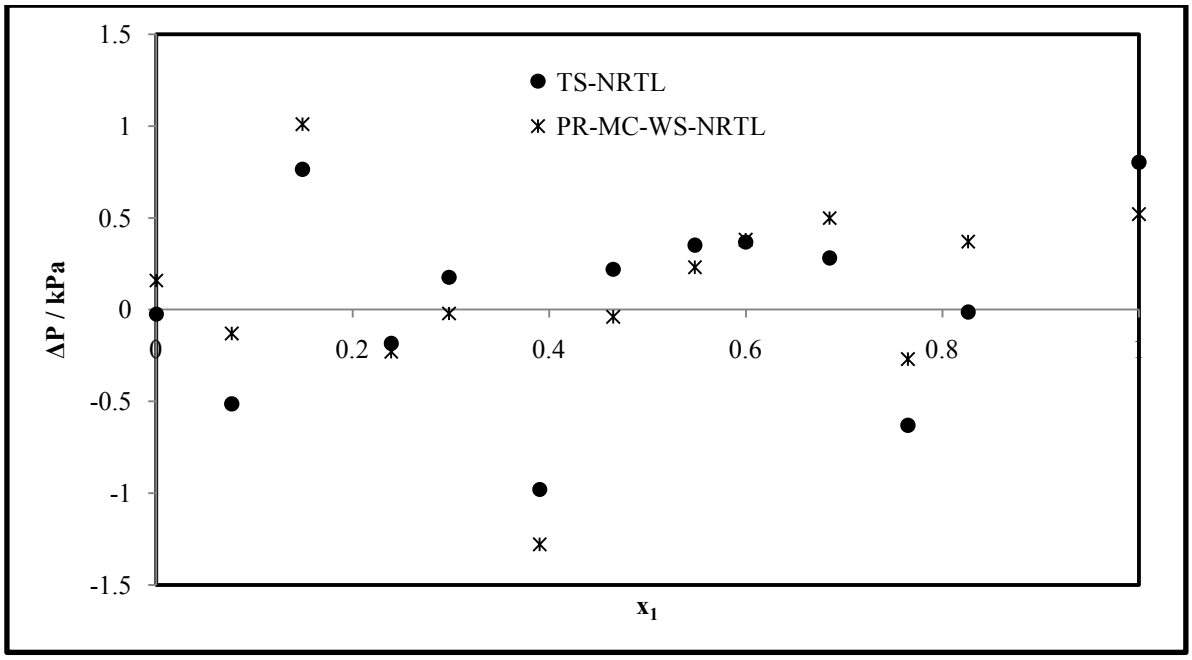

Figure 7-47: ΔP plot for the TS-NRTL and PR-MC-WS-NRTL model combinations for the 2-methoxy-2-methylpropane (1) + ethyl acetate (2) system at 373.17 K.

Table 7-29: Results obtained for the *direct test* when using a liquid phase activity coefficient model for the 2-methoxy-2-methylpropane (1) + ethyl acetate (2) system at 373.17 K.

	RMSD	
Model	**$\ln(\gamma_1/\gamma_2)$**	**Index***
TK-Wilson	0.044	2
NRTL (α = 0.3)	0.044	2
NRTL (α = 3.54)	0.043	2
mod UNIQUAC	0.044	2

*Ranges from 1 to 10, where 1 signifies excellent consistency and 10 poor consistency

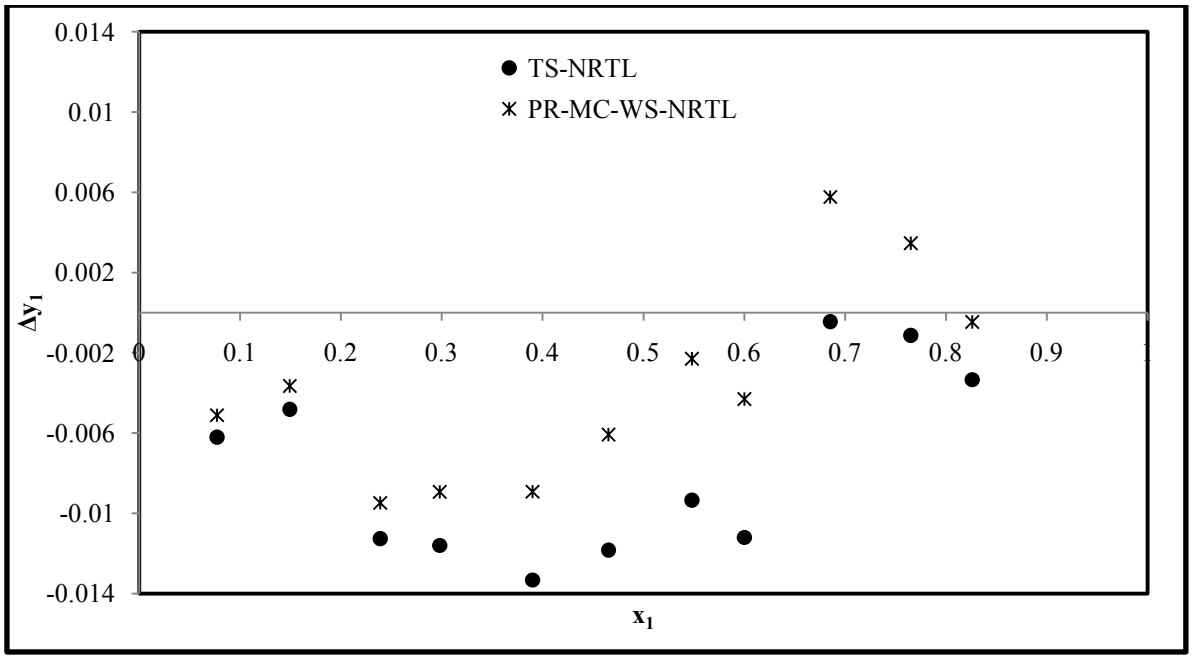

Figure 7-48: Δy_1 plot for the TS-NRTL and PR-MC-WS-NRTL model combinations for the 2-methoxy-2-methylpropane (1) + ethyl acetate (2) system at 373.17 K.

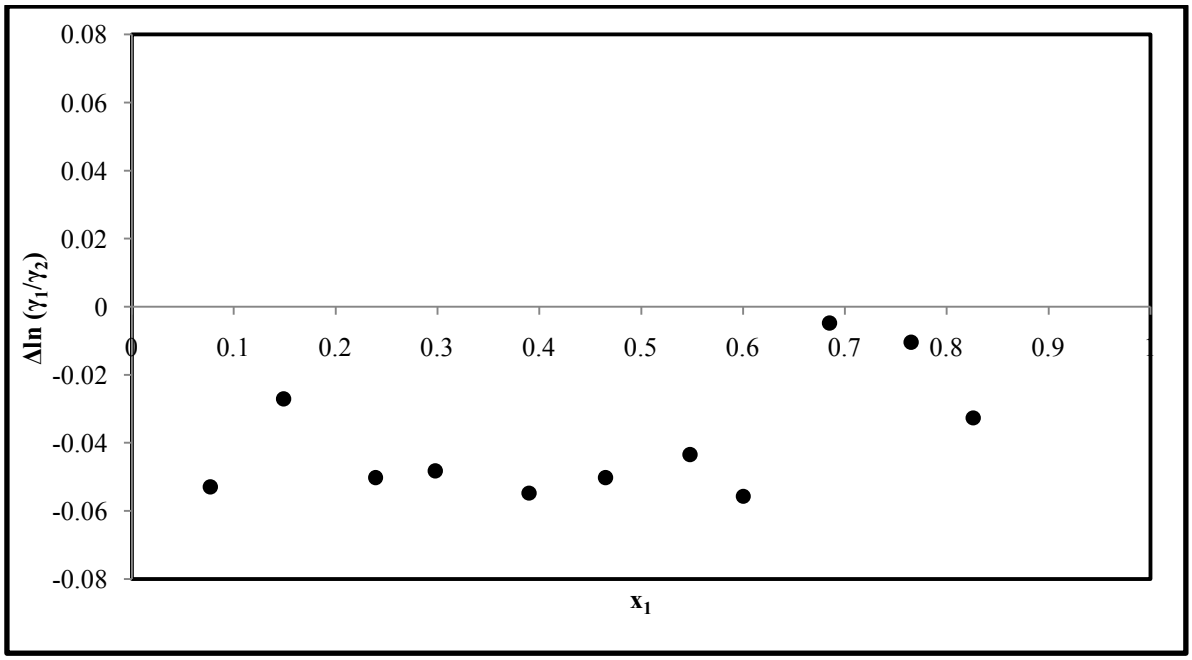

Figure 7-49: Δ ln (γ_1/γ_2) plot for the TS-NRTL model combination for the 2-methoxy-2-methylpropane (1) + ethyl acetate (2) system at 373.17 K.

7.7.2 Methanol (1) + Butan-2-one (2)

The values of the average absolute deviation (AAD) for the pressure and vapour composition values for the combined method and direct method models were presented in Tables 7-15 and 7-16 respectively. The vapour phase mole fraction AAD criterion of the *point test* is satisfied for both the combined and direct methods and each isotherm measured. The ΔP and Δy_1 plots for each isotherm with the direct method are presented in Figures 7-50 and 7-51 respectively. The ΔP plots for each isotherm show random scattering about the x-axis. However, more importantly the Δy_1 plots for each isotherm does not scatter randomly about the x-axis but displayed a positive bias. Hence as mentioned for the previously discussed system, it cannot be satisfactorily concluded that the data are thermodynamically consistent according to the *point test* applied to the direct method as only one of the two conditions were satisfied.

The ΔP and Δy_1 plots for each isotherm with the combined method are presented in Figures 7-52 and 7-53 respectively. For this method the ΔP and Δy_1 plots for each isotherm display random scattering about the x-axis. Hence, since all the conditions for the *point test* applied to the combined method are satisfied, it can be concluded that the data are thermodynamically consistent. Again, this illustrates that the *point test* is subjected to the model employed in the regression technique.

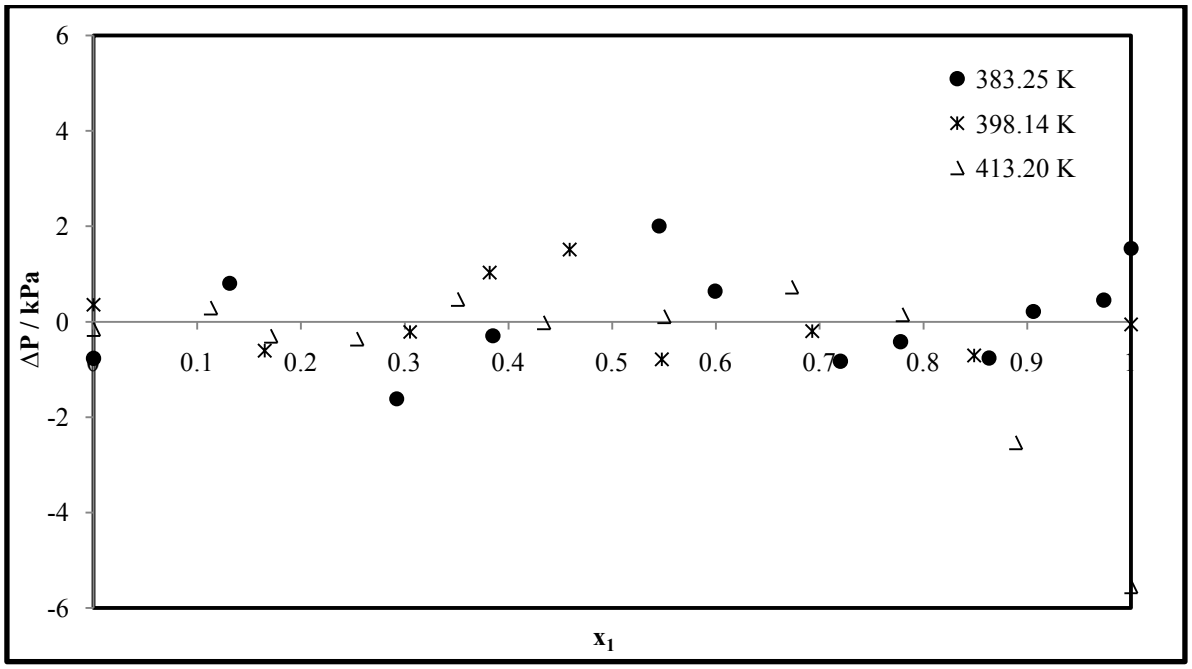

Figure 7-50: ΔP plot for the best fit direct method model combinations of the methanol (1) + butan-2-one (2) system at 383.25, 398.14 and 413.20 K.

With regards to Table 3-1 for the *direct test* of thermodynamic consistency, all the isotherms show excellent results as reported in Table 7-30, where an index value of 2 is observed for all isotherms, indicative of thermodynamic consistent data. The $\Delta \ln (\gamma_1/\gamma_2)$ plot in Figure 7-54 on the other hand, shows random scattering about the x-axis for the 383.25 and 413.20 K isotherms. The data for the 398.14 K isotherm however display a positive bias. Hence, according to the *direct test*, it can be concluded that the data for the 383.25 and 413.20 K isotherms are thermodynamically consistent, whereas the *direct test* for the 398.14 K isotherm data is inconclusive.

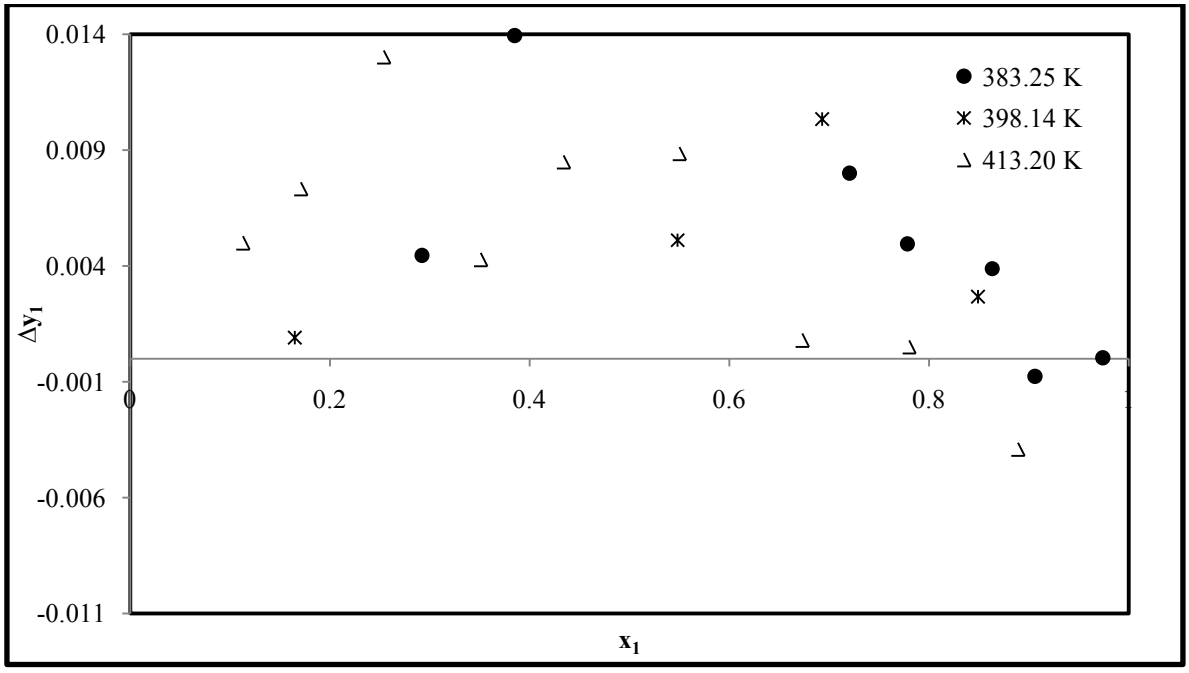

Figure 7-51: Δy_1 plot for the best fit direct method model combinations of the methanol (1) + butan-2-one (2) system at 383.25, 398.14 and 413.20 K.

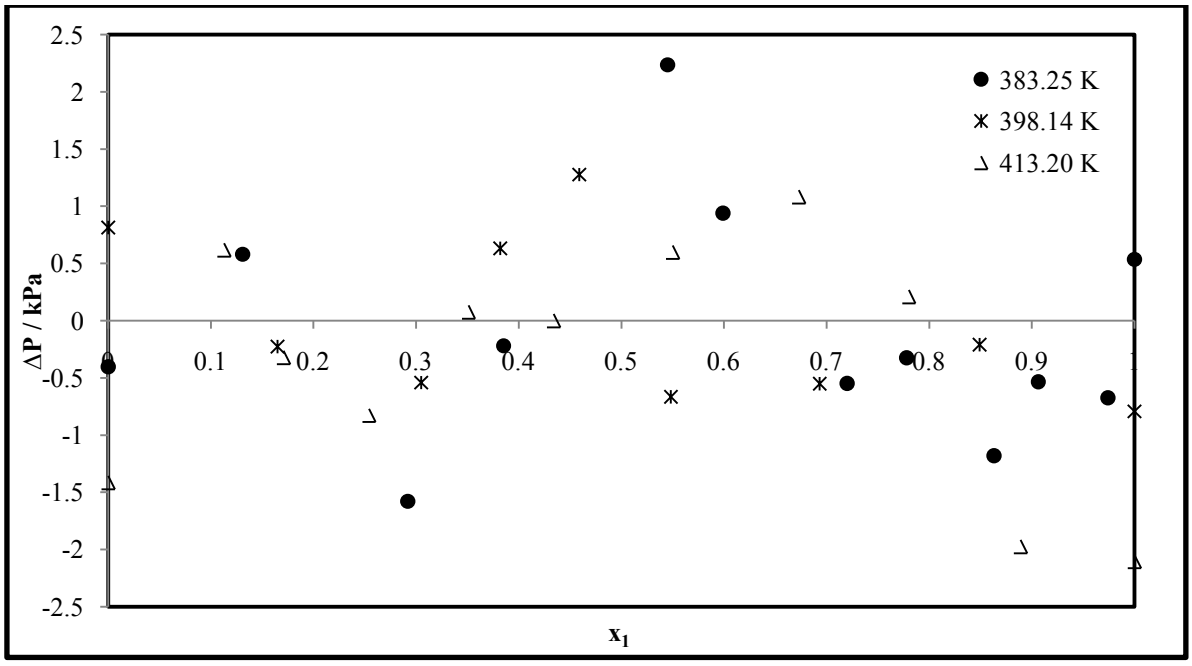

Figure 7-52: ΔP plot for the best fit combined method model combinations of the methanol (1) + butan-2-one (2) system at 383.25, 398.14 and 413.20 K.

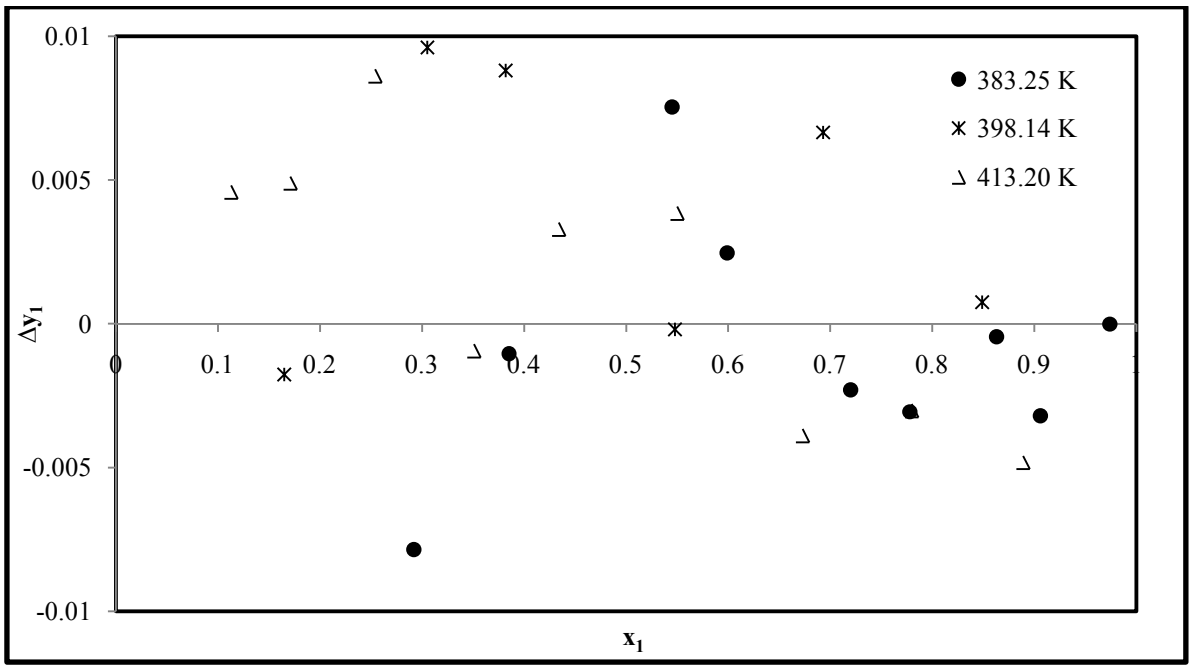

Figure 7-53: Δy_1 plot for the best fit combined method model combinations of the methanol (1) + butan-2-one (2) system at 383.25, 398.14 and 413.20 K.

Table 7-30: Results obtained for the *direct test* when using a liquid phase activity coefficient model for the methanol (1) + butan-2-one (2) system at 383.25, 398.14 and 413.20 K.

Model	RMSD $\ln(\gamma_1/\gamma_2)$	Index*
383.25 K		
TK-Wilson	0.036	2
NRTL (α = 0.3)	0.038	2
NRTL (α = 1.45)	0.036	2
mod UNIQUAC	0.036	2
398.14 K		
TK-Wilson	0.037	2
NRTL (α = 0.3)	0.035	2
NRTL (α = 0.077)	0.035	2
mod UNIQUAC	0.036	2
413.20 K		
TK-Wilson	0.027	2
NRTL (α = 0.3)	0.026	2
NRTL (α = 1.89)	0.028	2
mod UNIQUAC	0.026	2

*Ranges from 1 to 10, where 1 signifies excellent consistency and 10 poor consistency

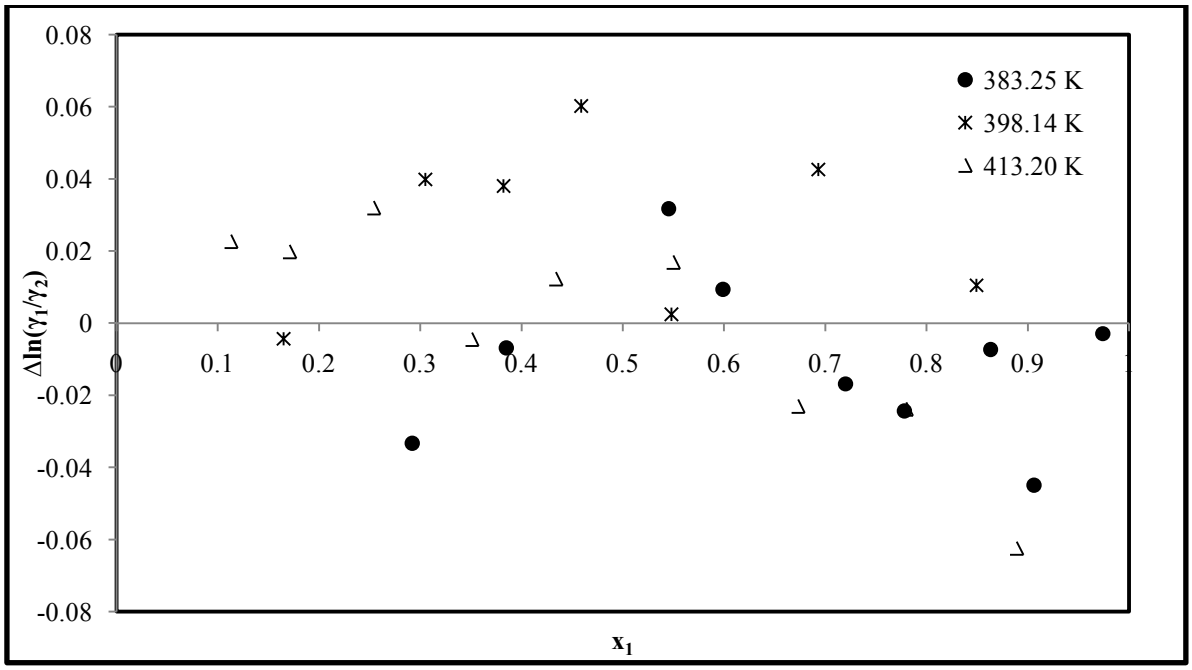

Figure 7-54: Δ ln (γ_1/γ_2) plot for the combined method best fit model combinations of the methanol (1) + butan-2-one (2) system at 383.25, 398.14 and 413.20 K.

7.7.3 Ethanol (1) + Butan-2-one (2)

The values of the average absolute deviation (AAD) for the pressure and vapour composition values for the combined method and direct method models are presented in Tables 7-17 and 7-18 respectively. Similar to the methanol + butan-2-one system, the vapour phase mole fraction AAD criterion of the *point test* is satisfied for both the combined and direct methods and each isotherm measured. The ΔP and Δy_1 plots for each isotherm with the direct method are presented in Figures 7-55 and 7-56 respectively. The ΔP plot for each isotherm shows random scattering about the x-axis. The Δy_1 plots for each isotherm do not scatter randomly about the x-axis but display a positive bias. Hence as mentioned for the previously discussed system, it cannot be satisfactorily concluded that the data are thermodynamically consistent according to the *point test* applied to the direct method as only one of the two conditions is satisfied.

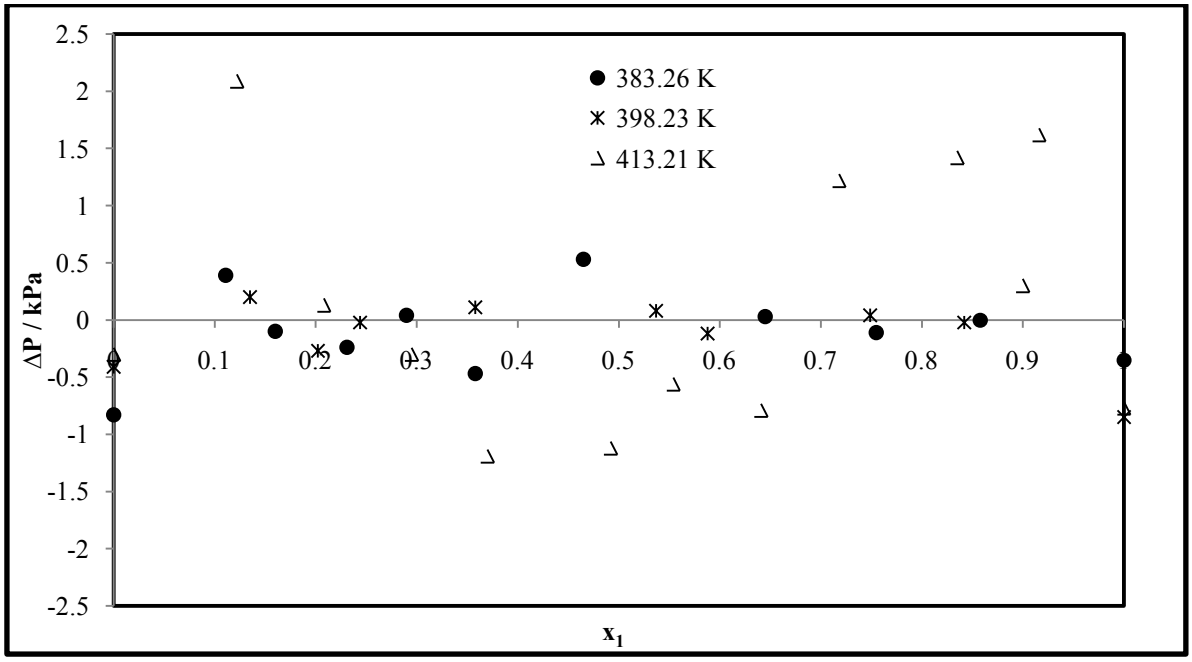

Figure 7-55: ΔP plot for the best fit direct method model combinations of the ethanol (1) + butan-2-one (2) system at 383.26, 398.23 and 413.21 K.

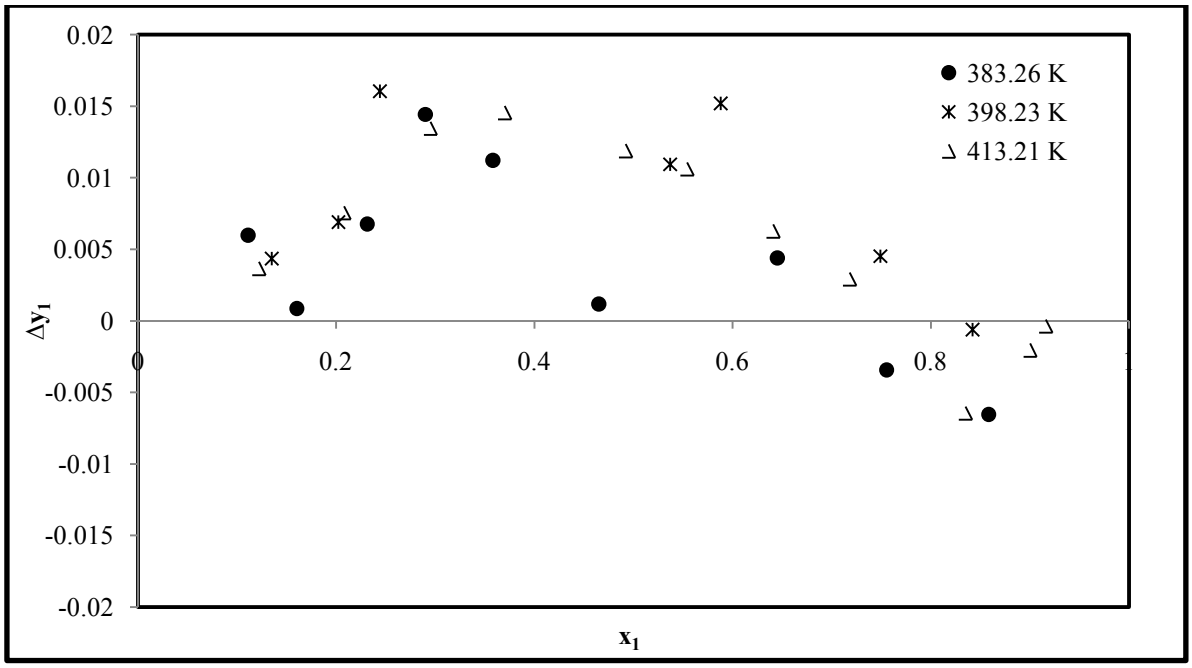

Figure 7-56: Δy_1 plot for the best fit direct method model combinations of the ethanol (1) + butan-2-one (2) system at 383.26, 398.23 and 413.21 K.

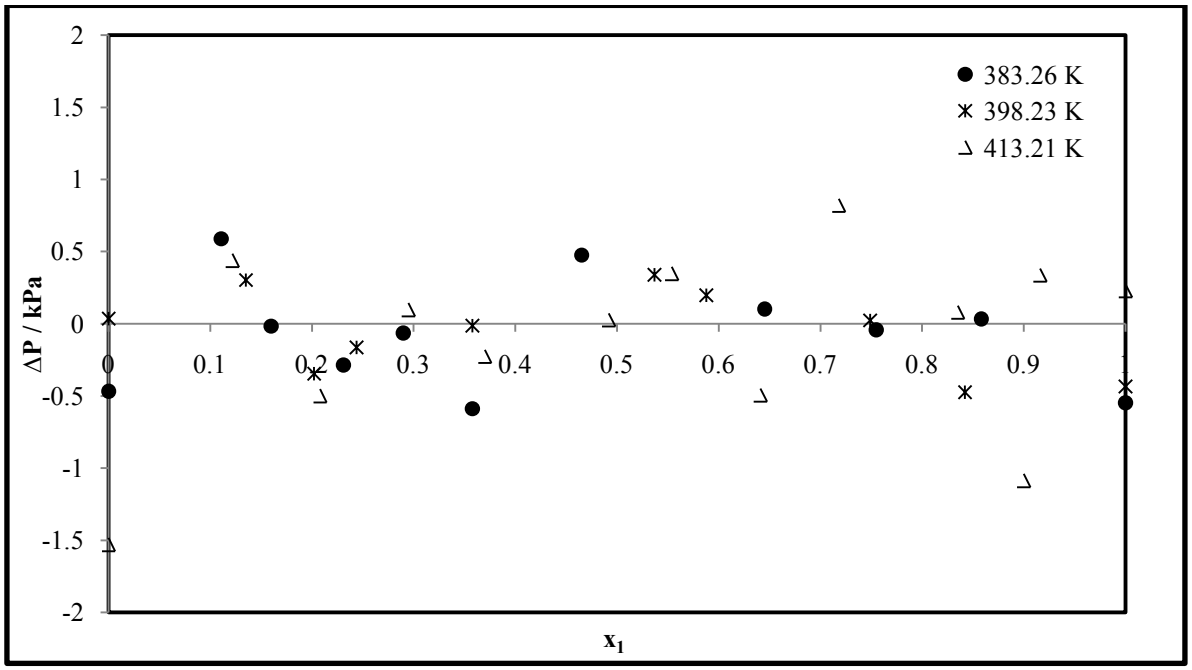

Figure 7-57: ΔP plot for the best fit combined method model combinations of the ethanol (1) + butan-2-one (2) system at 383.26, 398.23 and 413.21 K.

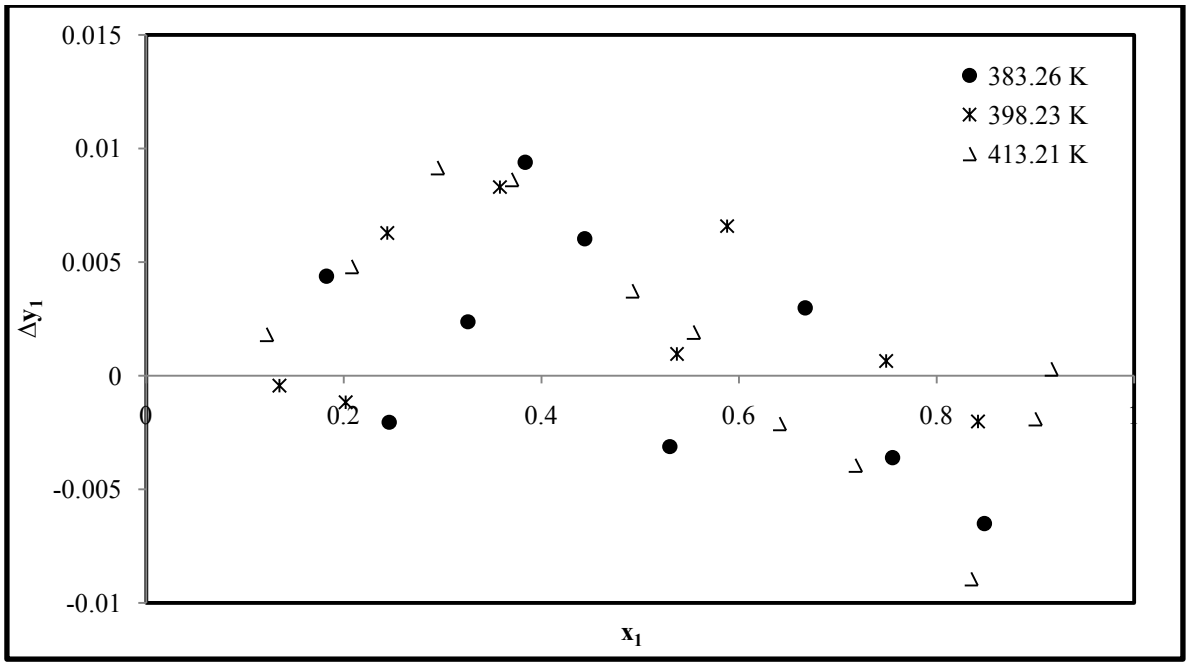

Figure 7-58: Δy_1 plot for the best fit combined method model combinations of the ethanol (1) + butan-2-one (2) system at 383.26, 398.23 and 413.21 K.

The ΔP and Δy_1 plots for each isotherm with the combined method are presented in Figures 7-57 and 7-58 respectively. For this method the ΔP and Δy_1 plots for each isotherm display random scattering about the x-axis. Thus all the conditions for the *point test* applied to the combined method are satisfied. It can be concluded that the data are thermodynamically consistent.

According to Table 3-1 for the *direct test* of thermodynamic consistency, all the isotherms show excellent results as reported in Table 7-31, where index values of 1 and 2 are observed for the isotherms, indicative of thermodynamic consistent data. The $\Delta \ln (\gamma_1/\gamma_2)$ plot in Figure 7-59 moreover shows random scattering about the x-axis for all the isotherms. Therefore, according to the *direct test*, it can be concluded that the data for all the isotherms are thermodynamically consistent.

Table 7-31: Results obtained for the *direct test* when using a liquid phase activity coefficient model for the ethanol (1) + butan-2-one (2) system at 383.26, 398.23 and 413.21 K.

Model	RMSD $\ln(\gamma_1/\gamma_2)$	Index
383.26 K		
TK-Wilson	0.029	2
NRTL (α = 0.3)	0.029	2
NRTL (α = 0.044)	0.028	2
mod UNIQUAC	0.025	1
398.23 K		
TK-Wilson	0.020	1
NRTL (α = 0.3)	0.040	2
NRTL (α = 0.028)	0.020	1
mod UNIQUAC	0.018	1
413.21 K		
TK-Wilson	0.022	1
NRTL (α = 0.3)	0.028	2
NRTL (α = 2.06)	0.028	2
mod UNIQUAC	0.020	1

*Ranges from 1 to 10, where 1 signifies excellent consistency and 10 poor consistency

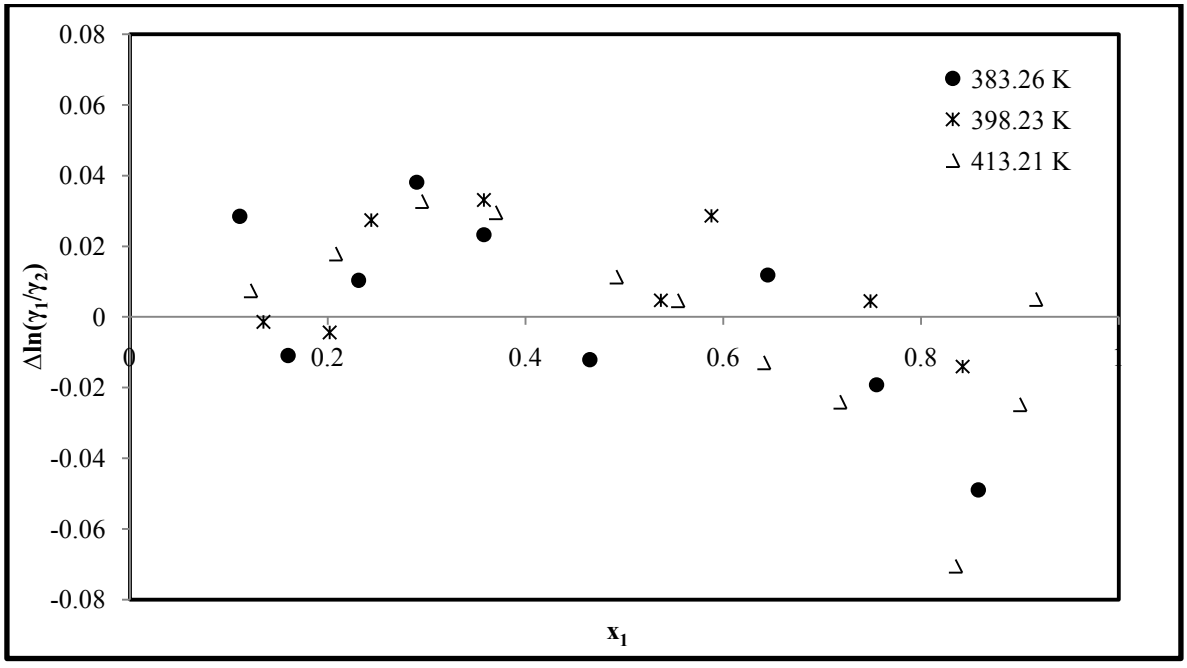

Figure 7-59: Δ ln (γ_1/γ_2) plot for the combined method best fit model combinations of the ethanol (1) + butan-2-one (2) system at 383.26, 398.23 and 413.21 K.

7.7.4 Ethanol (1) + 2-Methoxy-2-Methylbutane (2)

The values of the average absolute deviation (AAD) for the pressure and vapour composition values for the combined method and direct method models are presented in Tables 7-19 and 7-20 respectively. The vapour phase mole fraction AAD criterion of the *point test* is satisfied for both the combined and direct methods and both isotherms measured. The ΔP and Δy_1 plots for each isotherm with the direct method are presented in Figures 7-60 and 7-61 respectively. The ΔP plot for each isotherm shows random scattering about the x-axis. The Δy_1 plot at 398.25 K shows random scattering about the x-axis whereas at 413.19 K the Δy_1 plot displays a positive bias. Hence according to the *point test* applied to the direct method, only the data at 398.25 K can be considered thermodynamically consistent but the data at 413.19 K cannot be strictly considered thermodynamically consistent as only one of the two conditions is satisfied.

The ΔP and Δy_1 plots for both isotherms with the combined method are presented in Figures 7-62 and 7-63 respectively. For this method the ΔP and Δy_1 plots for each isotherm display random scattering about the x-axis. Hence, since all the conditions for the *point test* applied to the combined method are satisfied, it can be concluded that the data are thermodynamically consistent.

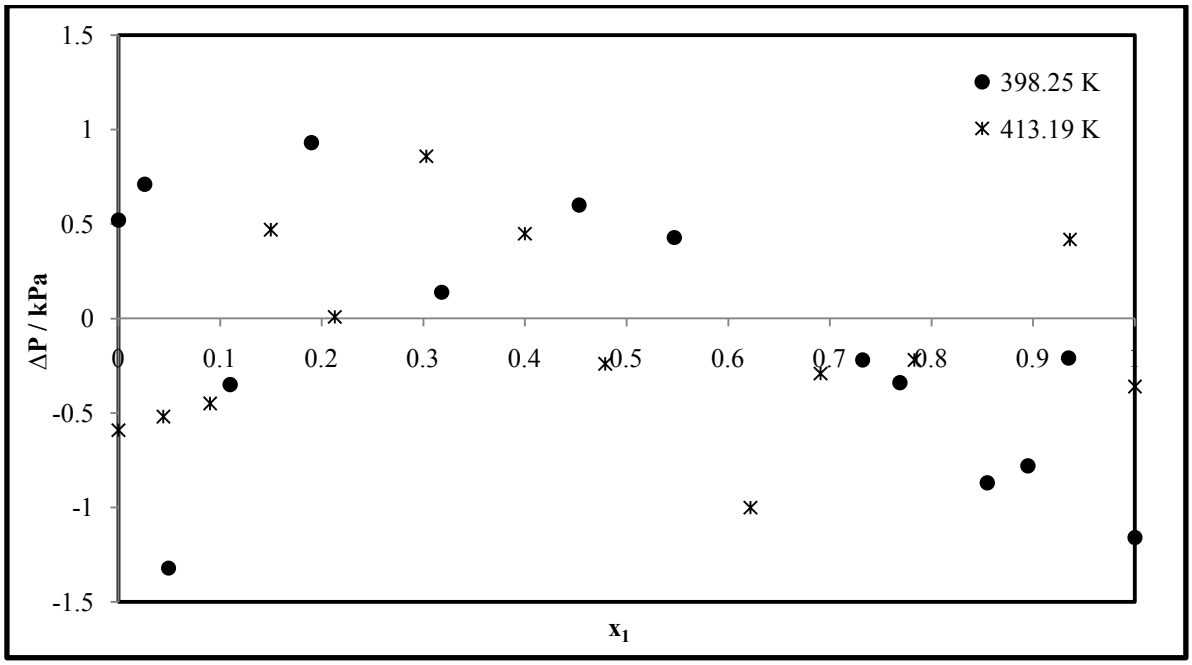

Figure 7-60: ΔP plot for the best fit direct method model combinations of the ethanol (1) + 2-methoxy-2-methylbutane (2) system at 398.25 and 413.19 K.

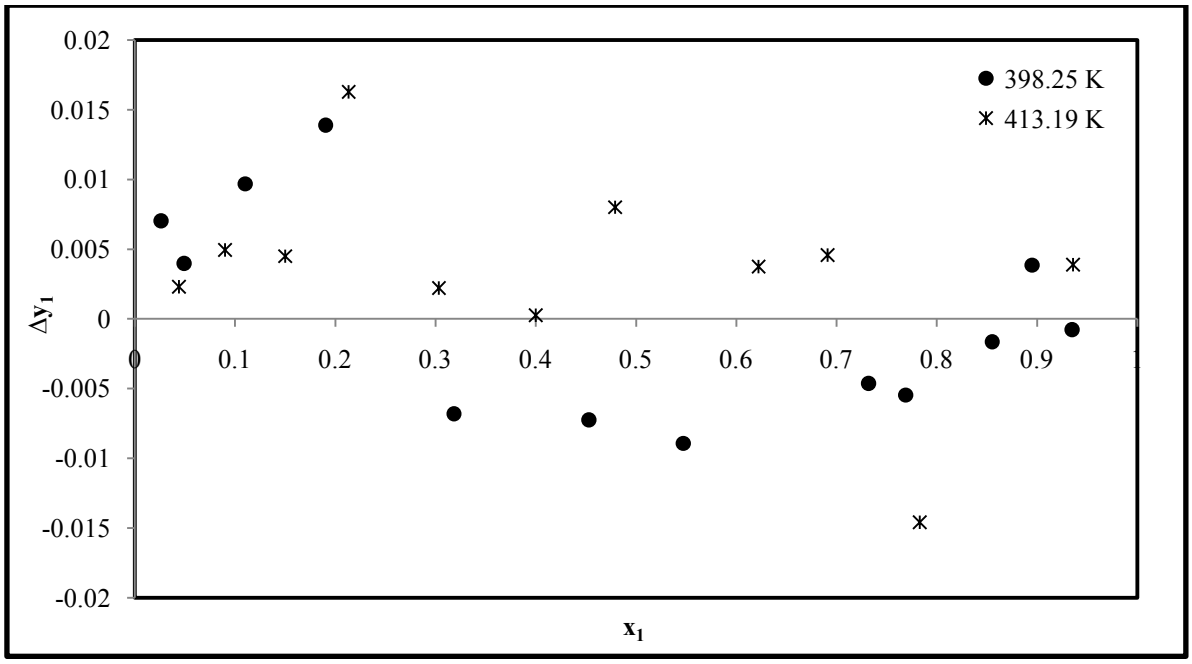

Figure 7-61: Δy_1 plot for the best fit direct method model combinations of the ethanol (1) + 2-methoxy-2-methylbutane (2) system at 398.25 and 413.19 K.

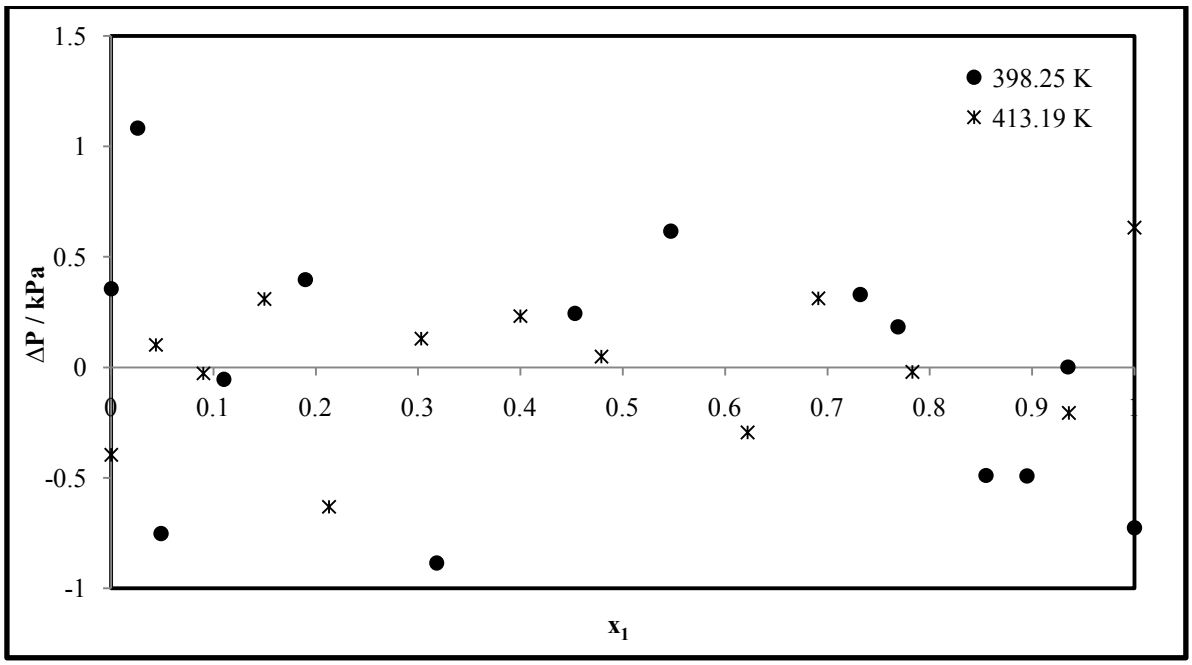

Figure 7-62: ΔP plot for the best fit combined method model combinations of the ethanol (1) + 2-methoxy-2-methylbutane (2) system at 398.25 and 413.19 K.

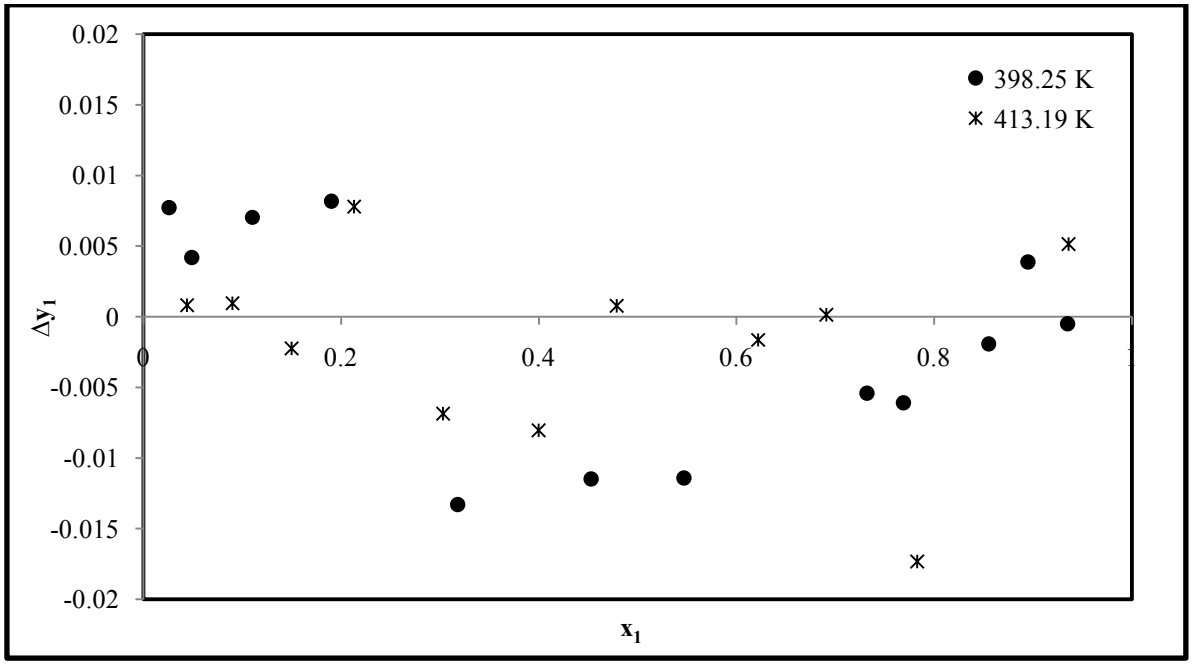

Figure 7-63: Δy_1 plot for the best fit combined method model combinations of the ethanol (1) + 2-methoxy-2-methylbutane (2) system at 398.25 and 413.19 K.

Table 7-32: Results obtained for the *direct test* when using a liquid phase activity coefficient model for the ethanol (1) + 2-methoxy-2-methylbutane (2) system at 398.25 and 413.19 K.

	RMSD	
Model	**$\ln(\gamma_1/\gamma_2)$**	**Index**
398.25 K		
TK-Wilson	0.042	2
NRTL (α = 0.3)	0.043	2
NRTL (α = 0.083)	0.043	2
mod UNIQUAC	0.040	2
413.19 K		
TK-Wilson	0.040	2
NRTL (α = 0.3)	0.038	2
NRTL (α = 0.56)	0.040	2
mod UNIQUAC	0.038	2

*Ranges from 1 to 10, where 1 signifies excellent consistency and 10 poor consistency

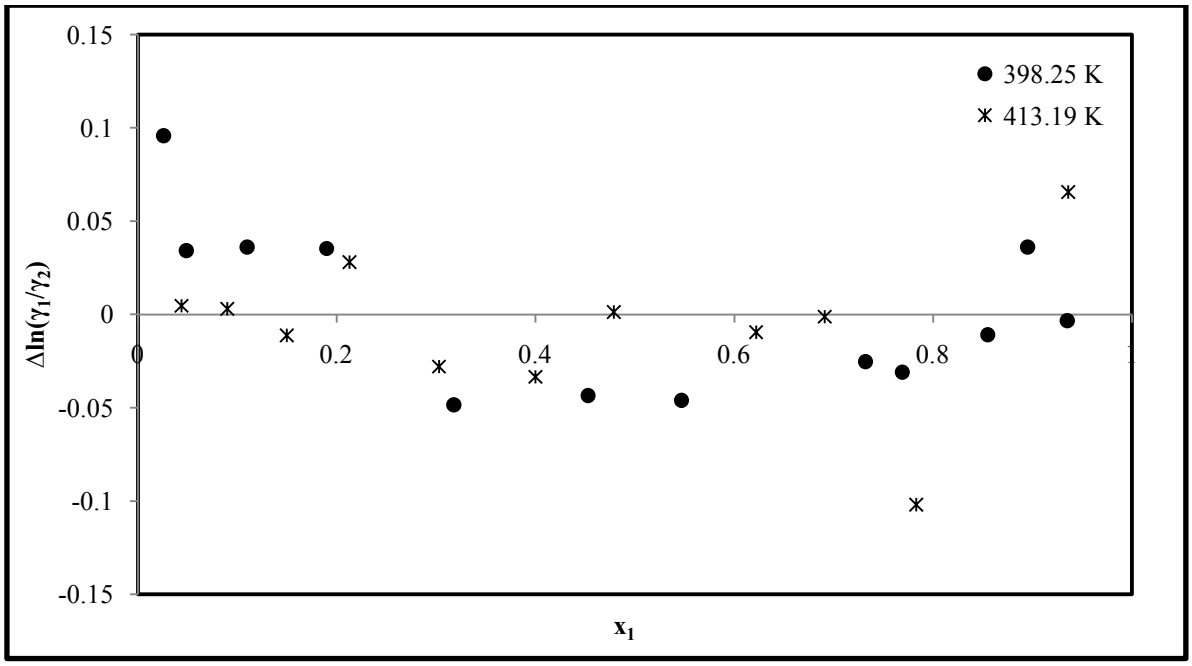

Figure 7-64: Δ ln (γ_1/γ_2) plot for the combined method best fit model combinations of the ethanol (1) + 2-methoxy-2-methylbutane (2) system at 398.25 and 413.19 K.

According to Table 3-1 for the *direct test* of thermodynamic consistency, both isotherms show excellent results as reported in Table 7-32, where an index value of 2 is observed for both isotherms, indicative of thermodynamic consistent data. Furthermore, the Δ ln (γ_1/γ_2) plot in Figure 7-64 shows random scattering about the x-axis for both isotherms. Therefore, according to the *direct test*, it can be concluded that the data for both isotherms are thermodynamically consistent.

7.7.5 2-Methylpent-2-ene (1) + Ethanol (2) System

The values of the average absolute deviation (AAD) for the pressure and vapour composition values for the combined method and direct method models are presented in Tables 7-21 and 7-22 respectively. The vapour phase mole fraction AAD criterion (< 0.01) of the *point test* is strictly not satisfied for the combined method as the AAD value is slightly higher (0.011). With regards to the direct method, the vapour phase mole fraction AAD value (0.009) is slightly lower than the criterion and therefore partly satisfies the *point test*. The ΔP and Δy_1 plots with the direct and combined methods and are presented in Figures 7-65 and 7-66 respectively. The ΔP plots show random scattering about the x-axis. The Δy_1 plots also show some degree of random scattering about the x-axis but display a slightly positive bias. The data can therefore be cautiously considered as thermodynamically consistent using the *point test*.

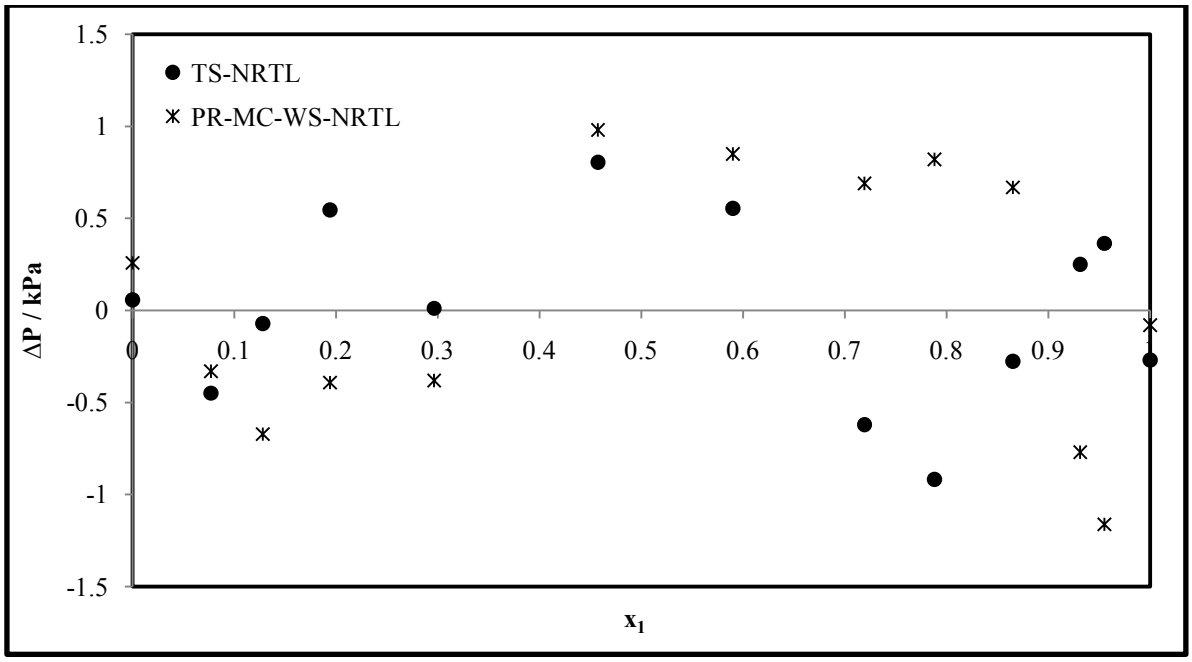

Figure 7-65: ΔP plot for the TS-NRTL and PR-MC-WS-NRTL model combinations for the 2-methylpent-2-ene (1) + ethanol (2) system at 383.20 K.

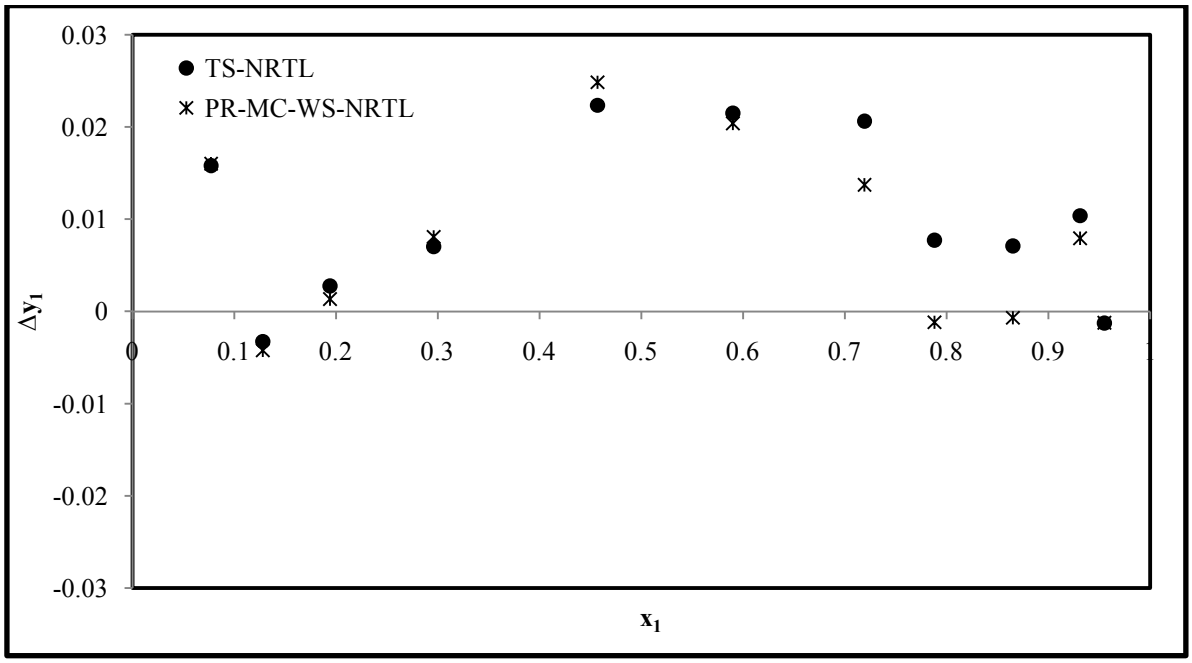

Figure 7-66: Δy_1 plot for the TS-NRTL and PR-MC-WS-NRTL model combinations for the 2-methylpent-2-ene (1) + ethanol (2) system at 383.20 K.

According to Table 3-1 for the *direct test* of thermodynamic consistency, the data shows very good thermodynamic consistency as reported in Table 7-33, where an index value of 3 is observed. On the other hand the $\Delta \ln (\gamma_1/\gamma_2)$ plot in Figure 7-67 shows very little degree of random scattering about the x-axis with a slightly positive bias. Therefore, according to the *direct test*, it could not be strictly concluded that the data are thermodynamically consistent.

Table 7-33: Results obtained for the *direct test* when using a liquid phase activity coefficient model for the 2-methylpent-2-ene (1) + ethanol (2) system at 383.20 K.

	RMSD	
Model	**$\ln(\gamma_1/\gamma_2)$**	**Index**
TK-Wilson	0.054	3
NRTL (α = 0.3)	0.058	3
NRTL (α = -0.55)	0.056	3
mod UNIQUAC	0.055	3

*Ranges from 1 to 10, where 1 signifies excellent consistency and 10 poor consistency

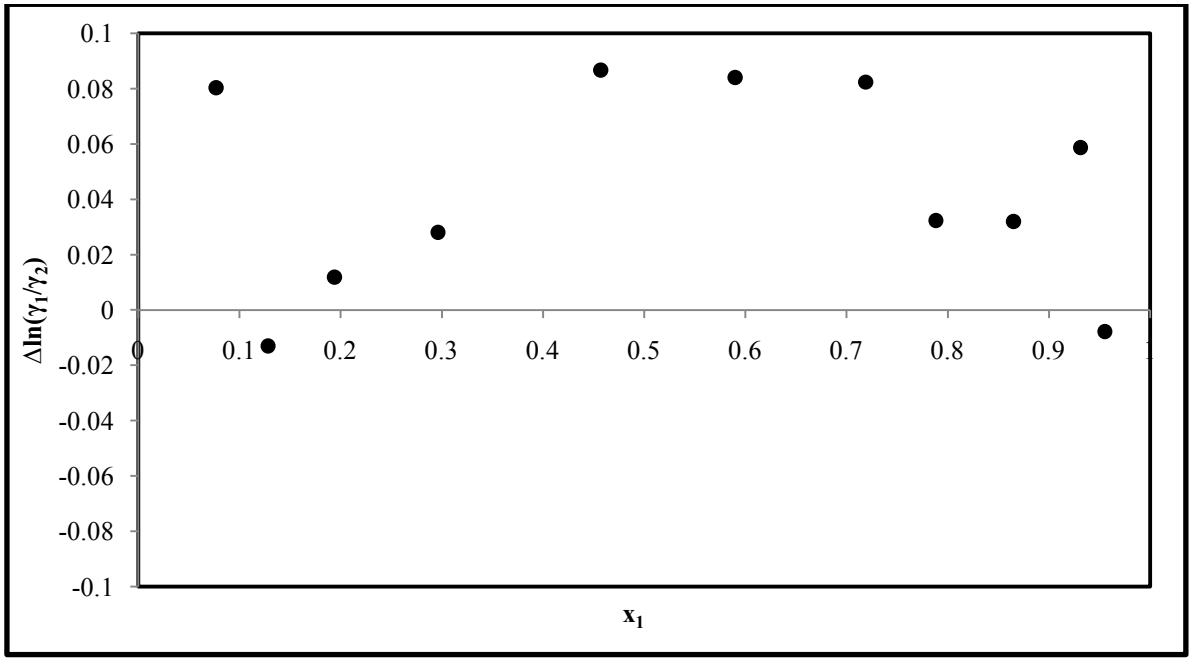

Figure 7-67: $\Delta \ln (\gamma_1/\gamma_2)$ plot for the TS-NRTL model combination for the 2-methylpent-2-ene (1) + ethanol (2) system at 383.20 K.

7.8 Concluding Remarks

All the vapour pressure and phase equilibrium data measured with the newly developed phase equilibrium apparatus were subjected to data analysis and discussed. All the vapour pressure data were regressed using the extended Antoine and Wagner empirical equations as well as the PR and SRK EoS. The combined and direct methods of data regression were used to obtain model parameters for VLE systems. For the combined method, the vapour phase non-ideality was accounted for by the virial EoS with the second virial coefficient correlation of Tsonopoulos (1974). The liquid phase non-ideality of the combined methods was accounted for by use of liquid phase activity coefficient models (viz. TK-Wilson, NRTL and modified UNIQUAC). With regards to the direct method, both the vapour and liquid phase non-idealities were accounted for by the use of a cubic EoS (viz. the PR and SRK EoS with the temperature dependent function (α) of Mathias and Copeman (1983)). The same liquid phase activity coefficient models used in the combined method were also used to regress data for the LLE systems measured. To show versatility of the equilibrium apparatus, VLLE data were also measured and analysed using the combined method of data regression.

Overall, the analysis revealed that all experimental data measured were satisfactorily modeled with an exception to the VLLE data. Thermodynamic consistency testing of the VLE data was also checked as part of the data analysis where the *point* and *direct tests* were employed. It was found that most of the data were thermodynamically consistent with a few being inconclusive.

L'étude décrite dans ce chapitre a consisté en la conception, la construction et la mise en route d'un nouvel appareil permettant, sur de petits volumes, des mesures fiables d'équilibres de phases, plusieurs phases liquides et une phase vapeur. La partie centrale de la cellule d'équilibre a été réalisée en saphir par Rayotek Scientific Inc. Le volume interne de cette cellule d'équilibre a un volume d'environ 17.4 cm^3. La température de fonctionnement de l'appareil s'étend de 253 et 473 K, tandis que la pression de fonctionnement s'étend du vide à 1600 k Pa. Une méthode expérimentale pour la mesure des équilibres de phase adaptée à l'utilisation de cet appareil a été développée avec succès. Les prélèvements des phases à l'équilibre ont été réalisés avec succès au moyen du « Rapid On Line sampling Injector » (ROLSI™).

En préalable aux mesures d' équilibres, chaque produit chimique a été dégazé au moyen de la méthode de distillation sous vide de Van Ness et Abbott (1978). L'appareillage de dégazage a été construit avec de la verrerie et des instruments disponibles à l'école du génie chimique, université KwaZulu Natal, Durban, Afrique du Sud.

Les données expérimentales de pression de vapeur obtenues ont été régressées en utilisant des modèles mathématiques, à savoir l'équation d'Antoine et de Wagner et ont été également régressées avec des équations d'état à savoir l'équation d'état (EdE) dite de Peng et Robinson et de Soave, Redlich et Kwong. Un test de cohérence thermodynamique quantitatif a été effectué pour examiner les données expérimentales de pression de vapeur, qui suite à ce test sai ont toutes été déclarées comme thermodynamiquement cohérentes.

Deux méthodes différentes ont été employées pour la régression des données expérimentales de d'équilibres « liquide-vapeur » (ELV) : les méthodes combinées et directes. La méthode combinée utilise le deuxième coefficient de la corrélation du viriel de Tsonopoulos (1974) pour la non-idéalité en phase vapeur et les modèles : TK-Wilson, NRTL et Modified UNIQUAC pour la non-idéalité phase liquide. La méthode directe fait appel aux équations d'état (EdE) de Peng et Robinson et de Soave, Redlich et Kwong avec une fonction alpha, (α), dépendante de la température, celle de Mathias et Copeman (1983). Dans l'ensemble, nous avons été amené à constater que tous les modèles : méthodes directe et combinée permettaient de décrire de manière satisfaisante les équilibres de phase. Cependant le modèle de NRTL, dans la méthode combinée, s'est avéré meilleur au niveau de la qualité de l'ajustement de la plupart des données obtenues, tandis que pour la méthode directe c'est l'équation d'état (EdE) de Peng et Robinson (PR) qui s'est révélée supérieure.

De manière générale, la comparaison des deux méthodes (directe et combinée) a permis de conclure que tous les systèmes sont mieux décrits par la méthode combinée.

De manière synthétique on peut dire que l'appareil a été conçu, construit et mis en oeuvre avec succès à l'école du génie chimique de l'université KwaZulu Natal, Durban, Afrique du Sud.

8

CHAPTER EIGHT

CONCLUSION

This study was concerned with the design, construction and commissioning of a new apparatus that enabled reliable equilibria measurements for multiple liquid and vapour phases for small volumes. The need for such a small volume apparatus was to enable reliable phase equilibrium measurements for new chemicals that are extremely costly to synthesize. The equilibrium cell was constructed of sapphire by Rayotek Scientific Inc. with a volume of approximately 17.4 cm^3. The operating temperature of the apparatus ranged from 253 to 473 K and the operating pressure ranged from absolute vacuum to 1600 kPa. A successful experimental method for the measurement of phase equilibrium was also developed. The novel technique for the sampling of the equilibrium phases was successfully accomplished using a Rapid-OnLine-Sampler-Injector (ROLSI^{TM}) that was capable of withdrawing as little as 1µl of sample from each phase. Overall the apparatus was successfully designed, constructed and commissioned at the School of Chemical Engineering, University of KwaZulu Natal, Durban, South Africa.

Prior to carrying out measurements, each chemical was thoroughly degassed successfully using the vacuum distillation method of Van Ness and Abbott (1978). The degassing apparatus was constructed of glassware and set-up in the School of Chemical Engineering, University of KwaZulu Natal, Durban, South Africa.

Vapour pressure and phase equilibrium data were measured for the following systems:

a) VLE for 2-methoxy-2-methylpropane + ethyl acetate at 373.17 K
b) LLE for methanol + heptane at 350 kPa
c) LLE for hexane + acetonitrile at 350 kPa
d) VLLE for hexane + acetonitrile at 348.20 K
e) VLE for methanol + butan-2-one at 383.25, 398.14 and 413.20 K

f) VLE for ethanol + butan-2-one at 383.26, 398.23 and 413.21 K
g) VLE for ethanol + 2-methoxy-2-methylbutane at 398.25 and 413.19 K
h) VLE for ethanol + 2-methylpent-2-ene at 383.20 K

The first three systems mentioned above (a – c) were used as test systems to verify that the newly developed apparatus was capable of vapour pressure and phase equilibrium measurements. This also demonstrated the successful versatility of the apparatus in measuring VLE, LLE and VLLE data. The novel technique for sampling was also found to be highly successful.

The experimental vapour pressure data obtained were regressed using mathematical models, viz. the extended Antoine and Wagner equation and were also regressed with equations of state viz. the PR and SRK EoS. A quantitative thermodynamic consistency test was also carried out to test the experimental vapour pressure data where it was found that all the data were thermodynamically consistent.

Two different methods were used for the regression of experimental VLE data: the combined and direct methods. The combined method made use of the second virial coefficient correlation of Tsonopoulos (1974) for the vapour phase non-ideality and the TK-Wilson, NRTL and modified UNIQUAC models for the liquid phase non-ideality. The direct method used the PR and SRK EoS with the temperature dependent function (α) of Mathias and Copeman (1983). On the whole, it was found that all the models of both the direct and combined method were able to describe the phase equilibrium measurements sufficiently well. However the NRTL model in the combined method was found to provide the best fit to most of the systems whilst the PR EoS in the direct method seemed to provide the best fit to most the systems as well. Overall, a comparison of the two methods suggested that the all systems were better described by the combined method.

Systems (e) to (h) above constituted as new experimental data and each was found to contain an azeotrope. For systems (e) and (f), pressure swing distillation was recommended to overcome the azeotrope whilst for systems (g) and (h) homogeneous or heterogeneous azeotropic distillation should be considered.

Experimental LLE data were carried out with the aid of high pressure nitrogen to enable sampling with the ROLSI^{TM}. The experimental LLE data measured were regressed with the TK-Wilson, NRTL and modified UNIQUAC liquid phase activity coefficient models. The regression revealed

that a second degree polynomial was sufficient to fit all the model parameters with a least squares deviation reasonably well.

A VLLE system (d) was also experimentally measured to demonstrate versatility of the apparatus. This data was regressed using the combined method with the same models as used for VLE. It was found that the experimental vapour compositions measured showed considerable deviations to that of the models. This was attributed to error in vapour composition measurements or that the models could not adequately describe the experimental data.

Thermodynamic consistency testing was also performed on all VLE data measured using the *point* and *direct tests*. Systems (e), (f) and (g) were found to show excellent thermodynamic consistency. However, systems (a) and (h) were found not to be strictly thermodynamically consistent as only one of the two conditions were met for both the *point* and *direct tests*.

Overall, the study was found to be highly successful. There are however some recommendations to modify the apparatus to enable low or very high pressure phase equilibrium measurements as well. These are further discussed in Chapter 9.

Ce chapitre présente les recommandations qui pourraient et devraient être mises en application afin d'améliorer la polyvalence et la mise en œuvre de l'appareil conçu et développé au cours de ce travail de thèse. Des modifications au ROLSI™ sont envisagées pour rendre efficace le prélèvement à basse pression et pour permettre l'échantillonnage des systèmes aqueux à haute température. Des modèles thermo-dynamiques plus complexes sont attendus pour régresser les données d'équilibres de phase de composés très polaires.

9

CHAPTER NINE

RECOMMENDATIONS

To further improve versatility and operation of the newly developed apparatus, the following recommendations should be considered:

1) The 6-port GC valve and ROLSI™ were successfully linked to the GC to enable sampling at low pressures. However, it was found that when the 6-port GC valve was "switched" to send the sample to the GC, a rather larger peak with a long tailing effect was observed. This could have been due to the change in pressure experienced when the 6-port GC valve was "switched". This should be further investigated by perhaps using a flame ionization detector instead of a thermal conductivity detector.

2) High pressure phase equilibrium systems could also be measured by simply replacing the pressure transmitter with a suitable one. Care however should be taken to thoroughly check the apparatus for pressure leaks.

3) The apparatus should be carefully maintained with regular checks done on the condition of the O-rings used and replaced when necessary or not compatible with the chemicals used. The apparatus must also be constantly checked for pressure leaks prior to operation.

4) Aqueous VLLE systems should be studied with the specialized polymer to consolidate that the newly developed apparatus is capable of undertaking experimental VLLE measurements.

5) The movement control of the ROLSI™ could be achieved with a stepper motor instead of manual operation.

6) More complex models can be used in regression to account for non-idealities, especially for VLLE systems. The use of a cubic equation of state to represent the vapour phase non-ideality in the combined method should be investigated.

7) VLE data from one or both homogeneous regions from VLLE data can be used to obtain activity coefficients. The activity coefficients can then be used to predict LLE data. One can also consider using the flexQUAC model which simultaneously regresses VLE and LLE data (Rarey, 2005).

8) A semi-theoretical approach should be considered to estimate the upper critical solution temperature for binary LLE data (José de Pablo and Prausnitz, 1988).

REFERENCES

Abbott, M. M., (1979), "Cubic Equations of State: An Interpretive Review", *Advances in Chemistry Series*, Vol. 182, pp. 47-70.

Abbott, M. M., (1986), "Low-Pressure Phase Equilibria: Measurement of VLE", *Fluid Phase Equilibria*, Vol. 29, pp. 193-207.

Abrams, D. S. and Prausnitz, J. M., (1975), "Statistical Thermodynamics of Liquid Mixtures: A New Expression for the Excess Gibbs Energy of Partly or Completely Miscible Systems", *American Institute of Chemical Engineers Journal*, Vol. 21(1), pp. 116-128.

Aim, K. and Ciprian, M., (1980), "Vapor Pressures, Refractive Index at 20.0 ^{o}C, and Vapor-Liquid Equilibrium at 101.325 kPa in the Methyl Tert-Butyl Ether - Methanol System", *Journal of Chemical and Engineering Data*, Vol. 25(2), pp. 100-103.

Aim, K., (1978), "Measurement of Vapor-Liquid Equilibrium in Systems with Components of Very Different Volatility by the Total Pressure Static Method", *Fluid Phase Equilibria*, Vol. 2(2), pp. 119-142.

Aizawa, T., Kanakubo, M., Ikushima, Y., Saitoh, N., Arai, K. and Smith Jr, R. L., (2004), ""Totsu"-Window Optical Cell for Absorption and Emission Studies of High Pressure Liquids and Supercritical Fluids", *Journal of Supercritical Fluids*, Vol. 29, pp. 313-317.

Anderko, A., (1990), "Equation-of-State Methods for the Modelling of Phase Equilibria", *Fluid Phase Equilibria*, Vol. 61(1-2), pp. 145-225.

Andersen, W. C., Sievers, R. E., Lagalante, A. F. and Bruno, T. J., (2001), "Solubilities of Cerium(IV), Terbium(III), and Iron(III) β-Diketonates in Supercritical Carbon Dioxide", *Journal of Chemical and Engineering Data*, Vol. 46(5), pp. 1045-1049.

Anderson, T. F. and Prausnitz, J. M., (1978), "Application of the UNIQUAC Equation to Calculation of Multicomponent Phase Equilibria. 1: Vapor-Liquid Equilibria; 2: Liquid-Liquid Equilibria", *Industrial and Engineering Chemistry. Process Design and Development*, Vol. 17(4), pp. 552-567.

Arce, A., Martínez-Ageitos, J. and Soto, A., (1996), "VLE Measurements of Binary Mixtures of Methanol, Ethanol, 2-Methoxy-2-methylpropane, and 2-Methoxy-2-methylbutane at 101.32 kPa", *Journal of Chemical and Engineering Data*, Vol. 41(4), pp. 718-723.

Arce, A., Martínez-Ageitos, J., Mendoza, J. and Soto, A., (1997), "Water + Ethanol + 2-Methoxy-2-Methylbutane: Properties of Mixing at 298.15 K and Isobaric Vapour-Liquid Equilibria at 101.32 kPa", *Fluid Phase Equilibria*, Vol. 141(1-2), pp. 207-220.

Arce, A., Martínez-Ageitos, J., Rodil, E. and Soto, A., (1998), "Isobaric (Vapour + Liquid) Equilibrium of (Ethanol + Methanol + 2-Methoxy-2-Methylbutane)", *Journal of Chemical Thermodynamics*, Vol. 30(11), pp. 1363-1372.

Ashcroft, S. J., Shearn, R. B. and Williams, G. J. J., (1983), "A Visual Equilibrium Cell for Multiphase Systems at Pressures up to 690 bar", *Chemical Engineering Research and Design*, Vol. 61(1), pp. 51-55.

Aspen Plus, (2004), "Physical Properties and Methods", Cambridge, MA: Aspen Technology Incorporation.

Baba-Ahmed, A., Guilbot, P. and Richon, D., "New Equipment using a Static Analytic Method for the Study of Vapour-Liquid Equilibria at Temperatures down to 77 K", *Fluid Phase Equilibria*, Vol. 166(2), pp. 225-236.

Bae, H.-K., Nagahama, K. and Hirata, M., (1981), "Measurement and Correlation of High Pressure Vapor-Liquid Equilibriums for the Systems Ethylene-1-Butene and Ethylene-Propylene", *Journal of Chemical Engineeering of Japan*, Vol. 14(1), pp. 1-6.

Bernabe, D., Romero-Martinez, A. and Trejo, A., (1988), "Liquid-Liquid Coexistence Curves for Binary Systems", *Fluid Phase Equilibria*, Vol. 40(3), pp. 279-288.

Besserer, G. J. and Robinson, D. B., (1971), "High-Pressure Autocollimating Refractometer for Determing Coexisting Liquid and Vapour Phase Densities", *Canadian Journal of Chemical Engineering*, Vol. 49(5), pp. 651-656.

Britton, E. C., Nutting, H. S. and Horsley, L. H., "Vapor-Liquid Equilibrium Diagrams of Alcohol-Ketone Azeotropes as a Function of Pressure", *Analytical Chemistry*, Vol. 19, pp. 601-602.

Brunner, G., Teich, J. and Dohrn, R., (1994), "Phase Equilibria in Systems Containing Hydrogen, Carbon Dioxide, Water and Hydrocarbons", *Fluid Phase Equilibria*, Vol. 100, pp. 253-268.

Cholinski, J., Szafranski, A and Wyrzykowska-Stankiewicz, D., (1986), "Computer Aided Second Virial Coefficient Data for Organic Individual Compounds and Binary Systems", PWN-Polish Scientific Publishers, Warsaw.

Christov, M. and Dohrn, R., "High-Pressure Fluid Phase Equilibria Experimental Methods and Systems Investigated (1994-1999)", *Fluid Phase Equilibria*, Vol. 202, pp. 153-218.

Coquelet, C. and Richon, D., (2009), "Experimental Determination of Phase Diagram and Modeling: Application to Refrigerant Mixtures", *International Journal of Refrigeration*, Vol. 32, pp. 1604-1614.

Corazza, M. L., Filho, L. C., Antunes, O. A. C. and Dariva, C., (2003), "High Pressure Phase Equilibria of the Related Substances in the Limonene Oxidation in Supercritical CO_2", *Journal of Chemical and Engineering Data*, Vol. 48(2), pp. 354-358.

da Cruz Francisco, J., Topgaard, D., Sivik, J. and Bergenståhl, B., (2004), "Phase Behavior of the System Lecithin-Water. The Effects of Addition of the Hydrocarbon 1, 8-Cineole and Supercritical Carbon Dioxide", *Journal of Supercritical Fluids*, Vol. 31(3), pp. 255-262.

Danesh, A. and Todd, A. A., (1990), "A Novel Sampling Method for Compositional Analysis of High Pressure Fluids", *Fluid Phase Equilibria*, Vol. 57(1-2), pp. 161-171.

Danner, R. P. and Gess, M. A., (1990), "A Data Base Standard for the Evaluation of Vapor-Liquid-Equilibrium Models", *Fluid Phase Equilibria*, Vol. 56, pp. 285-301.

Daubert, T. E., Sibul, H. M., Stebbins, C. and Kendall, R., (1990), "Policies and Procedures Documenting Compilation, Prediction, and Correlation for DIPPR Data Compilation Project", *American Institute of Chemical Engineers Symposium*, Vol. 86, pp. 62-92.

Doherty, M. F. and Caldarola, G. A., (1985), "Design and Synthesis of Homogeneous Azeotropic Distillations. 3. The Sequencing of Columns for Azeotropic and Extractive Distillations", *Industrial Engineering and Chemistry Fundamentals*, Vol. 24(4), pp. 474-485.

Dohrn, R., Bertakis, E., Behrend, O., Voutsas, E. and Tassios, D., (2007), "Melting Point Depression by using Supercritical CO_2 for a Novel Melt Dispersion Micronization Process", *Journal of Molecular Liquids*, Vol. 131-132, pp. 53-59.

Dohrn, R., Peper, S. and Fonseca, J. M. S., (2010), "High-Pressure Fluid-Phase Equilibria: Experimental Methods and Systems Investigated (2000-2004)", *Fluid Phase Equilibria*, Vol. 288, pp. 1-54.

Dortmund Data Bank, (2010), DDBST Software and Separation Technology GmbH, DDB Software Package Version 2010, Oldenburg.

Dymond, J. H. and Smith, E. B., (1980), "The Virial Coefficients of Gases and Gaseous Mixtures", Clarendon Press, Oxford.

Eduljee, G. H. and Tiwari, K. K., (1976), "Vapor-Liquid Equilibrium in Methanol + Methyl Ethyl Ketone and Methanol + Methyl Isobutyl Ketone at 760 mm Mercury", *Journal of Chemical Engineering of Japan*, Vol. 9(4), pp. 319-321.

Elliott, J. R. and Rainwater, J. C., (2000), "The Bancroft Point and Vapor-Liquid Equilibria in the System Benzene + Isopropanol", *Fluid Phase Equilibria*, Vol. 175(1-2), pp. 229-236.

Figuiere, P., Hom, J. F., Laugier, S., Renon, H., Richon, D. and Szwarc, H., (1980), "Vapor-Liquid Equilibriums up to 40000 kPa and 400 °C: A New Ststic Method", *American Institute of Chemical Engineers Journal*, Vol. 26(5), pp. 872-875.

Fischer, K. and Gmehling, J., (1994), "P-x and γ^{∞} Data for the Different Binary Butanol-Water Systems at 50 °C", *Journal of Chemical and Engineering Data*, Vol. 39, pp. 309-315.

Fontana, M. G. and Greene, N. D., (1967), "Corrosion Engineering", McGraw-Hill, USA.

Galicia-Luna, L. A., Ortega-Rodriguez, A. and Richon, D., (2000), "New Apparatus for the Fast

Determination of High-Pressure Vapor-Liquid Equilibria of Mixtures and of Accurate Critical Pressures", *Journal of Chemical and Engineering Data*, Vol. 45(2), 265-271.

Franceschi, E., Grings, M. B., Frizzo, C. D., Oliveira, J. V. and Dariva, C., (2004), "Phase Behavior of Lemon and Bergamot Peel Oils in Supercritical CO_2", *Fluid Phase Equilibria*, Vol. 226, pp. 1-8.

Garmroodi, A., Hassan, J. and Yamini, Y., (2004), "Solubilities of the Drugs Benzocaine, Metronidazole Benzoate, and Naproxen in Supercritical Carbon Dioxide", *Journal of Chemical and Engineering Data*, Vol. 49(3), pp. 709-712.

General Ruby and Sapphire Company, "Sapphire", available online from: http://www.generalruby.com/sapphire.html.

Gess, M. A., Danner, R. P. and Nagvekar, M., (1991), "Thermodynamic Analysis of Vapour-Liquid Equilibria: Recommended Models and a Standard Data Base", Design Institute for Physical Property Data, American Institute of Chemical Engineers.

Gibbs, R. E. and Van Ness, H. C., (1972), "Vapor-Liquid Equilibria from Total-Pressure Measurements. A New Apparatus", *Industrial and Engineering Chemistry Fundamentals*, Vol. 11(3), pp. 410-413.

Gmehling, J. and Onken, U., (1977-1982), "Vapor-Liquid Equilibrium Data Collection", DECHEMA Chemistry Data Series, Frankurt/Main.

Gómez-Nieto, M. and Thodos, G., (1978), "Vapor-Liquid Equilibrium Measurements for the Propane-Ethanol System at Elevated Pressures", *American Institue of Chemical Engineers Journal*, Vol. 24(4), pp. 672-678.

Guilbot, P., Valtz, A., Legendre, H. and Richon D., (2000), "Rapid On-Line Sampler-Injector: A Reliable Tool for HT-HP Sampling and On-Line GC Analysis", *Analusis*, Vol. 28(5), pp. 426-431.

Guillevic, J. L., Richon, D. and Renon, H., (1983), "Vapor-Liquid Equilibrium Measurements up to 558 K and 7 Mpa: A New Apparatus", *Industrial & Engineering Chemistry Fundamentals*, Vol. 22(4), pp. 495-499.

Hála, E ., P ick, J ., F ried, V . a nd Villim, O ., (1967), "Vapour-Liquid E quilibrium", 2nd e dition, Pergamon Press, Oxford.

Hayden, J . D . a nd O 'Connell, J. P ., (1975), "Generalized M ethod f or P redicting S econd Virial Coefficients", *Industrial and Engineering Chemistry. Process Design and Development*, Vol. 14(3), pp. 209-216.

Hellwig, L . R . a nd V an Winkle, M ., (1953), "Vapor-Liquid E quilibria f or E thyl A lcohol B inary Systems", *Journal of Industrial and Engineering Chemistry*, Vol. 45(3), pp. 624-629.

Herington, E. F. G., (1947), "A Thermodynamic Test for the Internal Consistency of Experimental Data on Volatility Ratios", *Nature*, Vol. 160, pp. 610-611.

Hernández-Garduza, O ., G arcía-Sánchez, F . a nd N eau, E ., (2001), "Generalization of C omposition-Dependent Mixing Rules for Multicomponent Systems: Prediction of Vapour-Liquid and Liquid-Liquid Equilibria", *Chemical Engineering Journal*, Vol. 84(3), pp. 283-294.

Higashiuchi, H ., S akuragi, Y ., I wai, Y ., A rai, Y . and N agatani, M ., (1987), "Measurement a nd Correlation o f L iquid-Liquid E quilibria of B inary a nd T ernary S ystems C ontaining M ethanol a nd Hydrocarbons", *Fluid Phase Equilibria*, Vol. 36, pp. 35-47.

Hill, W. D . a nd Van W inkle, M ., (1952), "Vapor-Liquid E quilibria in M ethanol B inary S ystems. I. Methanol - Propanol, M ethanol - Butanol, a nd M ethanol - Pentanol. I I. M ethanol - Methyl E thyl Ketone, Methanol - Methyl Propyl Ketone, Methanol - Methyl Isobutyl K etone", *Journal of Industrial and Engineering Chemistry*, Vol. 44, pp. 205-210.

Hodges, M . a nd K etley, G ., (2003), "Components f or B lending of T ransportation F uels", P atent Cooperation Treaty International Application, World Intellectual Property Organization.

Holldorff, H. and Knapp, H., (1988), "Vapor Pressures of n-Butane, Dimethyl Ether, Methyl Chloride, Methanol a nd the V apor-Liquid E quilibrium of D imethyl E ther - Methanol: E xperimental A pparatus, Results and Data Reduction", *Fluid Phase Equilibria*, Vol. 40(1-2), pp. 113-125.

Horstmann, S ., Jabloniec, A ., K rafczyk, J ., F ischer, K . a nd G mehling, J ., (2005), "PSRK G roup

Contribution Equation of State: Comprehensive Revision and Extension IV, including Critical Constants and α-function Parameters for 1000 Components", *Fluid Phase Equilibria*, Vol. 227(2), pp. 157-164.

Huang, S. S.-S., Leu, A.-D., Ng, H.-J. and Robinson, D. B., (1985), "The Phase Behavior of Two Mixtures of Methane, Carbon Dioxide, Hydrogen Sulfide, and Water", *Fluid Phase Equilibria*, Vol. 19(1-2), pp. 21-32.

Ignatius, J., Jaervelin, H. and Lindqvist, P., (1995), "Use TAME and Heavier Ethers to Improve Gasoline Properties", *Hydrocarbon Processing, International Edition*, Vol. 74(2), pp. 51-53.

José de Pablo, J. and Prausnitz, J. M., (1988), "Thermodynamics of Liquid-Liquid Equilibria Including the Critical Region", *American Institute of Chemical Engineers Journal*, Vol. 34(10), pp. 1595-1606.

Kaiser, T., Voßmerbaumer, C. and Schweiger, G., (1992), "A New Approach to the Determination of Fluid Phase Equilibria: Concentration Measurements by Raman Spectroscopy", *Berichte der Bunsengesellschaft für Physikalische Chemie*, Vol. 96(8), pp. 976-980.

Kalra, H. and Robinson, D. B., (1975), "Apparatus for the Simultaneous Measurement of Equilibrium Phase Composition and Refractive Index data at low Temperatures and High Pressures", *Cryogenics*, Vol. 15(7), pp. 409-412.

Kalra, H., Kubota, H., Robinson, D. B. and Ng, H.-J., (1978), "Equilibrium Phase Properties of the Carbon Dioxide-n-Heptane System", *Journal of Chemical and Engineering Data*, Vol. 23(4), pp. 317-321.

Kang, J. W., Lee. J. H., Yoo, K.-P. and Lee, C. S., (2002), "Evaluation of Equations of State Applicable to Polymers and Complex Systems", *Fluid Phase Equilibria*, Vol. 194-197, pp. 77-86.

Katayama, H. and Ichikawa, M.-A., (1995), "Liquid-Liquid Equilibria of Three Ternary Systems: Methanol - Heptane including 1,3-Dioxolane, 1,4-Dioxane and Tetrahydropyran in the Range of 253.15 to 303.15 K", *Journal of Chemical Engineering of Japan*, Vol. 28(4), pp. 412-418.

Katayama, T., Ohgaki, K., Maekawa, G., Goto, M. and Nagano, T., (1975), "Isothermal Vapor-Liquid

Equilibriums of Acetone-Carbon Dioxide and Methanol-Carbon Dioxide Systems at High Pressures", *Journal of Chemical Engineering of Japan*, Vol. 8(2), pp. 89-92.

Klink, A. E., Cheh, H. Y. and Amick, E. H. Jr., (1975), "The Vapor-Liquid Equilibrium of the Hydrogen-Butane System at Elevated Pressures", *American Institute of Chemical Engineers*, Vol. 21(6), pp. 1142-1148.

Knapp, J. P. and Doherty, M. F., (1992), "A New Pressure-Swing-Distillation Process for Separating Homogeneous Azeotropic Mixtures", *Industrial and Engineering Chemistry Research*, Vol. 31(1), pp. 346-357.

Kolbe, B. and Gmehling, J., (1985), "Thermodynamic Properties of Ethanol + Water. I. Vapour-Liquid Equilibria Measurements from 90 to 150 ^{o}C by the Static Method", *Fluid Phase Equilibria*, Vol. 23, pp. 213-226.

Konrad, R., Swaid, I. and Schneider, G. M., (1983), "High-Pressure Phase Studies on Fluid Mixtures of Low-Volatile Organic Substances with Supercritical Carbon Dioxide", *Fluid Phase Equilibria*, Vol. 10(2-3), pp. 307-314.

Lagarias, J. C., Reeds, J. A., Wright, M. H. and Wright, P. E., (1998), "Convergence Properties of the Nelder-Mead Simplex Method in Low Dimensions", *SIAM Journal of Optimization*, Vol. 9(1), pp112-147.

Laugier, S. and Richon, D., (1986), "New Apparatus to Perform Fast Determinations of Mixture Vapor-Liquid Equilibria up to 10 MPa and 423 K", *Review of Scientific Instruments*, Vol. 57(3), pp. 469-472.

Lauret, A., Richon, D. and Renon, H., (1994), "Measurements of Physical and Thermodynamic Properties of Products Obtained Through Direct Coal Liquefaction", *International Journal of Energy Research*, Vol. 18(2), pp. 267-275.

Laursen, T., Rasmussen, P. and Andersen, S. I., (2002), "VLE and VLLE Measurements of Dimethyl Ether Containing Systems", *Journal of Chemical and Engineering Data*, Vol. 47(2), pp. 198-202.

Lee, J.-D., Lee, T.-J. and Park, S.-J., (1995), "Infinite Dilution Activity Coefficients and Vapor-Liquid

Equilibria for the Binary Systems Containing MTBE", *Hwahak Konghak*, Vol. 33(5), pp. 527-534.

Lee, M.-J., Hsiao, C.-C. and Lin, H.-M., (1997), "Isothermal Vapor-Liquid Equilibria for Mixtures of Methyl Tert-Butyl Ether, Methyl Acetate, and Ethyl Acetate", *Fluid Phase Equilibria*, Vol. 137(1-2), pp. 193-207.

Legret, D., Richon, D. and Renon, H., (1980), "Static Still for Measuring Vapor-Liquid Equilibriums up to 50 bar", *Industrial & Engineering Chemistry Fundamentals*, Vol. 19(1), pp. 122-126.

Legret, D., Richon, D. and Renon, H., (1981), "Vapor Liquid Equilibria up to 100 MPa: A New Apparatus", *American Institute of Chemical Engineers Journal*, Vol. 27(2), pp. 203-207.

Maher, P. J. and Smith, B. D., (1979), "A New Total Pressure Vapor-Liquid Equilibrium Apparatus. The Ethanol + Aniline System at 313.15, 350.81, and 386.67 K", *Journal of Chemical and Engineering Data*, Vol. 24(1), pp. 16-22.

Malanowski, S., (1982), "Experimental Methods for Vapour-Liquid Equilibria. Part I. Circulation Methods", *Fluid Phase Equilibria*, Vol. 8, pp. 197-219.

Malanowski, S. and Anderko, A., (1992), *Modelling Phase Equilibria: Thermodynamic Background and Practical Tools*, John Wiley and Sons Inc., New York.

Marquardt, D. W., (1963), "An Algorithm for Least-Squares Estimation of Non-Linear Parameters", *Journal of the Society of Industrial and Applied Mathematics*, Vol., 11, pp. 431-441.

Martin, J. J., (1979), "Cubic Equations of State – Which?", *Industrial and Engineering Chemistry Fundamentals*, Vol. 18(2), pp. 81-97.

Martínez, N. F., Lladosa, E., Burguet, M. and Montón, J. B., (2008), "Isobaric Vapour-Liquid Equilibria for Binary Systems of 2-Butanone with Ethanol, 1-Propanol, and 2-Propanol at 20 and 101.3 kPa", *Fluid Phase Equilibria*, Vol. 270, pp. 62-68.

Mathias, P. M. and Copeman, T. W., (1983), "Extension of the Peng-Robinson Equation of State to Complex Mixtures: Evaluation of the Various Forms of the Local Composition Concept", *Fluid Phase Equilibria*, Vol. 13, pp. 91-108.

Matos, H. A., Gomes de Azevedo, E., Simoes, P. C., Carrondo, M. T. and Nunes de Ponte, M., (1989), "Phase Equilibria of Natural Flavors and Supercritical Solvents", *Fluid Phase Equilibria*, Vol. 52, pp. 357-364.

Matsuda, H., Kurihara, K., Ochi, K. and Kojima, K., (2002), "Prediction of Liquid-Liquid Equilibria at High Pressure for Binary Systems using EOS-G^E Models: Methanol + Hydrocarbon Systems", *Fluid Phase Equilibria*, Vol. 203(1-2), pp. 269-284.

McBee, E. T. and Christman, D. L., (1955), "Infrared Spectra of Halogenated Acetic Esters", *Journal of the American Chemical Society*, Vol. 77, pp. 755-756.

Michelsen, M. L. and Kistenmacher, H., (1990), "On Composition-Dependent Interaction Coefficients", *Fluid Phase Equilibria*, Vol. 58(1-2), pp. 229-230.

Mühlbauer, A. L. and Raal, J. D., (1991), "Measurements and Thermodynamic Interpretation of High-Pressure Vapor-Liquid Equilibria in the Toluene-Carbon Dioxide System", *Fluid Phase Equilibria*, Vol. 64, pp. 213-236.

Mühlbauer, A. L., (1990), PhD Dissertation: *Measurement and Thermodynamic Interpretation of High Pressure Vapour-Liquid Equilibrium Data*, University of Natal, Durban, South Africa.

Naidoo, P., (2004), PhD Dissertation: *High-Pressure Vapor-Liquid Equilibrium Studies*, University of KwaZulu Natal, Durban, South Africa.

Nakayama, T., Sagara, H., Arai, K. and Saito, S., (1987), "High Pressure Liquid-Liquid Equilibria for the System of Water, Ethanol and 1,1-Difluoroethane at 323.2 K", *Fluid Phase Equilibria*, Vol. 38(1-2), pp. 109-127.

Nasir, P., Martin, R. J. and Kobayashi, R., (1981), "A Novel Apparatus for the Measurement of the Phase and Volumetric Behavior at High Temperatures and Pressures and its Application to Study VLE in the Hydrogen-Tetralin System", *Fluid Phase Equilibria*, Vol. 5(3-4), pp. 279-288.

Ng, H.-J. and Robinson, D. B., (1978), "Equilibrium Phase Properties of the Toluene-Carbon Dioxide System", *Journal of Chemical and Engineering Data*, Vol. 23(4), pp. 325-327.

Ng, H. -J., Robinson, D. B. and Leu, A.-D., (1985), "Critical Phenomena in a Mixture of Methane, Carbon Dioxide and Hydrogen Sulfide", *Fluid Phase Equilibria*, Vol. 19(3), pp. 273-286.

Novák, J. P., Matouš, J. and Pick, J., (1987), "Liquid-Liquid Equilibria", Elsevier, Amsterdam.

Ohta, T., Koyabu, J. and Nagata, I., (1981), "Vapor-Liquid Equilibriums for the Ternary Ethanol-2-Butanone-Benzene System at 298.15 K", *Fluid Phase Equilibria*, Vol. 7(1), pp. 65-73.

Ohta, T., Todoriki, H. and Yamada, T., (2004), "Representation of Liquid-Liquid Equilibria at Low and High Pressures using EOS-G^E Mixing Rules", *Fluid Phase Equilibria*, Vol. 225(1-2), pp. 23-27.

Outcalt, S. L. and Lee, B.-C., (2004), "A Small-Volume Apparatus for the Measurement of Phase Equilibria", *Journal of Research of the National Institute of Standards and Technology*, Vol. 109, pp. 525-531.

Park, S. -J., Han, K.-J. and Gmehling, J., (2007), "Isothermal Phase Equilibria and Excess Molar Enthalpies for Binary Systems with Dimethyl Ether at 323. 15 K", *Journal of Chemical and Engineering Data*, Vol. 52(5), pp. 1814-1818.

Peng, C., Liu, H. and Hu, Y., (2002), "Liquid-Liquid Equilibria of Copolymer Mixtures based on an Equation of State", *Fluid Phase Equilibria*, Vol. 201(1), pp. 19-35.

Peng, D. Y. and Robinson, D. B., (1976), "A New Two Constant Equation of State", *Industrial and Engineering Chemistry Fundamentals*, Vol. 15(1), pp. 59-64.

Perry, R. H. and Green, D. W., (1998), "Perry's Chemical Engineers' Handbook", 7th edition, McGraw-Hill, New York.

Power Chemical Corporation, "Silicone Oil", available online from: http://www.powerchemical.net/library/Silicone_Oil.pdf

Prausnitz, J. M., Anderson, T. F., Grens, E. A., Eckert, C. A., Hseih, R. and O'Connell, J. P., (1980), "Computer Calculations for Multicomponent Vapour-Liquid and Liquid-Liquid Equilibria", Prentice-Hall, Englewood Cliffs, New Jersey.

Prausnitz, J. M., Lichtenthaler, R. N. and de Azevedo, E. G., (1999), "Molecular Thermodynamics of Fluid-Phase Equilibria", 3rd edition, Prentice-Hall, Upper Saddle River, New Jersey.

Privott, W. J., Paul, D. R., Jolls, K. R. and Schoenborn, E. M., (1966), "Vapor-Liquid Equilibriums of Methanol-Methyl Ethyl Ketone in the Presence of Diethyl Ketone", *Journal of Chemical and Engineering Data*, Vol. 11(3), pp. 331-333.

Professional Plastics, "Techtron® HVP - Bearing Grade PPS. Features and Benefits", available online from: http://www.professionalplastics.com

Raal, J. D. and Mühlbauer, A. L., (1998), "Phase Equilibria: Measurement and Computation", Taylor and Francis, Bristol, PA.

Rackett, H. G., (1970), "Equation of State for Saturated Liquids", *Journal of Chemical and Engineering Data*, Vol. 15(4), pp. 514-517.

Ramjugernath, D., (2000), PhD Dissertation: *High Pressure Phase Equilibrium Studies*, University of Natal, Durban, South Africa.

Rarey, J., (2005), "Extended Flexibility for G^E Models and Simultaneous Description of Vapor-Liquid Equilibrium and Liquid-Liquid Equilibrium using a Nonlinear Transformation of the Concentration Dependence", *Industrial and Engineering Chemistry Research*, Vol. 44, pp. 7600-7608.

Rarey, J. R. and Gmehling, J., (1993), "Computer-Operated Differential Static Apparatus for the Measurement of Vapor-Liquid Equilibrium Data", *Fluid Phase Equilibria*, Vol. 83, pp. 279-287.

Redlich, O. and Kister, A. T., (1948), "Thermodynamics of Nonelectrolyte Solutions. Algebraic Representation of Thermodynamic Properties and the Classification of Solutions", *Journal of Industrial and Engineering Chemistry*, Vol. 40, pp. 345-348.

Redlich, O. and Kwong, J. N. S., (1949), "On the Thermodynamics of Solutions. V. An Equation of State. Fugacities of Gaseous Solutions", *Chemical Reviews*, Vol. 44, pp. 233-244.

Reid, R. C., Prausnitz, J. M. and Poling, B. E., (1988), "The Properties of Gases and Liquids", 4th

edition, McGraw-Hill, New York.

Reiff, W. E., Peters-Gerth, P. and Lucas, K., (1987), "A Static Equilibrium Apparatus for (Vapor + Liquid) Equilibrium Measurements at High Temperatures and Pressures. Results for (Methane + n-Pentane)", *Journal of Chemical Thermodynamics*, Vol. 19(5), pp. 467-477.

Renon, H. and Prausnitz, J. M., (1968), "Local Compositions in Thermodynamic Excess Functions for Liquid Mixtures", *American Institute of Chemical Engineers Journal*, Vol. 14(1), pp. 135-144.

Richon, D., (2003), "New Measurements for Phase Equilibria and PVT Determinations in a Large Range of Pressures (0 to 100 Mpa) and Temperatures (0 to 770 K)", *Proceedings of the South African Chemical Engineering Congress*, 3-5 September 2003, Sun City, South Africa.

Rigas, T. J., Mason, D. F. and Thodos, G., (1958), "Vapor-Liquid Equilibrium. Microsampling Technique applied to a New Variable-Volume Cell", *Journal of Industrial and Engineering Chemistry*, Vol. 50, pp. 1297-1300.

Robinson, C. S. and Gilliland, E. R., (1950), "Elements of Fractional Distillation", 4th edition, McGraw-Hill, New York.

Rogers, B. L. and Prausnitz, J. M., (1970), "Sample-Extrusion for High-Pressure Vapor-Liquid Equilibria. Compositions and densities at pressures up to the critical", *Industrial & Engineering Chemistry Fundamentals*, Vol. 9(1), pp. 174-177.

ROLSI™ Evolution IV, "New ROLSI™ Electromagnetic Model Rapid On Line Sampler Injector", available online from: http://www.rolsi.com/English.htm.

Rowlinson, J. S., (1969), "Liquids and Liquid Mixtures", 2nd edition, Plenum Press, New York.

Schmitt, C. G. and Boord, C. E., (1932), "Nuclear Synthesis in the Olefin Series. III. Hexenes", *Journal of the American Chemical Society*, Vol. 54, pp. 751-761.

Schneider, G. M., (1998), "High-Pressure Investigations of Fluid Mixtures - Review and Recent Results", *Journal of Supercritical Fluids*, Vol. 13, pp. 5-14.

Scott, R . L ., (1956), "Corresponding-States Treatment o f N onelectrolyte S olutions", *Journal o f Chemical Physics*, Vol. 25, pp. 193-205.

Seader, J. D . a nd H enley, E . J ., (1998), "Separation P rocess P rinciples", John W iley & S ons, Incorporation, New York.

Secuianu, C., Feroiu, V. and Geana, D., (2003), "High-Pressure Vapor-Liquid Equilibria in the System Carbon Dioxide and 2-Propanol at Temperatures from 293.25 K to 323.15 K", *Journal of Chemical and Engineering Data*, Vol. 48(6), pp. 1384-1386.

Shieh, Y .-T., Liu, K .-H. and Lin, T .-L., (2004), " Effect o f S upercritical C O_2 on M orphology o f Compatible Crystalline/Amorphous PEO/PMMA blends", *Journal of Supercritical Fluids*, Vol. 28, pp. 101-112.

Sinnott, R . K., (2005), "Coulson and R ichardson's C hemical E ngineering V olume 6: C hemical Engineering Design", 4th edition, Butterworth-Heinemann, Oxford.

Slumpys, "Fiberfrax Durablanket Description", available online from: http://www.slumpys.com

Smith, J . M ., V an Ness, H . C. and Abbott, M . M ., (2001), "Introduction t o Chemical E ngineering Thermodynamics", 6th edition, McGraw-Hill, New York.

Soave, G., (1972), "Equilibrium Constants from a Modified Redlich-Kwong Equation of State", *Chemical Engineering Science*, Vol. 27(6), pp. 1197-1203.

Soave, G., (1993), "Improving the Treatment of Heavy Hydrocarbons by the SRK EOS", *Fluid Phase Equilibria*, Vol. 84, pp. 339-342.

Sørensen, J. M., Magnussen, T., R asmussen, P . a nd F redenslund, A ., (1979), "Liquid-Liquid Equilibrium D ata: Their Retrieval, C orrelation a nd P rediction, P art I : R etrieval", *Fluid P hase Equilibria*, Vol. 2(4), pp. 297-309.

Sørensen, J . M ., M agnussen, T ., Rasmussen, P . a nd F redenslund, A ., (1979), "Liquid-Liquid Equilibrium D ata: Their Retrieval, C orrelation a nd P rediction, P art I I: C orrelation", *Fluid P hase Equilibria*, Vol. 3(1), pp. 47-82.

Sørensen, J. M., Magnussen, T., Rasmussen, P. and Fredenslund, A., (1979), "Liquid-Liquid Equilibrium Data: Their Retrieval, Correlation and Prediction, Part III: Prediction", *Fluid Phase Equilibria*, Vol. 4(1-2), pp. 151-163.

Staby, A. and Mollerup, J., (1991), "Measurement of Solubilities of 1-Pentanol in Supercritical Ethene", *Journal of Supercritical Fluids*, Vol. 4(4), pp. 233-237.

Sugi, H. and Katayama, T., (1978), "Ternary Liquid-Liquid and Miscible Binary Vapor-Liquid Equilibrium Data for the Two Systems n-Hexane - Ethanol - Acetonitrile and Water - Acetonitrile - Ethyl Acetate", *Journal of Chemical Engineering of Japan*, Vol. 11(3), pp. 167-172.

Takagi, T., Fugita, K., Furuta, D. and Tsuji, T., (2003), "Bubble Point Pressure for Binary Mixtures of Propane and Pentafluoroethane", *Fluid Phase Equilibria*, Vol. 212, pp. 279-283.

Tarakad, R. R. and Danner, R. P., (1977), "An Improved Corresponding States Method for Polar Fluids: Correlation of Second Virial Coefficients", *American Institute of Chemical Engineers Journal*, Vol. 23(5), pp. 685-695.

Taylor, B. N., Mohr, P. J. and Douma, M., (2007), "The NIST Reference on Constants, Units, and Uncertainty", available online from: www.physics.nist.gov/cuu/index.html

Treybal, R. E., (1963), "Liquid Extraction", 2nd edition, McGraw-Hill, USA.

Tsonopoulos, C., (1974), "An Empirical Correlation of Second Virial Coefficients", *American Institute of Chemical Engineers Journal*, Vol. 20(2), pp. 263-272.

Tsuboka, T. and Katayama, T., (1975), "Modified Wilson Equation for Vapor-Liquid and Liquid-Liquid Equilibriums", *Journal of Chemical Engineering of Japan*, Vol. 8(3), pp. 181-187.

Twu, C. H. and Coon, J. E., (1996), "CEOS/AE Mixing Rules Constrained by vdW Mixing Rule and Second Virial Coefficient", *American Institute of Chemical Engineers Journal*, Vol. 42(11), pp. 3212-3222.

Twu, C. H., Bluck, D., Cunningham, J. R. and Coon, J. E., (1991), "A Cubic Equation of State with a

New Alpha Function and a New Mixing Rule", *Fluid Phase Equilibria*, Vol. 69, pp. 33-50.

Valderrama, J. O., (2003), "The State of the Cubic Equations of State", *Industrial and Engineering Chemistry Research*, Vol. 42(8), pp. 1603-1618.

Valtz, A., Coquelet, C., Baba-Ahmed, A. and Richon, D., (2002), "Vapor-Liquid Equilibrium data for the Propane + 1,1,1,2,3,3,3-heptafluoropropane (R227ea) system at temperatures from 293.16 to 353.18 K and Pressures up to 3.4 Mpa", *Fluid Phase Equilibrium*, Vol. 202(1), pp. 29-47.

Van der Waals, J. D., (1873), "Over de Continuitet van den Gas - en Vloeistoftoestand", Doctoral Dissertation, Leiden, as given by Anderko (1990).

Van Laar, J. J., (1910), "The Vapor Pressure of Binary Mixtures", *Zeitschrift feur Physik Chemie*, Vol. 72, pp. 723-751.

Van Ness, H. C. and Abbott, M. M., (1978), "A Procedure for Rapid Degassing of Liquids", *Industrial & Engineering Chemistry Fundamentals*, Vol. 17(1), pp. 66-67.

Van Ness, H. C. and Abbott, M. M., (1982), "Classical Thermodynamics of Nonelectrolyte Solutions: With Applications to Phase Equilibria", McGraw Hill, New York.

Van Ness, H. C., (1959), "Exact Forms of the Unrestricted Gibbs-Duhem Equation", *Chemical Engineering Science*, Vol. 10, pp. 225-228.

Van Ness, H. C., (1995), "Thermodynamics in the Treatment of Vapor/Liquid Equilibrium (VLE) Data", *Pure and Applied Chemistry*, Vol. 67(6), pp. 859-872.

Van Ness, H. C., Byer, S. M. and Gibbs, R. E., (1973), "Vapor-Liquid Equilibrium: Part I. An Appraisal of Data Reduction Methods", *American Institute of Chemical Engineers Journal*, Vol. 19(2), pp. 238-244.

Vetere, A., (2000), "A Simple Modification of the NRTL Equation", *Fluid Phase Equilibria*, Vol. 173, pp. 57-64.

Wagner, Z. and Wichterle, I., (1987), "High-Pressure Vapor-Liquid Equilibrium in Systems Containing Carbon Dioxide, 1-Hexene, and n-Hexane", *Fluid Phase Equilibria*, Vol. 33(1-2), pp. 109-123.

Walas, S. M., (1985), "Phase Equilibrium in Chemical Engineering", Butterworth, Boston.

Weast, R. C., Astle, M. J. and Beyer, W. H., (1984), "Handbook of Chemistry and Physics", 64th edition, CRC Press: Boca Raton, FL.

Wen, C.-C. and Tu, C.-H., (2007), "Vapor-Liquid Equilibria for Binary and Ternary Mixtures of Ethanol, 2-Butanone, and 2,2,4-Trimethylpentane at 101.3 kPa", *Fluid Phase Equilibria*, Vol. 258, pp. 131-139.

Wichterle, I. and Boublíková, L., (1969), "Semi-micromethod for Determination of Partial Pressures of Solutions", *Industrial and Engineering Chemistry Fundamentals*, Vol. 8(3), pp. 585-588.

Wichterle, I. and Hála, E., (1963), "Communication. Semi-micro Determination of Vapor-Liquid Equilibrium", *Industrial and Engineering Chemistry Fundamentals*, Vol. 2(2), pp. 155-157.

Wilson, G. M., (1964), Vapor-Liquid Equilibrium. XI. A New Expression for the Excess Free Energy of Mixing", *Journal of the American Chemical Society*, Vol. 86(2), pp. 127-130.

Wong, D. S. H. and Sandler, S. I., (1992), "A Theoretically Correct Mixing Rule for Cubic Equations of State", *American Institute of Chemical Engineers Journal*, Vol. 38(5), pp. 671-680.

Wu, X., Du, X. and Zheng, D., (2010), "Measurement of Vapor-Liquid Equilibrium for the DME + Diisopropyl Ether Binary System and Correlation for the DME + CO_2 + Diisopropyl Ether Ternary System", *International Journal of Thermophysics*, Vol. 31(2), pp. 308-315.

Zabaloy, M. S., Gros, H. P., Bottini, S. B. and Brignole, E. A., (1994), "Isohermal Vapor-Liquid Equilibrium Data for the Binaries Isobutane-Ethanol, Isobutane-1-Propanol, and Propane-Ethanol", *Journal of Chemical and Engineering Data*, Vol. 39(2), pp. 214-218.

Zimmermann, A. and Keller, J. U., (1989), "Vapor-Liquid Equilibrium in the System Water-Ammonia-Lithium Bromide", *Fluid Phase Equilibria*, Vol. 53, pp. 229-234.

Appendix A

Criterion For Phase Equilibrium

For any closed system, the temperature and pressure are related to the Gibbs energy using primary thermodynamic properties and the definition of the Gibbs energy:

$$d(nG) = (nV)dP - (nS)dT \tag{A-1}$$

Application of Equation (A-1) to a single-phase fluid, i n which there is no chemical reaction, implies that the composition of such a system is constant. This leads to the following deductions:

$$\left[\frac{\partial(nG)}{\partial P}\right]_{T,n} = nV \tag{A-2}$$

$$\left[\frac{\partial(nG)}{\partial T}\right]_{P,n} = -nS \tag{A-3}$$

where n is the number o f moles of all chemical species in t he system. The subscripts signify properties that are held constant.

With regards to an open system, the surroundings can interchange matter with the system. However, the Gibbs energy is still a function of temperature and pressure but also becomes a function of the number of moles of a specific chemical species in the system (n_i). Hence:

$$nG = g(P, T, n_i) \tag{A-4}$$

The total differential of Equation (A-4) yields:

$$d(nG) = (nV)dP - (nS)dT + \sum_i \mu_i dn_i \tag{A-5}$$

and

$$\mu_i = \left[\frac{\partial(nG)}{\partial n_i}\right]_{P,T,n_j} \tag{A-6}$$

where μ_i is known as the chemical potential of species *i* in the mixture.

Now when two phases (say α and β) are in equilibrium in an overall closed system, each phase can be considered an open system that is free to transfer mass with each other. If one assumes the equilibrium temperature and pressure to be uniform throughout the closed system, Equation (A-5) can be used to express each phase:

$$d(nG)^{\alpha} = (nV)^{\alpha} dP - (nS)^{\alpha} dT + \sum_i \mu_i^{\alpha} dn_i^{\alpha} \tag{A-7}$$

$$d(nG)^{\beta} = (nV)^{\beta} dP - (nS)^{\beta} dT + \sum_i \mu_i^{\beta} dn_i^{\beta} \tag{A-8}$$

The sum of Equations (A-7) and (A-8) gives the change in the total Gibbs energy for this system. The total system property can be expressed by the following relation:

$$nM = (nM)^{\alpha} + (nM)^{\beta} \tag{A-9}$$

where *M* represents any extensive thermodynamic property. Application of Equation (A-9) shows:

$$d(nG) = (nV)dP - (nS)dT + \sum_i \mu_i^{\alpha} dn_i^{\alpha} + \sum_i \mu_i^{\beta} dn_i^{\beta} \tag{A-10}$$

Since the system is a closed system, Equation (A-1) is applicable. A comparison of Equation (A-1) and (A-10) at equilibrium reveals that:

$$\sum_i \mu_i^{\alpha} dn_i^{\alpha} + \sum_i \mu_i^{\beta} dn_i^{\beta} = 0 \tag{A-11}$$

The terms dn_i^{α} and dn_i^{β} represent changes and result from the mass transfer between the two phases. For a non-reactive system, the law of mass conservation requires that $dn_i^{\alpha} = -dn_i^{\beta}$. Hence Equation (A-11) becomes:

$$\sum_i \left(\mu_i^{\alpha} - \mu_i^{\beta}\right) dn_i^{\alpha} = 0 \tag{A-12}$$

Since the changes dn_i^{α} are independent and arbitrary, the only way that Equation (A-12) can in general be zero is when each term in parentheses is separately equated to zero:

$$\mu_i^{\alpha} = \mu_i^{\beta} \tag{A-13}$$

Equation (A-13) can be generalized to include more than two phases by successively considering pairs of phases. In the case of a closed system consisting N chemical species and π phases at the same temperature and pressure, the general result is:

$$\mu_i^{\alpha} = \mu_i^{\beta} = \ldots = \mu_i^{\pi} \tag{A-14}$$

where $i = 1, 2, \ldots, N$.

Hence the criterion for phase equilibrium of a system consisting of multiple phases at the same temperature and pressure is achieved when the chemical potential of each species is the same in all phases (Smith et al, 2001).

Appendix B

Pure Component Properties

The critical properties and the UNIQUAC pure component constants for all the chemicals used in this study were taken the Dortmund Data Bank (2009).

Table B-1: Physical properties of chemicals used in this study.

Chemical	T_c / K	P_c / kPa	V_c / $cm^3.mol^{-1}$	ω
2-methoxy-2-methylbutane	534.0	3113.72	377	0.3103
2-methoxy-2-methylpropane	497.1	3434.92	319	0.2670
2-methylpent-2-ene	518.0	3282.93	351	0.2290
acetonitrile	548.0	4833.20	173	0.3210
butan-2-one	535.6	4154.33	267	0.3290
ethanol	516.2	6383.48	167	0.6350
ethyl acetate	523.3	3830.09	286	0.3630
heptane	540.3	2733.75	432	0.3457
hexane	507.4	3014.42	370	0.2975
methanol	512.6	8084.00	118	0.5590

Table B-2: Pure component constants for the modified UNIQUAC model.

Chemical	r	q	q'
2-methoxy-2-methylbutane	4.7422	4.172	4.172
2-methoxy-2-methylpropane	4.0678	3.632	3.632
2-methylpent-2-ene	4.2663	3.760	3.760
acetonitrile	1.8701	1.724	1.724
butan-2-one	3.2479	2.876	2.876
ethanol	2.1055	1.972	0.920
ethyl acetate	3.4786	3.116	3.116
heptane	5.1742	4.396	4.396
hexane	4.4998	3.856	3.856
methanol	1.4311	1.432	1.432

Appendix C

C.1 Temperature Calibrations

Table C-1: Calibration results for temperature probes/sensors used in this study.

Probe/Sensor Description	Calibration Equation	Temperature Range	Calibration Uncertainty ΔT / K
Equilibrium cell upper 316 SS flange	$T_{actual} = 0.9941 T_{display} + 0.5649$	298 to 355 K	0.02
	$T_{actual} = 0.9969 T_{display} - 0.3778$	354 to 465 K	0.05
Equilibrium cell lower 316 SS flange	$T_{actual} = 0.9941 T_{display} + 0.5385$	298 to 355 K	0.02
	$T_{actual} = 0.9975 T_{display} - 0.5801$	354 to 465 K	0.05
Temperature control upper 316 SS flange	$T_{actual} = 0.9972 T_{display} - 0.3068$	303 to 465 K	0.04
Low pressure transmitter aluminum block	$T_{actual} = 0.9955 T_{display} - 2.3180$	298 to 371 K	0.02
Moderate pressure transmitter aluminum block	$T_{actual} = 0.9933 T_{display} - 1.5931$	298 to 371 K	0.01
Temperature sensor in ROLSI™ expansion chamber	$T_{actual} = 1.0001 T_{display} - 3.9244$	330 to 465 K	0.04
Sensor in the lines between the ROLSI™ and the 6-port GC valve	$T_{actual} = 0.9989 T_{display} - 3.1732$	324 to 465 K	0.05
Sensor in the lines between the 6-port GC valve and the GC	$T_{actual} = 0.9981 T_{display} - 2.9661$	330 to 465 K	0.03
Sensor in the lines between the pressure transmitters and the equilibrium cell	$T_{actual} = 0.9990 T_{display} - 3.1715$	298 to 465 K	0.05
Sensor in the aluminum block for the GC valve	$T_{actual} = 0.9984 T_{display} - 2.8543$	330 to 465 K	0.03

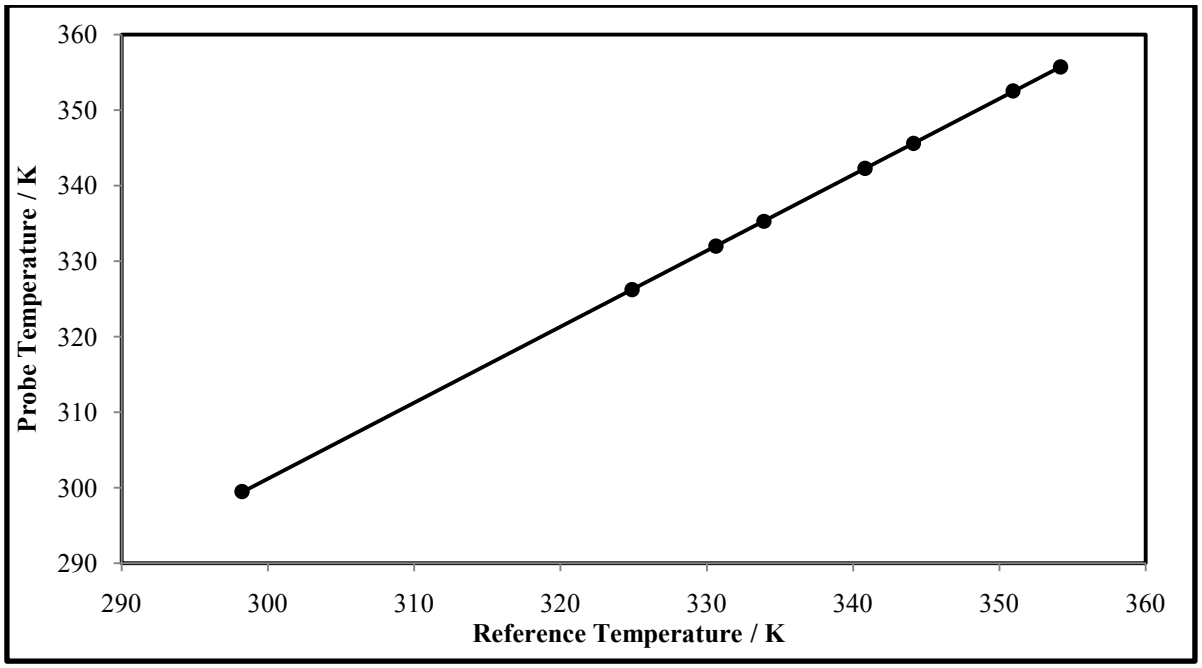

Figure C-1: Temperature calibration plot for the probe of the upper 316 SS flange of the equilibrium cell (low temperature range).

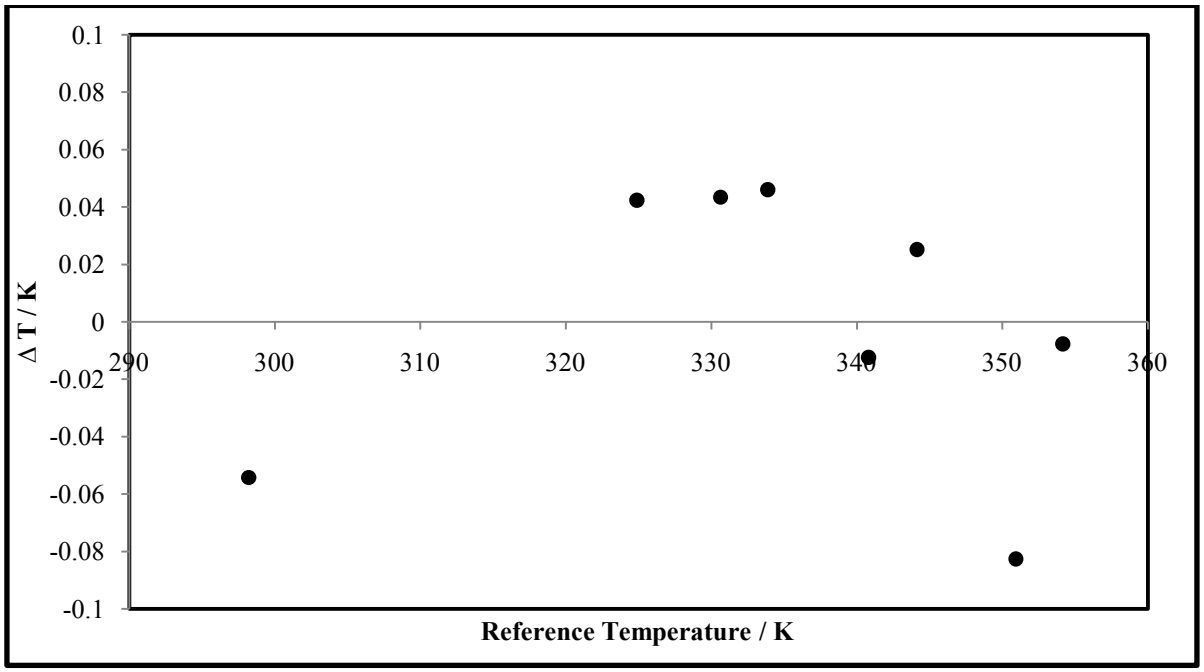

Figure C-2: Temperature deviation plot for the probe of the upper 316 SS flange of the equilibrium cell (low temperature range).

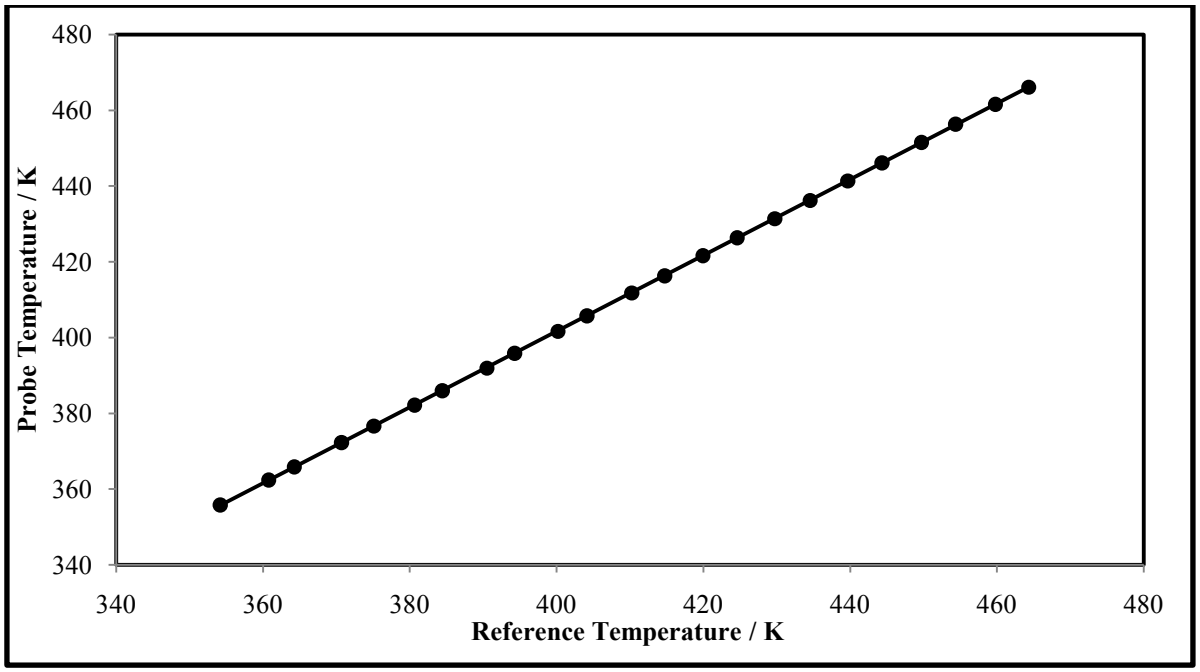

Figure C-3: Temperature calibration plot for the probe of the upper 316 SS flange of the equilibrium cell (high temperature range).

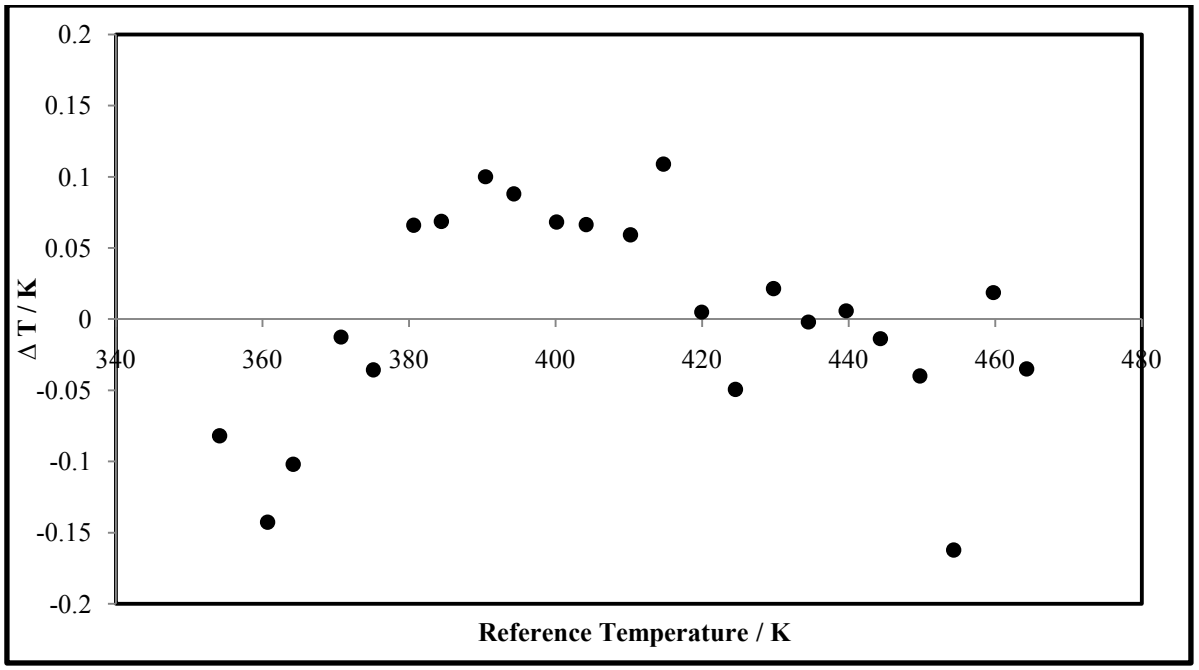

Figure C-4: Temperature deviation plot for the probe of the upper 316 SS flange of the equilibrium cell (high temperature range).

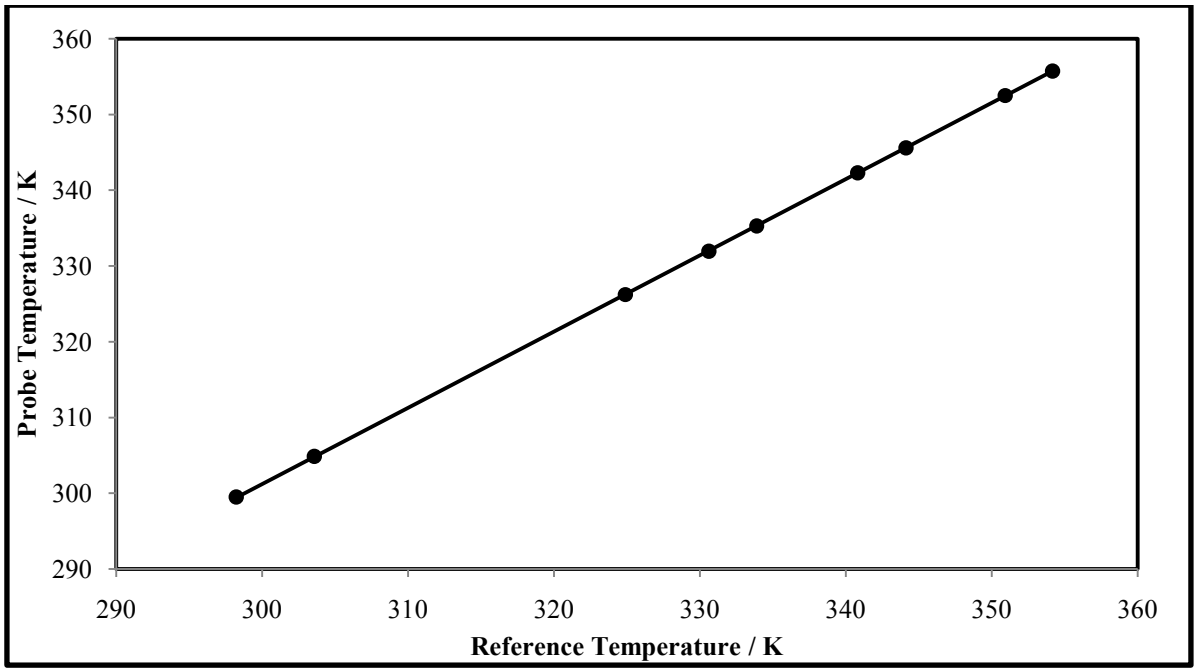

Figure C-5: Temperature calibration plot for the probe of the lower 316 SS flange of the equilibrium cell (low temperature range).

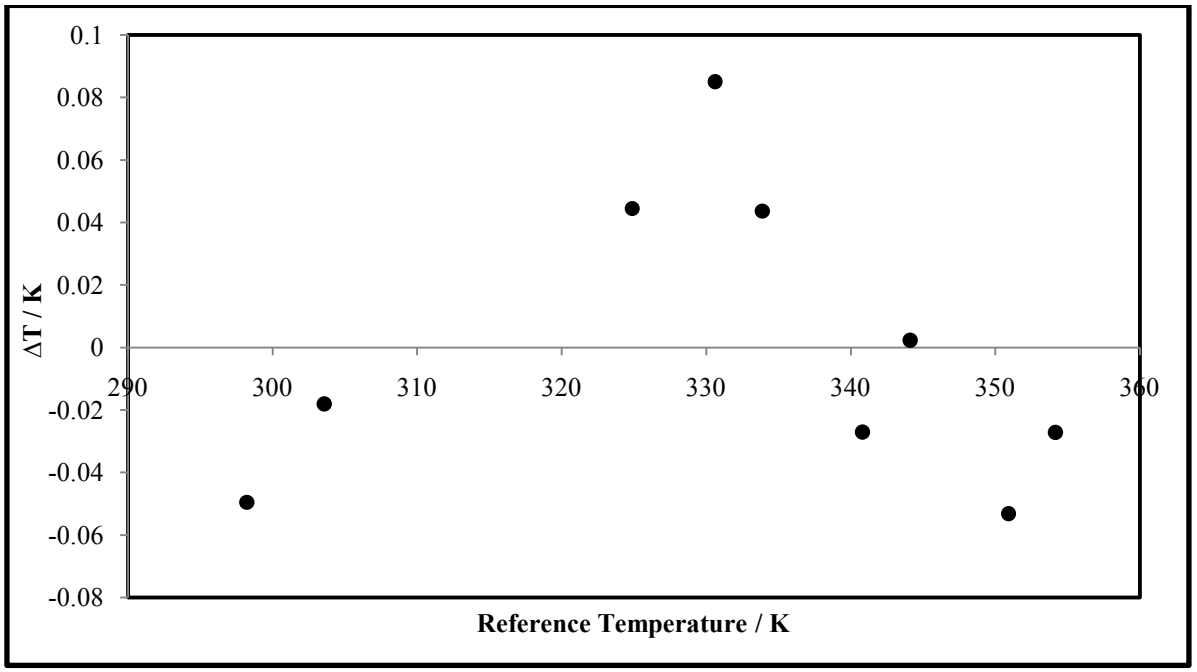

Figure C-6: Temperature deviation plot for the probe of the lower 316 SS flange of the equilibrium cell (low temperature range).

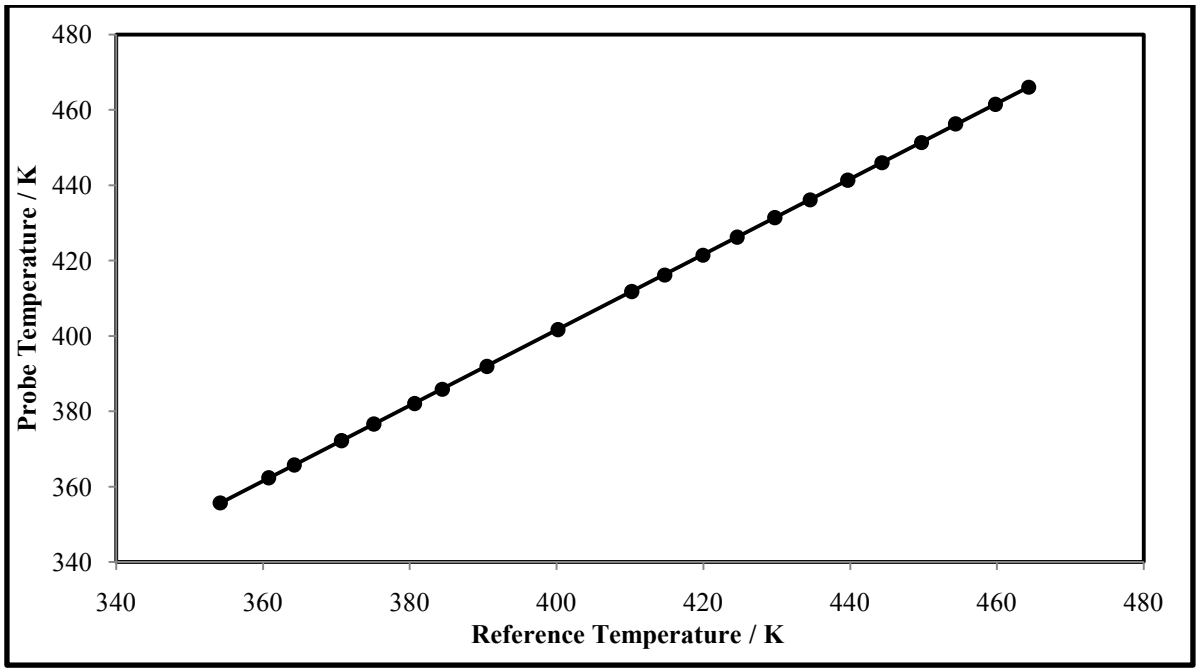

Figure C-7: Temperature calibration plot for the probe of the lower 316 SS flange of the equilibrium cell (high temperature range).

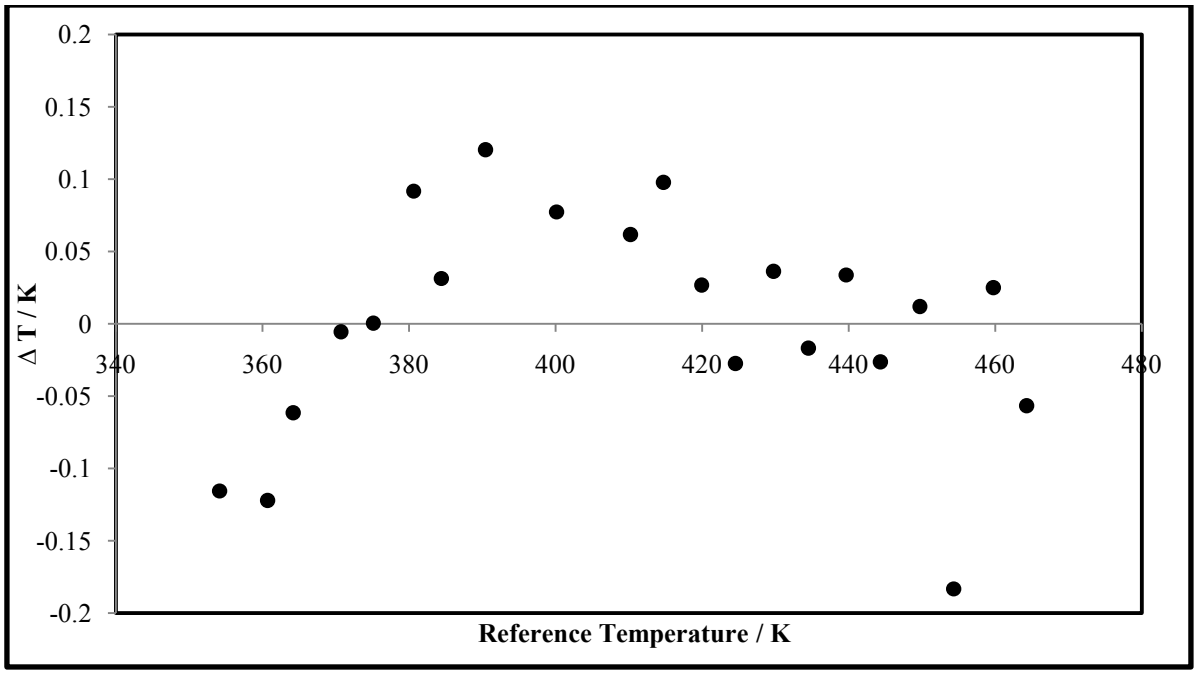

Figure C-8: Temperature deviation plot for the probe of the lower 316 SS flange of the equilibrium cell (high temperature range).

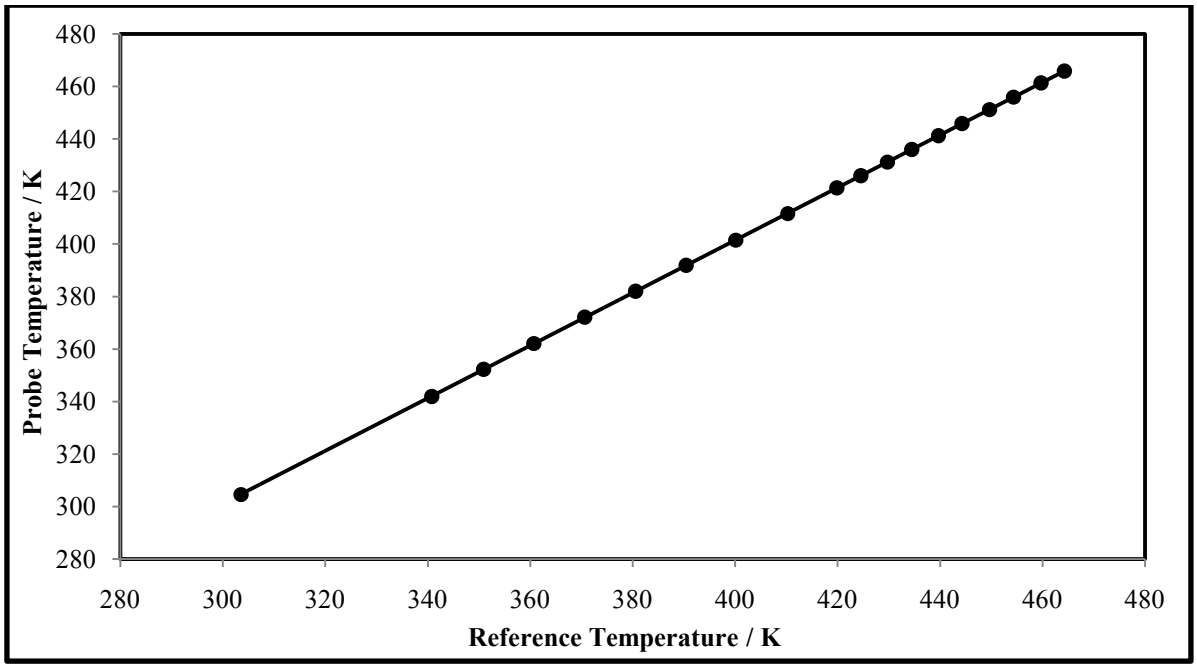

Figure C-9: Temperature calibration plot for the probe of the upper 316 SS flange of the equilibrium cell used to control the heater cartridge.

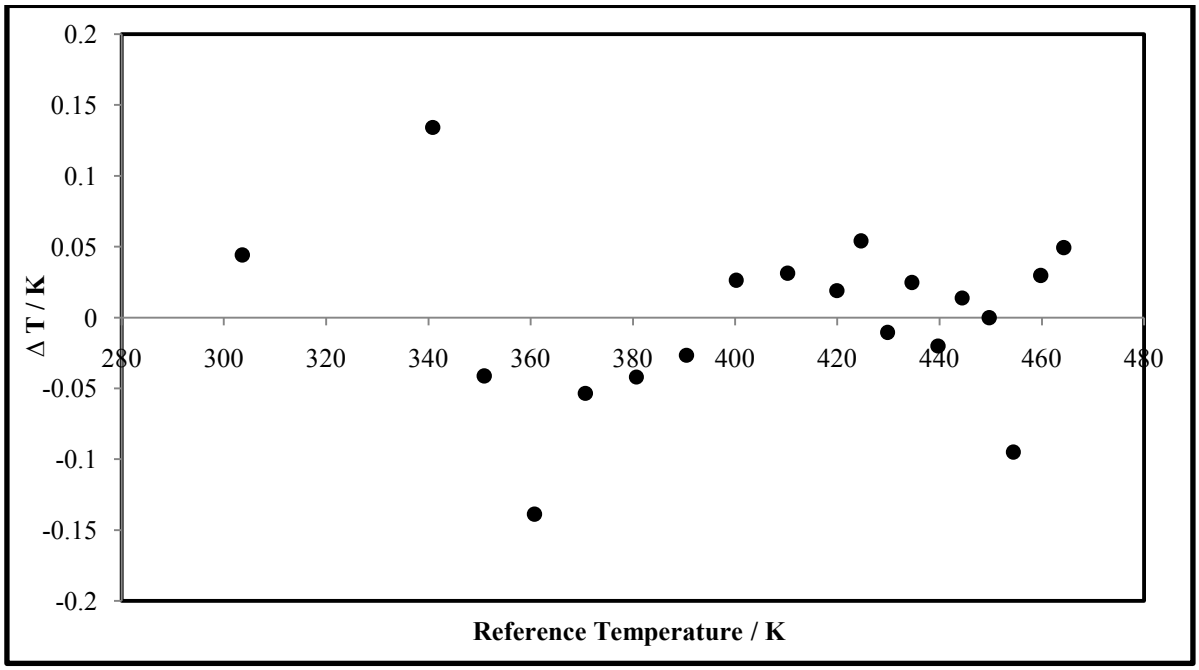

Figure C-10: Temperature deviation plot for the probe of the upper 316 SS flange of the equilibrium cell used to control the heater cartridge.

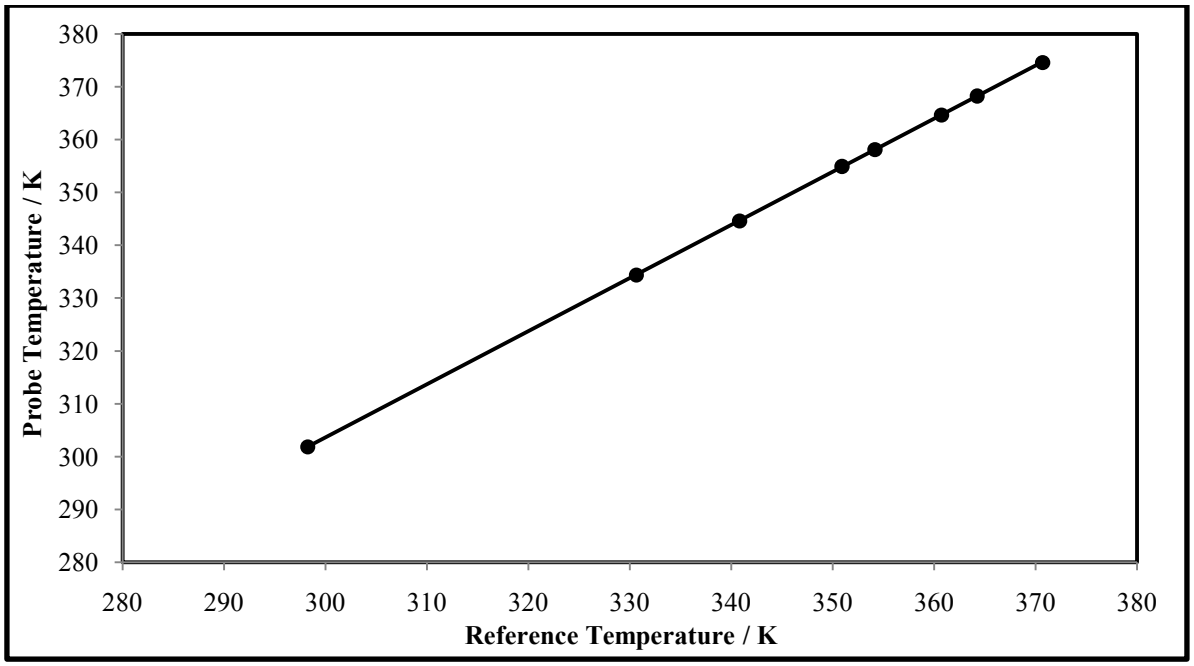

Figure C-11: Temperature calibration plot for the sensor on the low pressure transmitter aluminum block.

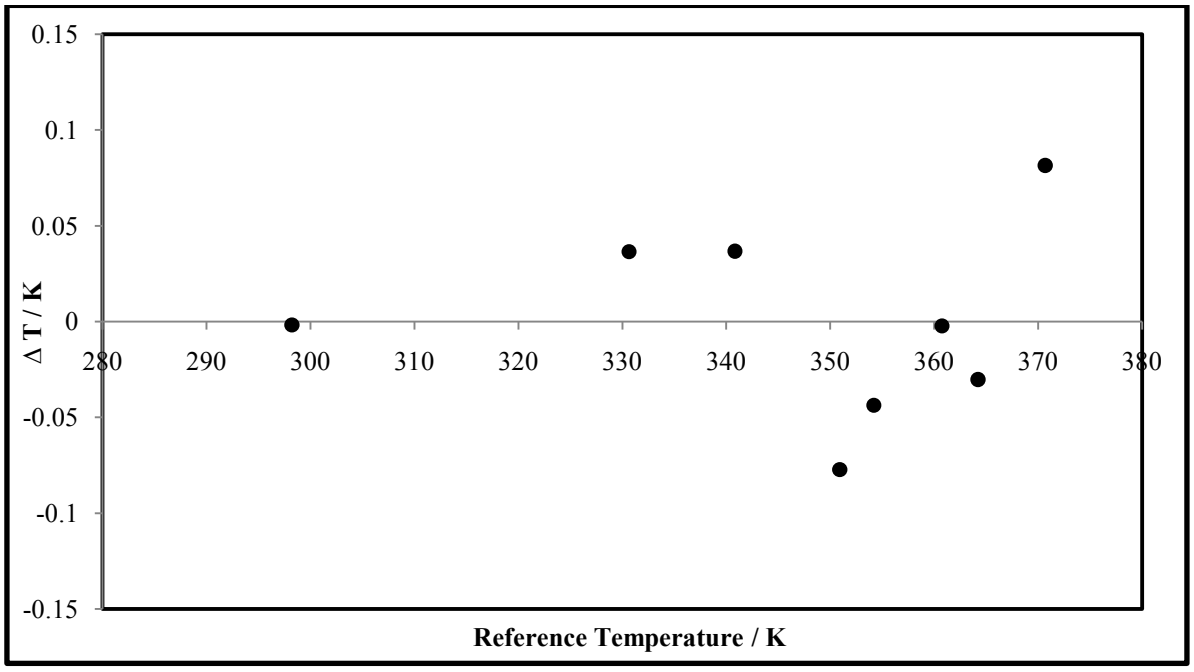

Figure C-12: Temperature deviation plot for the sensor on the low pressure transmitter aluminum block.

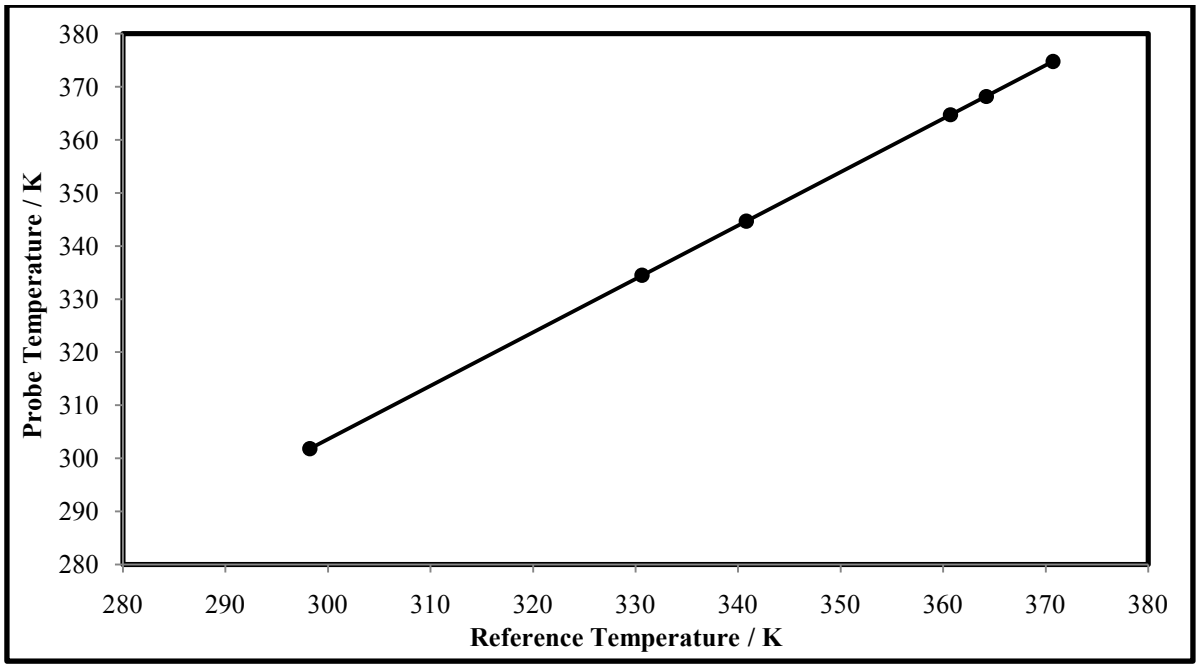

Figure C-13: Temperature calibration plot for the sensor on the high pressure transmitter aluminum block.

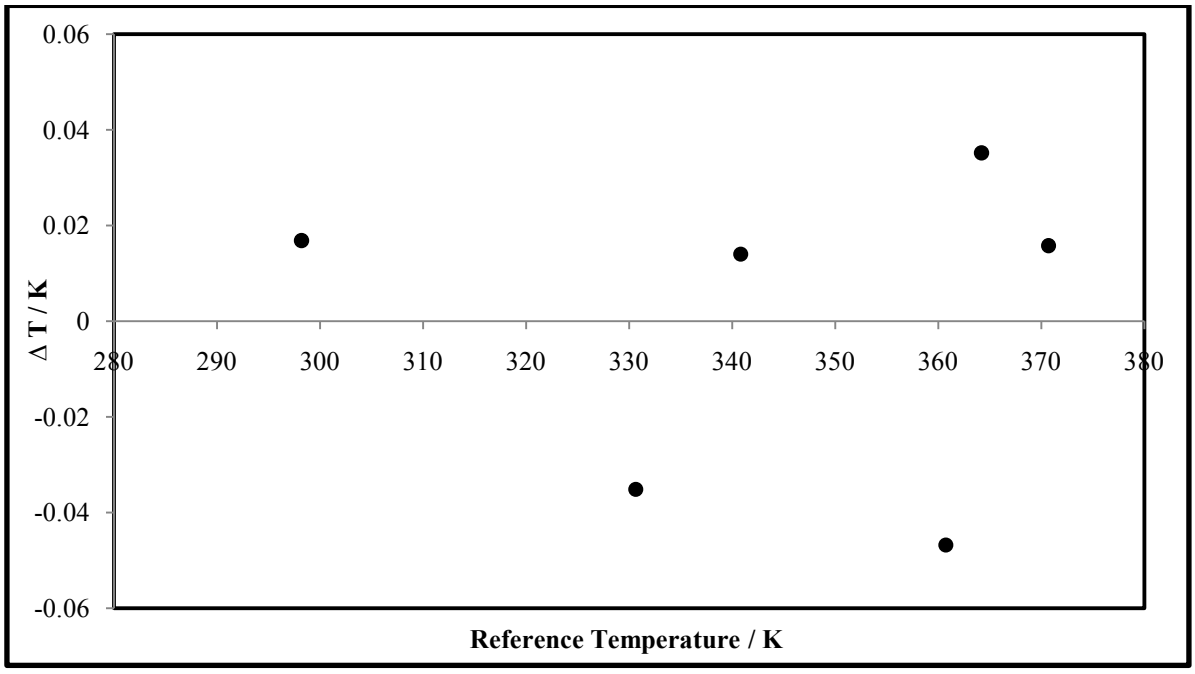

Figure C-14: Temperature deviation plot for the sensor on the high pressure transmitter aluminum block.

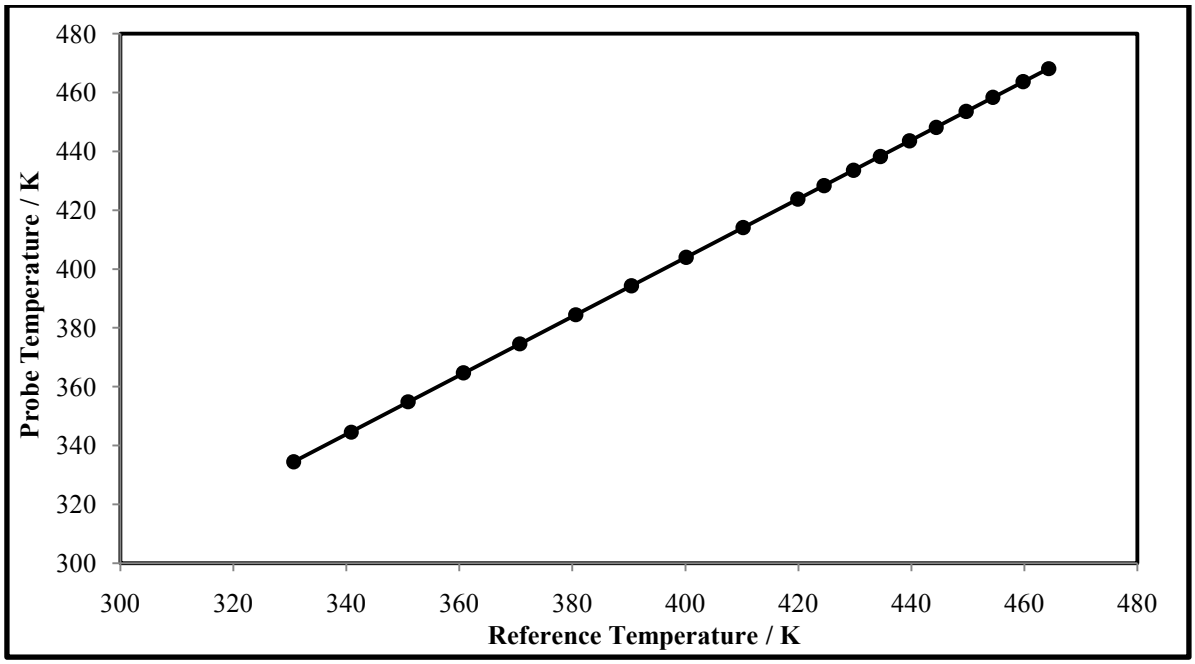

Figure C-15: Temperature calibration plot for the sensor in the ROLSI™ expansion chamber.

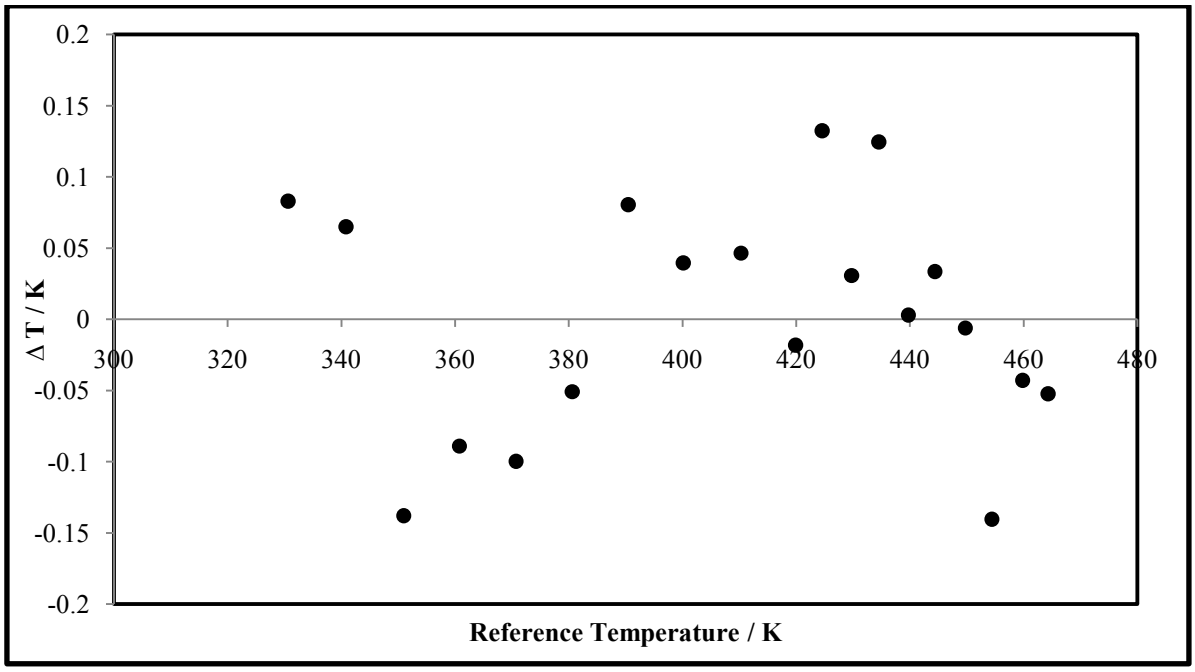

Figure C-16: Temperature deviation plot for the sensor in the ROLSI™ expansion chamber.

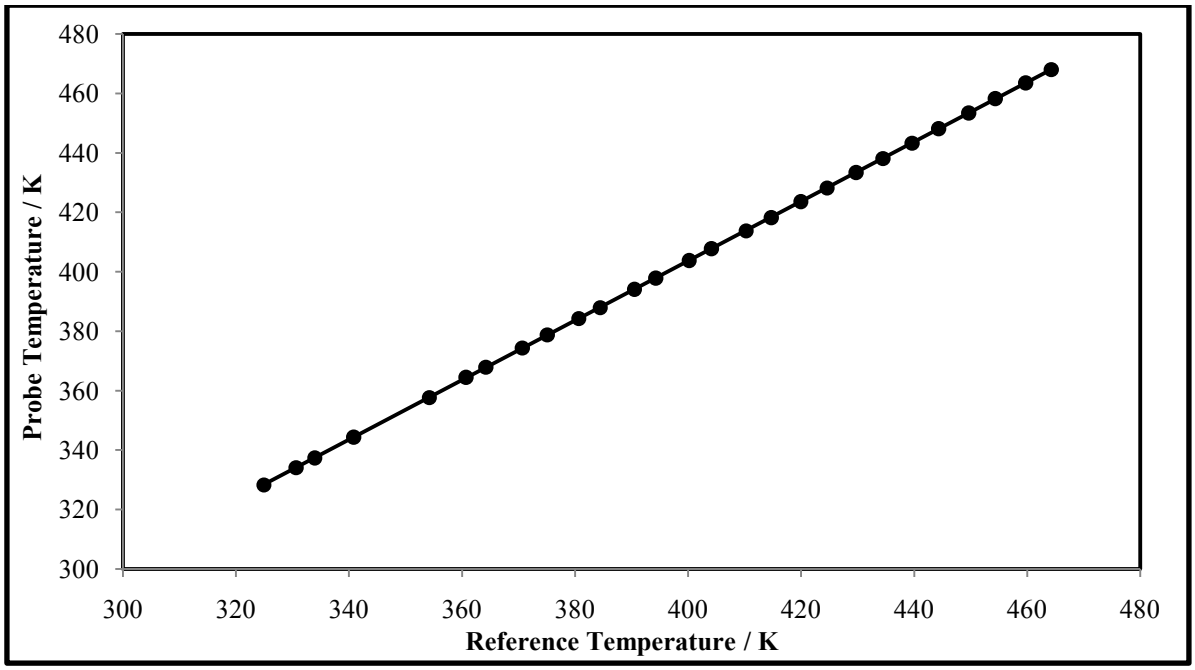

Figure C-17: Temperature calibration plot for the sensor in the lines between the ROLSI™ and the 6-port GC valve.

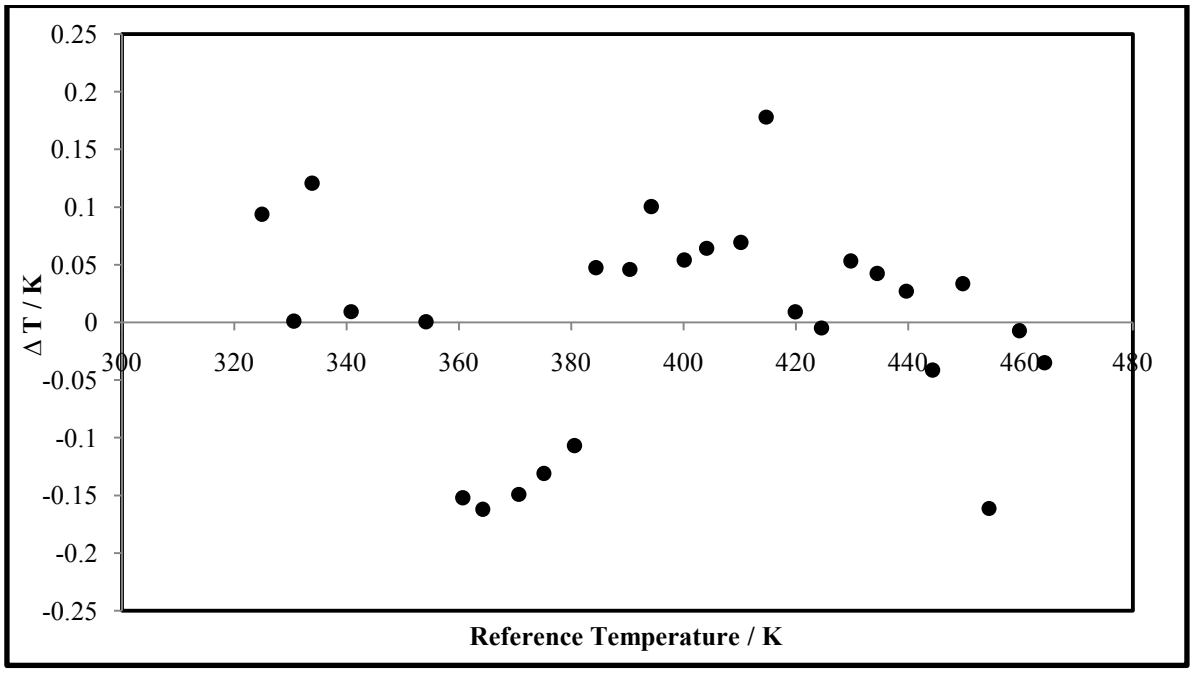

Figure C-18: Temperature deviation plot for the sensor in the lines between the ROLSI™ and the 6-port GC valve.

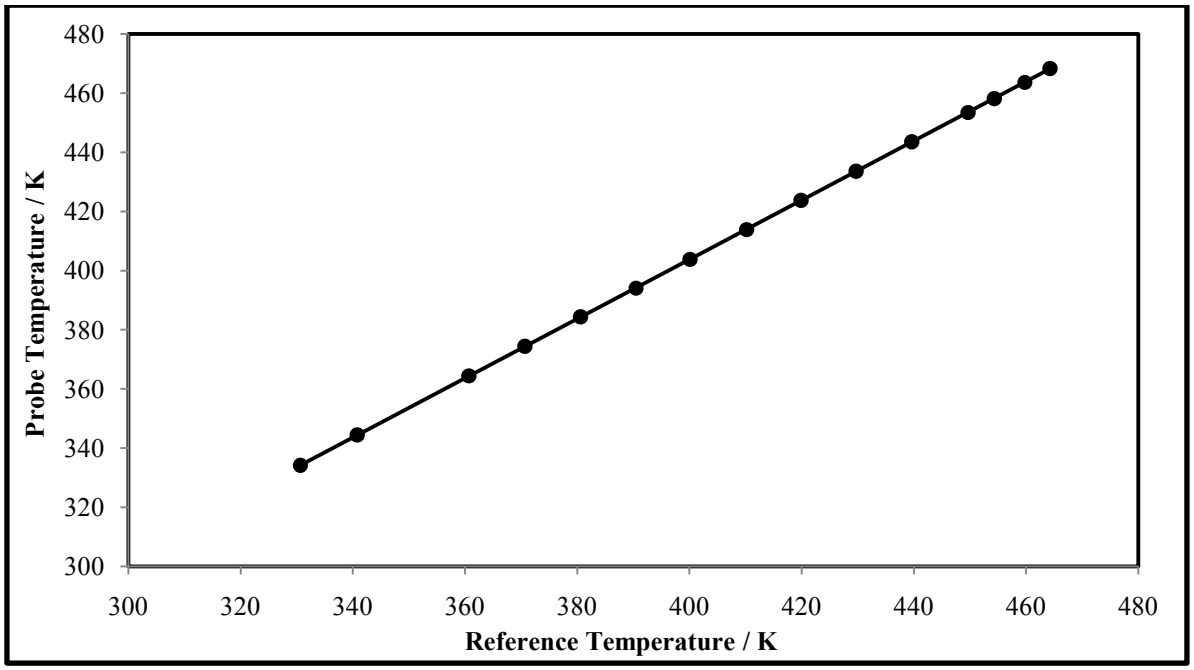

Figure C-19: Temperature calibration plot for the sensor in the lines between the 6-port GC valve and the GC.

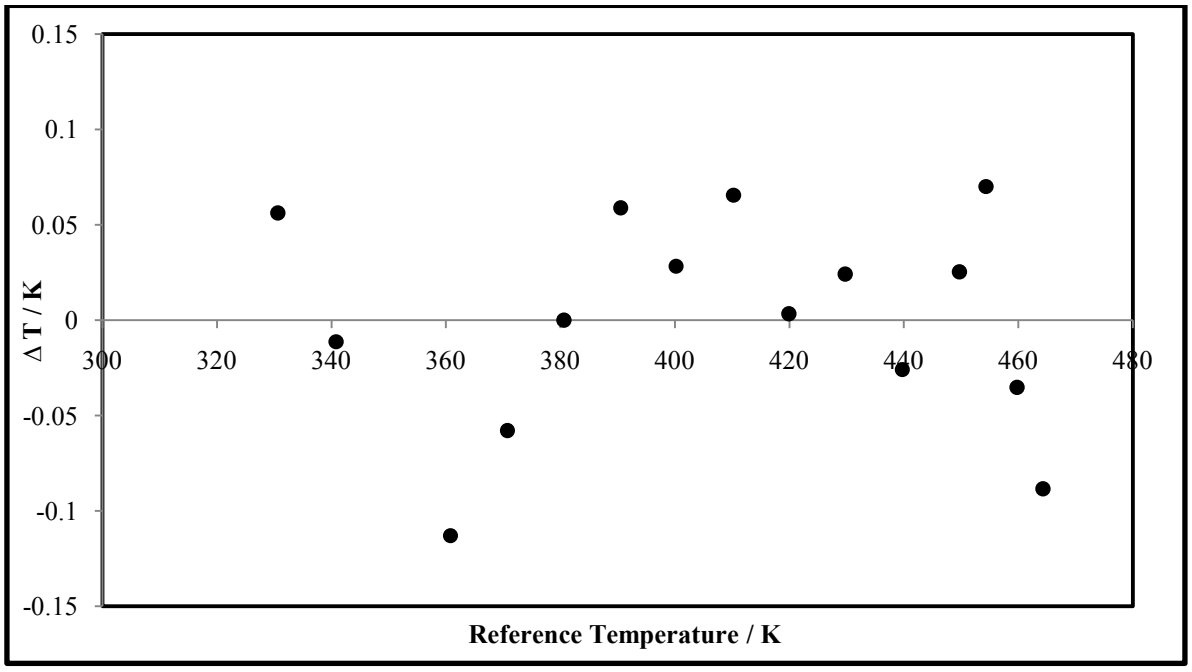

Figure C-20: Temperature deviation plot for the sensor in the lines between the 6-port GC valve and the GC.

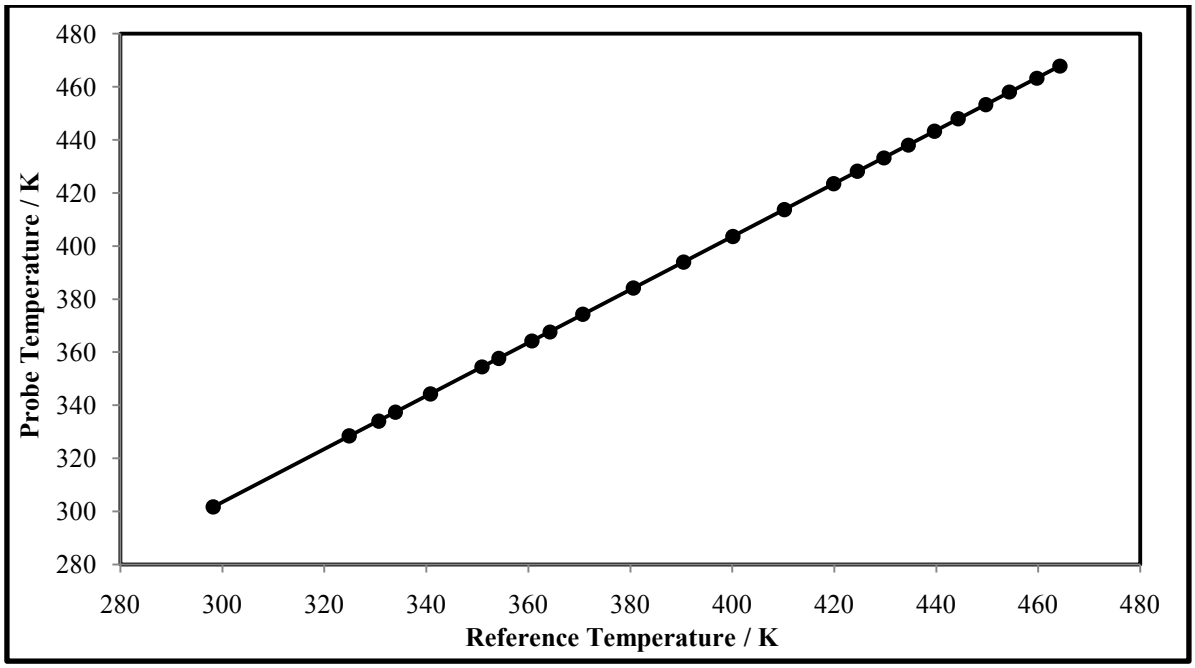

Figure C-21: Temperature calibration plot for the sensor in the lines between the pressure transmitters and the equilibrium cell.

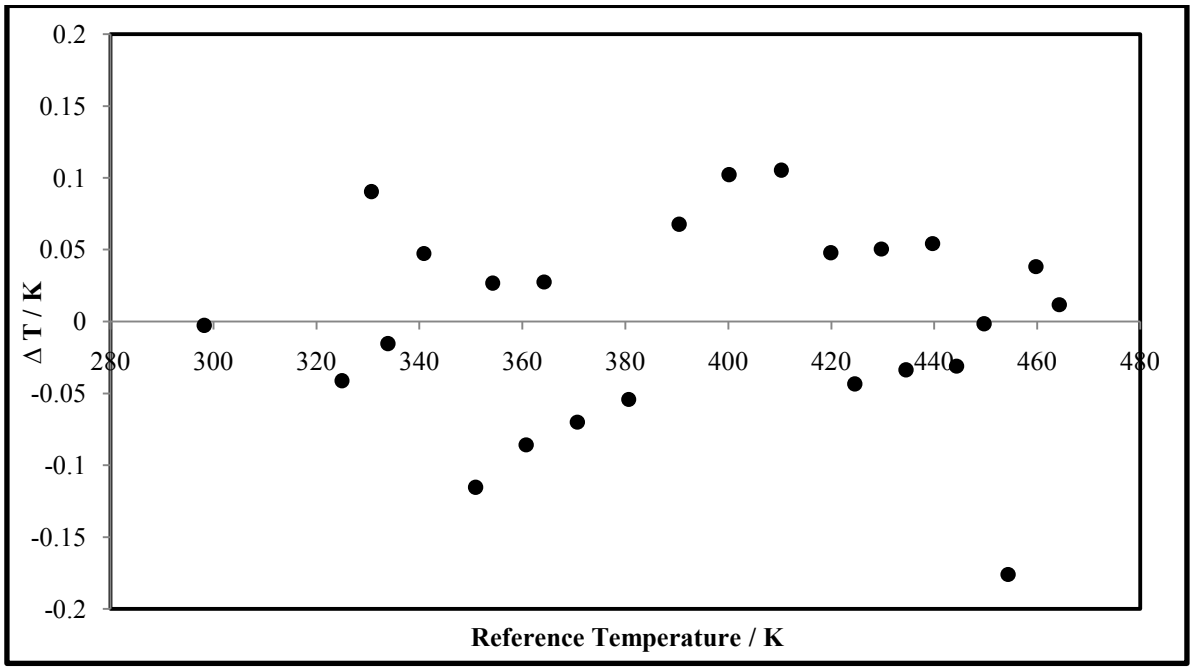

Figure C-22: Temperature deviation plot for the sensor in the lines between the pressure transmitters and the equilibrium cell.

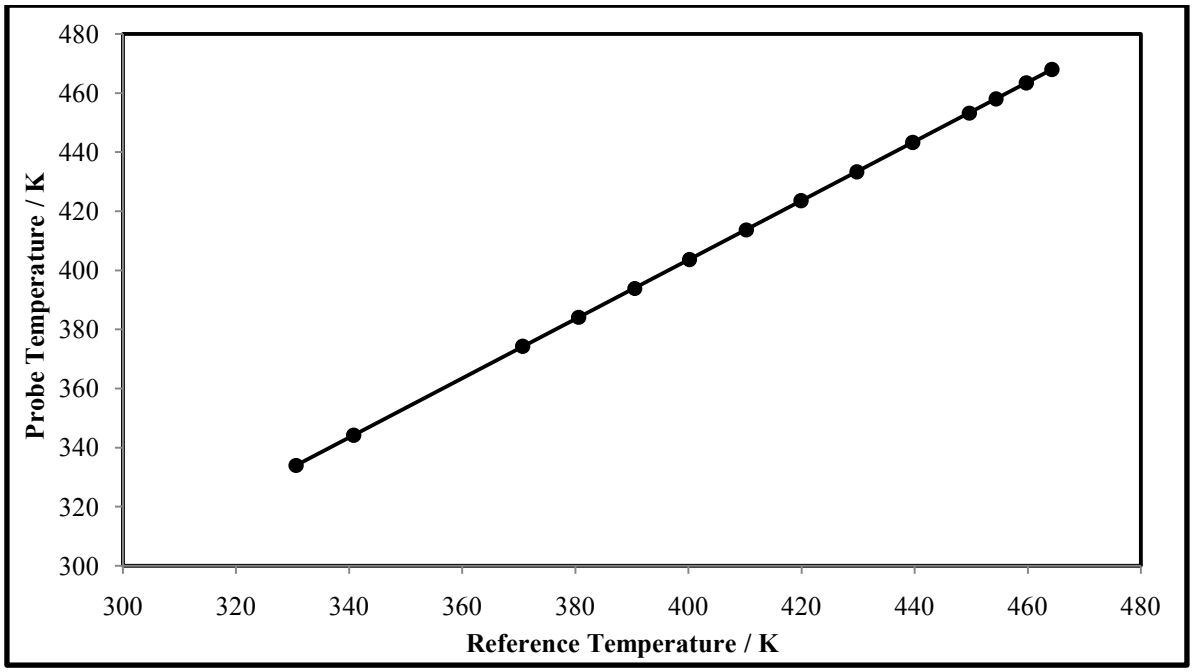

Figure C-23: Temperature calibration plot for the sensor in the aluminum block for the GC valve.

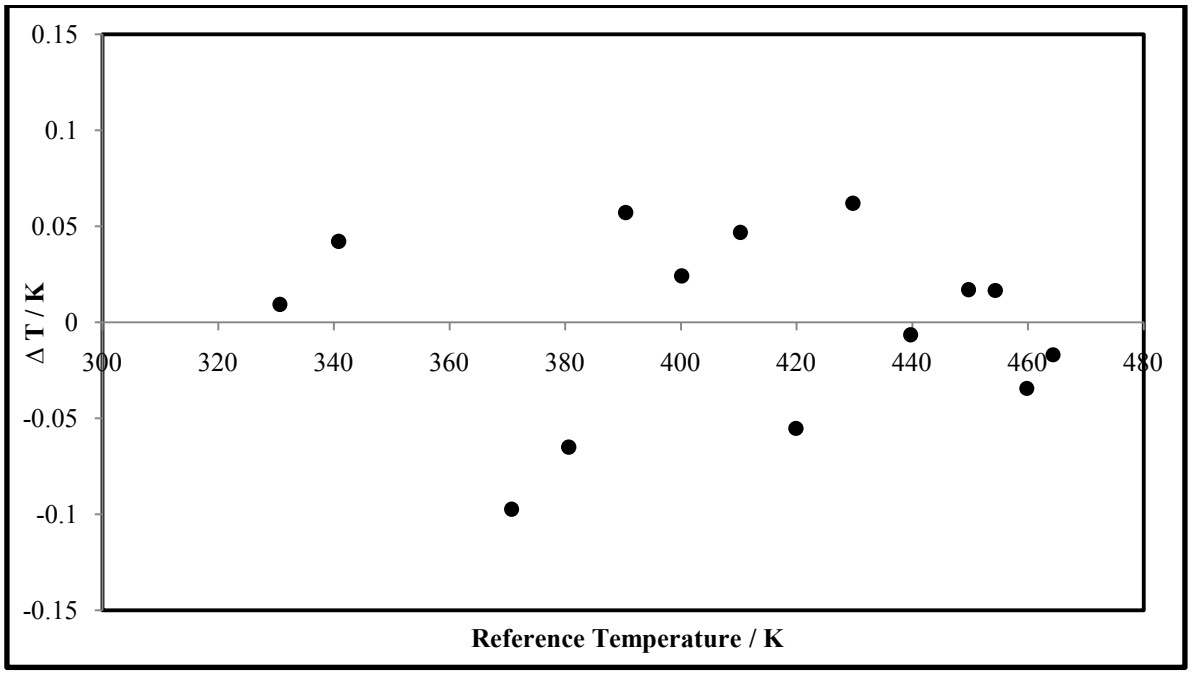

Figure C-24: Temperature deviation plot for the sensor in the aluminum block for the GC valve.

C.2 Pressure Calibrations

Table C-2: Calibration results for pressure transmitters used in this study.

Transmitter Description	Calibration Equation	Pressure Range	Calibration Uncertainty ΔP / kPa
Low pressure transmitter	$P_{actual} = 1.0002 P_{display} + 0.0027$	5 to 99 kPa	0.003
Moderate pressure transmitter	$P_{actual} = 0.9996 P_{display} - 0.4898$	97 to 1313 kPa	0.6

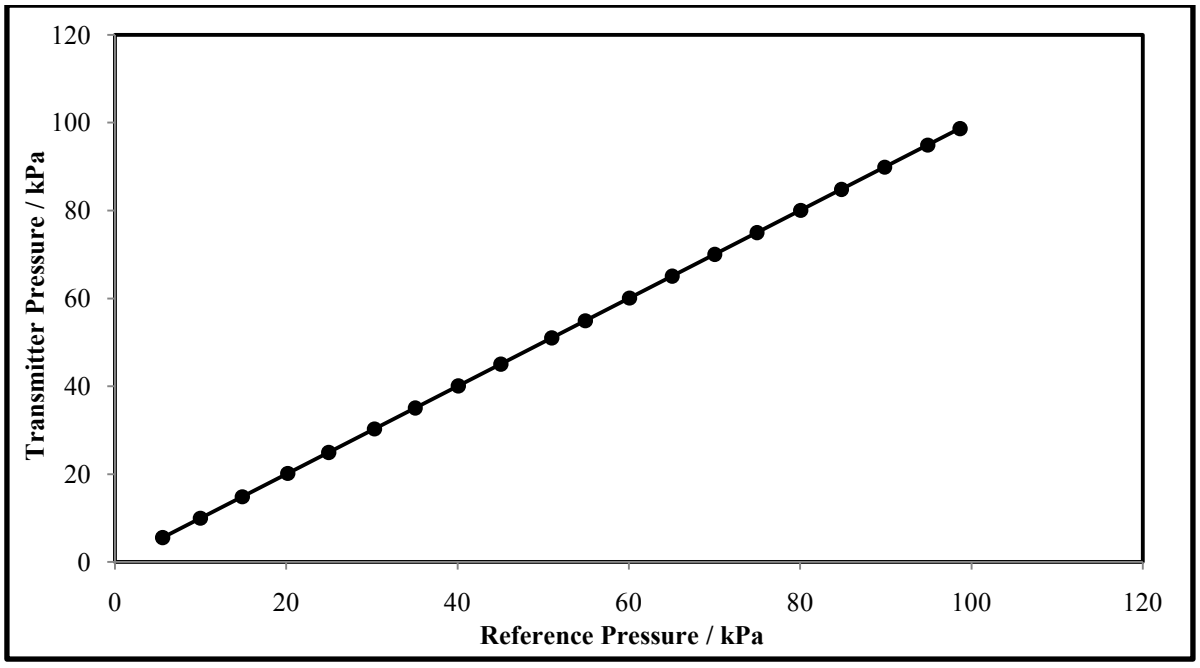

Figure C-25: Pressure calibration plot for the low pressure transmitter.

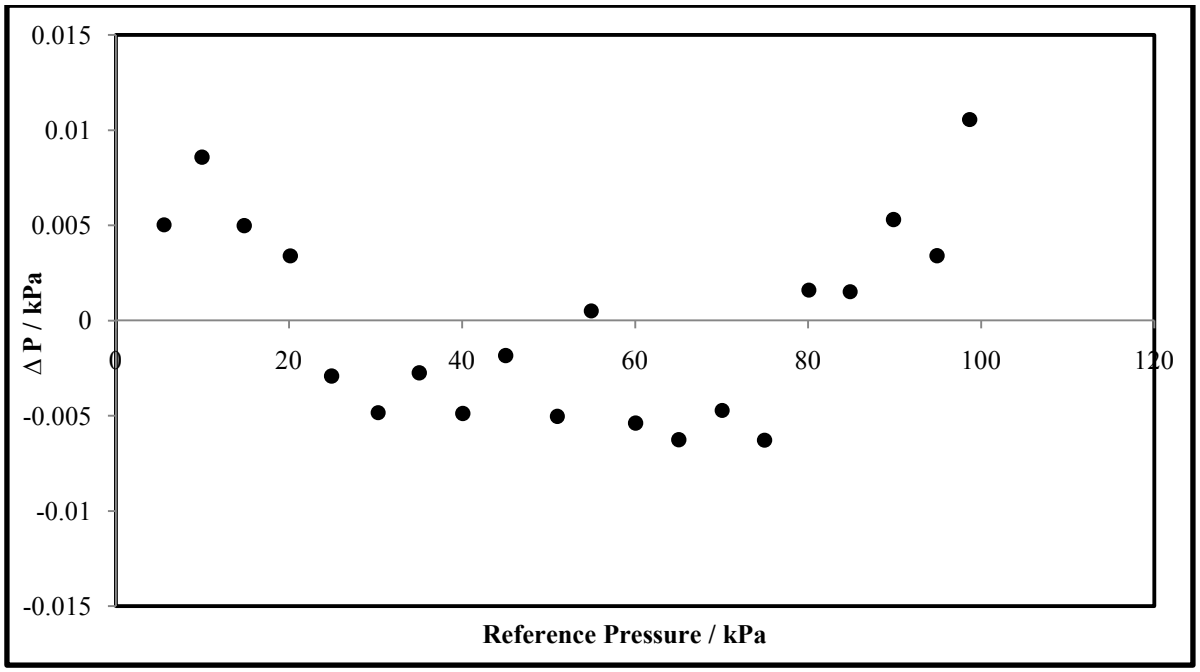

Figure C-26: Pressure deviation plot for the low pressure transmitter.

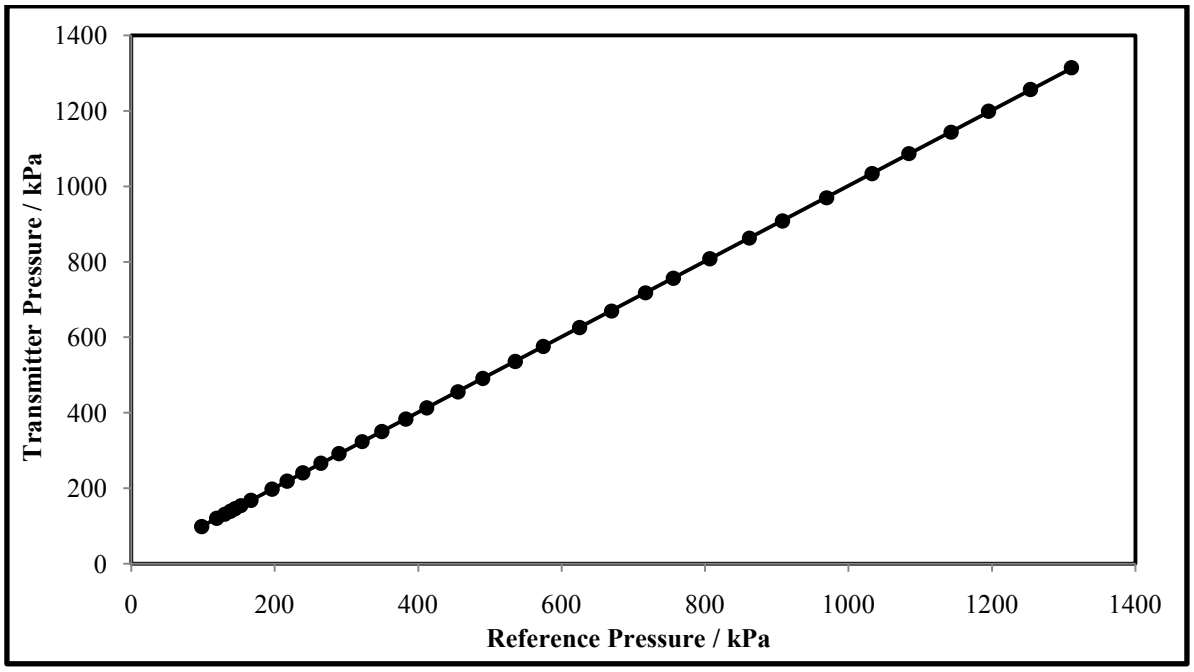

Figure C-27: Pressure calibration plot for the moderate pressure transmitter.

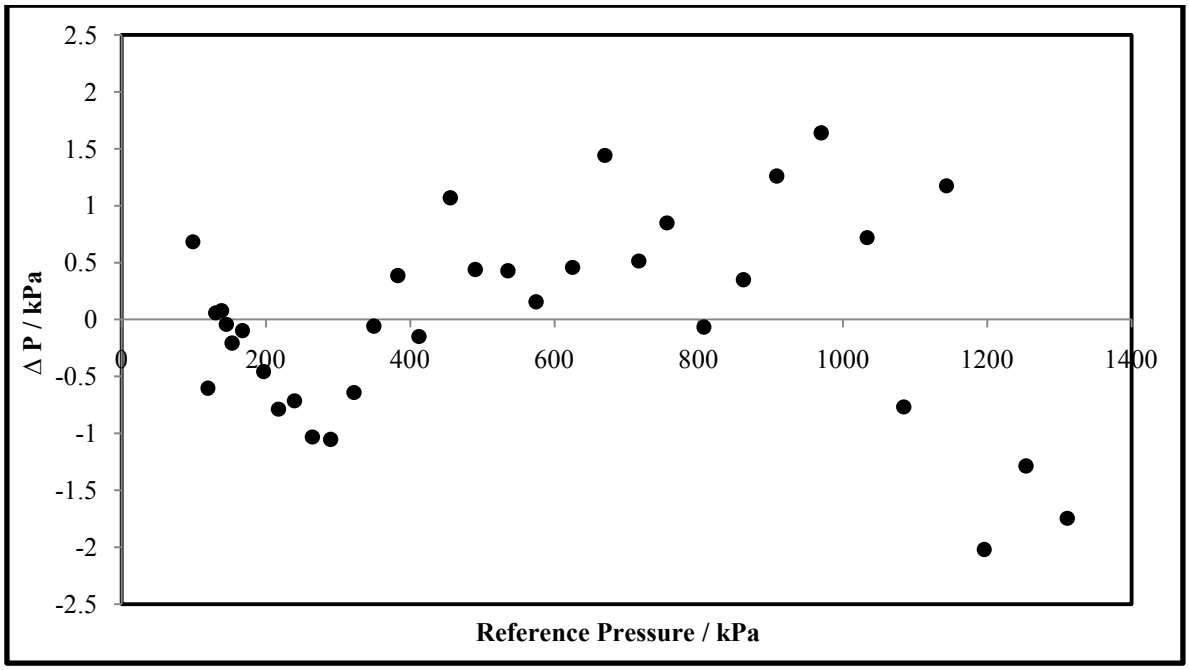

Figure C-28: Pressure deviation plot for the moderate pressure transmitter.

C.3 Gas Chromatograph Operating Conditions

Table C-3: Specifications of the gas chromatograph capillary columns used in this study.

Name	JW Scientific	HP-5
Phase loading	GS-Q: polarity with phases between Porapak® Q and Porapak® N	Crosslinked 5% PH ME Silicone
Serial number	6271935	19091J-413
Maximum temperature / K	523.15	523.15
Length / m	30	30
Internal diameter / mm	0.53	0.32
Film thickness / µm	1.5	0.25

The GC operating conditions are presented in Table C4 for the following systems:

a) 2-methoxy-2-methylpropane (1) + ethyl acetate (2)

b) methanol (1) + butan-2-one (2)

c) ethanol (1) + butan-2-one (2)

d) ethanol (1) + 2-methoxy-2-methylbutane (2)

e) 2-methylpent-2-ene (1) + ethanol (2)

f) hexane (1) + acetonitrile (2)

g) methanol (1) + heptane (2)

Table C-4: Gas chromatograph (GC) operating conditions for the systems studied in this work.

System	a	b	c	d	e	f	g
GC column	JW Scientific	HP-5	HP-5	HP-5	HP-5	HP-5	HP-5
Carrier gas	Helium	Helium	Helium	Helium	Helium	Helium	Helium
Column pressure (gauge) / kPa	16.1	22	22.4	22.8	22.4	20	25.1
Column flow / $mL.min^{-1}$	2.92	0.53	0.51	0.5	0.51	0.5	0.64
Flow control mode	linear velocity	linear velocity	linear velocity	linear velocity	linear velocity	linear velocity	linear velocity
Split ratio	20	60	80	80	80	40	60
Injector temperature / K	473.15	473.15	473.15	473.15	473.15	473.15	473.15
Column temperature / K	323.15	333.15	343.15	353.15	343.15	323.15	323.15
Detector temperature / K	473.15	473.15	473.15	473.15	473.15	473.15	473.15

C.4 Gas Chromatograph Calibrations

C.4.1 VLE Systems

For each calibration point, at least five samples were used for repeatability with a maximum error of 1%, where the error was found from the following equation:

$$Repeatibility\ \ Error = \frac{Average}{Standard\ \ Deviation} \times 100\% \tag{C-1}$$

The absolute average deviation (AAD) for mole fraction composition in gas GC TCD detector calibration was found from:

$$AAD = \frac{\sum_{i=1}^{k} \left| (\Delta x_1)_i \right|}{k} \tag{C-2}$$

where:

$$\Delta x_1 = (x_1)_{calibration} - (x_1)_{standard} \tag{C-3}$$

Table C-5: Gas chromatograph calibration results for all VLE systems used in this study.

System	Calibration Equation	AAD for x_1
2-methoxy-2-methylpropane (1) + ethyl acetate (2)	2-methoxy-2-methylpropane dilute region: $\frac{A_1}{A_2} = 1.0261 \frac{x_1}{x_2}$ ethyl acetate dilute region: $\frac{A_2}{A_1} = 0.9738 \frac{x_2}{x_1}$	2-methoxy-2-methylpropane dilute region: 0.002 ethyl acetate dilute region: 0.002
methanol (1) + butan-2-one (2)	methanol dilute region: $\frac{A_1}{A_2} = 0.4916 \frac{x_1}{x_2}$ butan-2-one dilute region: $\frac{A_2}{A_1} = 2.0006 \frac{x_2}{x_1}$	methanol dilute region: 0.006 butan-2-one dilute region: 0.004

Table C-5: Gas chromatograph calibration results for all VLE systems used in this study (continued).

System	Calibration Equation	AAD for x_1
ethanol (1) + butan-2-one (2)	ethanol dilute region: $\frac{A_1}{A_2} = 0.7187\frac{x_1}{x_2}$ butan-2-one dilute region: $\frac{A_2}{A_1} = 1.3686\frac{x_2}{x_1}$	ethanol dilute region: 0.004 butan-2-one dilute region: 0.003
ethanol (1) + 2-methoxy-2-methylbutane (2)	ethanol dilute region: $\frac{A_1}{A_2} = 0.5599\frac{x_1}{x_2}$ 2-methoxy-2-methylbutane dilute region: $\frac{A_2}{A_1} = 1.7239\frac{x_2}{x_1}$	ethanol dilute region: 0.007 2-methoxy-2-methylbutane dilute region: 0.006
2-methylpent-2-ene (1) + ethanol (2)	2-methylpent-2-ene dilute region: $\frac{A_1}{A_2} = 0.0518\left(\frac{x_1}{x_2}\right)^2 + 1.3440\left(\frac{x_1}{x_2}\right)$ ethanol dilute region: $\frac{A_2}{A_1} = 0.3109\left(\frac{x_2}{x_1}\right)^2 + 0.4208\left(\frac{x_2}{x_1}\right)$	2-methylpent-2-ene dilute region: 0.002 ethanol dilute region: 0.004

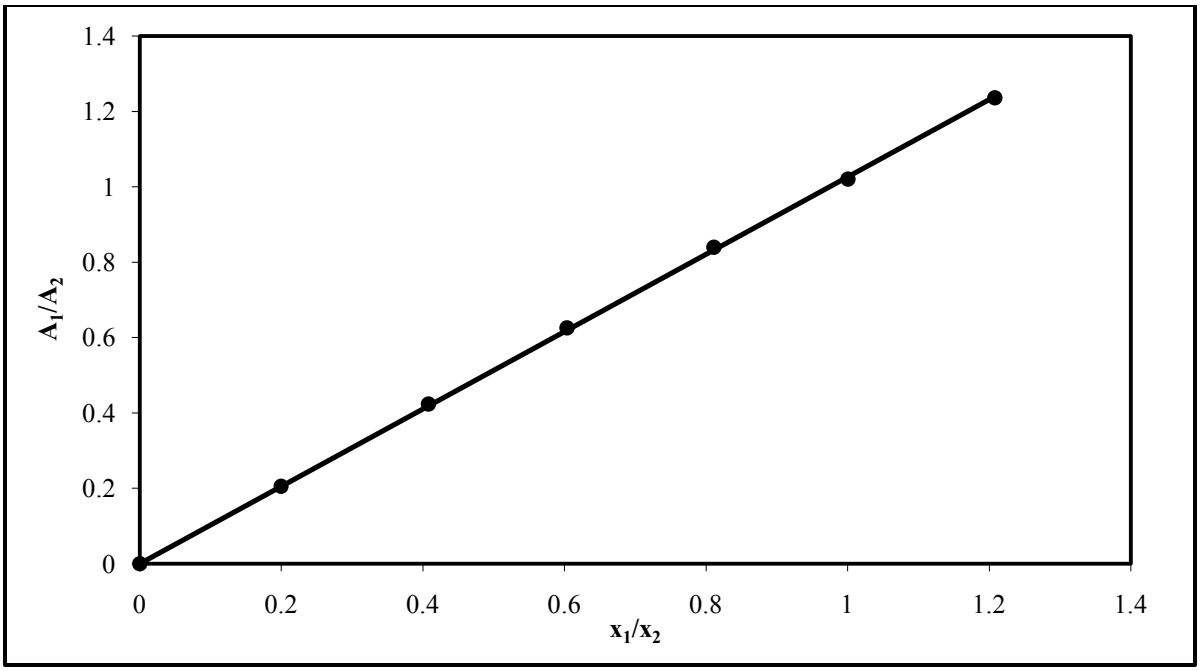

Figure C-29: GC calibration graph for the 2-methoxy-2-methylpropane (1) + ethyl acetate (2) system (2-methoxy-2-methylpropane dilute region).

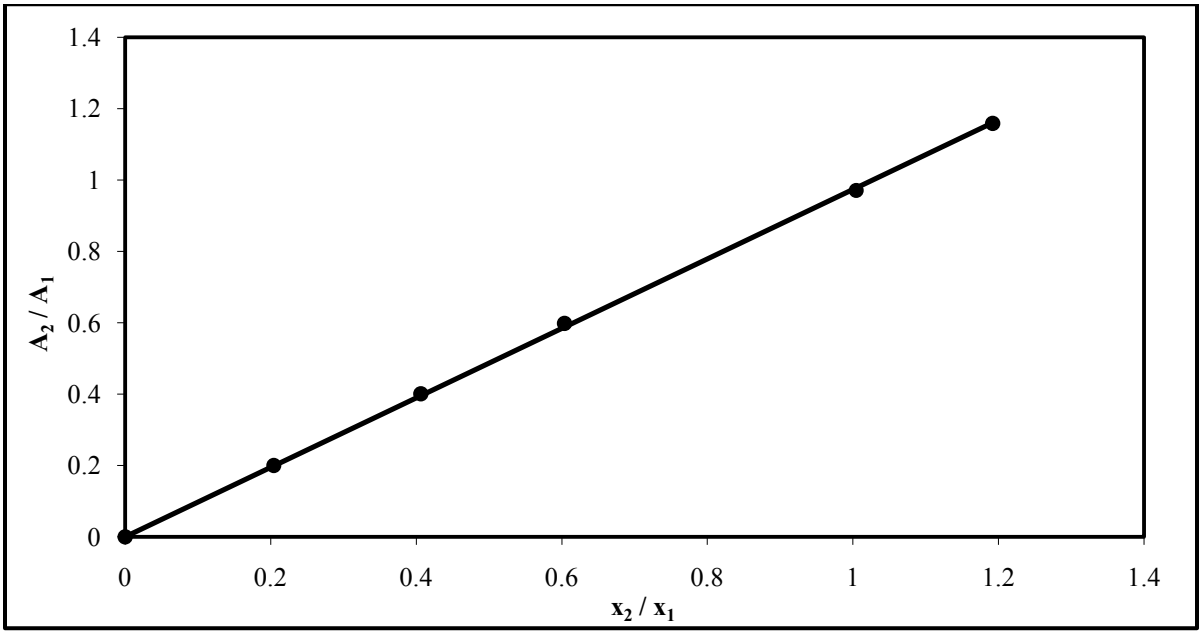

Figure C-30: GC calibration graph for the 2-methoxy-2-methylpropane (1) + ethyl acetate (2) system (ethyl acetate dilute region).

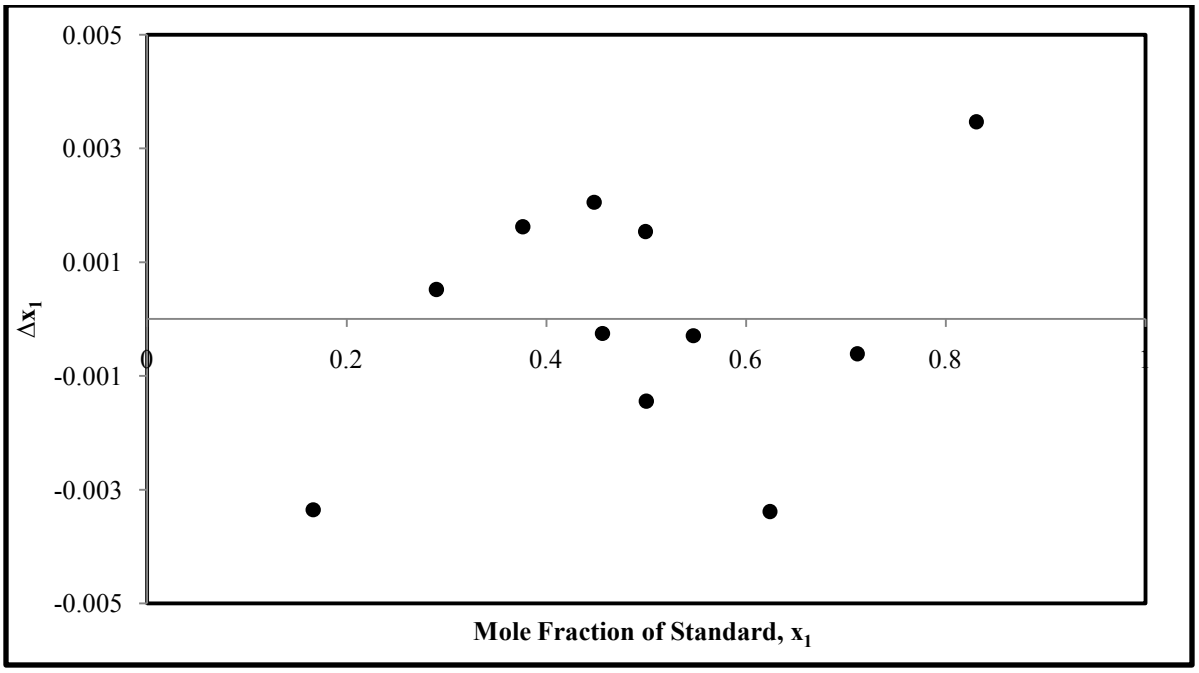

Figure C-31: Composition deviation plot for the 2-methoxy-2-methylpropane (1) + ethyl acetate (2) system.

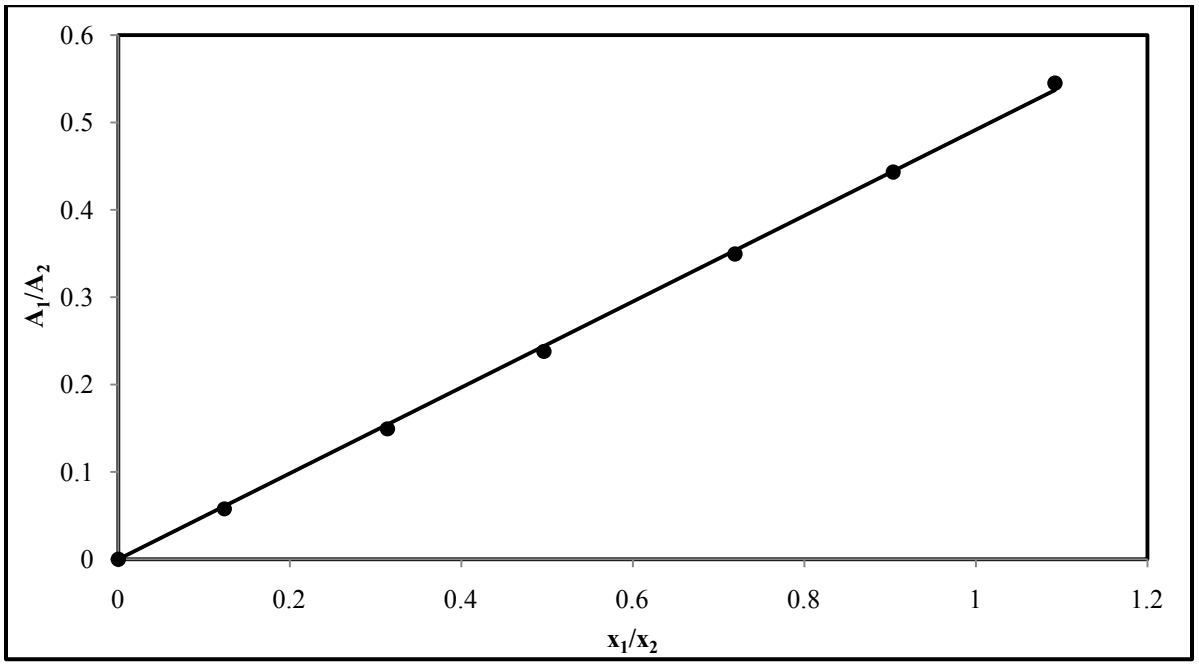

Figure C-32: GC calibration graph for the methanol (1) + butan-2-one (2) system (methanol dilute region).

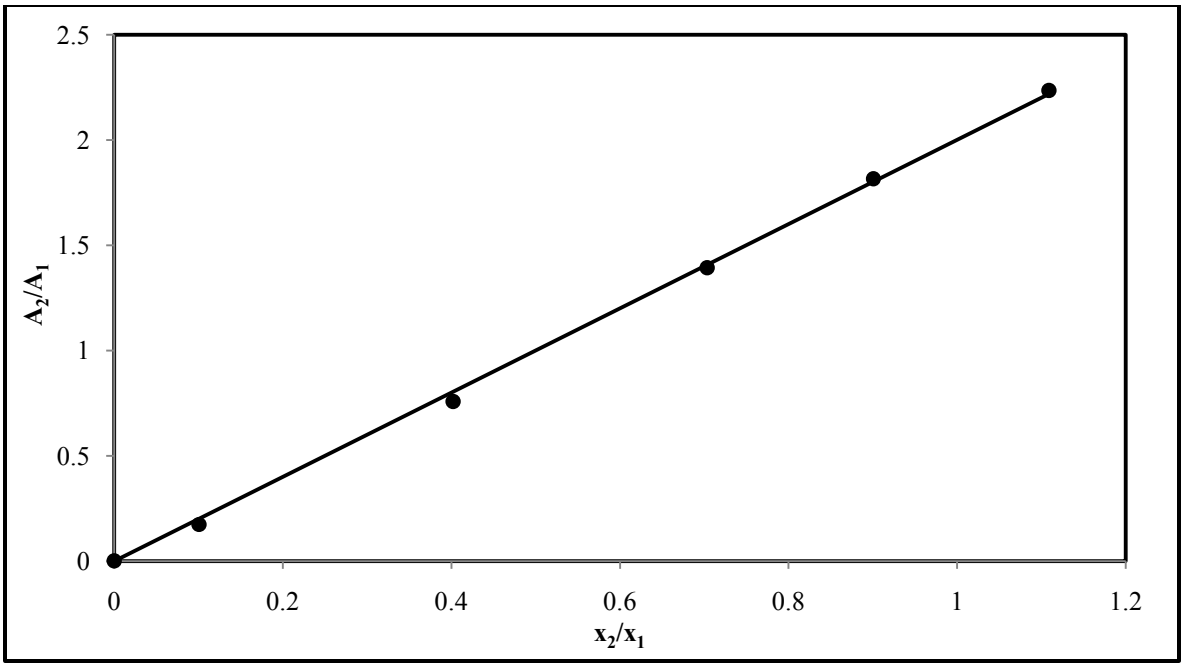

Figure C-33: GC calibration graph for the methanol (1) + butan-2-one (2) system (butan-2-one dilute region).

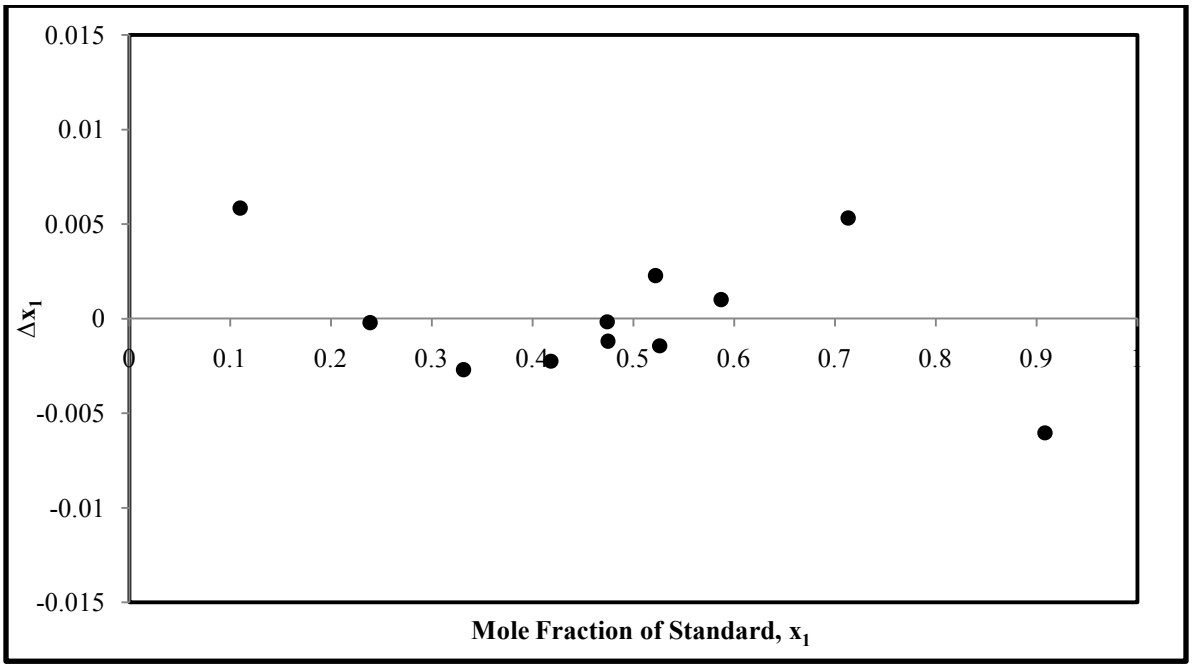

Figure C-34: Composition deviation plot for the methanol (1) + butan-2-one (2) system.

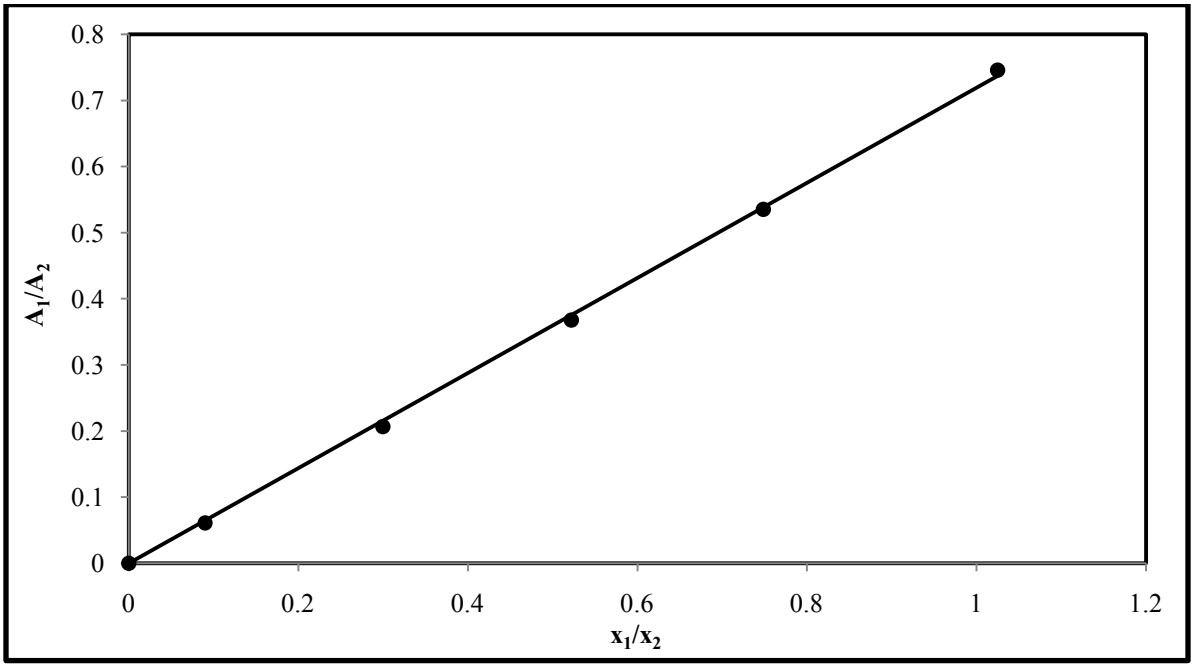

Figure C-35: GC calibration graph for the ethanol (1) + butan-2-one (2) system (ethanol dilute region).

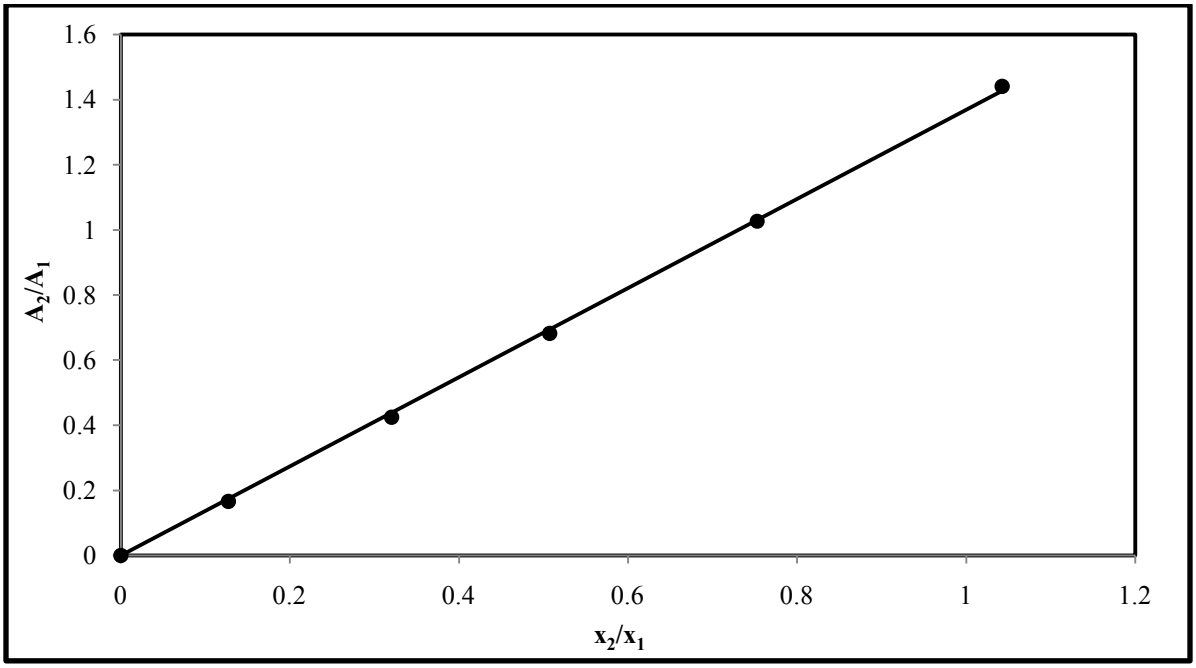

Figure C-36: GC calibration graph for the ethanol (1) + butan-2-one (2) system (butan-2-one dilute region).

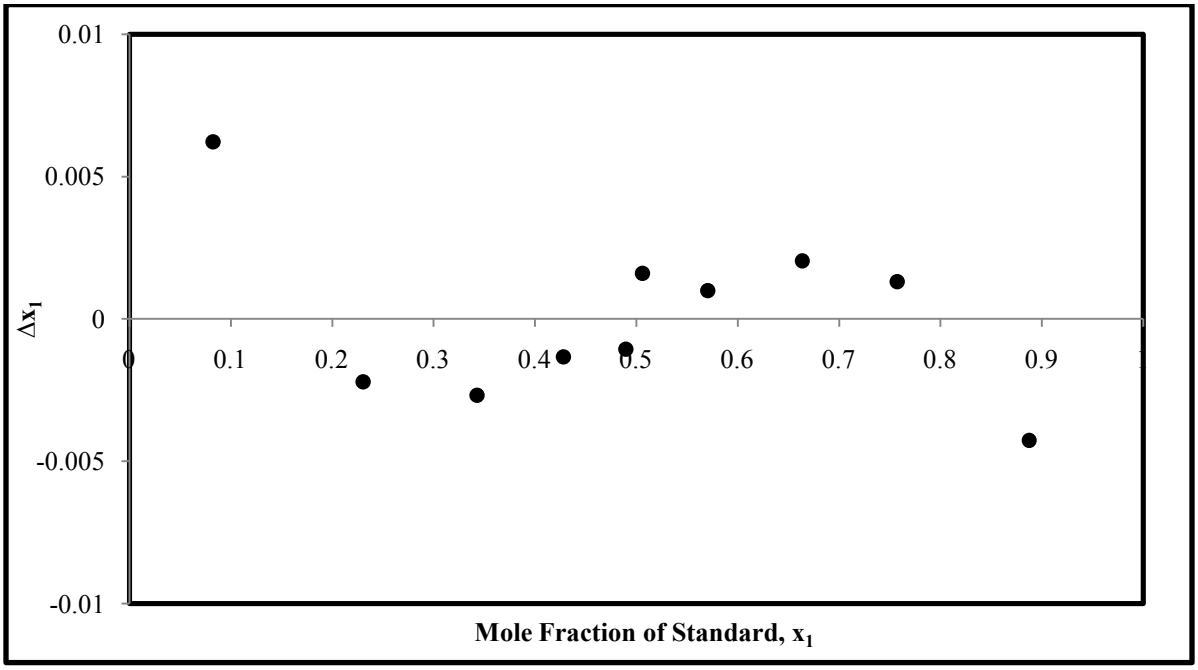

Figure C-37: Composition deviation plot for the ethanol (1) + butan-2-one (2) system.

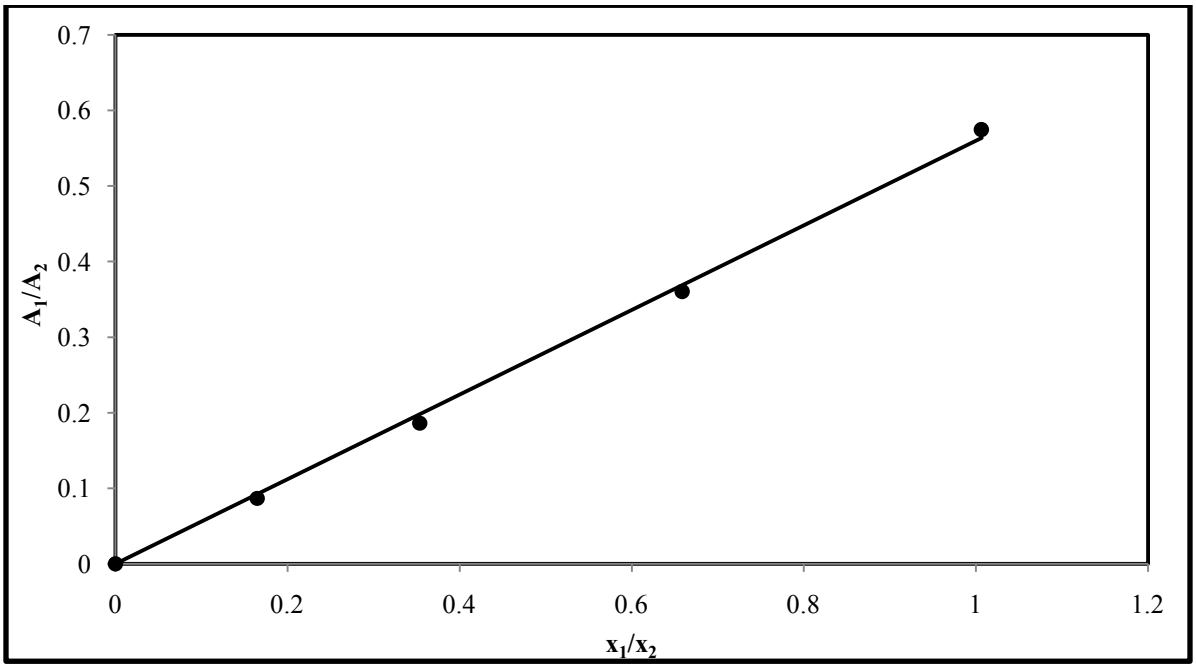

Figure C-38: GC calibration graph for the ethanol (1) + 2-methoxy-2-methylbutane (2) system (ethanol dilute region).

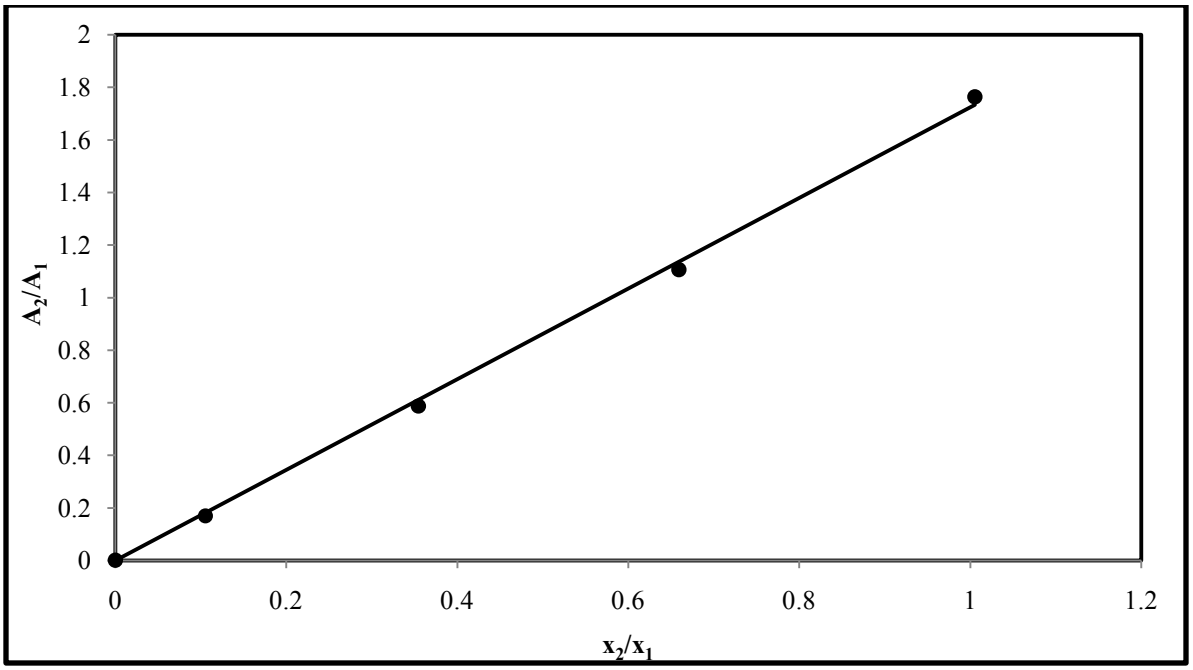

Figure C-39: GC calibration graph for the ethanol (1) + 2-methoxy-2-methylbutane (2) system (2-methoxy-2-methylbutane dilute region).

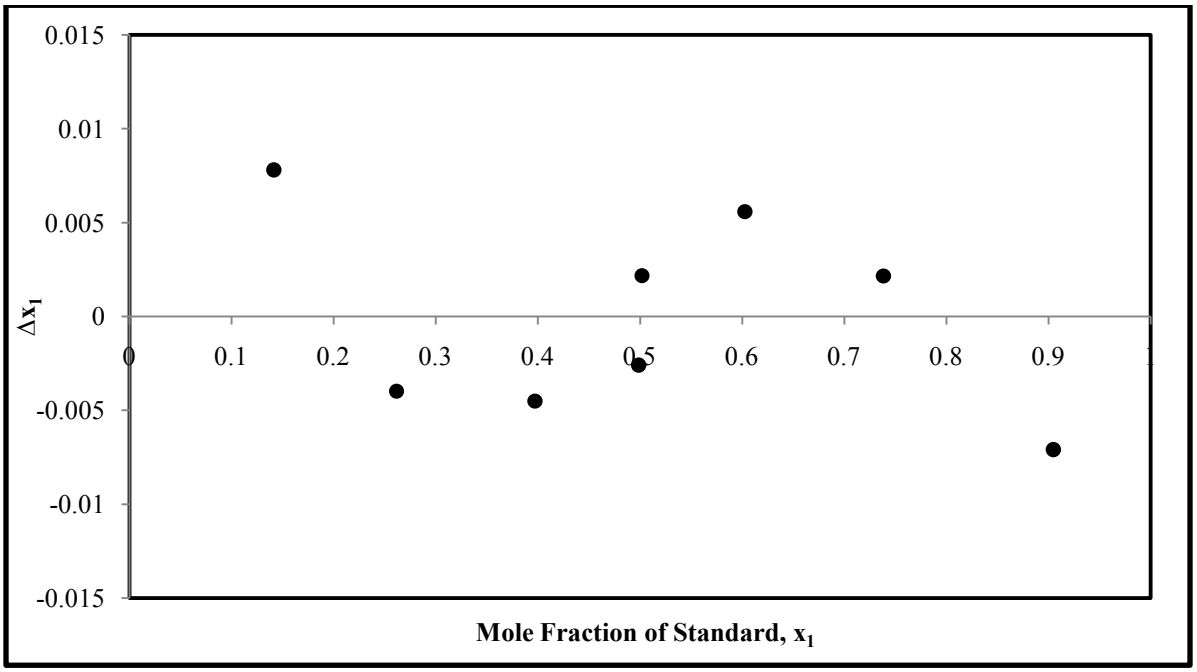

Figure C-40: Composition deviation plot for the ethanol (1) + 2-methoxy-2-methylbutane (2) system.

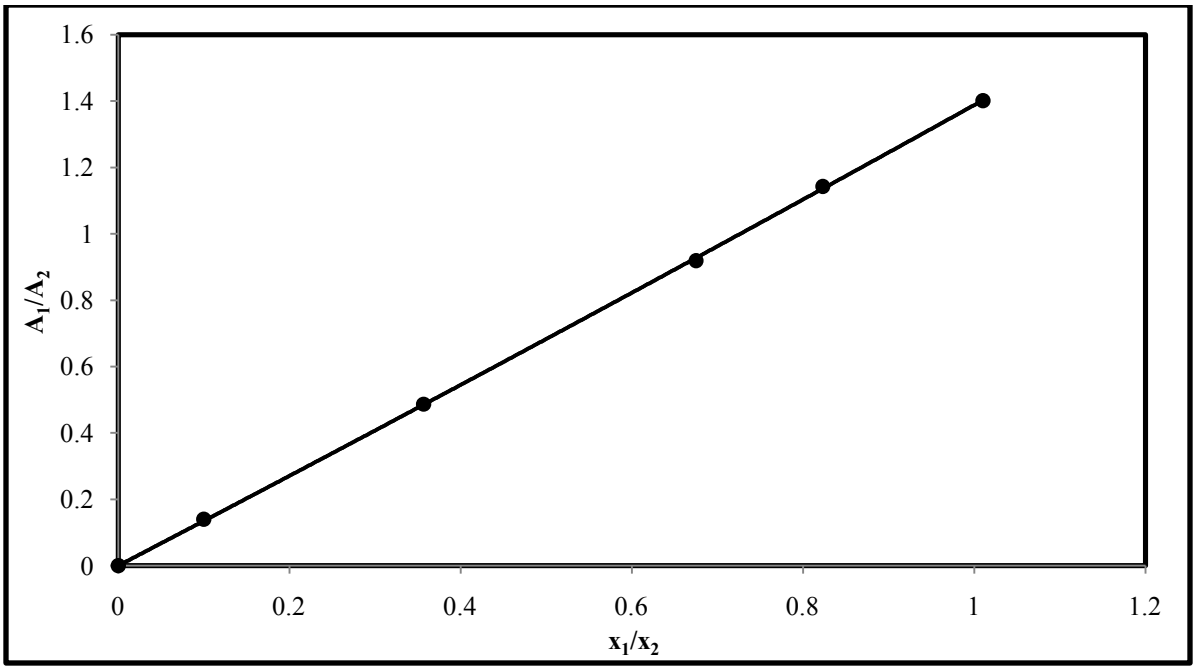

Figure C-41: GC calibration graph for the 2-methylpent-2-ene (1) + ethanol (2) system (2-methylpent-2-ene dilute region).

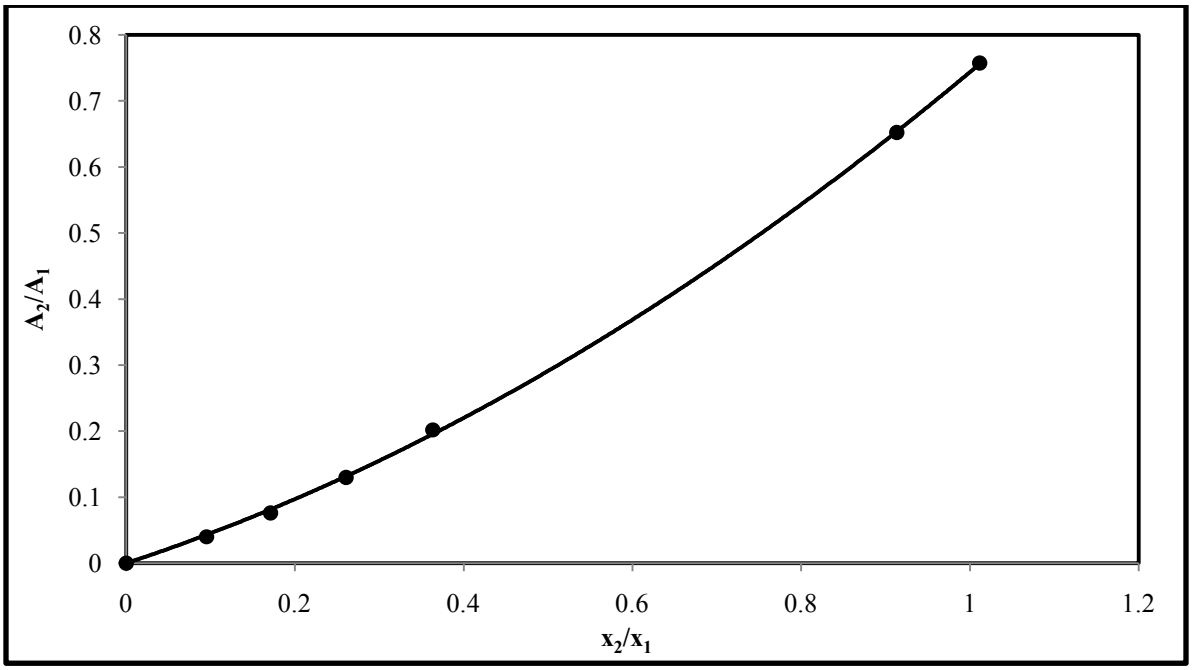

Figure C-42: GC calibration graph for the 2-methylpent-2-ene (1) + ethanol (2) system (ethanol dilute region).

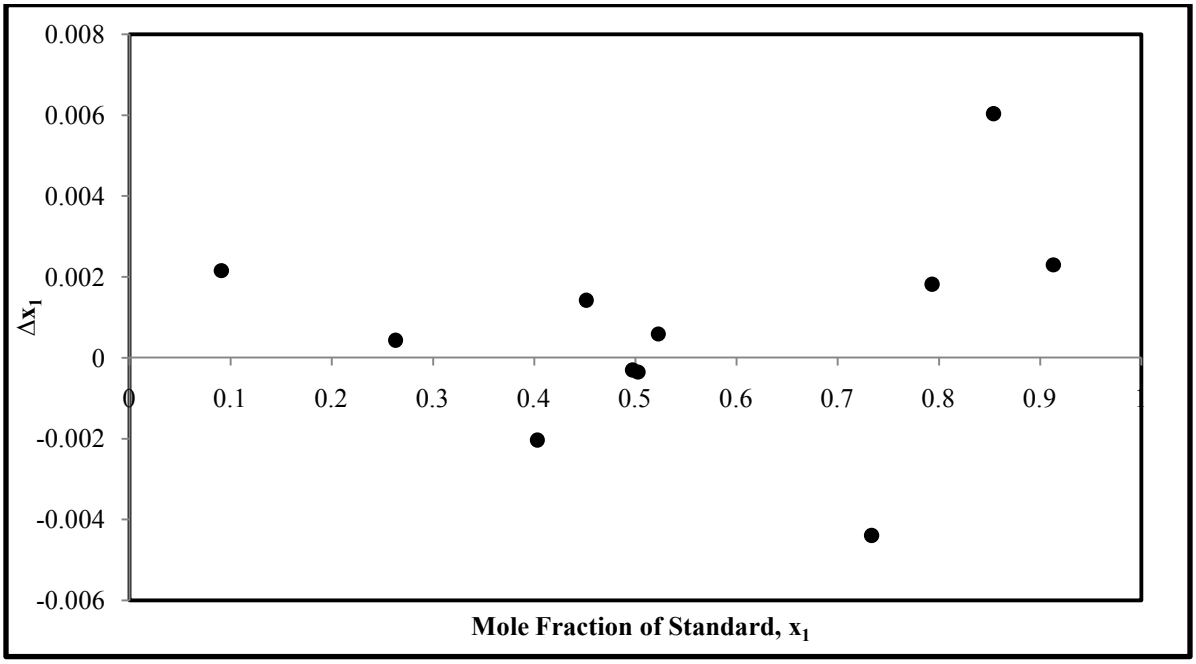

Figure C-43: Composition deviation plot for the 2-methylpent-2-ene (1) + ethanol (2) system.

C.4.2 LLE and VLLE Systems

Table C-6: Gas chromatograph calibration results for all LLE and VLLE systems used in this study.

System	Calibration Equation	AAD for n
hexane (1) + acetonitrile (2)	hexane: $n_1 = 2.9878\times10^{-18} A_1^2 + 2.1516\times10^{-11} A_1$ acetonitrile: $n_2 = 4.236\times10^{-19} A_2^2 + 3.4711\times10^{-11} A_2$	hexane: 8.39×10^{-8} acetonitrile: 1.92×10^{-7}
methanol (1) + heptane (2)	methanol: $n_1 = 4.3938\times10^{-18} A_1^2 + 5.3131\times10^{-11} A_1$ heptane: $n_2 = 2.4020\times10^{-20} A_2^2 + 1.7723\times10^{-11} A_2$	methanol: 7.11×10^{-7} heptane: 7.31×10^{-8}

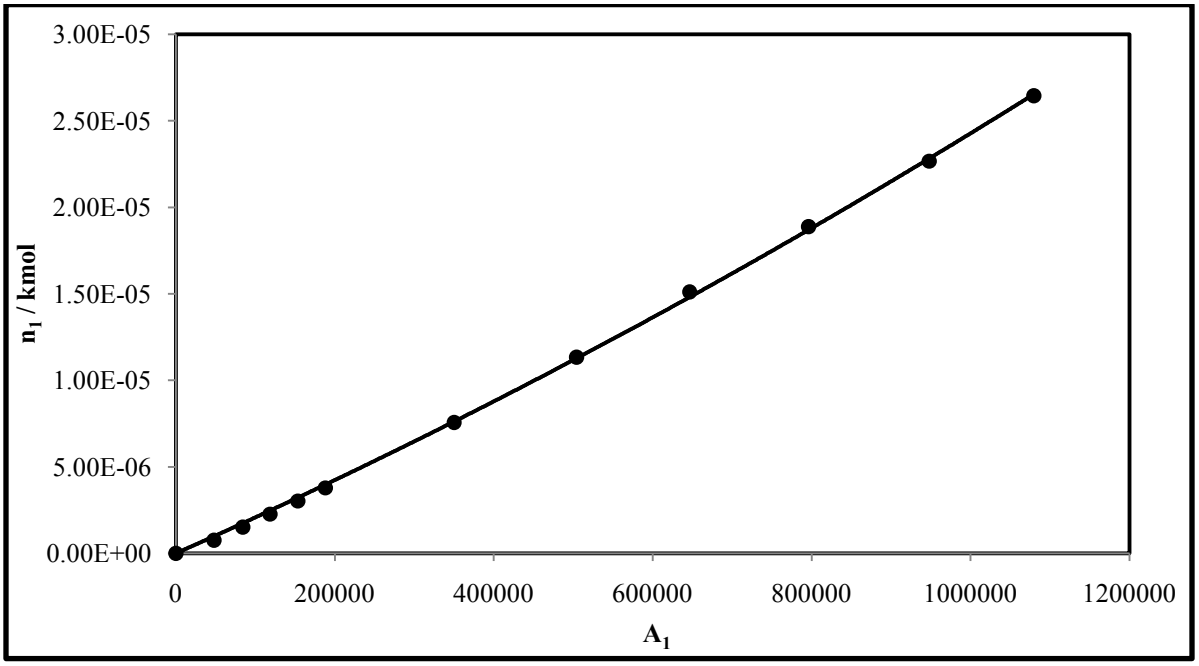

Figure C-44: GC calibration graph for the hexane (1) + acetonitrile (2) system (hexane calibration, second order polynomial fit).

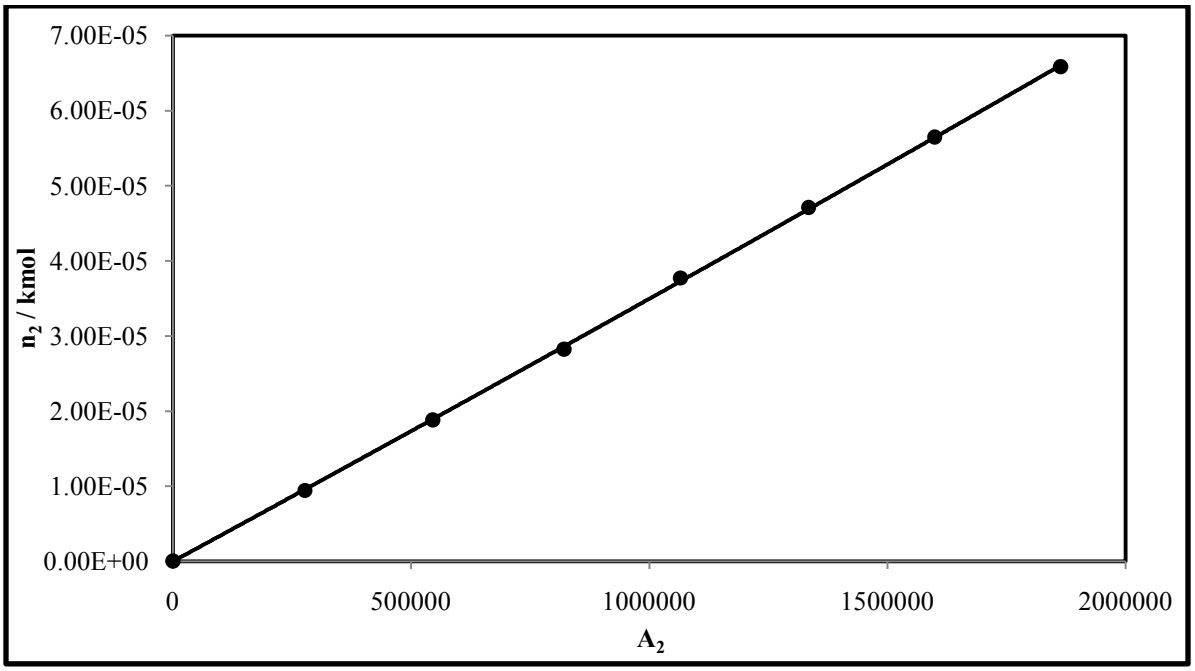

Figure C-45: GC calibration graph for the hexane (1) + acetonitrile (2) system (acetonitrile calibration, second order polynomial fit).

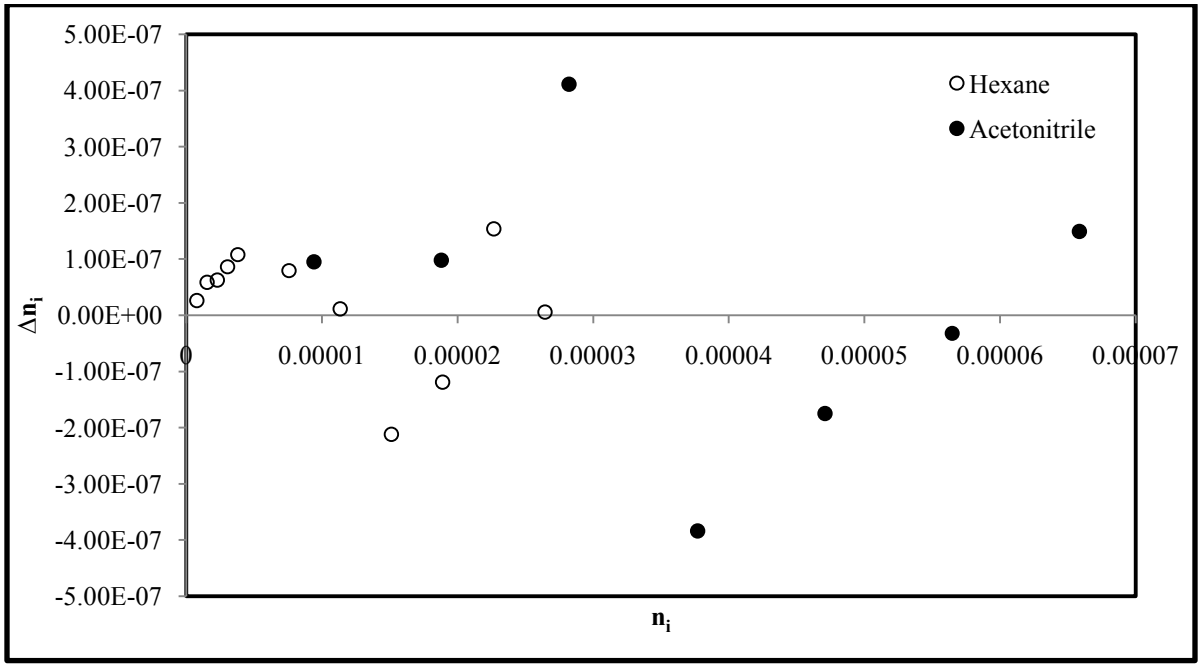

Figure C-46: Composition deviation plot for the hexane (1) + acetonitrile (2) system.

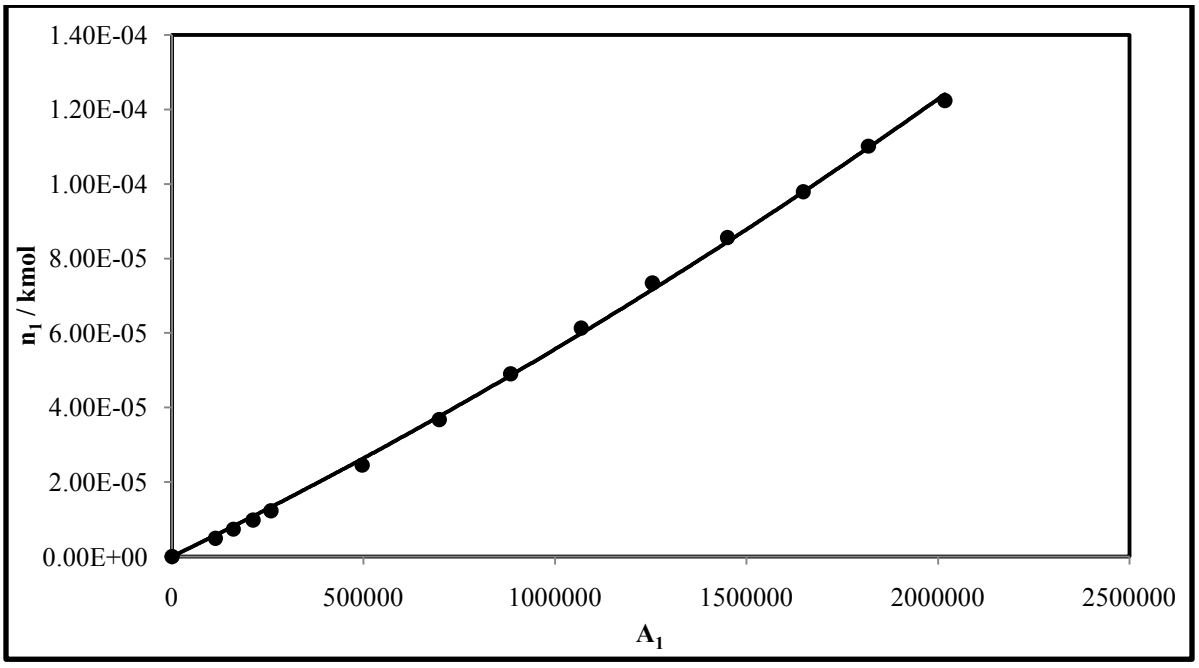

Figure C-47: GC calibration graph for the methanol (1) + heptane (2) system (methanol calibration, second order polynomial fit).

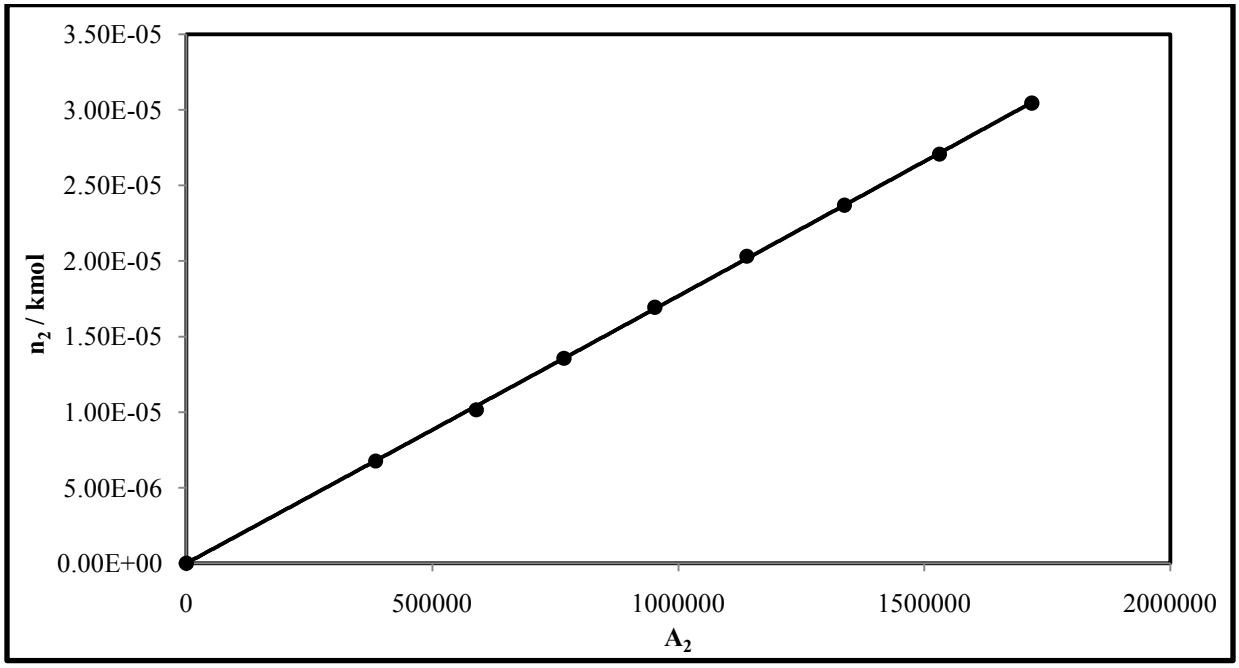

Figure C-48: GC calibration graph for the methanol (1) + heptane (2) system (heptane calibration, second order polynomial fit).

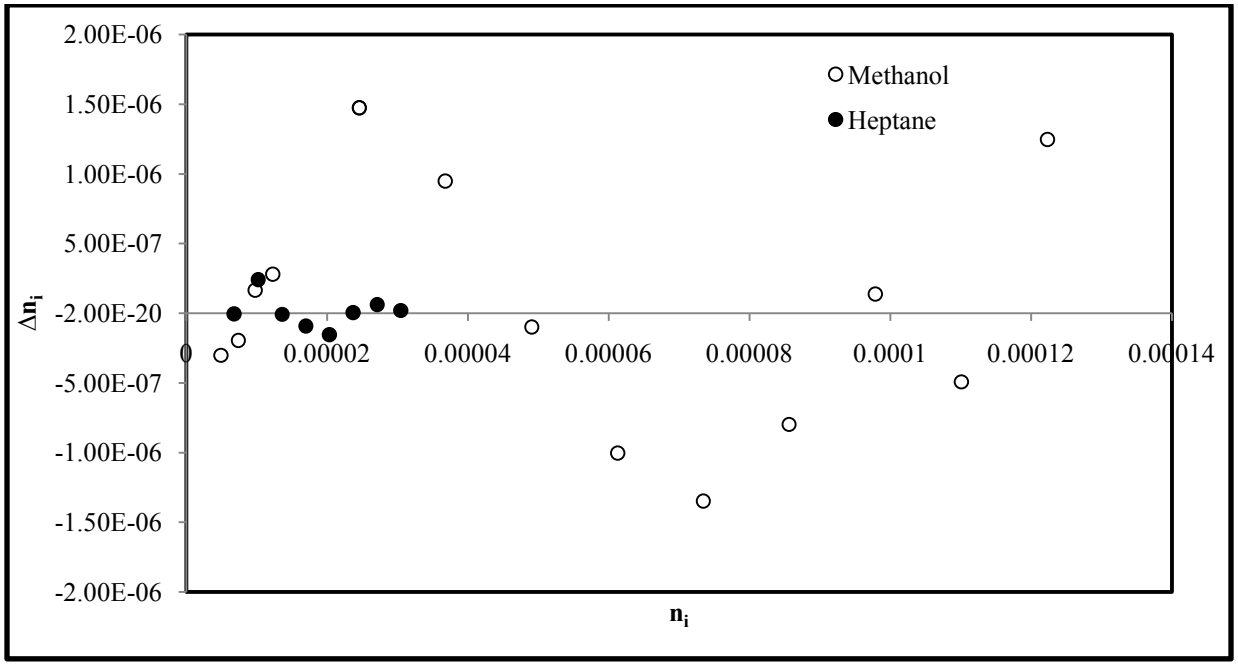

Figure C-49: Composition deviation plot for the methanol (1) + heptane (2) system.

Appendix D

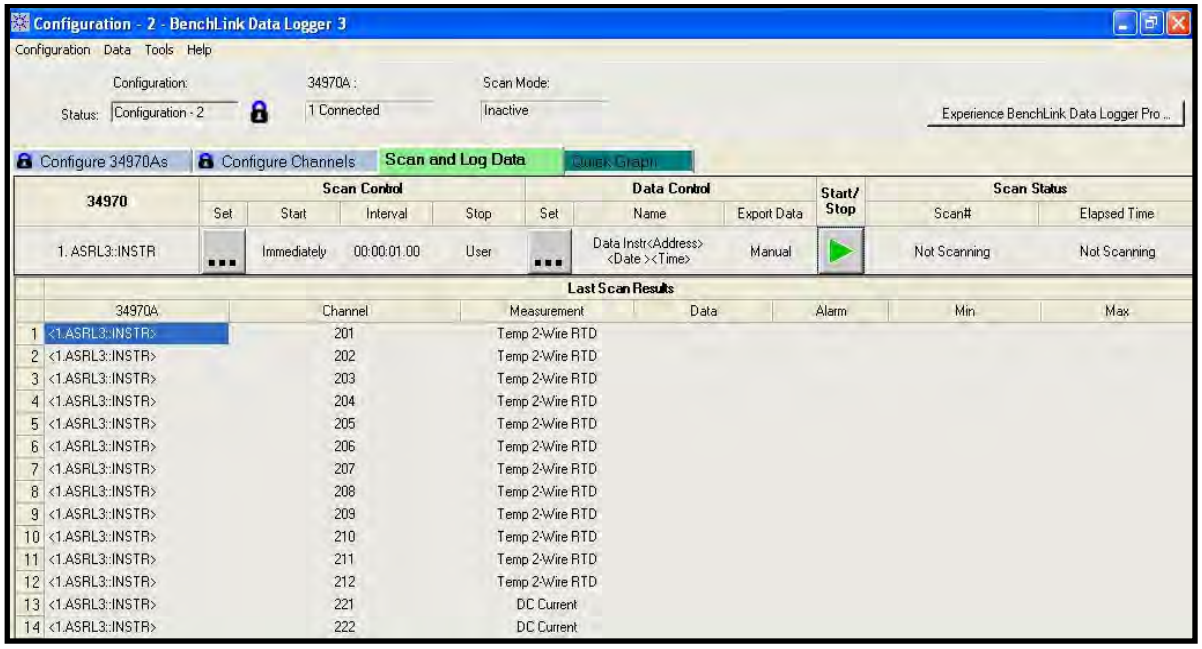

Figure D-1: User-interface of the software for the 34970A Agilent data acquisition unit.

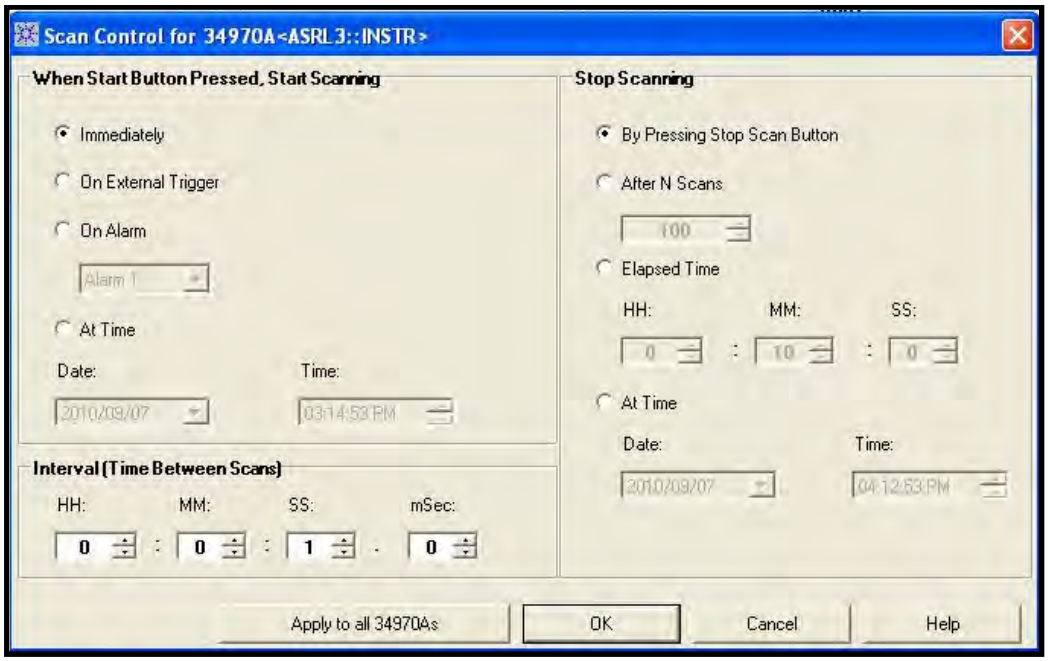

Figure D-2: User-interface of the software for the 34970A Agilent data acquisition unit, showing the scan control options.

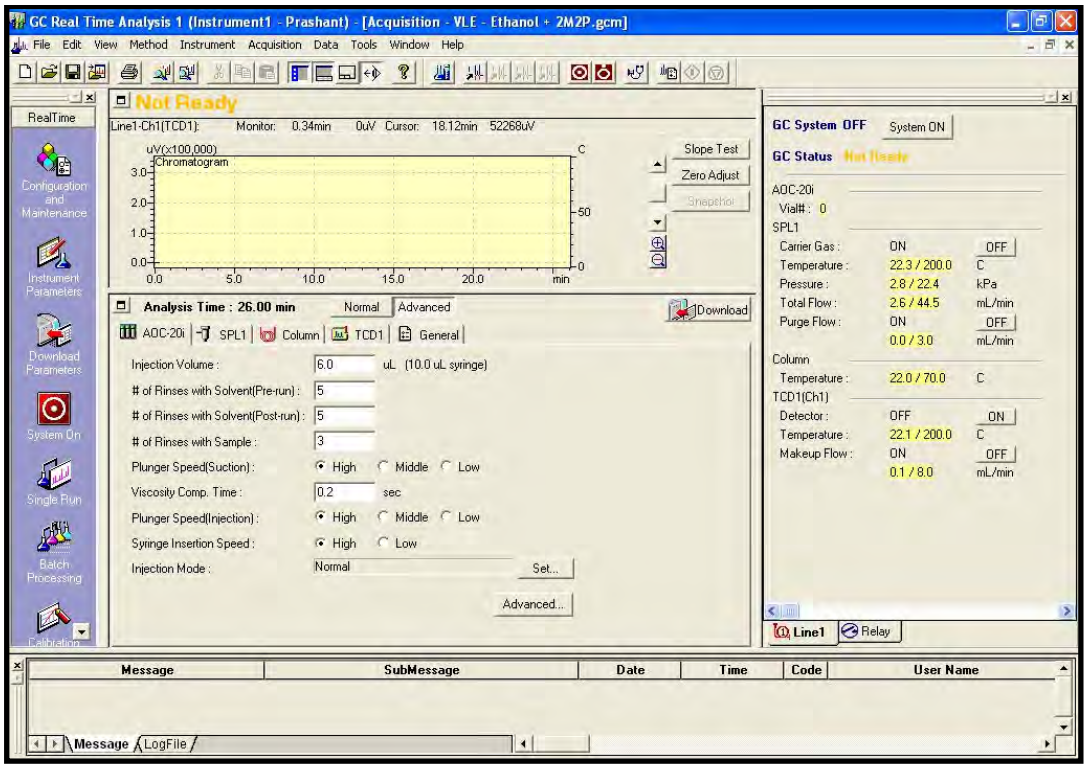

Figure D-3: User-interface of the GC Solutions software used for the equilibrium phase composition analysis.

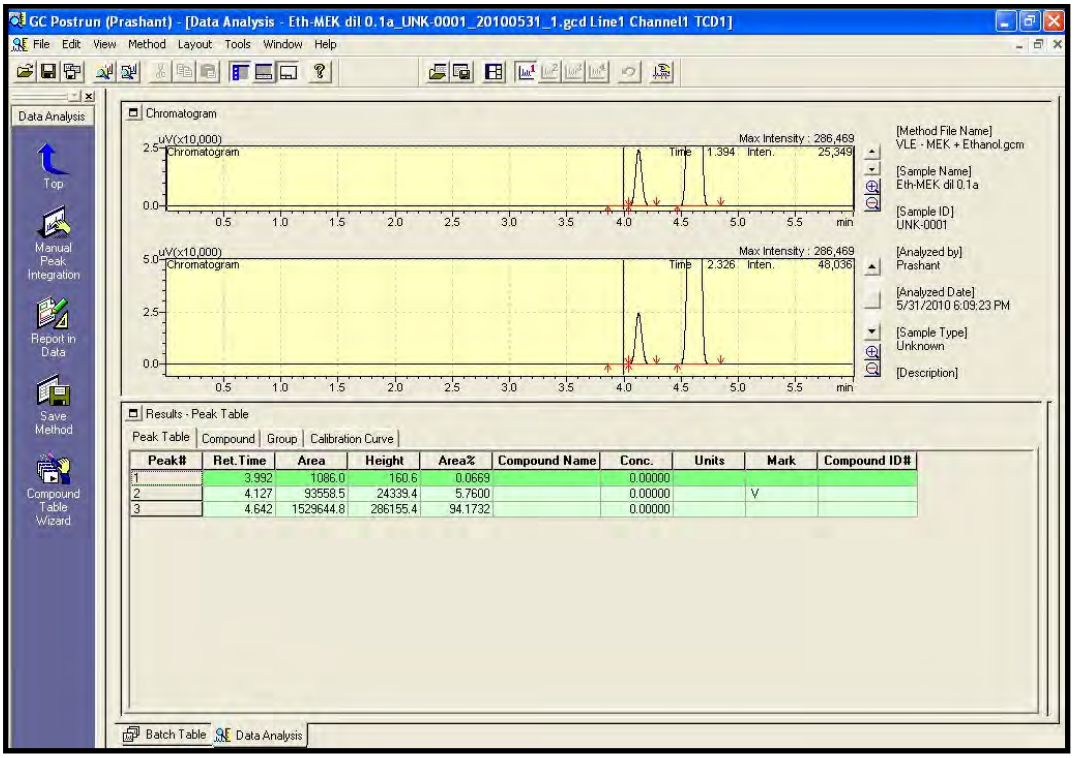

Figure D-4: User-interface for the integration of the peak areas.

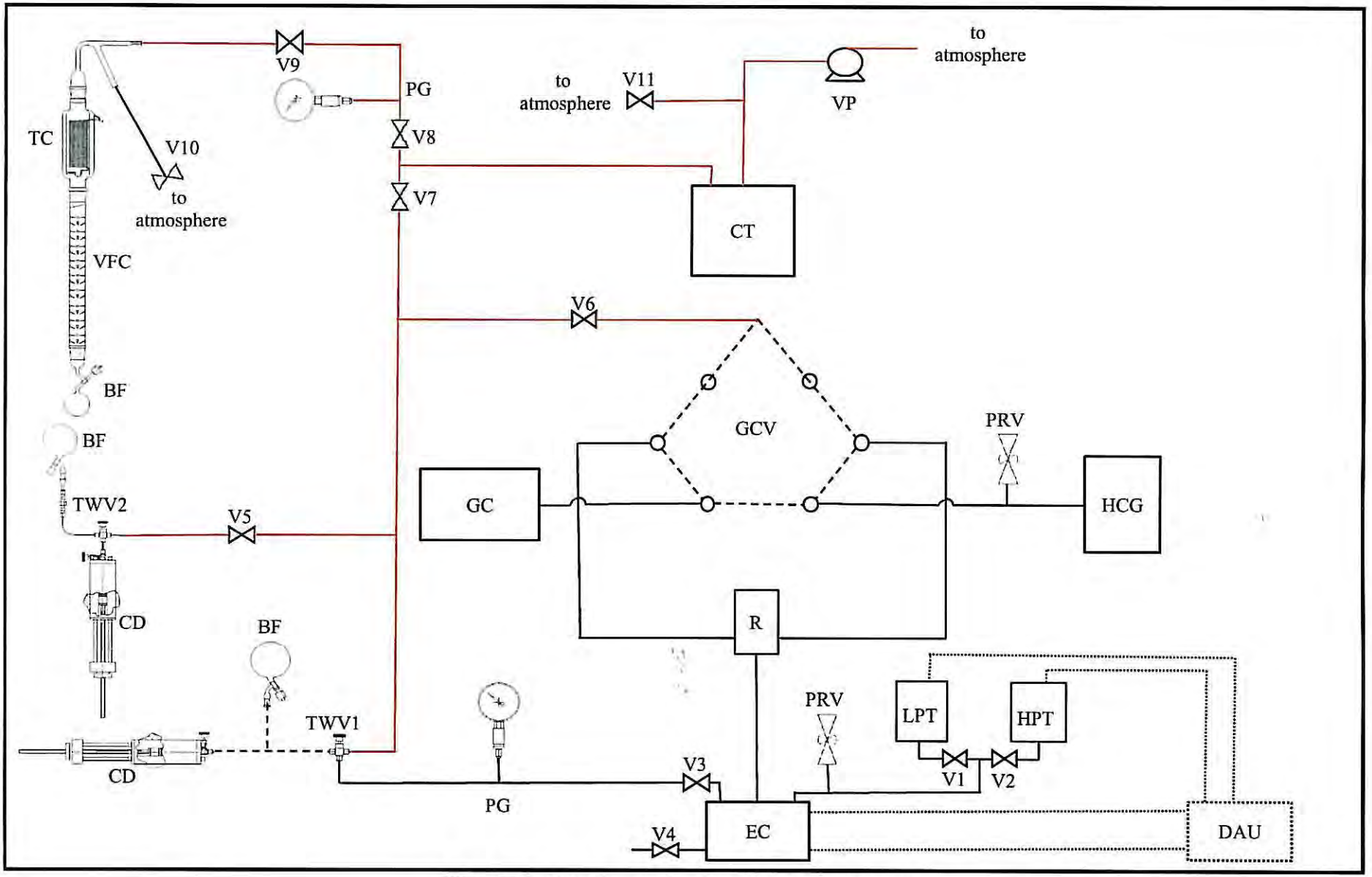

Figure E-1: Flow diagram for the entire apparatus set-up.

BF: boiling flask; CD: compression device; CT: cold-trap; DAU: data acquisition unit; EC: equilibrium cell; GC: gas chromatograph; HCG: helium carrier gas; HPT: high pressure transmitter; LPT: low pressure transmitter; PG: pressure gauge; PRV: pressure relief valve; R: ROLSI™; TC: total condenser; TWV: three-way valve; V: stainless steel valves; VFC: Vigreux fractionating column.

Appendix F

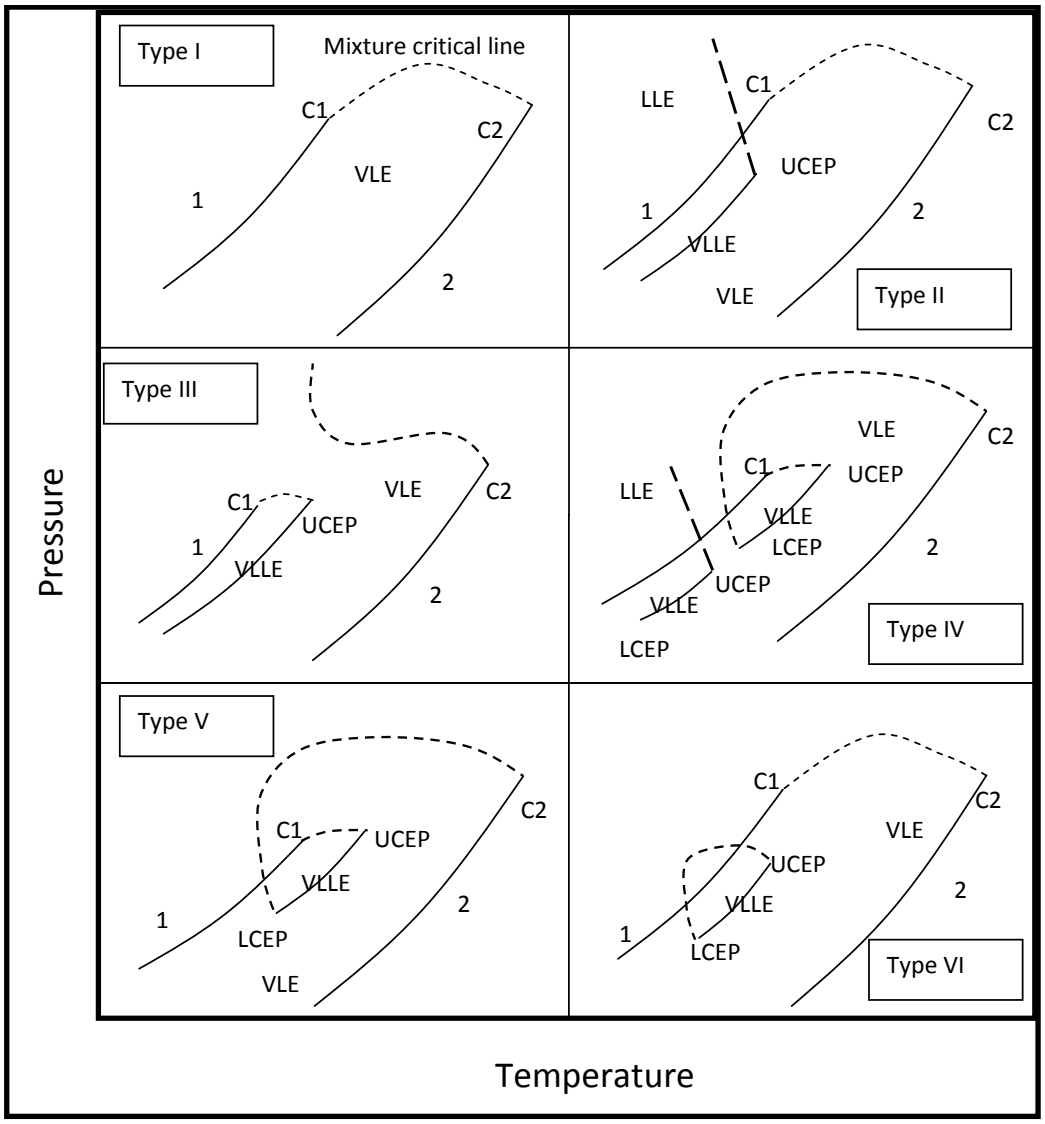

Figure F1: Six types of phase behaviour in binary fluid systems, C: critical point; L: liquid; V: vapour; UCEP; upper critical end point; LCEP: lower critical end point. The dashed curve represents the critical line (Coquelet and Richon, 2009).

In Figure F2 the following notation are used which are described below:

Stable node: this is the point at which all residue curves in a given region terminate. Hence, it is the component or azeotrope with the highest boiling point in the region.

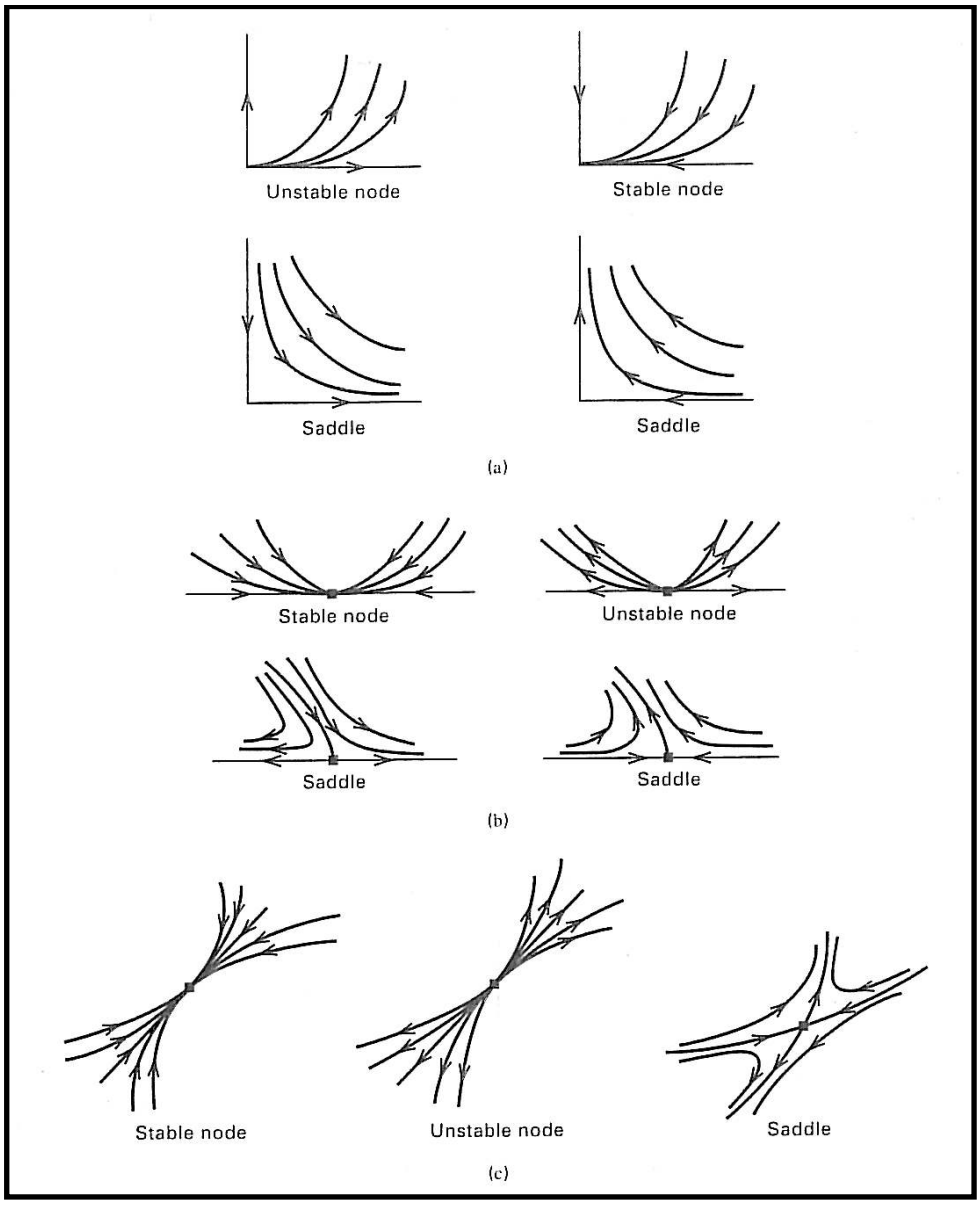

Figure F2: Residue curve patterns (a) near pure component vertices; (b) near binary azeotropes; (c) near ternary azeotropes (Doherty and Caldarola, 1985).

Unstable node: this is the point from which all residue curves in a given region originate. Hence, it is the component or azeotrope with the lowest boiling point in the region.

Saddle: in this case, the residue curves within the triangle move toward and then away from a point. For a given distillation region, all pure components and azeotropes intermediate in boiling point between the stable node and unstable node are saddles (Seader and Henley, 1998).

Appendix G

G.1 Publications

1. Narasigadu, C., J. D. Raal, P. Naidoo and D. Ramjugernath, " Ternary Liquid-Liquid Equilibria of Acetonitrile and Water with Heptanoic Acid and Nonanol at 323.15 K and 1 atm", Journal of Chemical and Engineering Data, Vol. 54, pp. 735-738, 2009.
2. Narasigadu, C., S. C. Subramoney, P. Naidoo, D. Ramjugernath, C. Coquelet and D. Richon, "Vapour-Liquid Equilibrium Measurments Using the "Dynamic-Analytic" Method for 1-Propanol and n-Dodecane at 323.0, 343.4, 353.2, 363.1 and 369.2 K", Journal of Chemical and Engineering Data, *in review*.
3. Narasigadu, C., P. Naidoo, D. Ramjugernath, C. Coquelet and D. Richon, "A Novel Static Analytical Apparatus for Phase Equilibrium Measurements", Fluid Phase Equilibria, *in review*.

G.2 Conferences

1. Narasigadu, C., D. Ramjugernath, J.D. Raal and P. Naidoo, "Measurement and Correlation of Ternary Liquid-Liquid Equilibria of Acetonitrile and Water with n-Dodecane, 1-Dodecene, Nonanol and Heptanoic Acid at 323.15 K and 1 atm", 19th International Conference on Chemical Thermodynamics, p. 635, Boulder, USA, 30 July to 4 August 2006. [Extended abstract, peer-reviewed].
2. Narasigadu, C., D. Ramjugernath, J.D. Raal and P.Naidoo, "Measurement and Correlation of Ternary Liquid-liquid Equilibria at 323.15 K and 1 atm", Electronic proceedings, 2006 South African Chemical Engineering Conference, Durban, RSA, 20-22 September 2006. [Full-manuscript, peer reviewed].
3. Narasigadu, C., P. Naidoo, C. Coquelet, D. Richon and D. Ramjugernath, "Vapour-Liquid Equilibrium Measurements using the Static and Dynamic Analytical Methods for 1-Propanol and n-Dodecane at 343.4, 363.1, 369.2 and 377.9 K", Electronic proceedings, 2009 South African Chemical Engineering Conference, Somersetwest, RSA, 20-32 September 2009. [Full-manuscript, peer reviewed].
4. Narasigadu, C., P. Naidoo, K. Robertson, C. Coquelet, D. Richon and D. Ramjugernath, "A Novel Static Analytical Apparatus for Phase Equilibrium Measurements for Small Volumes (18 cm^3)", Electronic proceedings, 2009 South African Chemical Engineering Conference, Somersetwest, RSA, 20-32 September 2009. [Full-manuscript, peer reviewed].

5. Narasigadu, C. P. Naidoo, D. Ramjugernath, C. Coquelet and D. Richon, "A Novel Static Analytical Apparatus for Phase Equilibrium Measurements for Small Volumes (18 cm^3)", Thermodynamics 2011, p. 105-106, Athens, Greece, 31 August to 03 September 2011. [Extended abstract, peer-reviewed].

Conception d'une Micro-Cellule pour Mesures d'Équilibres de Phases : Mesures et Modélisation

Résumé : Cette étude couvre la conception d'un nouvel appareil qui permet la mesure fiable de pressions de vapeur d'équilibres à plusieurs phases à partir de petits volumes (un maximum de 18 c m^3). Les mesures d'équilibres de phase concernant la présente étude incluent : des équilibres "liquide-vapeur" (ELV), "liquide-liquide" (ELL) et " liquide-liquide-vapeur" (ELLV). La température de fonctionnement de l 'appareil s 'étend de 253 à 47 3 K pour une pression de fonctionnement qui s'étend du vide absolu à 1600 kPa. Le prélèvement des phases est réalisé grâce au Rapid On line Sampling Injector (ROLSI™). Une technique originale est ajoutée en complément du R OLSI™ pour éviter des chutes de pressions lors du prélèvement. Cette technique utilise une tige métallique afin de compenser les changements de volume lors des prélèvements. Des mesures de tensions de vapeur et d'équilibres de phase ont été entreprises pour caractériser le fonctionnement de l'appareil conçu et développé. Ensuite de nouvelles mesures de tensions de vapeur et d'ELV ont été mesurées sur des systèmes intéressant les compagnies pétrochimiques. Les données expérimentales de pression de vapeur obtenues ont été régressées en utilisant les équations étendues d' Antoine et de Wagner. Les données expérimentales d'ELV mesurées ont été régressées avec des modèles thermodynamiques au moyen des méthodes directes et combinées. Pour la méthode directe les équations d'état de Soave-Redlich-Kwong et de Peng-Robinson ont été employées avec la fonction (α) de Mathias et Copeman (1983) dépendante de la température. Pour la méthode combinée, l'équation du viriel (deuxième coefficient du viriel de la corrélation de Tsonopoulos (1974)) a été employée associée à un modèle de solution (coefficient d'activité) pour la phase liquide: TK-Wilson, NRTL et UNIQUAC modifié. Des tests de cohérence thermodynamique ont été exécutés pour toutes les données expérimentales de VLE mesurées. Presque tous les systèmes mesurés ont déclarés thermodynamiquement cohérents (test de point de Van Ness et autres (1973) et test direct de Van Ness (1995).

Mots clés : équilibres de phase, nouvel appareil, modélisation thermodynamique

Design of a Static Micro-Cell for Phase Equilibrium Measurements : Measurements and Modelling

Abstract: This study covers the design of a new apparatus that enables reliable vapour pressure and equilibria measurements for multiple liquid and vapour phases of small volumes (a maximum of 18 c m^3). These phase equilibria measurements include: vapour-liquid equilibrium (VLE), liquid-liquid equilibrium (LLE) and vapour-liquid-liquid (VLLE). The operating temperature of the apparatus ranges from 253 to 473 K and the operating pressure ranges from absolute vacuum to 1600 kPa. The sampling of the phases is accomplished using a single Rapid-OnLine-Sampler-Injector (ROLSI™). A novel technique is used to achieve sampling for each phase. The technique made use of a metallic rod in an arrangement to compensate for volume changes during sampling. As part of this study, vapour pressure and phase equilibrium data were measured to test the operation of the newly developed apparatus. New experimental vapour pressure and VLE data were also measured for systems of interest to petrochemical companies. The experimental vapour pressure data obtained were regressed using the extended Antoine and Wagner equations. The experimental VLE data measured were regressed with thermodynamic models using the direct and combined methods. For the direct method the Soave-Redlich-Kwong and Peng-Robinson equations of state were used with the temperature dependent function (α) of Mathias and Copeman (1983). For the combined method, the virial equation of state with the second virial coefficient correlation of Tsonopoulos (1974) was used together with one of the following liquid-phase activity coefficient model: TK-Wilson, NRTL and modified UNIQUAC. Thermodynamic consistency testing was also performed for all the VLE experimental data measured where almost all the systems measured showed good thermodynamic consistency for the point test of Van Ness et al. (1973) and direct test of Van Ness (1995).

Keywords : phase equilibria, novel apparatus, thermodynamic modelling